USGS
science for a changing world

In cooperation with the
JOSHUA BASIN WATER DISTRICT

Evaluation of Geohydrologic Framework, Recharge Estimates, and Ground-Water Flow of the Joshua Tree Area, San Bernardino County, California

Scientific Investigations Report 2004-5267

U.S. DEPARTMENT OF THE INTERIOR
U.S. GEOLOGICAL SURVEY

125 years of science for America ★ ★ ★ ★ ★ *1879–2004*

Evaluation of Geohydrologic Framework, Recharge Estimates, and Ground-Water Flow of the Joshua Tree Area, San Bernardino County, California

By Tracy Nishikawa, John A. Izbicki, Joseph A. Hevesi, Christina L. Stamos, and Peter Martin

In cooperation with the
Joshua Basin Water District

Scientific Investigations Report 2004-5267

U.S. Department of the Interior
U.S. Geological Survey

U.S. Department of the Interior
Gale A. Norton, Secretary

U.S. Geological Survey
Charles G. Groat, Director

U.S. Geological Survey, Reston, Virginia: 2004
For sale by U.S. Geological Survey, Information Services
Box 25286, Denver Federal Center
Denver, CO 80225-0286

For more information about the USGS and its products:
Telephone: 1-888-ASK-USGS
World Wide Web: http://www.usgs.gov/

Suggested citation:
Nishikawa, T. Izbicki, J.A., Hevesi, J.A., Stamos, C.L., and Martin, P., 2004, Evaluation of geohydrologic framework, recharge estimates, and ground-water flow of the Joshua Tree area, San Bernardino County, California: U.S. Geological Survey Scientific Investigations Report 2004–5267, 115 p.

Contents

Figures

Tables

Conversion Factors, Datum, and Abbreviations

Multiply	By	To obtain
Length		
inch (in.)	2.54	centimeter
inch (in.)	25.4	millimeter
foot (ft)	0.3048	meter
mile (mi)	1.609	kilometer
yard (yd)	0.9144	meter
Area		
acre	4,047	square meter
acre	0.4047	hectare
acre	0.004047	square kilometer
square foot (ft^2)	929.0	square centimeter
square foot (ft^2)	0.09290	square meter
square inch (in^2)	6.452	square centimeter
square mile (mi^2)	259.0	hectare
square mile (mi^2)	2.590	square kilometer
Volume		
gallon (gal)	3.785	liter
gallon (gal)	0.003785	cubic meter
cubic inch (in^3)	16.39	cubic centimeter
cubic inch (in^3)	0.01639	cubic decimeter
cubic inch (in^3)	0.01639	liter
cubic foot (ft^3)	28.32	cubic decimeter
cubic foot (ft^3)	0.02832	cubic meter
acre-foot (acre-ft)	1,233	cubic meter
Flow rate		
acre-foot per day (acre-ft/d)	0.01427	cubic meter per second
acre-foot per year (acre-ft/yr)	1,233	cubic meter per year
foot per hour (ft/hr)	0.3048	meter per hour
foot per day (ft/d)	0.3048	meter per day
foot per year (ft/yr)	0.3048	meter per year
cubic foot per second (ft^3/s)	0.02832	cubic meter per second
cubic foot per day (ft^3/d)	0.02832	cubic meter per day
gallon per minute (gal/min)	0.06309	liter per second
inch per year (in/yr)	25.4	millimeter per year
Pressure		
atmosphere, standard (atm)	101.3	kilopascal
bar	100	kilopascal
Density		
pound per cubic foot (lb/ft^3)	16.02	kilogram per cubic meter
pound per cubic foot (lb/ft^3)	0.01602	gram per cubic centimeter
Energy		
kilowatthour (kWh)	3,600,000	joule
Hydraulic conductivity		
foot per second (ft/sec)	0.3048	meter per second
foot per day (ft/d)	0.3048	meter per day

Temperature in degrees Celsius (°C) may be converted to degrees Fahrenheit (°F) as follows:

$$°F=1.8\ °C+32$$

Temperature in degrees Fahrenheit (°F) may be converted to degrees Celsius (°C) as follows:

$$°C=(°F-32)/1.8$$

Water-quality and unsaturated-zone data are generally reported in metric units. The use of dual units in this report is intended to facilitate application of the data by maintaining the integrity of the original units of measurement.

*Transmissivity: The standard unit for transmissivity is cubic foot per day per square foot times foot of aquifer thickness [$(ft^3/d)/ft^2$]ft. In this report, the mathematically reduced form, foot squared per day (ft^2/d), is used for convenience.

WATER-QUALITY INFORMATION

Concentrations of chemical constituents in water are given in milligrams per liter (mg/L) or micrograms per liter (µg/L). Milligrams per liter is approximately equivalent to parts per million. Micrograms per liter is approximately equivalent to parts per billion. Specific conductance is given in microsiemens per centimeter at 25 degrees Celsius (µS/cm at 25°C).

Data for the isotopes oxygen-18 and deuterium are reported in delta (δ) notation as per mil (parts per thousand); tritium data are reported in tritium units (TU); carbon-14 data are reported as percent modern carbon (pmc).

DATUM

Vertical coordinate information is referenced to the North American Vertical Datum of 1988 (NAVD 88).

Horizontal coordinate information is referenced to North American Datum of 1983 (NAD 83).

Altitude, as used in this report, refers to distance above the vertical datum.

ABBREVIATIONS

asl	above sea level
bls	below land surface
^{14}C	carbon-14
DVRFS	Death Valley Regional Flow System
δD	delta deuterium
$\delta^{18}O$	delta oxygen-18
DEM	digital elevation model
ENSO	El Nino-Southern Oscillation
ET_0	evapotranspiration rate
F1	hydraulic characteristic of Pinto Mountain Fault, in per day
F2	hydraulic characteristic of inferred north-south trending fault, in per day
GAP	California Gap Analysis Program
GHBN	general-head conductance northern boundary in feet squared per day
GHBS	general-head conductance southern boundary in feet squared per day
IN	mass balance inflow
INFILv3	distributed-parameter watershed model

K	hydraulic conductivity in feet per day
Kz	vertical hydraulic conductivity in feet per day
LSD	land surface datum
MCL	Maximum Contaminant Level
MSE	mean-square error
MF2K	MODFLOW-2000 ground-water flow model
MUID	map unit identifier
NCDC	National Climatic Data Center
NI	not included in mass balance caluclation
NTS	Nevada Test Site
NWISweb	USGS National Water Information System Web page
OUT	mass balance outflow
PDO	Pacific Decadal Oscillation
pmc	percent modern carbon
PVC	polyvinyl chloride
PRISM	Parameter Regression on Independent Slope Model
RAWS	Remote Automated Weather Stations
Rech	recharge in acre-feet per year
S	storativity
SMCL	Secondary Maximum Contaminant Level
STATSGO	state soil geographic database
Ss	specific storage in per feet
S_y	specific yield in feet per feet
TU	tritium units
UT	Utah
VSMOW	Vienna Standard Mean Ocean Water

Organizations

JBWD	Joshua Basin Water District
NWS	National Weather Service
USEPA	U.S. Environmental Protection Agency
USGS	U.S. Geological Survey

Well-Numbering System

Wells are identified and numbered according to their location in the rectangular system for the subdivision of public lands. Identification consists of the township number, north or south; the range number, east or west; and the section number. Each section is divided into sixteen 40-acre tracts lettered consecutively (except I and O), beginning with "A" in the northeast corner of the section and progressing in a sinusoidal manner to "R" in the southeast corner. Within the 40-acre tract, wells are sequentially numbered in the order they are inventoried. The final letter refers to the base line and meridian. In California, there are three base lines and meridians; Humboldt (H), Mount Diablo (M), and San Bernardino (S). All wells in the study area are referenced to the San Bernardino base line and meridian (S) Well numbers consist of 15 characters and follow the format 001N006E025M003. In this report, well numbers are abbreviated and written 1N/6E-25M3. Wells in the same township and range are referred to only by their section designation, 25M3. The following diagram shows how the number for well 1N/6E-25M3 is derived.

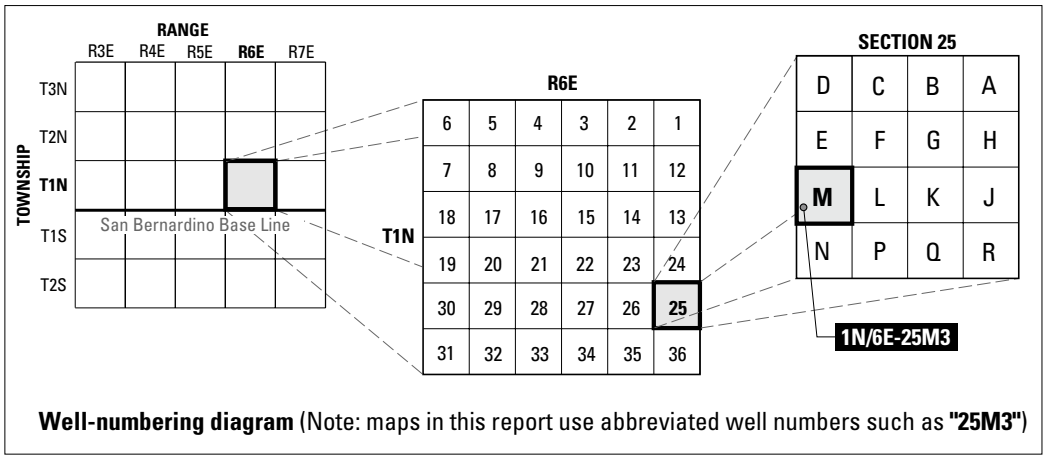

Well-numbering diagram (Note: maps in this report use abbreviated well numbers such as **"25M3"**)

Evaluation of Geohydrologic Framework, Recharge Estimates, and Ground-Water Flow of the Joshua Tree Area, San Bernardino County, California

By Tracy Nishikawa, John A. Izbicki, Joseph A. Hevesi, Christina L. Stamos, and Peter Martin

Summary of Major Findings

To manage the ground-water resources in the Joshua Tree and Copper Mountain ground-water subbasins and to identify future mitigating measures, a thorough understanding of the ground-water system is needed.

Geohydrology

The geohydrology of the study area was refined by collecting and interpreting water-level and water-quality data, geologic and electric logs, and gravity data. The specific goals were to identify the thickness of the water-bearing units, define the aquifers, and study ground-water-level changes. Major findings regarding the geohydrology from this study are the following:

- On the basis of geophysical data, the ground-water subbasins are as deep as 4,500 feet east of the community of Joshua Tree and 2,000 feet beneath Coyote Lake.
- The water-bearing deposits were divided into three aquifers (referred to as the "upper," "middle," and "lower" aquifers). Most wells in the ground-water subbasins extract water from the upper and middle aquifers. The lower aquifer is the thickest aquifer; however, it is the least permeable and yields little water to wells.
- Ground-water withdrawals have resulted in as much as 35 ft of drawdown in the Joshua Tree ground-water subbasin.

Ground-Water Quality

The ground-water quality of the Joshua Tree and Copper Mountain ground-water subbasins was defined by analyzing ground-water samples for major ions, nutrients, and selected trace elements. Selected samples also were analyzed for oxygen-18, deuterium, tritium, and carbon-14. Major findings on ground-water quality from this study are the following:

- With the exception of one well, the water-quality data indicated that the dissolved solids concentrations are less than 375 mg/L. A sample from well 1N/7E-3D1 in the northern part of the Copper Mountain ground-water subbasin had a dissolved solids concentration of 809 mg/L, which exceeds regulatory limits.
- Fluoride and arsenic concentrations in samples collected from wells perforated in the lower aquifer exceeded regulatory limits.
- Carbon-14 analyses indicated that the time since recharge of the ground-water system is about 32,300 to 2,700 years before present.

Estimates of Natural Recharge

Field and numerical techniques were applied to determine the distribution and quantity of natural recharge. Field techniques included the installation of instrumented boreholes in selected washes and at a nearby control site. Numerical techniques included the use of a distributed-parameter watershed model and a ground-water flow model. Major findings from the recharge-estimate effort are the following:

- In general, the results from the field and numerical techniques indicate that natural recharge in the Joshua Tree area is very limited.
- The results from the field techniques indicated that as much as 71 acre-feet per year (acre-ft/yr) of water infiltrated into the streambed of the two principal washes during the study period (2001–03).
- The results from the watershed model indicated that the average recharge in the ground-water subbasins is about 158 acre-ft/yr.
- The results from the calibrated ground-water flow model indicated that the average recharge for the same area is about 123 acre-ft/yr.

Ground-Water Flow Model

To better understand the dynamics of ground-water flow in the Joshua Tree and Copper Mountain ground-water subbasins, a ground-water flow model was developed. Major findings from the model development are the following:

- The Pinto Mountain Fault restricts ground-water flow between the Joshua Tree and Copper Mountain ground-water subbasins. Therefore, the historical pumpage in the Joshua Tree ground-water subbasin has not affected water levels in the Copper Mountain ground-water subbasin.
- The steady-state hydrologic budget from the ground-water flow model indicates that the sources of natural recharge to the Joshua Tree ground-water subbasin include 123 acre-ft/yr of streamflow infiltration and 84 acre-ft/yr of underflow across the Yucca Barrier from the Warren ground-water subbasin. The hydrologic budget also indicates that an average of about 200 acre-ft/yr leaves the Copper Mountain ground-water subbasin entering the Surprise Spring ground-water subbasin.
- The cumulative volume of water pumped from the ground-water subbasins between 1958–2001 was 42,210 acre-feet (acre-ft); of this total pumpage, the model simulated that 99 percent (41,930 acre-ft) was removed from ground-water storage.
- The results from the ground-water flow model are in good agreement with measured data, indicating that the model can be used to determine the potential effects of water-management strategies (for example, artificial recharge, areal distribution of pumping, and well design) on ground-water levels.
- In this model, septage was not simulated as a source of recharge; however, this source of recharge may reach the water table. In order to simulate future conditions, the timing and quantity of this potential source of recharge should be considered.

Abstract

Ground water historically has been the sole source of water supply for the community of Joshua Tree in the Joshua Tree ground-water subbasin of the Morongo ground-water basin in the southern Mojave Desert. The Joshua Basin Water District (JBWD) supplies water to the community from the underlying Joshua Tree ground-water subbasin. The JBWD is concerned with the long-term sustainability of the underlying aquifer. To help meet future demands, the JBWD plans to construct production wells in the adjacent Copper Mountain ground-water subbasin. As growth continues in the desert, there may be a need to import water to supplement the available ground-water resources. In order to manage the ground-water resources and to identify future mitigating measures, a thorough understanding of the ground-water system is needed.

The purpose of this study was threefold: (1) improve the understanding of the geohydrologic framework of the Joshua Tree and Copper Mountain ground-water subbasins, (2) determine the distribution and quantity of recharge using field and numerical techniques, and (3) develop a ground-water flow model that can be used to help manage the water resources of the region.

The geohydrologic framework was refined by collecting and interpreting water-level and water-quality data, geologic and electric logs, and gravity data. The water-bearing deposits in the Joshua Tree and Copper Mountain ground-water subbasins are Quarternary alluvial deposits and Tertiary sedimentary and volcanic deposits. The Quarternary alluvial deposits were divided into two aquifers (referred to as the "upper" and the "middle" alluvial aquifers), which are about 600 feet (ft) thick, and the Tertiary sedimentary and volcanic deposits were assigned to a single aquifer (referred to as the "lower" aquifer), which is as thick as 1,500 ft.

The ground-water quality of the Joshua Tree and Copper Mountain ground-water subbasins was defined by collecting 53 ground-water samples from 15 wells (10 in the Joshua Tree ground-water subbasin and 5 in the Copper Mountain ground-water subbasin) between 1980 and 2002 and analyzing the samples for major ions, nutrients, and selected trace elements. Selected samples also were analyzed for oxygen-18, deuterium, tritium, and carbon-14. The water-quality data indicated that dissolved solids and nitrate concentrations were below regulatory limits for potable water; however, fluoride concentrations in the lower aquifer exceeded regulatory limits. Arsenic concentrations and chromium concentrations were generally below regulatory limits; however, arsenic concentrations measured in water from wells perforated in the lower aquifer exceeded regulatory limits. The carbon-14 activities ranged from 2 to 72 percent modern carbon and are consistent with uncorrected ground-water ages (time since recharge) of about 32,300 to 2,700 years before present. The oxygen-18 and deuterium composition of water sampled from the upper aquifer is similar to the volume-weighted composition of present-day winter precipitation indicating that winter precipitation was the predominant source of ground-water recharge.

Field studies, conducted during water years 2001 through 2003 to determine the distribution and quantity of recharge, included installation of instrumented boreholes in selected washes and at a nearby control site. Core material and cuttings from the boreholes were analyzed for physical, chemical, and hydraulic properties. Instruments installed in the boreholes were monitored to measure changes in matric potential and temperature. Borehole data were supplemented with temperature data collected from access tubes installed at additional sites along study washes. Streambed hydraulic properties and the response of instruments to infiltration were measured using infiltrometers. Physical and geochemical data collected away from the stream channels show that direct infiltration of precipitation to depths below the root zone and subsequent ground-water recharge do not occur in the Joshua Tree area. The simulation of measured temperature data indicated that as much as 71 acre-feet per year (acre-ft/yr) of water infiltrated as a result of streamflow during the study period. Most infiltration was along stream reaches where upstream urbanization resulted in increased runoff.

Numerical simulations to determine the distribution and quantity of recharge included applying a distributed-parameter watershed model, INFILv3, to estimate spatially and temporally distributed recharge under 1950–2003 climate conditions for the area of the Joshua Tree and Copper Mountain ground-water subbasins and for the areas of the surface-water drainage basins upstream from the subbasins. The average annual simulated recharge in the Joshua Tree surface-water drainage basin is about 1,090 acre-ft/yr, which includes 158 acre-ft/yr in the Joshua Tree and Copper Mountain subbasins ground-water model area. The simulated total annual streamflow is 2 to 10 times greater than the measured total annual streamflow indicating that the recharge values estimated using the watershed model may be overestimated. Results from the watershed model indicated that recharge throughout the Joshua Tree surface-water drainage basin is strongly dependent on winter-season runoff generation during wetter than average periods and the subsequent infiltration of surface-water run-on routed to downstream locations.

Data collected during the study were used to develop and calibrate a ground-water flow model of the Joshua Tree and Copper Mountain ground-water subbasins. The simulation period of the ground-water flow model was 1958–2001. The ground-water flow model was developed using MODFLOW-2000. The model cell size was about 820 ft by 820 ft and was discretized vertically into three layers (the upper, middle, and lower aquifers). Recharge was simulated using the net infiltration estimates from the watershed model. The model was calibrated using a trial-and-error approach using water-level data collected between 1958 and 2001; however, the MODFLOW-2000 sensitivity process was used for the sensitivity analysis. In order to better match the measured data, little flow was allowed to cross the Pinto Mountain Fault, thereby compartmentalizing the Joshua Tree and Copper Mountain ground-water subbasins. The calibrated total natural inflow was about 207 acre-ft/yr, consisting of 123 acre-ft/yr of recharge and 84 acre-ft/yr of underflow from the adjacent Warren subbasin. The simulated value of recharge is very close to those values estimated using measured temperature differences (71 acre-ft/yr) and a distributed-parameter watershed model (158 acre-ft/yr). The cumulative volume of water pumped from the ground-water subbasins between 1958–2001 was 42,210 acre-feet (acre-ft); of this total pumpage, the model simulated that 99 percent (41,930 acre-ft) was removed from ground-water storage.

Introduction

Ground water historically has been the sole source of water supply for the community of Joshua Tree in the Joshua Tree ground-water subbasin of the Morongo ground-water basin in the southern Mojave Desert (fig. 1). The Joshua Basin Water District (JBWD) supplies water to the community from the underlying Joshua Tree ground-water subbasin. The JBWD is concerned with the long-term sustainability of the underlying aquifer. To help meet future demands, the JBWD plans to construct production wells in the adjacent Copper Mountain ground-water subbasin (fig. 1). As growth continues in the desert, there may be a need to import water from outside the Morongo ground-water basin to supplement the available ground-water resources. To manage the ground-water resources and to identify future mitigating measures, a thorough understanding of the ground-water system is needed.

Description of Study Area

The study area is in the southern Mojave Desert approximately 120 miles (mi) east of Los Angeles and includes the community of Joshua Tree (fig. 1). The principal areas of interest for this study are the Joshua Tree and Copper Mountain ground-water subbasins, which cover about 18 and 54 square miles (mi^2), respectively. The Joshua Tree ground-water subbasin is bounded by the Little San Bernardino Mountains to the south, the Yucca Barrier and the Warren ground-water subbasin to the west, the Pinto Mountain Fault to the north, and the Twentynine Palms ground-water subbasin to the east. The Copper Mountain ground-water subbasin lies directly north of the Joshua Tree ground-water subbasin and is separated from the Joshua Tree ground-water subbasin by the Pinto Mountain Fault. The Copper Mountain ground-water subbasin is bounded by the Pinto Mountain Fault to the south, basement-complex highs to the west, Giant Rock ground-water subbasin to the north, and the Copper Mountain Fault and Copper Mountain to the east and northeast.

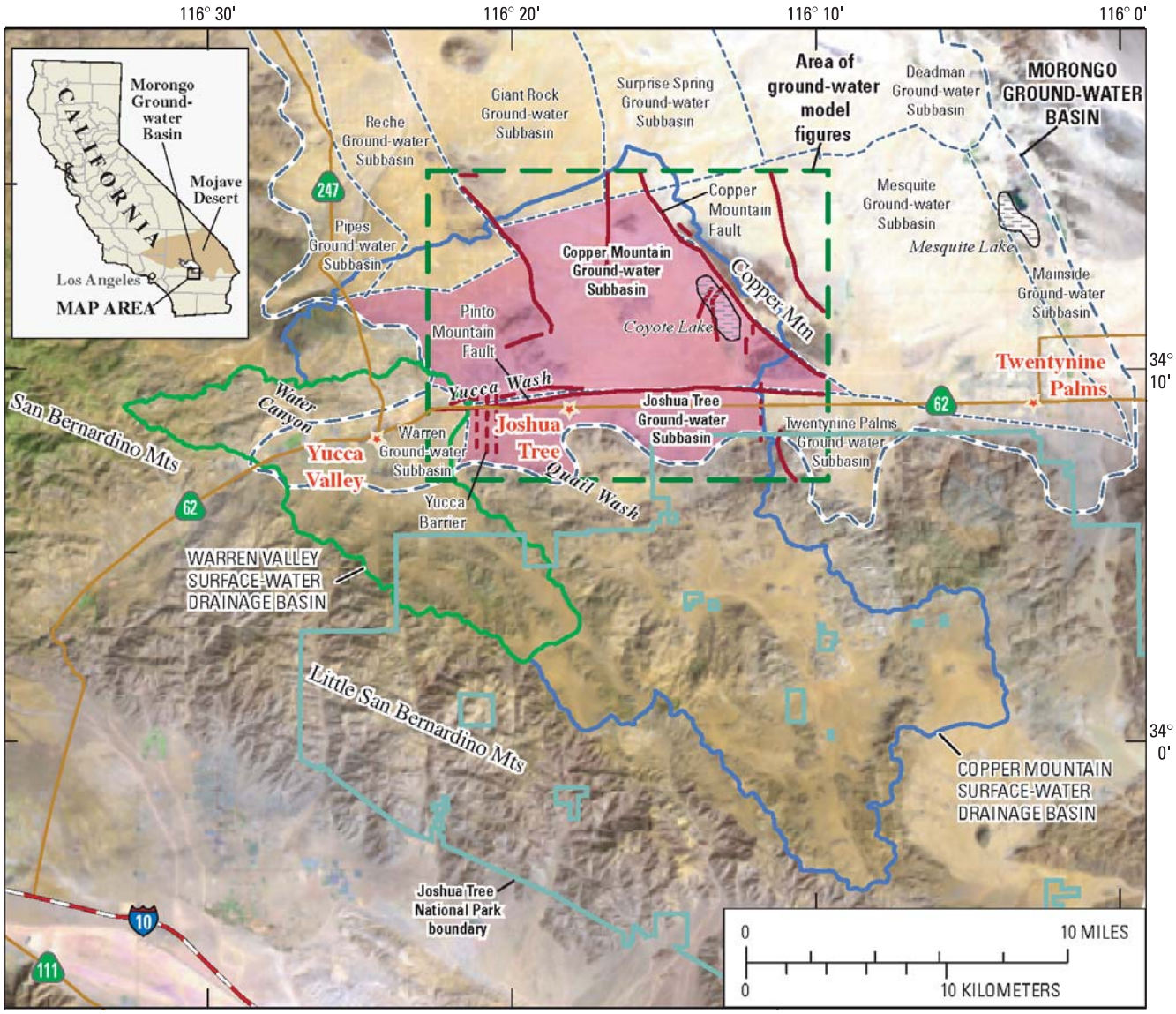

Base from U.S. Geological Survey digital data, 1:100,000, 1981–89; Universal Transverse Mercator Projection, Zone 11. Background image from satellite data compiled by U.S. Geological Survey, Geologic Division, 2000.

Faults modified from Bortugno, 1986.

EXPLANATION

Joshua Tree and Copper Mountain ground-water subbasins

Selected faults—Dashed where approximately located

Cities

Figure 1. Location of study area, Joshua Tree, San Bernardino County, California.

The ground-water subbasins receive surface-water runoff from the Warren Valley and Copper Mountain surface-water drainage basins (fig. 1). These surface-water drainage basins cover a total of about 260 mi^2. A large part of the surface-water drainage area lies within Joshua Tree National Park (fig. 1). The Warren Valley surface-water drainage basin covers 54 mi^2 and discharges into the Copper Mountain surface-water drainage basin. The Copper Mountain surface-water drainage basin covers 203 mi^2 and is a closed basin that discharges into Coyote Lake (dry) (fig. 1). The Warren Valley and Copper Mountain surface-water drainage basins are combined and referred to in this report as the "Joshua Tree surface-water drainage basin." The Joshua Tree surface-water drainage basin includes the areas of the Warren, Joshua Tree, and Copper Mountain ground-water subbasins (fig. 1).

Purpose and Scope

In 2000, the U.S. Geological Survey (USGS) began a cooperative study with JBWD to (1) improve the understanding of the geohydrologic framework of the Joshua Tree and Copper Mountain ground-water subbasins, (2) determine the distribution and quantity of recharge in the subbasins using field and numerical techniques, and (3) develop a ground-water flow model to help manage the water resources of the region. This report presents the results of this cooperative study.

Understanding of the geohydrologic framework was refined by collecting and interpreting water-level and water-quality data, geologic and electric logs, and gravity data. Field studies to determine the distribution and quantity of recharge included installation of instrumented boreholes in selected washes and at a nearby control site. Core material and cuttings from the boreholes were analyzed for physical, chemical, and hydraulic properties. Instruments installed in the boreholes were monitored to measure changes in matric potential and temperature. Borehole data were supplemented with temperature data collected from access tubes installed at additional sites along study washes. Streambed hydraulic properties were measured using infiltrometers. Numerical simulations to determine the distribution and quantity of recharge included applying a distributed-parameter watershed model to estimate spatially and temporally distributed recharge under 1950–2003 climate conditions for the area of the Joshua Tree and Copper Mountain ground-water subbasins and for the areas of the surface-water drainage basins upstream from the subbasins. The 2000–03 simulated recharge was compared with field data obtained during the 2001–03 study period. To better understand the physics and dynamics of ground-water flow in the Joshua Tree and Copper Mountain ground-water subbasins, a numerical flow model of the subbasins was developed. In order to develop the model, a conceptual model of the subbasins first was developed where boundary conditions, parameters, and inflows and outflows were defined. Data collected during the study were used to calibrate the ground-water flow model. A sensitivity analysis was performed and the model limitations discussed.

Definition of the Hydrologic System

The hydrologic system includes the surface-water and ground-water systems. Surface water is affected by climate characteristics, topography, drainage-basin characteristics, and flow characteristics. Ground water is affected by surface-water recharge and by the geology of the aquifers, including stratigraphy, depth-to-basement complex, and faulting.

Climate Characteristics

The climate of the area is typical of the southern Mojave Desert: sunny days, low amounts of rainfall, hot summers, and relatively cool winters. Within the study area, climate varies from arid for the lower altitudes in the area of Coyote Lake to semiarid for the higher altitudes along the Little San Bernardino Mountains. Precipitation primarily occurs as rain, although some snow occurs, especially in the higher altitudes. Precipitation data presented in this section are based on published data (EarthInfo Inc., 2003).

Precipitation data from two National Climatic Data Center (NCDC) climate stations located in the western part of the study area, Kee Ranch in the San Bernardino Mountains (NCDC station code 44467), and Morongo Valley in the Little San Bernardino Mountains (NCDC station code 45863) (fig. 2, table 1), indicate that about 50 percent of the annual precipitation in this mountainous area occurs during winter months (January through March), and about 10 percent occurs during summer months (July through September) (fig. 3). January tends to be the wettest month of the year, with an average monthly precipitation of more than 2 inches (in.) (fig. 3). May and June tend to be the driest months at both sites, with an average monthly precipitation of 0.1 in. or less. Average annual precipitation is 8.32 in. at Kee Ranch and 7.84 in. at Morongo Valley.

A 53-year (1948–2002) record of daily precipitation from the climate station at Twentynine Palms (NCDC station code 49099) (fig. 2, table 1) indicates that the precipitation on the desert floor east of the Warren Valley and Copper Mountain surface-water drainage basins follows a bimodal distribution: about 30 percent of annual precipitation occurs during the winter months and 44 percent occurs during the summer months (fig. 3). July and August tend to be the two wettest months, with an average monthly precipitation of 0.59 in. for July and 0.69 in. for August (fig. 3). June tends to be the driest month, with an average monthly precipitation of 0.01 in. Average annual precipitation at Twentynine Palms is 4.07 in.

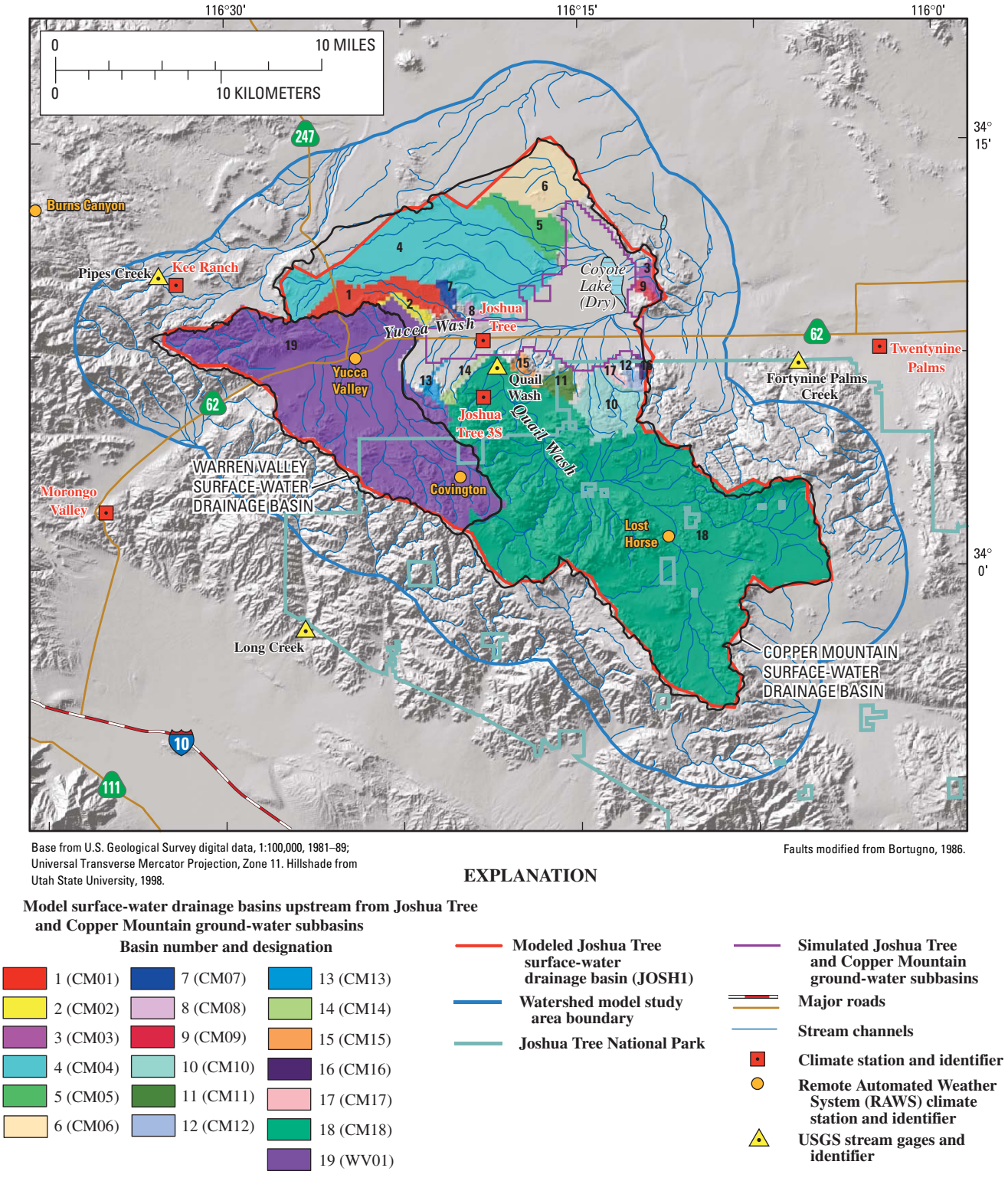

Figure 2. Modeled Joshua Tree surface-water drainage basin area, modeled surface-water drainage basins upstream of Joshua Tree and Copper Mountain ground-water subbasins, and Warren Valley and Copper Mountain surface-water drainage basins, San Bernardino County, California.

Table 1. Summary of daily climate records for six National Weather Service stations in the vicinity of Warren Valley and Copper Mountain surface-water drainage basins, San Bernardino County, California

[—, not available; °F, degrees Farenheit; NCDC, National Climatic Data Center]

	Station name					
	Palm Springs	Twentynine Palms	Joshua Tree	Joshua Tree 3 S	Kee Ranch	Morongo Valley
NCDC station code	46635	49099	44405	44407	44467	45863
Latitude	N33:49:39	N34:07:41	N34:08:00	N34:06:00	N34:10:00	N34:02:00
Longitude	W116:30:35	W116:02:13	W116:19:00	W116:19:00	W116:32:00	W116:35:00
Altitude[1] (feet)	425	1,975	2,723	3,491	4,334	2,562
Record start date	01/01/1927	07/01/1948	06/01/1959	04/01/1974	07/01/1948	10/01/1948
Record end date	12/31/2002	12/31/2002	03/31/1974	06/30/1977	01/31/1979	02/28/1972
Included in climate input	Yes	Yes	Yes	No	Yes	Yes
Subset of record for water years 1947–99						
Daily precipitation data:						
Number of days in record	18,739	18,333	5,233	1,187	9,868	6,713
Number of years in record	51.3	50.2	14.3	3.3	27.0	18.4
Average annual precipitation (inches)	4.99	4.14	4.83	5.26	8.32	7.84
Maximum daily precipitation (inches)	2.80	2.64	1.86	3.30	7.45	4.64
Date of maximum daily precipitation	06/23/1948	09/10/1976	09/17/1963	09/10/1976	02/10/1976	01/26/1969
Daily maximum air temperature data:						
Number of days in record	18,681	18,310				
Number of years in record	51.2	50.1	0	0	0	0
Average daily maximum air temperature (°F)	88.8	84.0	—	—	—	—
Maximum daily air temperature (°F)	123.0	118.0	—	—	—	—
Date of maximum daily air temperature	07/10/1979	07/11/1961	—	—	—	—
Daily minimum air temperature data:						
Number of days in record	18,590	18,316				
Number of years in record	50.9	50.2	0	0	0	0
Average daily minimum air temperature (°F)	57.2	52.0	—	—	—	—
Minimum daily air temperature (°F)	22.0	10.0	—	—	—	—
Date of minimum daily air temperature	01/14/1963	12/23/1990	—	—	—	—

[1]Datum unknown.

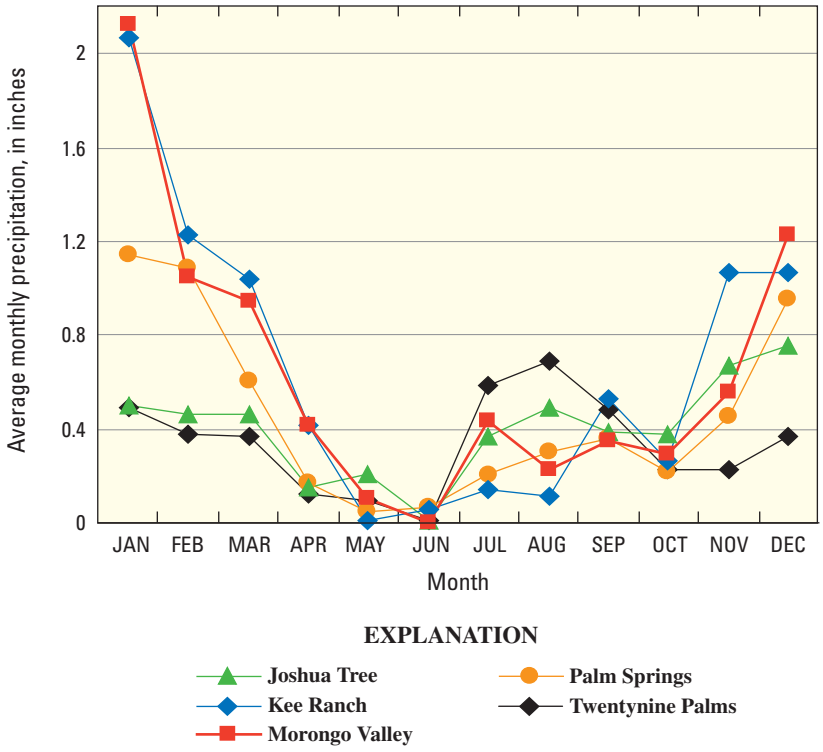

Figure 3. Average monthly precipitation measured at five locations in the vicinity of the Warren Valley and Copper Mountain surface-water drainage basins, San Bernardino County, California.

A 14-year (1959–74) record of daily precipitation from the climate station near the community of Joshua Tree (NCDC station code 44405) (fig. 2, table 1) indicates a less distinct bimodel distribution in comparison with the record at Twentynine Palms (fig. 3). November, December, and January are the three wettest months during the period of record, with an average monthly precipitation of 0.76 in. for December (the wettest month). August is the fourth-wettest month at this site, with an average monthly precipitation of 0.49 in. June is the driest month, with an average monthly precipitation of 0.01 in. Average annual precipitation at the Joshua Tree site is 4.83 in.

The Palm Springs climate station (NCDC station code 46635) is located outside the study area shown in figure 2 in the northwestern part of the Coachella Valley, about 20 mi southwest of the community of Joshua Tree. A 73.5-year (1927–2002) record of daily precipitation from the climate station at Palm Springs (table 1), indicates that December, January, and February tend to be the wettest months at this site (fig. 3). Average monthly precipitation is more than 0.8 in. for each month from December through February. January is the wettest month, with an average monthly precipitation of 1.14 in. May and June are the two driest months, with average monthly precipitation of 0.05 and 0.07 in., respectively. Average annual precipitation at the Palm Springs site is 5.64 in.

Winter (January through March), spring (April through June), and fall (October through December) precipitation primarily results from frontal-type storms moving eastward from the Pacific Ocean (Pyke, 1972). Summer precipitation primarily occurs as isolated convective storms (thunderstorms) or mesoscale convective storm clusters in response to the southwestern summer monsoon (Pyke, 1972). Winter storms tend to be of longer duration (1 or more days) in comparison with summer storms (1 to several hours), whereas summer storms typically generate higher intensity precipitation than do winter storms. Although rare, hurricanes also can affect the Joshua Tree area. Hurricanes tend to occur during the late summer through fall months and usually result in greater precipitation amounts and higher precipitation intensities relative to other storm types.

Most of the precipitation falling in the mountains and on the desert floor is lost through evapotranspiration. The total average potential evapotranspiration rate (or the reference evapotranspiration rate, ET_0, which represents the evapotranspiration rate when the availability of water is not a limiting factor) of the Joshua Tree area is 66.5 inches per year (in/yr) (California Irrigation Management Information System, 2002).

Topography and Drainage Basin Characteristics

The topography of the Joshua Tree surface-water drainage basin varies from the flat, dry lakebed at Coyote Lake and the gently sloping alluvial fans in the lower parts of the Copper Mountain and Warren Valley surface-water drainage basins to the rugged terrain in the higher parts of Joshua Tree National Park and the Little San Bernardino Mountains (fig. 1). Altitudes range from 2,097 ft above sea level (asl) at Coyote Lake to 6,670 ft asl in the Little San Bernardino Mountains. The average altitude for the Copper Mountain surface-water drainage basin is 3,705 ft asl, and the average altitude for the Warren Valley surface-water drainage basin is 3,996 ft asl. Altitudes generally decrease from the Little San Bernardino Mountains in the south and southwestern part of the study area to Coyote Lake dry lakebed in the north and northeastern part of the study area.

The description of the drainage-basin characteristics is based on published textural data (U.S. Department of Agriculture, 1994). The lowest parts of the Copper Mountain and Warren Valley surface-water drainage basins are underlain by thick (more than 100 ft) unconsolidated deposits. Most of the unconsolidated material consists of medium to coarse alluvial fan deposits characterized by a high percentage of sand. The Coyote Lake dry lakebed consists of finer grained lacustrine deposits with higher clay content in comparison with the surrounding alluvial fans. For some locations, finer grained sand and silt have accumulated from aeolian deposition. The upland areas of the drainage basins are characterized by thin soils, and a high percentage of the area is outcropping bedrock. The soils are medium to coarse grained with a high percentage of sand, and the bedrock consists of predominantly low-permeability granitic and metamorphic rocks.

Surface Water

Streamflow in the Joshua Tree surface-water drainage basin is intermittent, and occurs primarily in response to Hortonian overland flow. Hortonian overland flow occurs when the rainfall intensity is greater than the infiltration capacity of the soil (or the infiltration capacity of the bedrock for locations with thin soils) (Chow and others, 1988). The infiltration capacity is a function of the soil or bedrock hydraulic conductivity and the available storage capacity of the soil or bedrock. In contrast to overland flow, streamflow—in response to ground-water discharge—is limited to a few isolated springs in the Joshua Tree surface-water drainage basin. The springs generally are located in the higher altitudes and in the upper parts of the drainage basins. Discharge from many of the springs occurs only during wetter than average conditions. For all locations, spring discharge is not adequate to sustain streamflow but for a short distance downstream from the spring.

The major streams (having intermittent streamflow) in the Joshua Tree surface-water drainage basin discharging into Coyote Lake are Quail Wash in the Copper Mountain surface-water drainage basin and the unnamed wash that enters the Warren Valley surface-water drainage basin from the town of Yucca Valley (fig. 2). For the purposes of this report, this unnamed wash will be referred to as the "Yucca Wash." Quail Wash flows from the southeast to the northwest across the southern part of Copper Mountain basin and is the main tributary of Yucca Wash. The Quail Wash drainage basin (fig. 2, CM18) covers approximately 102 mi^2 (most of which lies within Joshua Tree National Park) and is the largest single drainage basin discharging into Coyote Lake. Yucca Wash drains the Warren Valley surface-water drainage basin and flows north in the upper reaches and then eastward through the town of Joshua Tree before terminating at Coyote Lake. Several unnamed streams discharge into the northern part of Coyote Lake, the largest of which flows from west to east within a drainage basin of approximately 30 mi^2.

Historical records of streamflow are available at four gaging stations in the Joshua Tree study area. The streamflow data can be retrieved from the USGS National Water Information System Web page (NWISweb) located at http://waterdata.usgs.gov/ca/nwis/ using the USGS station numbers given below.

Within the Joshua Tree surface-water drainage basin, streamflow was measured from April 1, 1964, through September 30, 1971, at a gaging station located in the lower part of Quail Wash (USGS station number 10253320), approximately 1.5 mi upstream from the juncture of Quail Wash with Yucca Wash (fig. 2; table 2). In the 2,759 days of record, only 7 days had measurable streamflow at the gaging station: 4 days in August, 1 day in July, 1 day in October, and 1 day in January. No measurable streamflow occurred during water years 1964–66. The wettest recorded water year was 1970, with 3 days of measurable streamflow and a total discharge of 7.3 acre-ft. A maximum daily mean discharge of 1.8 cubic feet per second (ft^3/s) was measured on August 26, 1970. Total discharge for the period of record was 9 acre-ft, with 8.3 acre-ft occurring during the summer months (July through September) and 0.7 acre-ft occurring during the remaining months.

Historical records of streamflow are available for three gaging stations located adjacent to the Joshua Tree surface-water drainage basin at: Pipes Creek (USGS station number 10260200), Long Creek (USGS station number 10257800), and Fortynine Palms Creek (USGS station number 10253350) (fig. 2, table 2). Streamflow was measured at Pipes Creek, adjacent to the western boundary of the Joshua Tree surface-water drainage basin, from September 1, 1958, through September 30, 1971. The maximum daily mean discharge was 53 ft^3/s on February 25, 1969. The average discharge rate for the period of record is 0.03 ft^3/s (20 acre-ft/yr). Streamflow was measured at Long Creek from May 1, 1963, through September 30, 1971. The maximum daily mean discharge was 340 ft^3/s on August 7, 1963. The average discharge rate for the period of record is 0.11 ft^3/s (79.7 acre-ft/yr). Streamflow was measured at Fortynine Palms Creek from October 1, 1962, through September 30, 1971. The maximum daily mean discharge was 69 ft^3/s on October 18, 1963. The average discharge rate for the period of record is 0.10 ft^3/s (74 acre-ft/yr).

Streamflow records for the Fortynine Palms and Longs Creek gaging stations indicate intermittent occurrences of streamflow in direct response to storms similar to conditions recorded at the Quail Wash gaging site. The duration of streamflow in response to the storms is only 1 to 2 days. Although the record for the Pipes Creek gage also indicates intermittent streamflow, the record includes the occurrence of longer duration streamflow during the period of February 24, 1969, through May 31, 1969. The average discharge rate for this period was 0.95 ft^3/s with a maximum daily mean discharge of 53 ft^3/s. Unlike the streamflow characteristic for Quail Wash, this relatively long period of sustained streamflow at the Pipes Creek gage was likely caused by the wetter than normal conditions for the higher altitudes in the upstream sections of the Pipes Creek drainage basin, where releases from streambank storage, saturated bedrock fractures, saturated conditions along the alluvium bedrock contact, and possibly snowmelt may have contributed to the sustained streamflow.

Ground-Water Hydrology

The geohydrology of the Joshua Tree and Copper Mountain ground-water subbasins was defined by summarizing previously published research [for example, Dibblee (1967) and Lewis (1972)], completing a gravity survey, and collecting geologic and hydrologic data from new and existing wells. The available well-construction data for wells used in this report are presented in table 3.

Geology

The geology of the study area was defined by compilation of information on the stratigraphy, depth-to-basement complex, and faulting.

Table 2. Gaged drainage basins and streamflow records, Warren Valley and Copper Mountain surface-water drainage basins, San Bernardino County, California

[mi^2, square miles; ft, feet; acre-ft/yr, acre-feet per year]

Station name	Station No.	Latitude	Longitude	Alititude (ft above NGVD 29)	Drainage basin area (mi^2)	Start of record	End of record	Average annual discharge (acre-ft/yr)	Modeled drainage basin area (mi^2)
Quail Wash Near Joshua Tree	10253320	N34:07:04	W116:18:27	2,917	100.00	04/01/1964	09/30/1971	1.2	95.88
Fortynine Palms Creek Near Twentynine Palms	10253350	N34:07:12	W116:05:43	2,315	8.55	10/01/1962	09/30/1971	74.3	7.84
Long Creek Near Desert Hot Springs	10257800	N33:57:53	W116:26:35	1,560	19.60	05/01/1963	09/30/1971	79.7	19.00
Pipes Creek Near Yucca Valley	10260200	N34:10:19	W116:32:45	4,440	15.10	09/01/1958	09/30/1971	20.0	15.16

Table 3. Well construction for selected wells, Joshua Tree and Copper Mountain ground-water subbasins, San Bernardino County, California

[ft, feet; asl, above sea level; LSD, land surface datum]

State well No.	Local ID	Year drilled	LSD (ft asl)	Hole depth (ft)	Well depth (ft)	Well screen top (ft)	Well screen bottom (ft)
1N/6E-13R1	Las Casitas	1956	2,650	715	710	455	470
						674	710
1N/6E-25K1	Lacy Richardson	1957	2,700	562	552	427	552
1N/6E-25K2	JBWD #11	1975	2,705	740	740	450	740
1N/6E-25M1	JT Serv Co #1 (JBWD #1)	1936	2,714	512	500	440	500
1N/6E-25M2	JBWD #2	1961	2,723.9	500	500	200	500
1N/6E-25M3	JBWD #10	1968	2,720	704	704	452	704
1N/6E-25M4	JBWD #3	Unknown	2,720	Unknown	Unknown	Unknown	Unknown
1N/6E-26N1	Lee & Wikoff	1949	2,853	610	610	545	610
1N/6E-34D3	Cemetery #1	1999	3,030	1,000	999	979	999
1N/6E-34D4	Cemetery #2	1999	3,030	1,000	920	900	920
1N/6E-34D5	Cemetery #3	1999	3,030	1,000	820	780	820
1N/6E-35C1	Lloyd land	1951	2,830	630	630	518	630
1N/7E-3D2	unknown	Unknown	2,480	Unknown	Unknown	240	330
1N/7E-4R1	Bratmon	1955	2,407	337	330	240	330
1N/7E-10D1	Robinson	1952	2,394	264	264	240	264
1N/7E-10N1	Reagan	1949	2,385	267	267	240	267
1N/7E-14N1	Peters	1943	2,363	450	450	386	425
1N/7E-16P1	Lanfair Water (Peterman)	1947	2,437	360	360	264	360
1N/7E-16P2	JBWD #12	1952	2,440	328	324	264	324
1N/7E-20P1	JBWD #9	1956	2,550.5	494	494	366	494
1N/7E-20P2	JBWD #15	2001	2,550	752	750	380	490
						560	700
						720	730
1N/7E-20Q1	LaFerney	Unknown	2,553	400	400	380	400
1N/7E-20Q2	Rumsy	1963	2,554	508	505	400	505
1N/7E-21H1	JBWD #16	2001	2,430	1,013	860	360	410
						540	640
						680	850
1N/7E-21J1			2,446			250	300
1N/7E-21Q1	Zastrow	Unknown	2,463	300	300	250	300
1N/7E-22D1	test hole #2	1971	2,405	750	506	464	506
1N/7E-22E1	Peterman	1946	2,428			105	251
1N/7E-22J1	Fjell	1961	2,388	416	395	230	250
						325	395
1N/7E-22L1	Webb	Unknown	2,411	251	251	105	251
1N/7E-22L2	Webb	1963	2,411	393	390	241	387
1N/7E-23A1	County Park #1	1970	2,376	380	370	360	370
1N/7E-23A2	County Park #2	1968	2,373	380	370	360	370

Table 3. Well construction for selected wells, Joshua Tree and Copper Mountain ground-water subbasins, San Bernardino County, California—Continued

State well No.	Local ID	Year drilled	LSD (ft asl)	Hole depth (ft)	Well depth (ft)	Well screen top (ft)	Well screen bottom (ft)
1N/7E-23N1	Lovegren	1955	2,383	230	230	170	230
1N/7E-23P1	Hallstead	1947	2,382	429	429	205	429
1N/7E-25E1	Brooks	1956	2,296	250	245	175	245
1N/7E-25E2	Giannelli	1959	2,308	294	194	254	294
1N/7E-26D1	Evans	~1946	2,388	250	250	170	250
1N/7E-26J1	College of Desert	1980	2,510	405	401	277	401
1N/7E-26N1	Rollard	1946	2,475	208	200	175	200
1N/7E-26P1	Akkerman	1949	2,463	210	210	160	210
1N/7E-26R1	Fergurson	Unknown	2,493	268	268	218	268
1N/7E-27D1	Cutler	1949	2,438	305	305	265	305
1N/7E-27E1	Beaumont	1958	2,448	220	215	165	215
1N/7E-28P1	Paul	Unknown	2,493	238	238	195	238
1N/7E-28Q1	JBWD #8	1947	2,483	412	412	180	412
1N/7E-28R1	Ray	1929	2,492	262	262	190	262
1N/7E-28R2	Stanlind	1957	2,464.6	262	262	5	75
1N/7E-29Q1	Solk	1961	2,553	333.5	257	5	257
1N/7E-30K1	JBWD #14	1982	2,625	740	740	470	720
1N/7E-30P1	Leach	1952	2,668	430	424	370	424
1N/7E-32C1	Thurlow	1952	2,610	392	385	320	385
1N/7E-33B1	Thompson	1952	2,543	292	287	240	287
1N/7E-33B2	Glass	1958	2,533	314	314	254	304
1N/7E-33C1	Hall	Unknown	2,543	Unknown	Unknown	240	287
1N/7E-34B1	Test hole #1	1971	2,489	785	590	527	590
1N/7E-34D1	Webster	1962	2,546.5	396	391	261	391
1N/7E-35D1	JBWD #13	1951	2,485	256	246	156	246
2N/7E-20Q1	Surprise Spring WA	1970	2,643	651	640	495	620

Stratigraphic Units

For this report, the geologic units compiled by Bedford and Miller (1997) were grouped into three generalized stratigraphic units: (1) a basement complex of pre-Tertiary granitic and metamorphic rocks (Kg, Jg, TRg, ZXsg, Xg, and Xm), (2) Tertiary sedimentary and volcanic deposits (Tsy and Tvy), and (3) Quaternary alluvial deposits (Qsu and Qp) (fig. 4*A*). The definitions of the stratigraphic units were based on analyses of drillers' logs and geophysical data; these data are on file at the USGS office in San Diego, California.

The pre-Tertiary basement complex underlies the Joshua Tree and Copper Mountain ground-water subbasins and crops out in the surrounding hills (fig. 4*A–B*). Except for small quantities of water in the fractures and weathered zones in this stratigraphic unit, the basement complex is not a major water-bearing unit.

Tertiary, sedimentary, and volcanic deposits overlie the basement complex throughout most of the study area. This stratigraphic unit consists primarily of partly consolidated alluvial deposits, which contain granitic and gneissic clasts derived from the surrounding bedrock, and probably yields only small quantities of water to wells. The volcanic deposits crop out in the northwestern part of the study area (fig. 4*A*). On the basis of drillers' logs and geophysical data, this stratigraphic unit reaches a maximum thickness of about 2,000 ft and is much less permeable than are the overlying alluvial fan deposits and alluvium.

Quaternary alluvial deposits overlie the Tertiary sedimentary and volcanic deposits and the pre-Tertiary basement complex throughout much of the basin (fig. 4*A–B*). On the basis of drillers' logs and geophysical data, this stratigraphic unit ranges in thickness from a few feet along the boundary of the basin to more than 1,000 ft near the center of the Joshua Tree ground-water subbasin. These deposits consist predominantly of poorly sorted sand and gravel with interbedded layers of silt and clay. The alluvial deposits are unconsolidated at land surface and become slightly more consolidated at depth. The most permeable alluvial deposits lie beneath the active washes in the subbasins. These permeable deposits range from about 0 to 100 ft in thickness and lie within the unsaturated zone. The dry-lakebed deposits (Qp) are found primarily at Coyote Lake in the Copper Mountain surface-water drainage basin (fig. 4*A*).

Depth to Basement Complex

The total thickness of the unconsolidated deposits in the Joshua Tree ground-water subbasin is unknown; however, several production wells were drilled to depths in excess of 800 ft below land surface (bls) without encountering bedrock. The total thickness of the unconsolidated deposits in the Copper Mountain ground-water subbasin is not thoroughly defined, but wells were drilled in the unconsolidated deposits in the subbasin to depths ranging from 230 to 750 ft.

A gravity survey was used to understand the three-dimensional structure and estimate the depth to basement complex (thickness of the basin fill) of the Morongo ground-water basin (Roberts and others, 2002). However, only a few wells penetrate the basement complex; therefore, there were few data to constrain the interpretation of the gravity data. Roberts and others (2002) developed four different basin-thickness models assuming various density profiles. For this study, the results from model 3 of Roberts and others (2002) were used because the results were deemed to be the most reasonable in terms of agreeing with existing well data.

In the Joshua Tree ground-water subbasin, the results from model 3 of Roberts and others (2002) indicate an east-west linear basin parallel to the Pinto Mountain Fault. The maximum thickness of the Joshua Tree ground-water subbasin may be greater than 4,500 ft in two locations east of the community of Joshua Tree (fig. 5). In the Copper Mountain ground-water subbasin, the gravity data indicate a north-south trending basin perpendicular to the Pinto Mountain Fault. The maximum thickness of the Copper Mountain ground-water subbasin may be greater than 2,000 ft beneath Coyote Lake (fig. 5).

The extent of each ground-water subbasin was determined by intersecting the 1998 water-table altitude with the depth-to-basement-complex estimates of Roberts and others (2002). These results indicate that the area of the Joshua Tree ground-water subbasin is about 12.4 mi^2 and that the area of the Copper Mountain ground-water subbasin is about 13.4 mi^2, which is about 0.6 mi^2 less than the surface area of the unconsolidated deposits estimated by Lewis (1972) (14 mi^2).

Faults and Ground-Water Barriers

The most prominent fault in the study area is the Pinto Mountain Fault, which trends east–west (fig. 4*B*) and separates the Joshua Tree ground-water subbasin from the Copper Mountain ground-water subbasin. The Pinto Mountain Fault has either juxtaposed the pre-Tertiary basement complex against unconsolidated alluvial deposits or displaced preferential flow paths in unconsolidated alluvial deposits. This juxtaposition and displacement, along with cementation, compaction, and extreme deformation of the water-bearing deposits adjacent to faults, can create low-permeability zones that can act as barriers to ground-water flow. The Pinto Mountain Fault is a barrier to flow as evidenced by water levels that are 100 to 70 ft higher in the Joshua Tree ground-water subbasin than water levels in the Copper Mountain ground-water subbasin (Lewis, 1972).

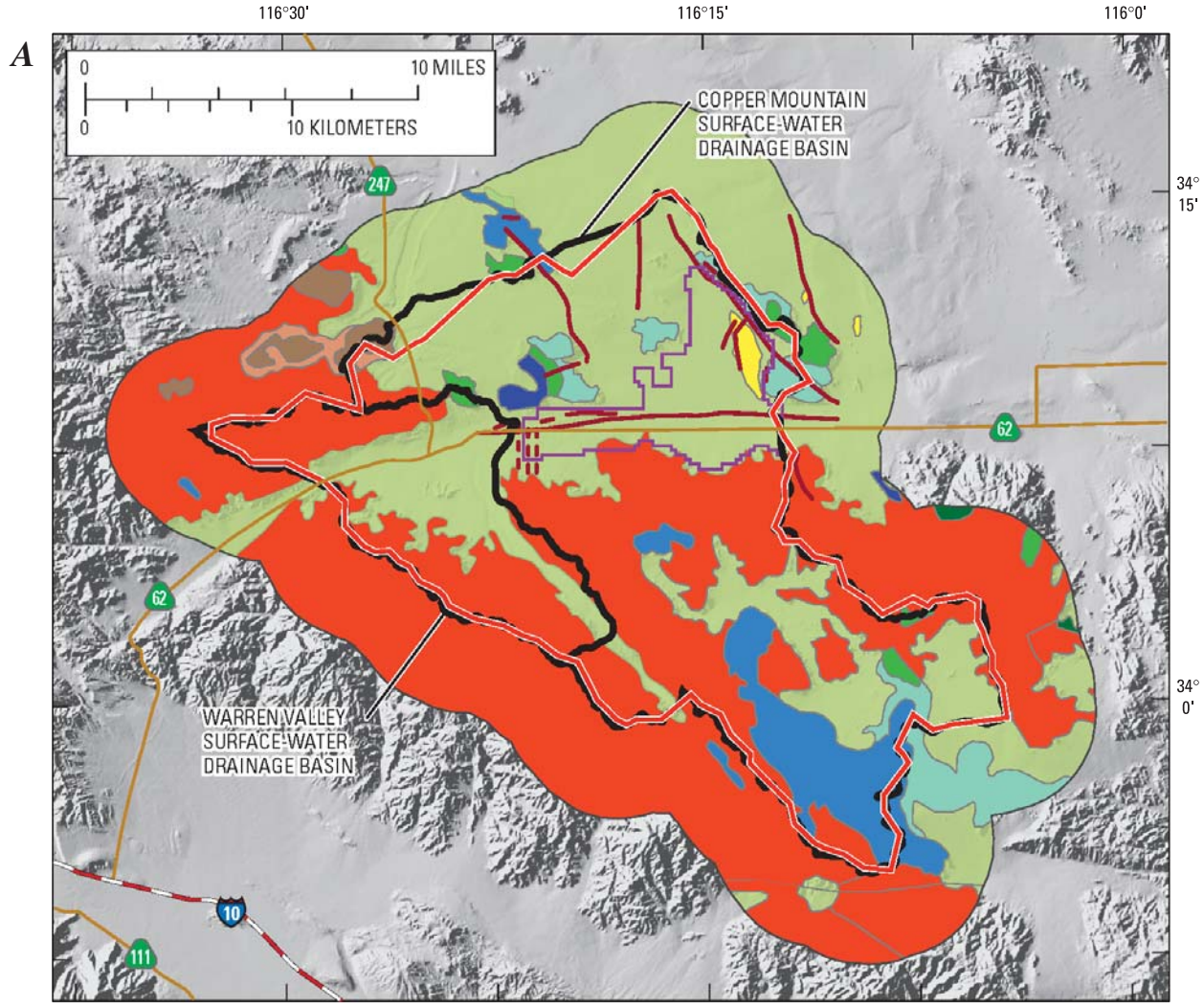

Base from U.S. Geological Survey digital data, 1:100,000, 1981–89; Universal Transverse Mercator Projection, Zone 11. Hillshade from Utah State University, 1998.

Geology from Utah State University, 1998. Faults modified from Bortugno, 1986.

EXPLANATION

Mojave regional geology map code (type-age)

Quaternary alluvial deposits

- Qsu — (Undifferentiated surface deposits-Quaternary/Pliocene)
- Qp — (Playa deposits-Quaternary/Pliocene)

Tertiary sedimentary and volcanic deposits

- Tsy — (Young sedimentary rocks-Late to Middle Pliocene)
- Tvy — (Volcanic rocks-Late to Middle Pliocene)

Pre-Tertiary basement complex

- Kg — (Granitoid rocks-Cretaceous)
- Jg — (Granitoid rocks-Jurassic)
- TRg — (Granitoid rocks-Triassic)
- ZXsg — (Sedimentary rocks and gneiss-Precambrian)
- Xg — (Granitoid rocks-Precambrian)
- Xm — (Metamorphic rocks-Precambrian)

- **Major roads**
- **Modeled Joshua Tree and Copper Mountain ground-water subbasins**
- **Modeled Joshua Tree surface-water drainage basin (JOSH1)**
- **Selected faults**—Dashed where approximately located

Figure 4. (*A*) geologic map of Warren Valley and Copper Mountain surface-water drainage basins and (*B*) generalized surficial geology, major faults, traces of geologic sections, and location of wells shown on geologic sections for the Joshua Tree and Copper Mountain ground-water subbasins, San Bernardino County, California.

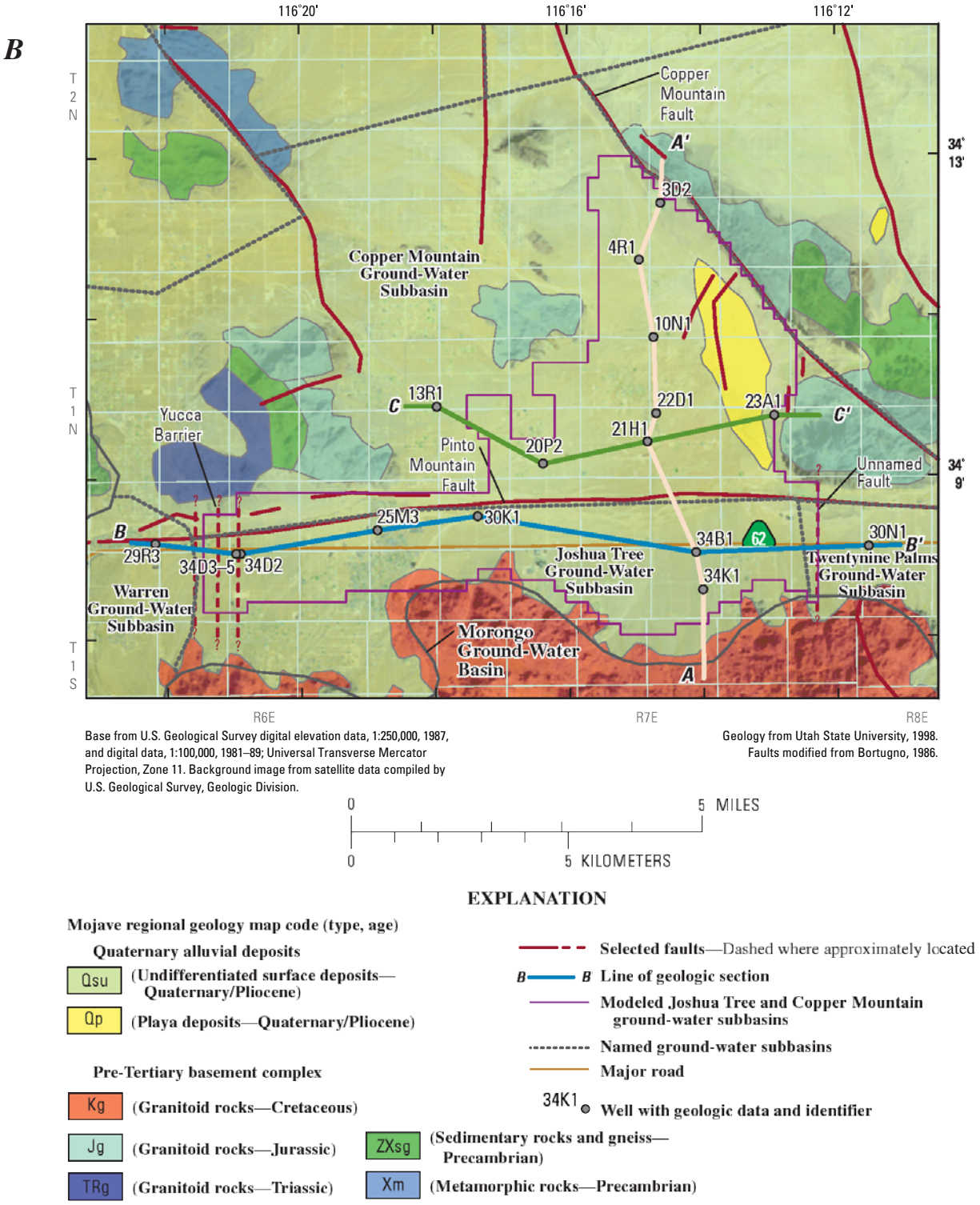

Figure 4.—Continued.

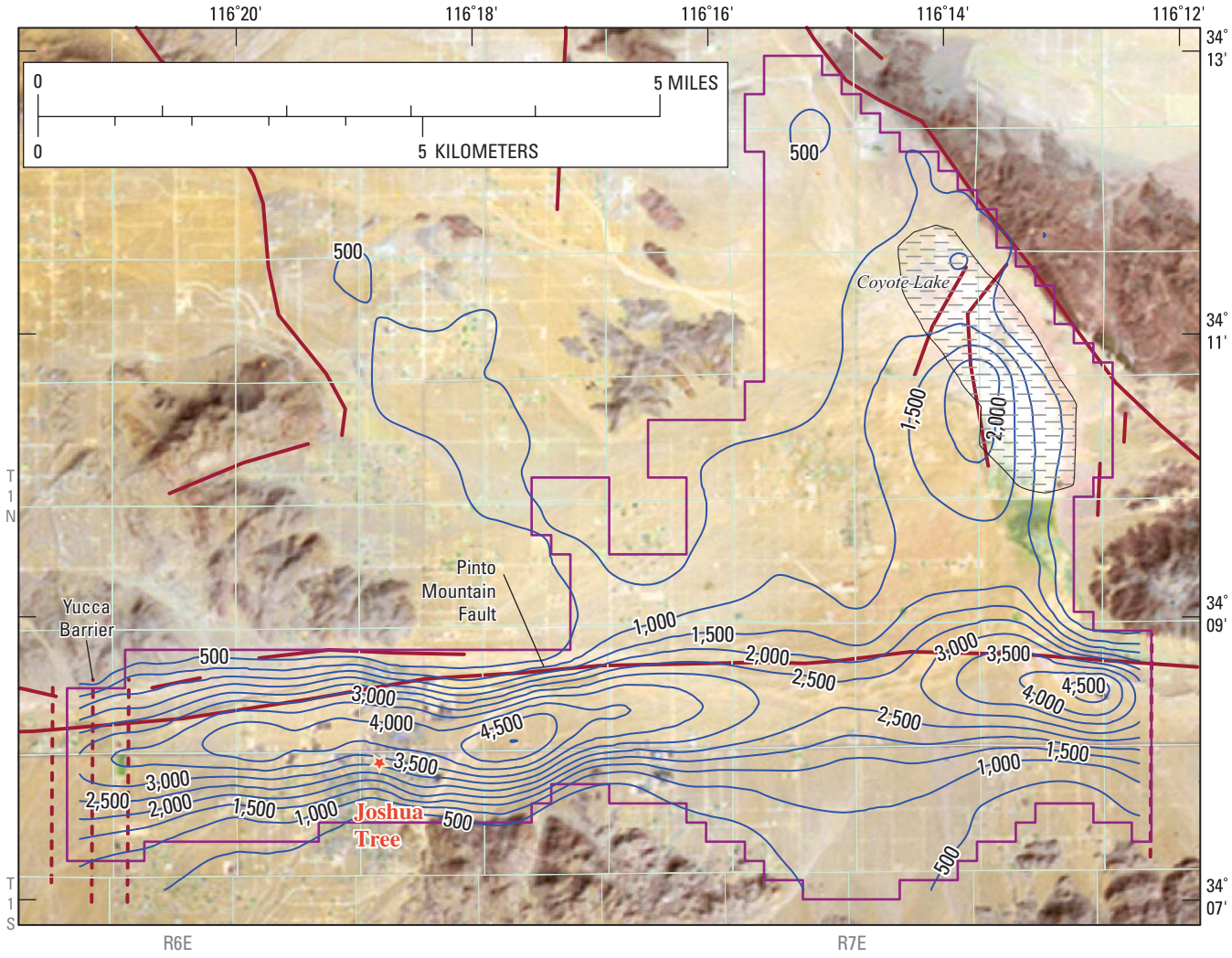

Base from U.S. Geological Survey, digital data, 1:100,000, 1981–89; Universal Transverse Mercator Projection, Zone 11. Background image from satellite data compiled by U.S. Geological Survey, Geologic Division, 2000.

Faults modified from Bortugno, 1986.

EXPLANATION

Line of equal depth to pre-Tertiary basement complex. Contour interval is 500 feet

Selected fault—Dashed where approximately located

Modeled Joshua Tree and Copper Mountain ground-water subbasins

Figure 5. Thickness of water-bearing units based on gravity data, Joshua Tree and Copper Mountain ground-water subbasins, San Bernardino County, California.

Lewis (1972) identified the Yucca Barrier as the boundary between the Warren and Joshua Tree ground-water subbasins (fig. 4*B*). The barrier was located on the basis of water-level data; water levels on the east side of the Yucca Barrier are as much as 400 ft lower than water levels on the west side (Lewis, 1972). Water-level data collected for this study indicate that the barrier may comprise several parallel unnamed north-south trending faults. It was inferred that one of these unnamed faults is located between monitoring wells 1N/6E-34D5 and 1N/6E-34D2 (dry) (fig. 4*B*) because the water-level altitude measured at 34D5 is 80 ft higher than the altitude of the bottom of well 34D2.

An unnamed fault separates the Joshua Tree ground-water subbasin from the Twentynine Palms ground-water subbasin (fig. 4*B*). It was inferred that this unnamed fault is located between monitoring wells 1N/7E-34B1 and 1N/8E-30N1(fig. 4*B*) because the water-level altitude measured at 34B1 was 91 ft higher than measured water levels at well 30N1 in 1994 (Trayler and Koczot, 1995) and in 1996 (Mendez and Christensen, 1997).

The eastern boundary of the Copper Mountain ground-water subbasin is the Copper Mountain Fault. In addition, there are two unnamed mapped faults in the vicinity of Coyote Lake; there are no water-level data to determine if these faults are barriers to ground-water flow. Other faults may be present in the Joshua Tree and Copper Mountain ground-water subbasins; however, they have not been defined by geologic mapping or water-level data.

Definition of Aquifer System

The water-bearing deposits in the Joshua Tree and Copper Mountain ground-water subbasins comprise the Quarternary alluvial deposits and the Tertiary sedimentary and volcanic deposits. On the basis of lithologic and downhole geophysical logs, the Quarternary alluvial deposits were divided into two aquifers (referred to as the “upper” and the “middle” aquifers) and the Tertiary sedimentary and volcanic deposits were assigned to a single aquifer (referred to as the “lower” aquifer). Transmissivity estimates reported in this section are based on specific-capacity tests reported in drillers’ logs and performed by Southern California Edison, and pumping tests performed for JBWD; these data are on file at the USGS office in San Diego, California.

The upper and middle aquifers constitute the saturated part of the Quaternary alluvial deposits. The upper aquifer is mainly sand and gravel as indicated by drillers’ logs and downhole geophysical logs. The thickness of this aquifer ranges from about 300 ft in the Joshua Tree ground-water subbasin to less than 175 ft in the Copper Mountain ground-water subbasin (fig. 6). Most of the production wells are perforated in the upper aquifer only. Estimates of transmissivity, based on specific capacity and pumping test data, range from about 580 to 55,580 square feet per day (ft^2/d), measured at 1N/7E-20P1 and 1N/6E-25K2, respectively. There were nine wells perforated solely in the upper aquifer that had associated estimated transmissivity values, and the mean transmissivity equalled 6,183 ft^2/d. Lewis (1972) estimated that the specific yield of the saturated deposits is 15 percent in the Joshua Tree ground-water subbasin and 14 percent in the Copper Mountain ground-water subbasin by inspecting geologic logs from wells in each subbasin.

The middle aquifer is mainly sand, silt, and clay with occasional gravel layers, and it is more indurated than is the upper aquifer. The middle aquifer is about 450 ft thick. Downhole geophysical logs are less resistive opposite the middle aquifer than opposite the upper aquifer, suggesting higher percentages of silt and clay. No production wells are perforated solely opposite the middle aquifer. Based on specific capacity and pumping test data from a production well in the Joshua Tree ground-water subbasin and two recently completed production wells in the Copper Mountain ground-water subbasin that are perforated in the upper and middle aquifers, estimates of transmissivity were about 38,000, 48,000, and 98,000 ft^2/d at 1N/7E-30K1, 1N/7E-21H1, and 1N/7E-20P2, respectively.

The lower aquifer is contained within the Tertiary sedimentary and volcanic deposits and is as much as 1,500 ft thick. The aquifer mainly consists of partly consolidated fanglomerates, and the downhole geophysical logs indicate very low resistivity. There are no production wells perforated in the deep aquifer. Nishikawa and others (2003) estimated that the Tertiary deposits have a hydraulic conductivity of 0.5 ft/d in the nearby Warren ground-water subbasin. Assuming that this value is representative of the Tertiary deposits in the Joshua Tree and Copper Mountain ground-water subbasins, the maximum transmissivity would be about 750 ft^2/d.

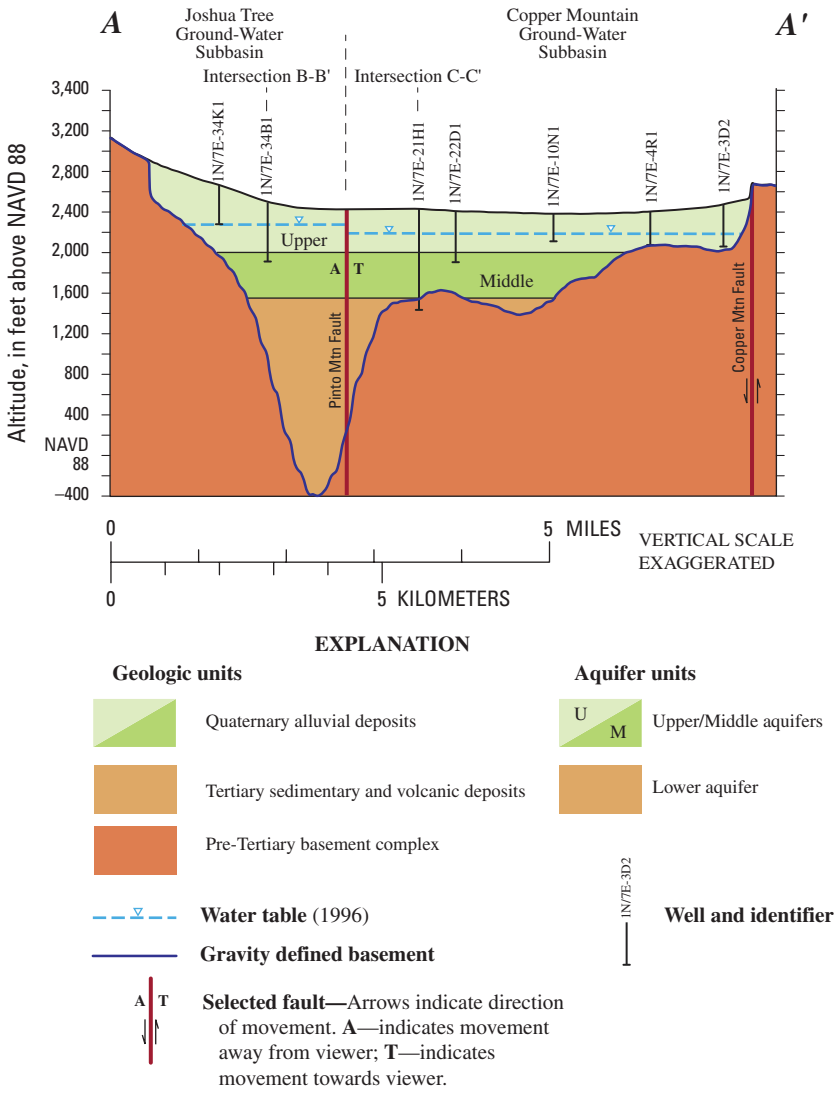

Figure 6. Locations and depths of production and monitoring wells and the upper, middle, and lower aquifer systems of the Joshua Tree and Copper Mountain ground-water subbasins, San Bernardino County, California.

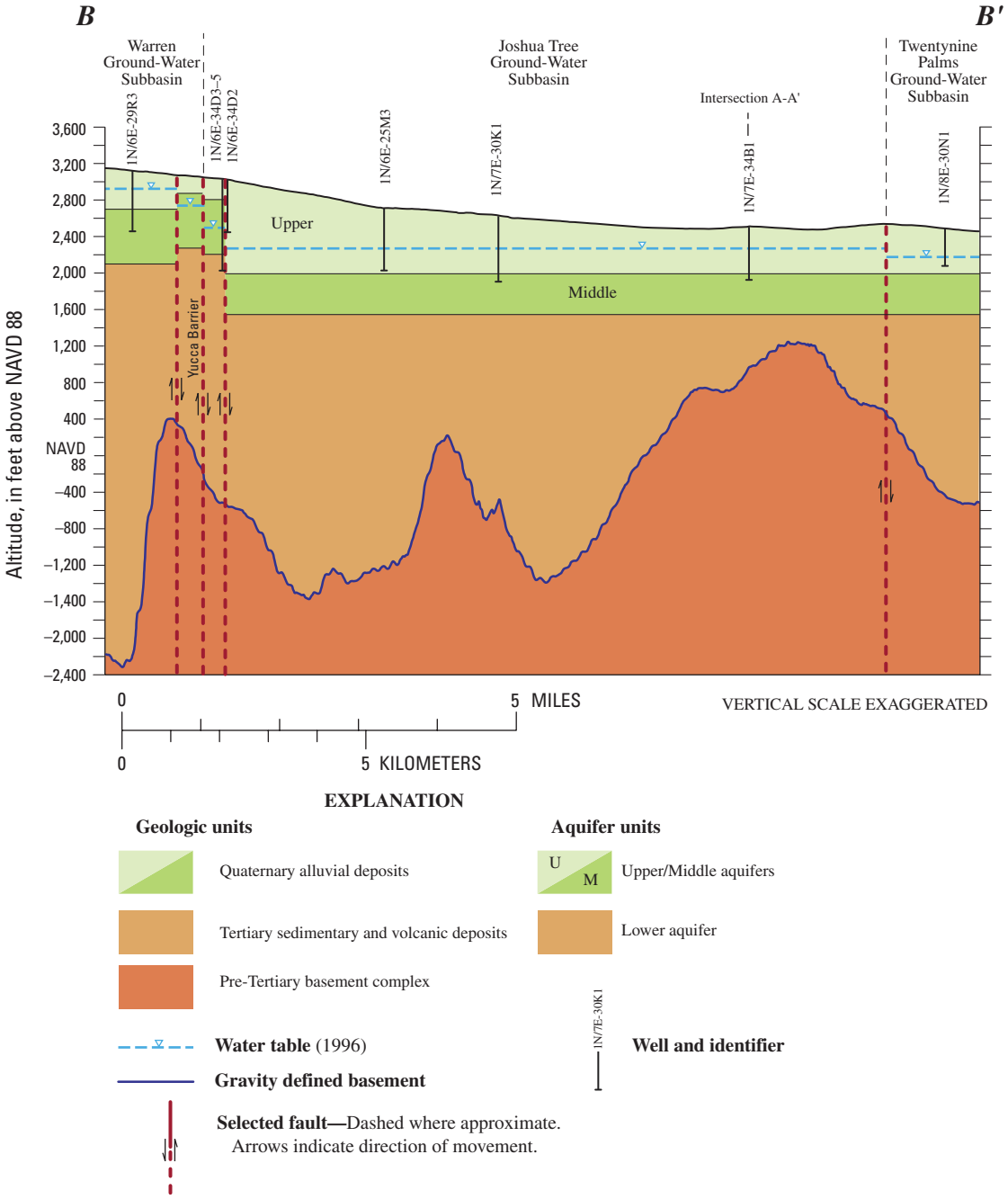

Figure 6.—Continued.

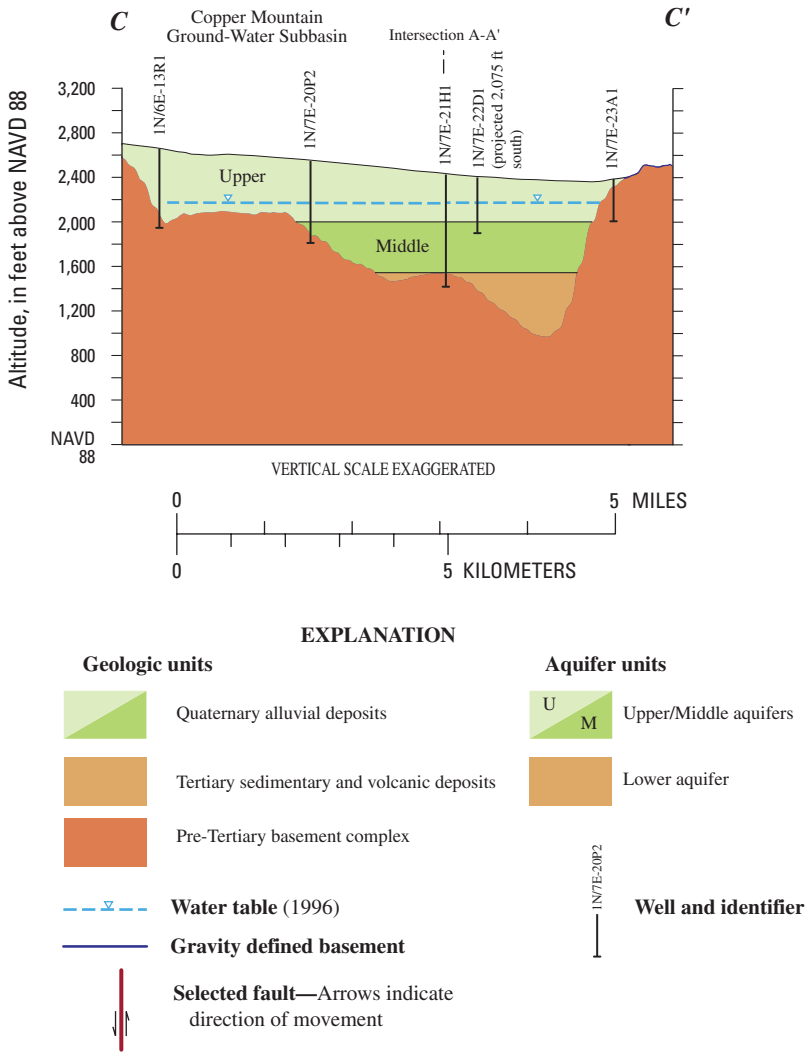

Figure 6.—Continued.

Ground-Water Recharge and Discharge

The principal sources of recharge to the Joshua Tree ground-water subbasin are runoff of precipitation from the Little San Bernardino Mountains to the south and ground-water underflow from the neighboring Warren Valley ground-water subbasin. Infiltration of precipitation runoff in stream channels and through fractures in the bedrock is the principal pathway for recharge to the Joshua Tree ground-water subbasin (Lewis, 1972). Whitt and Jonker (1998) estimated that the annual recharge from precipitation to the Joshua Tree ground-water subbasin was 975 acre-ft, on the basis of a percentage (2.8 to 5 percent) of the total precipitation (assumed 4.65 in. or 0.39 ft) falling on the Quail Springs watershed. The USGS used field and numerical techniques as part of this study to better estimate natural recharge owing to the infiltration of precipitation. Lewis (1972) estimated that less than 200 acre-ft/yr, and Nishikawa and others (2003) estimated about 85 acre-ft/yr of underflow entered the Joshua Tree ground-water subbasin from the Warren Valley ground-water subbasin.

The principal sources of recharge to the Copper Mountain ground-water subbasin are ground-water underflow and runoff of precipitation. Under predevelopment conditions, ground-water discharge from the Joshua Tree ground-water subbasin occurs as underflow across the Pinto Mountain Fault into the Copper Mountain ground-water subbasin. Lewis (1972) speculated that this underflow is the primary source of recharge to the Copper Mountain ground-water subbasin and that underflow from the Giant Rock ground-water subbasin to the northwest is a minor source of recharge. Whitt and Jonker (1998) estimated that the annual recharge from precipitation to the Copper Mountain ground-water subbasin was 728 to 1,300 acre-ft on the basis of a percentage (2.8 to 5 percent) of the total precipitation (assumed 4.65 in. or 0.39 ft) falling on watersheds that surround the ground-water subbasin.

In addition to ground-water discharge into the Copper Mountain ground-water subbasin, ground water may also discharge from the Joshua Tree ground-water subbasin into the Twentynine Palms ground-water subbasin. However, the unnamed fault between the Joshua Tree and Twentynine Palms ground-water subbasins appears to restrict flow between the subbasins.

Lewis (1972) noted that some natural ground-water discharge from the Copper Mountain ground-water subbasin may occur through a narrow gap between the Pinto Mountain Fault and Copper Mountain (fig. 4*B*); however, this could not be verified from available data. Ground-water discharge by evapotranspiration from the Coyote Lake dry lakebed is unlikely, even under undeveloped conditions, because water levels were more than 200 ft bls. Lewis (1972) estimated that the total pumpage from the Copper Mountain subbasin did not exceed 25 acre-ft/yr in 1970. Ground-water underflow into the Surprise Spring ground-water subbasin may occur between the Copper Mountain Fault and an unnamed fault to the west (fig. 4*B*).

Under present conditions, pumping of ground water by JBWD for domestic and commercial use is the main discharge from the Joshua Tree ground-water subbasin. The location of the production wells is shown in figure 7A. Total ground-water production by JBWD from 1958 to 2001 was about 42,000 acre-ft. The total annual pumpage increased from about 135 acre-ft/yr in 1958 to a maximum of about 1,700 acre-ft/yr in 1990 (fig. 8).

Septic tanks are the primary form of wastewater treatment in the Joshua Tree ground-water subbasin; therefore, septage maybe a source of ground-water recharge. Assuming that pumpage in the winter months (December–March) is representative of the average pumping and assuming that 73 percent [70 gal/capita-day septage (Eckenfelder, 1980) and 96 gal/capita-day water usage (total of 1,076 acre-ft/yr of water pumped in winter 2001, about 10,000 users in 2004 (Marina West, Joshua Tree Water District, written commun., 2004))] of the pumped ground water is returned by way of septage, then the average potential recharge flux from 1977 to 2001 is about 660 acre-ft/yr. This rate is an overestimation because some of the septic systems are located outside of the ground-water basins. Umari and others (1995) reported that the vertical rate of a wastewater wetting front at sites in Victorville, California (located in the Mojave Desert about 60 mi northwest of the study area), ranged from 0.07 to 1 ft/d, with the higher value in the upper part of the unsaturated zone. Assuming that these values represent travel times in the Joshua Tree ground-water subbasin and that the thickness of the unsaturated zone was about 500 ft in 1994, a travel time of 1.4 to 20 years would be required for the septage to reach the water table.

Ground-Water Levels and Movement

1996 water-level measurements and water-level measurements from other years (1958–2002) were compiled to develop water-level contours representing 1996 conditions (fig. 9). Water levels ranged from about 2,510 ft asl on the west side of the inferred north-south trending fault east of the Yucca Barrier to about 2,280 ft asl in the remainder of the Joshua Tree ground-water subbasin. On the eastern side of the Joshua Tree ground-water subbasin, water levels were about 90 ft higher than at wells in the western part of the Twentynine Palms ground-water subbasin (fig. 9). Water levels ranged from about 2,180 to 2,170 ft asl in the Copper Mountain ground-water subbasin. The contours indicate that water enters the Joshua Tree ground-water subbasin along the Little San Bernardino Mountains, flows north across the Pinto Mountain Fault, flows through the Copper Mountain ground-water subbasin, and exits the Copper Mountain ground-water subbasin north of Copper Mountain into the Surprise Spring ground-water subbasin.

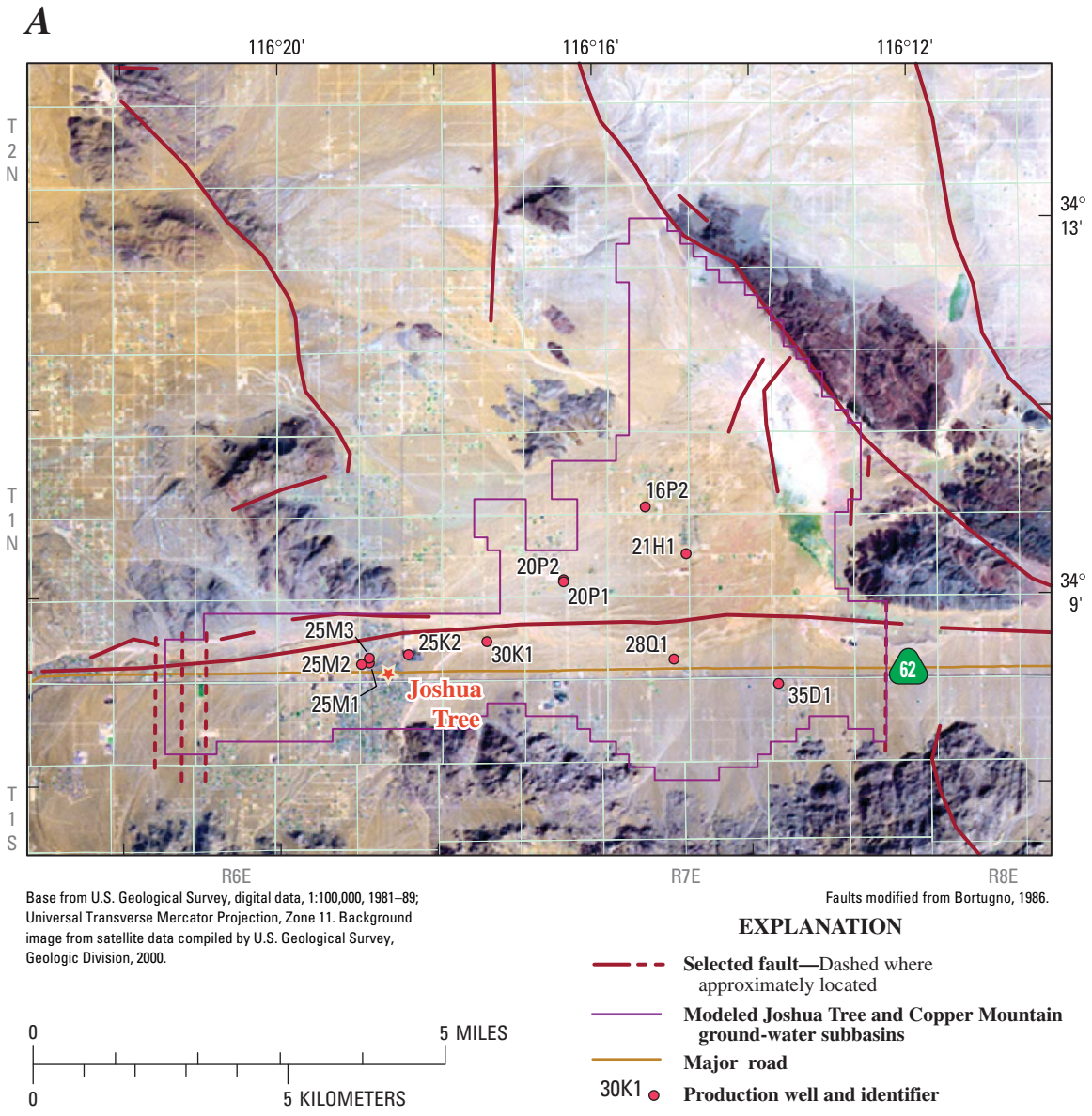

Figure 7. (*A*) location of production wells operated by Joshua Basin Water District, (*B*) water-level wells, and (*C*) water-quality wells, Joshua Tree and Copper Mountain ground-water subbasins, San Bernardino County, California.

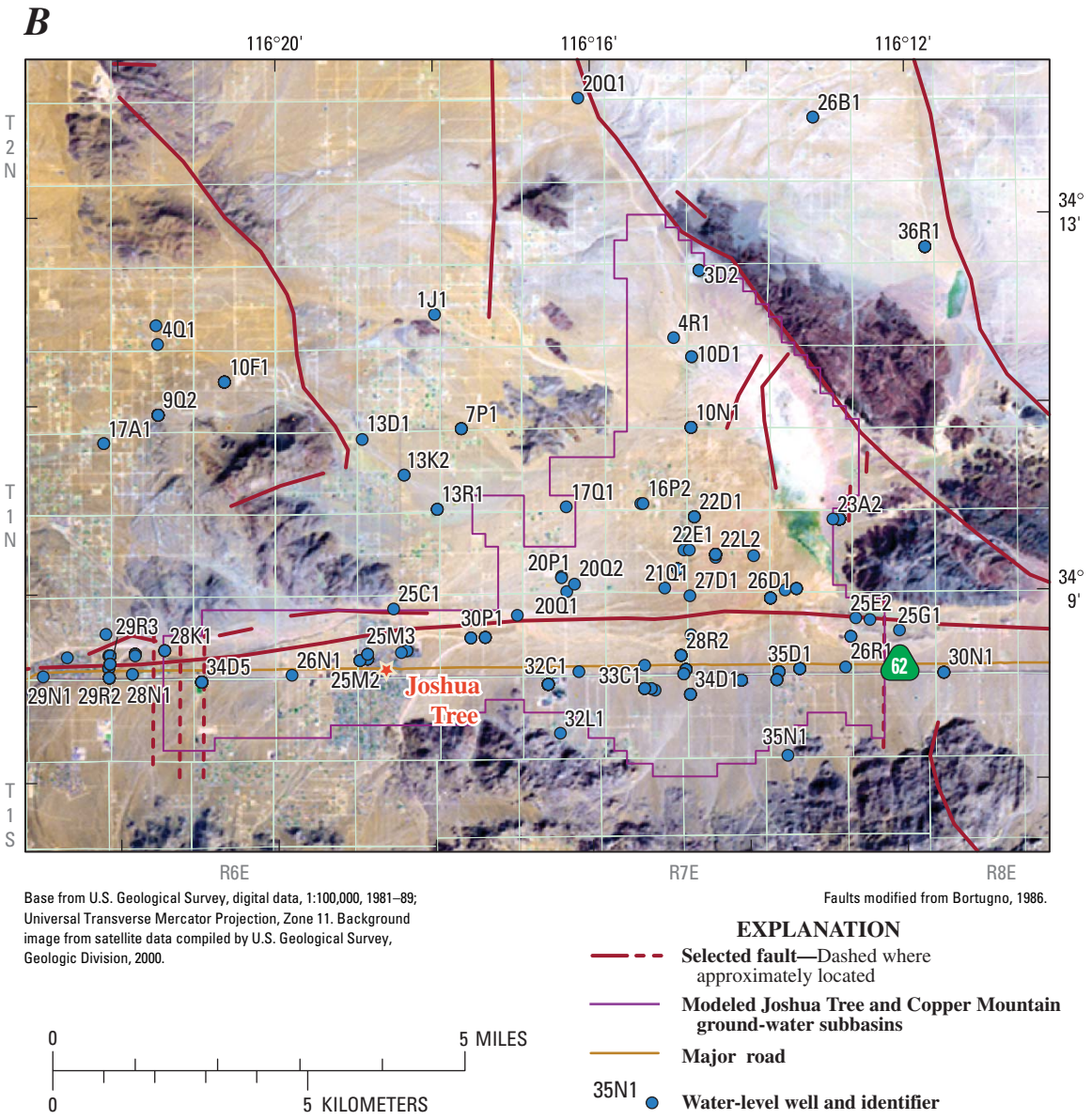

Figure 7.—Continued.

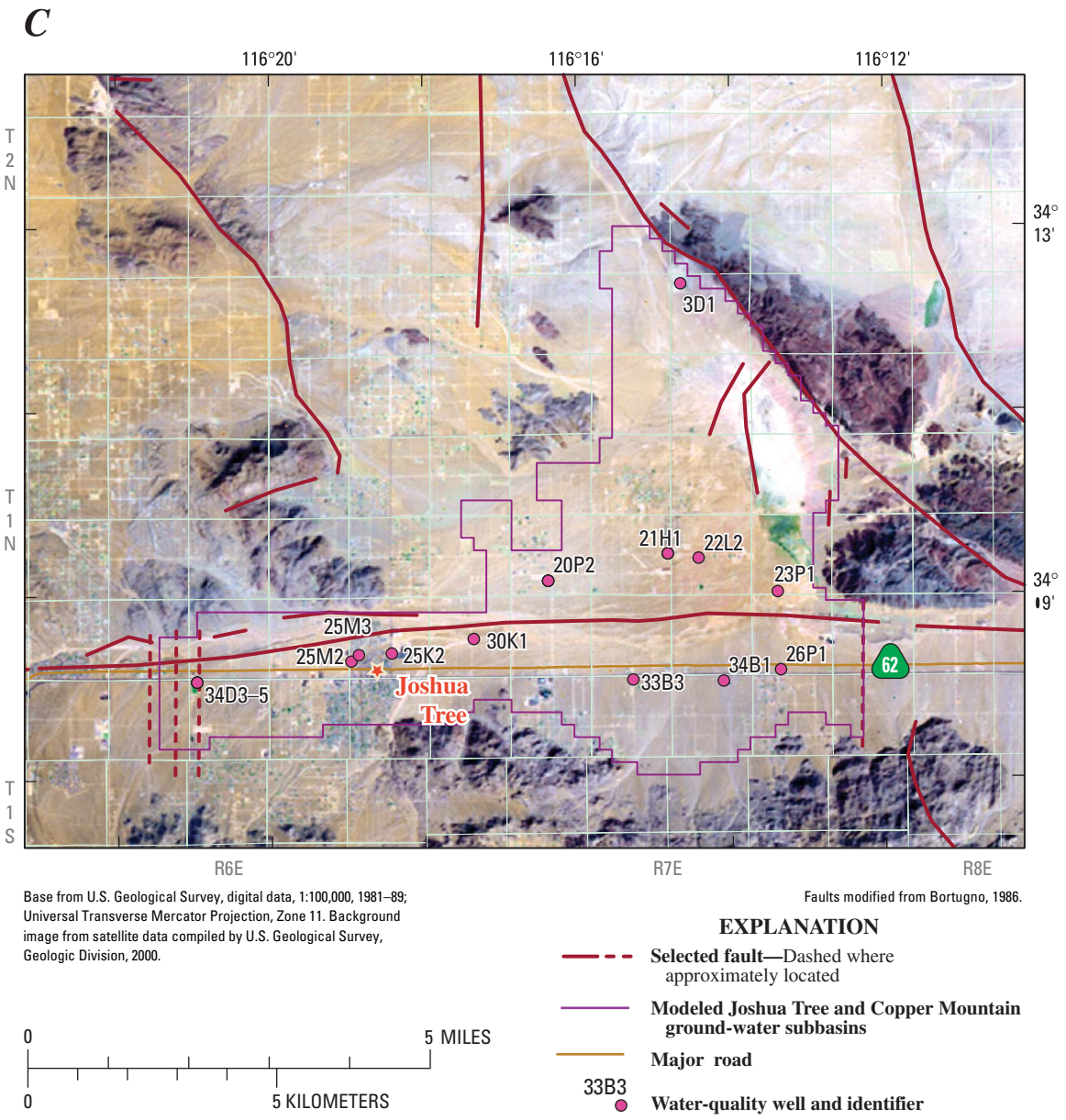

Figure 7.—Continued.

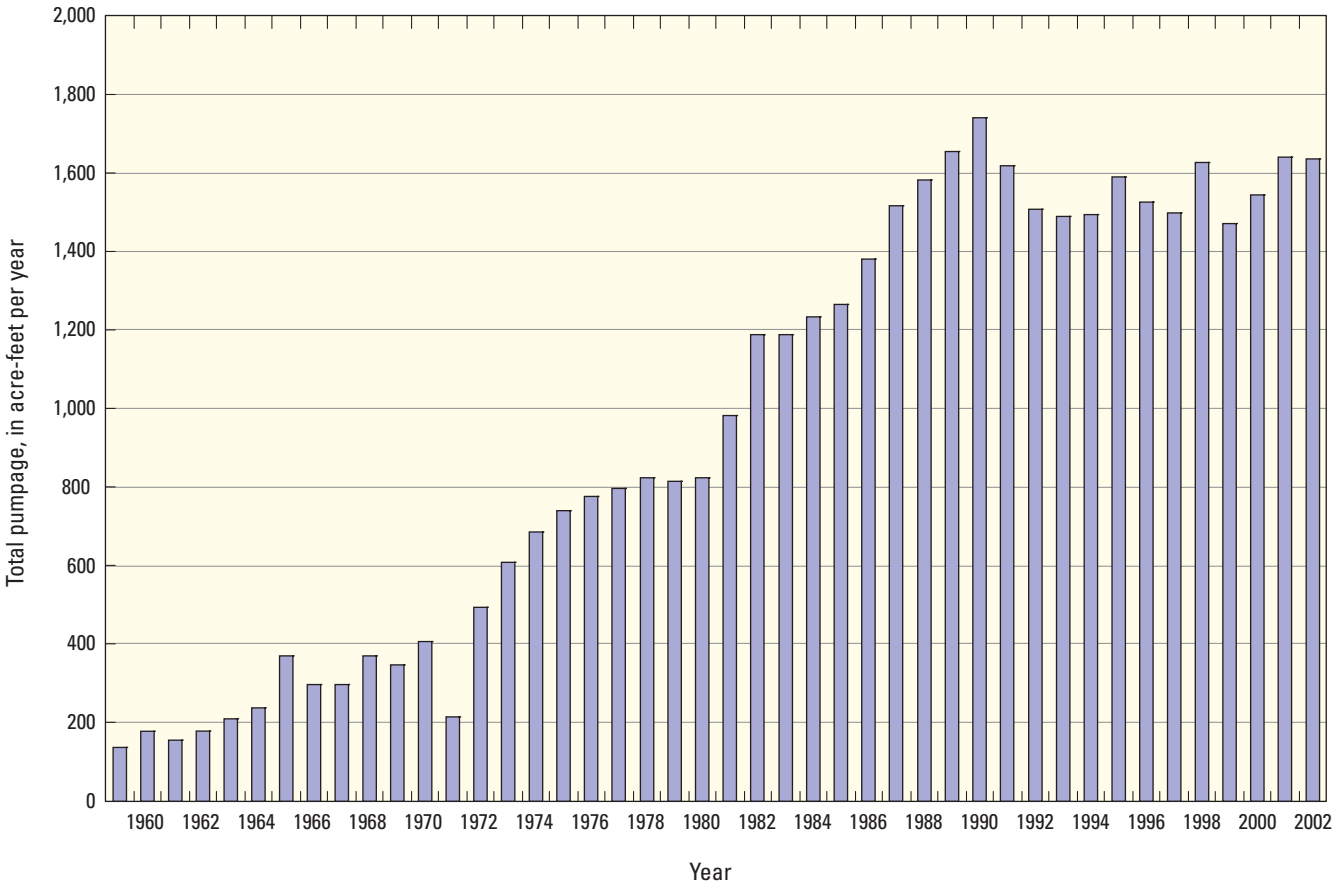

Figure 8. Total annual ground-water pumpage by Joshua Basin Water District, 1958–2001, Joshua Tree ground-water basin, San Bernardino County, California.

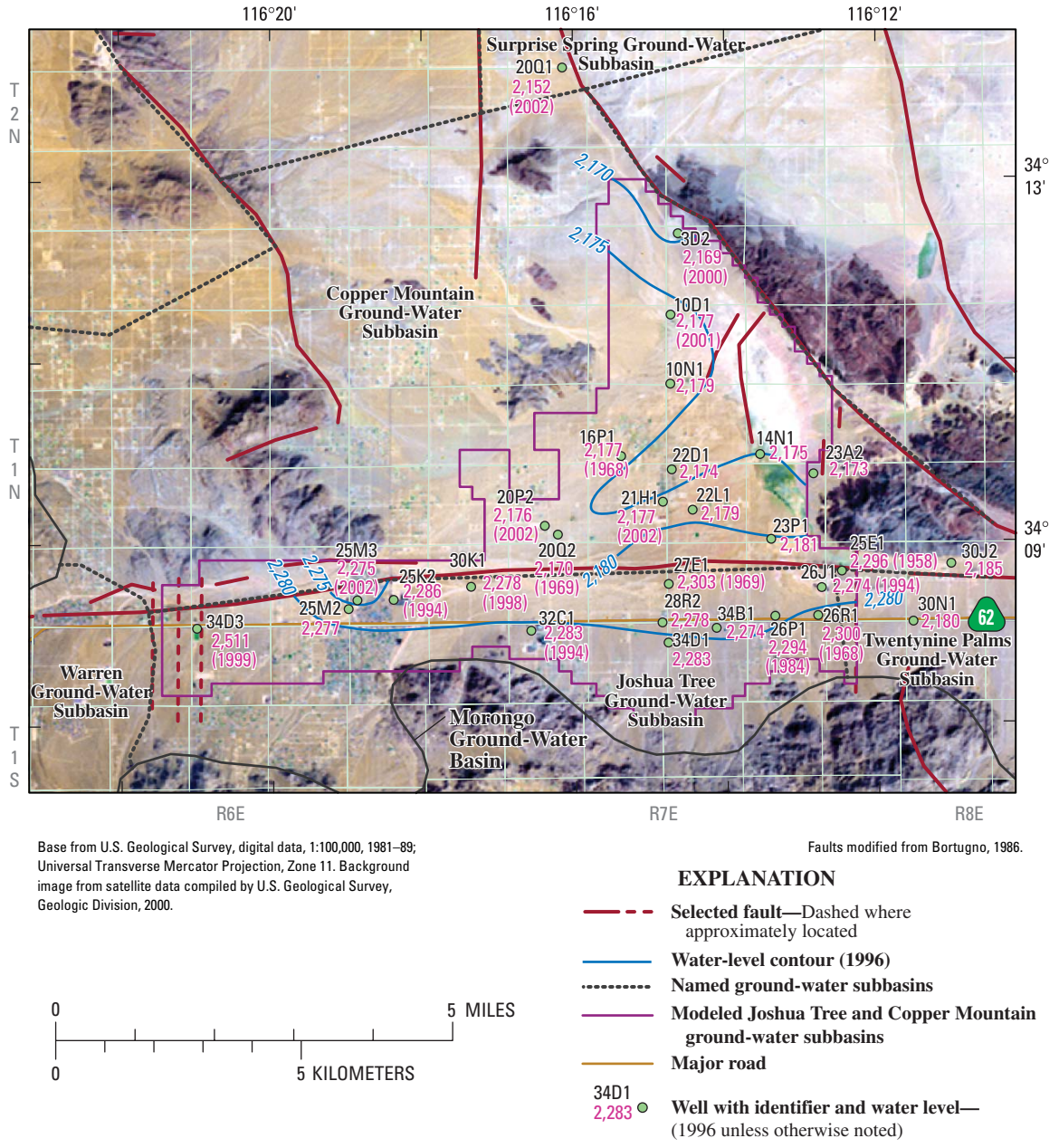

Base from U.S. Geological Survey, digital data, 1:100,000, 1981–89; Universal Transverse Mercator Projection, Zone 11. Background image from satellite data compiled by U.S. Geological Survey, Geologic Division, 2000.

Faults modified from Bortugno, 1986.

Figure 9. 1996 water levels, Joshua Tree and Copper Mountain ground-water subbasins, San Bernardino County, California.

Representative hydrographs are presented in figure 10. There were no early-time data available for wells located between the Yucca Barrier and the inferred north-south trending fault. A multiple-well site (1N/6E-34D3–5) was constructed in 1999 by the USGS in cooperation with JBWD (fig. 7*B*). All the wells at this site are perforated in the lower aquifer (Tertiary sedimentary and volcanic deposits) (fig. 6*B*). The hydrograph for well 1N/6E-34D4 indicates that water levels declined about 8 ft immediately following the Hector Mine earthquake (October 16, 1999) and then declined an additional 2 ft between October 1999 and July 2001 (fig. 10*A*).

Well 1N/6E-25M2 is a JBWD production well (JBWD #2) in the western part of the Joshua Tree ground-water subbasin (fig. 7*A*). Well 25M2 is perforated in the upper aquifer only and is adjacent to two other production wells. The hydrograph for well 25M2 indicates that water levels declined about 6 ft between early 1994 and early 1998 (fig. 10*B*)

Well 1N/7E-32C1 is in the central part of the Joshua Tree ground-water subbasin (fig. 7*B*) and is perforated in the upper aquifer only. The long-term hydrograph for well 32C1 indicates a steady, long-term water-level decline of about 31 ft between 1968 and 2000 (fig. 10*C*); this decline corresponded to an increase in ground-water pumpage (fig. 8).

Well 1N/7E-14N1 is in the Copper Mountain ground-water subbasin (fig. 7*B*) and is perforated in the middle aquifer only. The hydrograph for well 14N1 shows a water-level decline of about 1 ft between 1958 and 1977 (fig. 10*D*).

Ground-Water Quality

The ground-water quality of the Joshua Tree and Copper Mountain ground-water subbasins was defined by collecting 53 ground-water samples between 1980 and 2002 from 15 wells (10 in the Joshua Tree ground-water subbasin and 5 in the Copper Mountain ground-water subbasin) (fig. 7*C*) that were analyzed for major ions, nutrients, and selected trace elements (table 4). The wells included the three deep observation wells at the multiple-well site 1N/6E-34D3–5. Selected samples were analyzed for the stable isotopes of oxygen and hydrogen (oxygen-18 and deuterium, respectively); tritium, a naturally occurring radioactive isotope of hydrogen; and carbon-14 (^{14}C), a naturally occurring radioactive isotope of carbon. Some wells were sampled several times during this period. Complete analyses for all the samples can be retrieved from the USGS National database: http://waterdata.usgs.gov/ca/nwis/ using the USGS site numbers given in table 4.

Chemical Composition of Water from Wells

The chemical concentrations and composition of water from wells was determined by plotting selected data using box plots (fig. 11) and Piper diagrams (fig. 12), respectively. The box plots show the maximum, minimum, 25th quartile, median, and 75th quartile concentration values. A Piper diagram (Piper, 1945) shows the relative contribution of major cations and anions, on a charge-equivalent basis, to the ionic content of the water. Percentage scales along the sides of the diagram indicate the relative concentration, in milliequivalents per liter (meq/L), of each major ion. Cations are shown in the left triangle, anions are shown in the right triangle, and the central diamond integrates the data (fig. 12). For clarity, only the most recent analysis from each well is shown in figure 12; no trends in major-ion composition were observed in water from wells having more than one analysis.

Dissolved-solids concentrations in ground-water samples collected from 13 wells between October 1980 and February 2002 ranged from 142 to 809 milligrams per liter (mg/L) with a median concentration of 178 mg/L (fig. 11). Samples from all the wells, with the exception of the sample from well 1N/7E-3D1 (3D1), had dissolved-solids concentrations of less than 375 mg/L. The sample from well 3D1 had a dissolved-solids concentration of 809 mg/L, which exceeded the U.S. Environmental Protection Agency (USEPA) Secondary Maximum Contaminant Level (SMCL) of 500 mg/L (U.S. Environmental Protection Agency, 2003a). Nitrogen concentrations, measured as nitrate plus nitrite, were low and ranged from less than the detection limit of 0.05 to 4.78 mg/L as nitrogen with a median concentration of 2.5 mg/L as nitrogen. No samples exceeded the nitrate USEPA Maximum Contaminant Level (MCL) of 10 mg/L as nitrogen (U.S. Environmental Protection Agency, 2003b).

The major-ion composition of water from wells in the Joshua Tree ground-water subbasin is primarily sodium bicarbonate (fig. 12). Ground-water samples from the multiple-well monitoring site 1N/6E-34D3–5, perforated in the lower aquifer (Tertiary sedimentary deposits), contain low percentages of both calcium and magnesium and the highest percentage of sodium of all wells sampled. The high sodium percentages may be the result of a combination of calcite precipitation and cation exchange occurring over long periods of time as water reacts with aquifer materials. These processes have been shown to cause similar changes in ground-water chemistry in alluvial aquifers elsewhere in the Mojave Desert (Izbicki and others, 1995) and in southern California (Izbicki and Martin, 1997; Izbicki and others, 1997). Water from wells 34D3–5 had fluoride concentrations of about 6, 7, and 9 mg/L, respectively, and exceeded the USEPA SMCL for fluoride of 2 mg/L (U.S. Environmental Protection Agency, 2003a). The lower aquifer is not pumped for water supply.

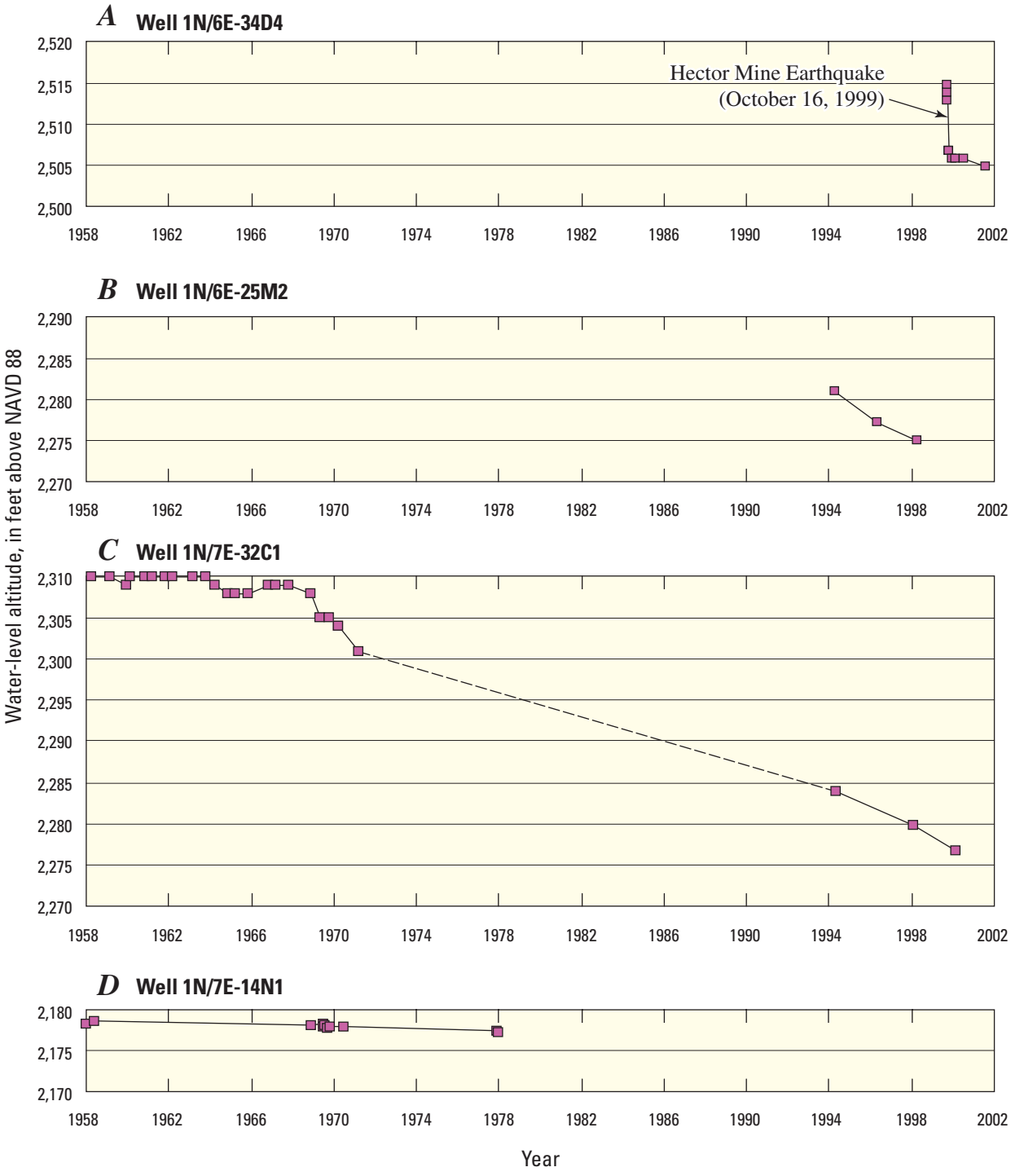

Figure 10. Water levels for wells (*A*) 1N/6E-34D4, (*B*) 1N/6E-25M2 (JBWD #2), (*C*) 1N/7E-32C1, and (*D*) N/7E-14N1, Joshua Tree and Copper Mountain groundwater subbasins, San Bernardino County, California.

Table 4. Water-quality data from ground-water samples, Joshua Tree and Copper Mountain ground-water subbasins, San Bernardino County, California

[—, no data collected]

State well No.	USGS site No.	Ground-water subbasin	Nutrients	Major ions	Isotopes	Tritium	Carbon-14
1N/6E-25K2	340822116182601	Joshua Tree	X	X	X	—	X
1N/6E-25M2	340817116185801	Joshua Tree	X	X	X	—	X
1N/6E-25M3	340821116185801	Joshua Tree	X	X	X	X	X
1N/6E-34D3	340804116205901	Joshua Tree	X	X	X	—	X
1N/6E-34D4	340804116205902	Joshua Tree	X	X	X	—	X
1N/6E-34D5	340804116205903	Joshua Tree	X	X	X	—	X
1N/7E-03D1	341222116143801	Copper Mountain	X	X	X	—	—
1N/7E-20P2	340909116162601	Copper Mountain	X	X	X	—	X
1N/7E-21H1	340926116144901	Copper Mountain	X	X	X	—	X
1N/7E-22L2	340923116142501	Copper Mountain	X	X	X	—	—
1N/7E-23P1	340901116132301	Copper Mountain	X	X	X	X	X
1N/7E-26P1	340810116132101	Joshua Tree	X	X	—	—	—
1N/7E-30K1	340831116172201	Joshua Tree	X	—	X	—	—
1N/7E-33B3	340804116151701	Joshua Tree	X	X	X	—	—
1N/7E-34B1	340803116140601	Joshua Tree	X	X	X	X	X

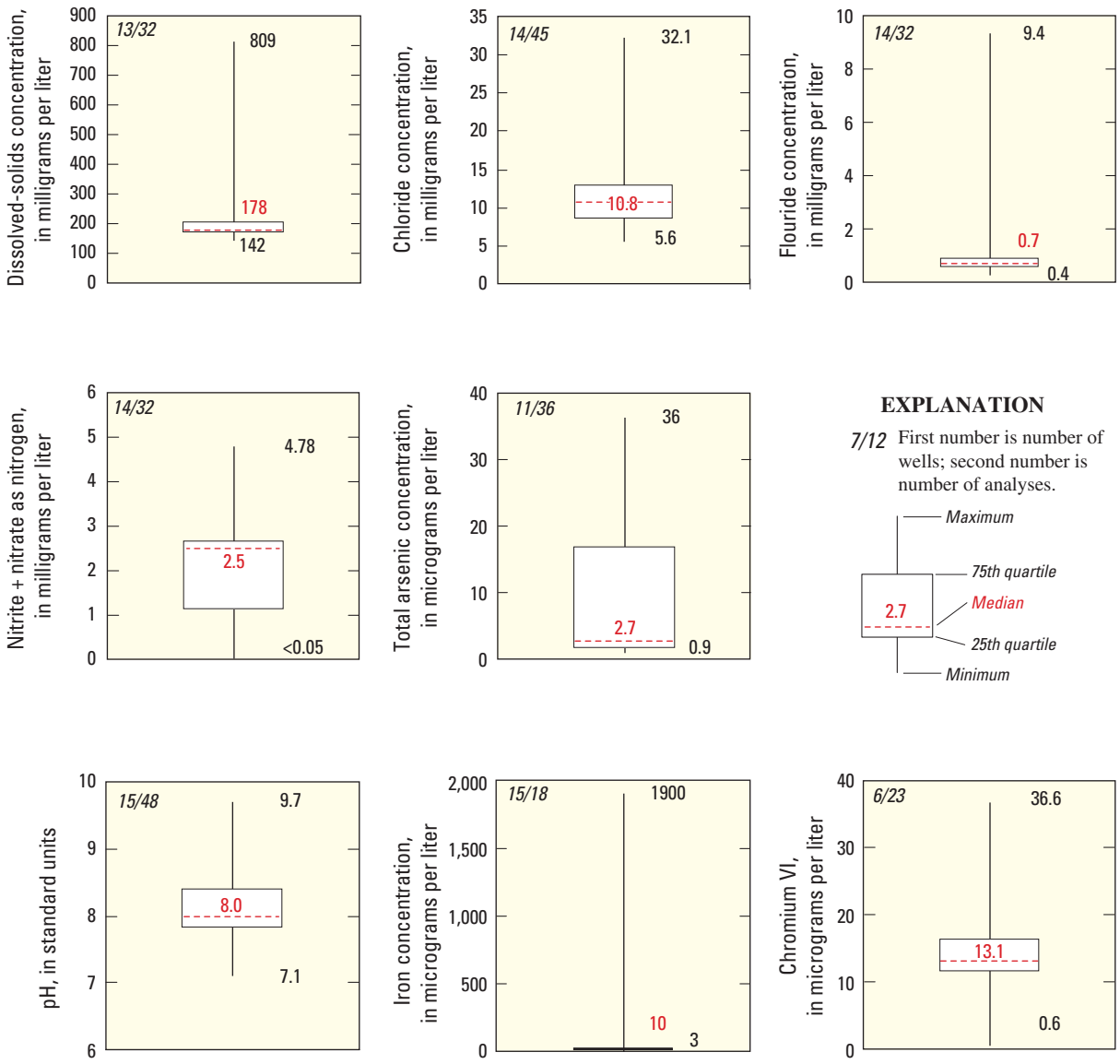

Figure 11. Chemical composition of ground water, Joshua Tree and Copper Mountain ground-water subbasins, San Bernardino County, California.

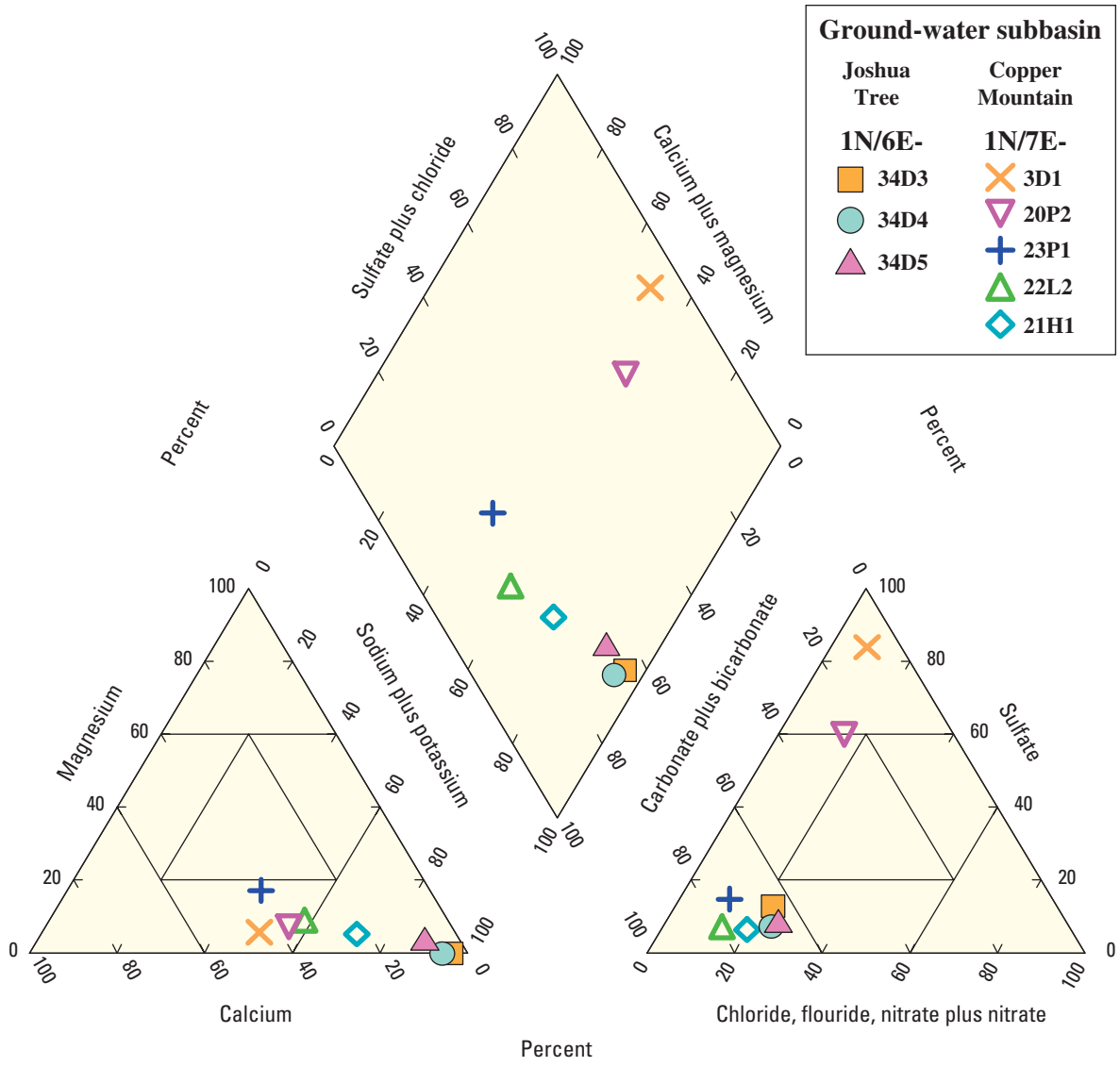

Figure 12. Major-ion composition of surface-discharge water from selected wells 1995–2002, Joshua Tree and Copper Mountain ground-water subbasins, San Bernardino County, California.

The major-ion composition of water sampled from wells in the Copper Mountain ground-water subbasin is more variable than that in water sampled in the Joshua Tree ground-water subbasin (fig. 12). Water sampled from well 1N/7E-23P1, perforated in the upper aquifer, has a calcium-sodium carbonate composition. Water sampled from well 1N/7E-22L2, perforated in the upper aquifer, and well 21H1 (JBWD #16), perforated primarily in the middle aquifer, has a sodium bicarbonate composition similar to the water sampled in the Joshua Tree ground-water subbasin. The water sampled from well 21H1 had a higher percentage of sodium than did water sampled from well 22L2, indicating that water in the middle aquifer may have a higher sodium percentage than water in the upper aquifer. Water sampled from wells 1N/7E-3D1, perforated in the upper aquifer, and 20P2 (JBWD #15), perforated in the upper and middle aquifers, has a sodium sulfate composition. Water sampled from well 1N/7E-3D1 had the highest dissolved-solids concentration (809 mg/L) of all wells sampled and is similar in composition to water from some deep wells sampled in the lower aquifer underlying the Surprise Spring Basin farther to the north (Londquist and Martin, 1991). Water sampled from well 20P2 is intermediate in composition and dissolved-solids concentration between water from well 3D1 and most other wells sampled. The higher dissolved-solids concentrations in water sampled from wells 3D1 and 20P2 and the variability in chemical composition of shallow ground water in alluvial deposits in the Copper Mountain ground-water subbasin may reflect greater contribution of water from the Tertiary-sedimentary and volcanic deposits.

Selected Trace Elements

The USEPA MCL for arsenic was lowered recently to 10 micrograms per liter (µg/L) (U.S. Environmental Protection Agency, 2003b); this has resulted in increased interest in the concentrations of arsenic and other trace elements (for example, chromium) in drinking water. Concentrations of naturally occurring arsenic and chromium may exceed MCLs in some alluvial aquifers in the western Mojave Desert (Christensen and Fields-Garland, 2001; Ball and Izbicki, 2004). Although the reactions occur slowly, weathering of primary silicate minerals in aquifer material derived from relatively nonreactive granitic or metamorphic rocks may increase ground water pH. As pH increases to values greater than 8, trace elements sorbed on mineral grains may come into solution. In addition, except for lacustrine deposits, aquifer material generally contains little carbon and the ground water is oxic, containing several milligrams per liter of dissolved oxygen (fig. 13*A–B*). As a result of the relatively high pH and oxidizing conditions, arsenic and chromium in water from wells in these aquifers commonly are present as As+5 (As V) and Cr+6 (Cr VI). Hexavalent chromium (Cr VI) is considered more toxic than is Cr+3 (Cr III).

Total arsenic concentrations in water sampled from wells within the study area ranged from 0.9 to 36 µg/L with a median concentration of 2.7 µg/L (fig. 11). Water sampled from the observation wells 1N/6E-34D3–5 (perforated in the lower aquifer) exceeded the USEPA MCL of 10 µg/L, with arsenic concentrations of about 26, 29, and 36 µg/L, respectively. Arsenic concentrations in water sampled from well 1N/7E-21H1 (perforated primarily in the middle aquifer) and well 1N/7E-33B3 (unknown perforated interval) were also relatively high, with concentrations of about 4 and 8 µg/L, respectively.

Chromium concentrations in water sampled from wells within the study area ranged from 0.6 to 36.6 µg/L with a median concentration of 13.1 µg/L (fig. 11). The highest chromium concentration was in water sampled from well 21H1. These values are within the range of naturally occurring chromium concentrations measured previously in water from wells in the western Mojave Desert (Ball and Izbicki, 2004), and almost all the chromium was in the form of Cr VI. No wells sampled exceeded the USEPA MCL for chromium of 100 µg/L (U.S. Environmental Protection Agency, 2003b) or the California MCL of 50 µg/L (California Department of Health Services, 2003).

Vertical Variations in Ground-Water Quality

Vertical variations in ground-water quality were evaluated in two production wells [1N/7E-20P2 (JBWD #15) and 1N/7E-21H1 (JBWD #16)] in the Copper Mountain ground-water subbasin. Variations in major-ion composition and trace-element concentrations with depth were evaluated in the wells on the basis of flowmeter and depth-dependent ground-water-quality data. The combination of flowmeter data and depth-dependent ground-water-quality data is especially effective for determining the distribution of water quality in heterogeneous aquifers where wells are perforated in multiple aquifer zones having different hydraulic properties and different water quality (Izbicki and others, 1999).

The wells were each pumped for at least 24 hours prior to flowmeter data and depth-dependent sample collection to ensure stable hydraulic conditions. Flowmeter data were collected using a vertical-axis flowmeter. Depth-dependent water-quality samples were collected under pumping conditions using a small-diameter sampling hose following the techniques described by Izbicki and others (1999). To collect a water-quality sample, the hose is pressurized to greater than the hydrostatic pressure of water at the sample depth and lowered into the well. When the sample depth is reached, the hose is vented at the surface and water from the well enters the hose at the sample depth. The hose is retrieved and the sample is expelled from the hose using nitrogen gas. The process is repeated at several depths to construct a water-quality profile within the well.

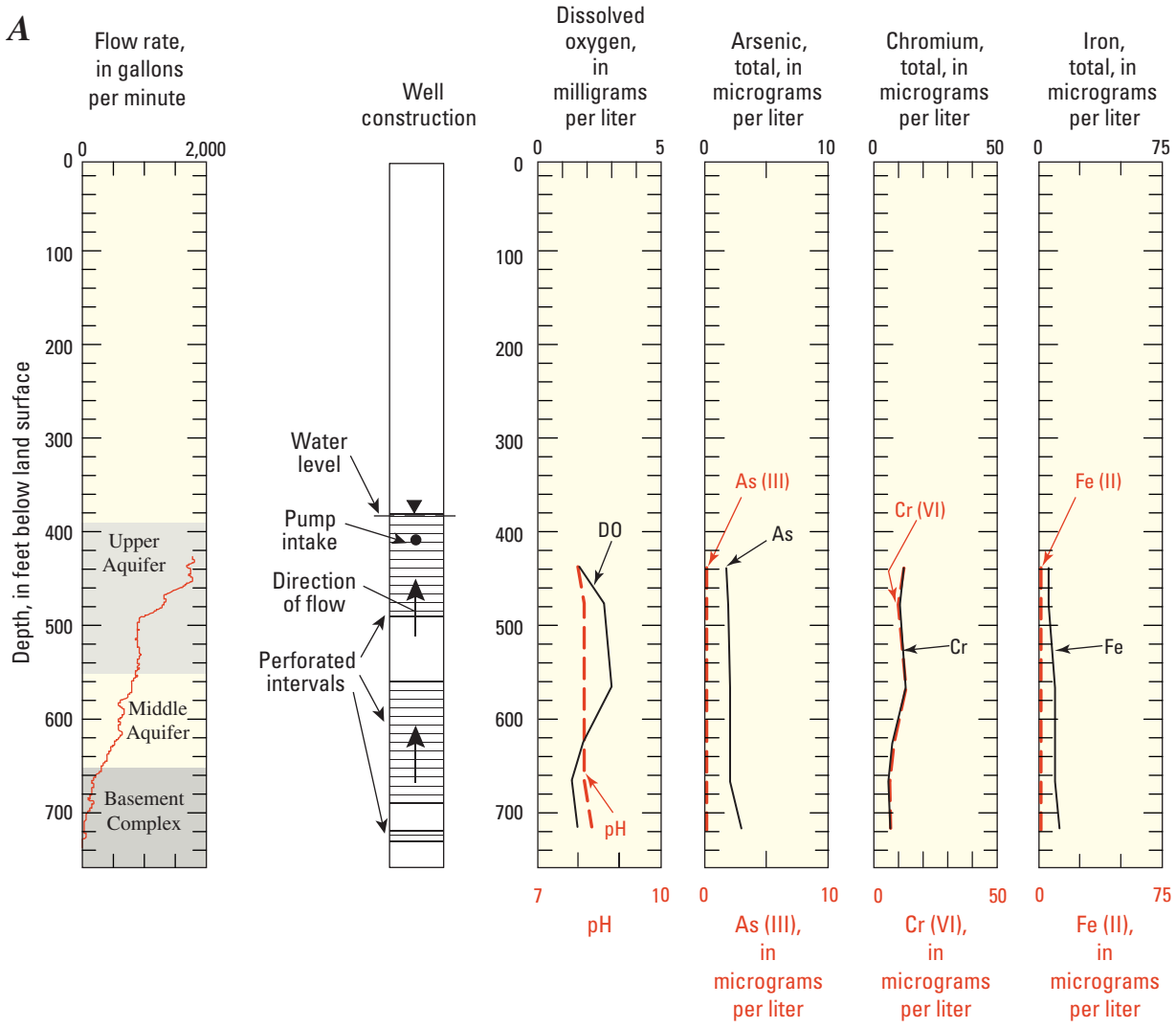

Figure 13. Fluid flow rate, well construction, and concentrations of selected dissolved constituents with depth in ground water from wells (*A*) 1N/7E-20P2 (sampled February 12, 2002) and (*B*) 1N/7E-21H1 (sampled December 3, 2001), Copper Mountain ground-water subbasin, San Bernardino County, California.

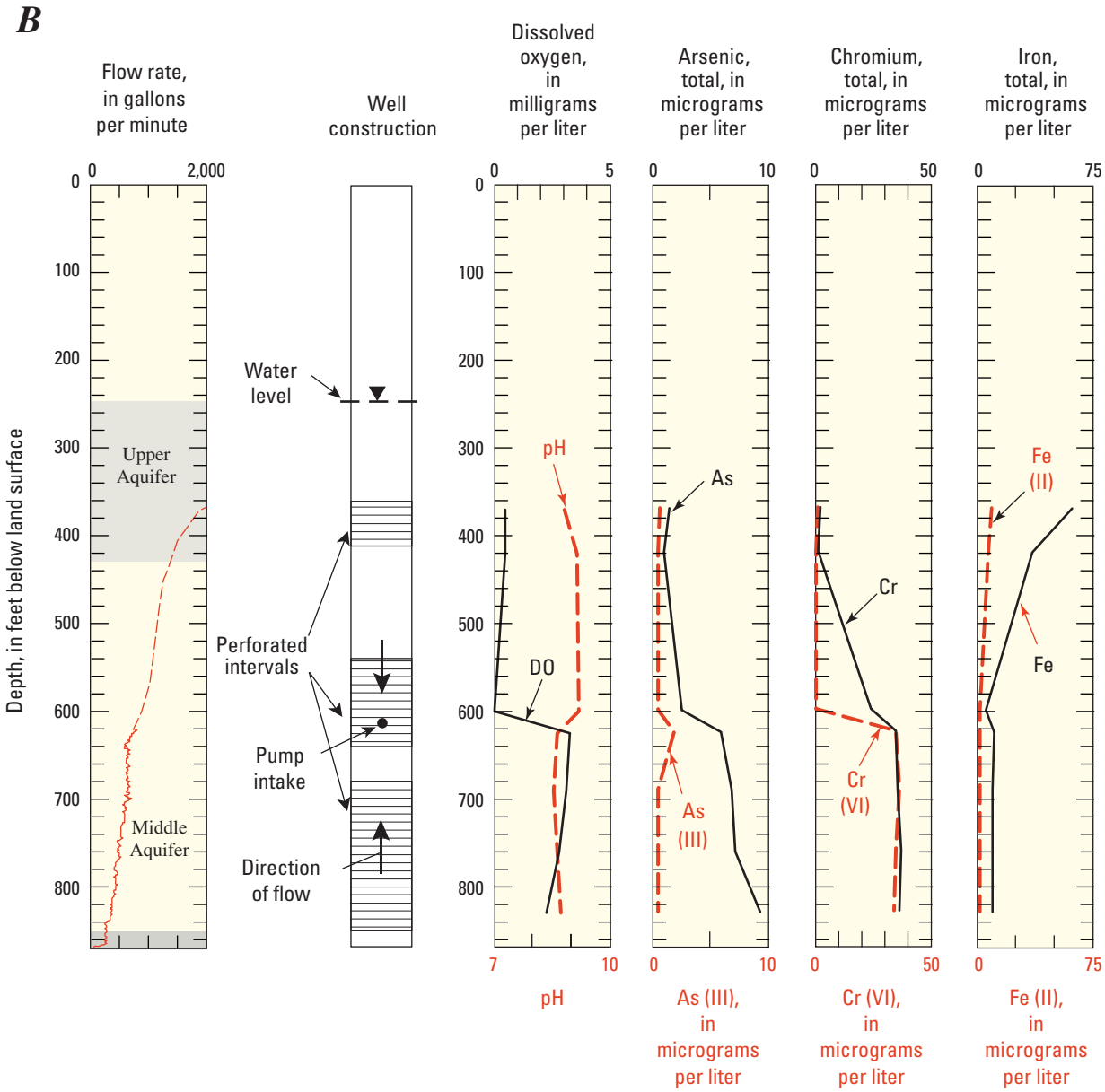

Figure 13.—Continued.

Well 1N/7E-20P2 is perforated from 380 to 490, 560 to 700, and 720 to 730 ft bls in the upper aquifer, middle aquifer, and the pre-Tertiary basement complex, respectively (fig. 13*A*). During sample collection, the pump intake was located near the top of the well screen and water sampled within the well was flowing upward toward the pump intake. On the basis of the velocity log shown in figure 13*A*, most water entered the well in two intervals from about 440 to 490 and 610 to 660 ft bls (changes in slope of the velocity log indicates water entering the well). The deepest sample, collected about 710 ft bls, represents water in the aquifer at that depth, and the next deepest sample, collected about 660 ft bls, is a mixture of water that entered the well between the two sample depths. Assuming simple mixing, the chemical composition of water in the aquifer between sample-collection depths could be estimated on the basis of the flowmeter and depth-dependent water-quality data (Izbicki and others, 1999).

Water sampled from well 20P2 was alkaline, with pH values ranging from 8 to 8.3, and contained dissolved-oxygen concentrations as high as 2.6 mg/L. Water sampled at 710 ft bls had the lowest dissolved-solids concentration (less than 250 mg/L). Water sampled at 660 ft bls had the highest concentrations of dissolved solids (474 mg/L) and sulfate (245 mg/L) and is more similar to the major-ion composition of water from well 1N/7E-3D1 than that of water sampled from the lower aquifer (fig. 12). In general, the dissolved-solids concentrations decreased with decreasing depth above the sample at 660 ft, with the surface-discharge concentration of 369 mg/L about 100 mg/L less than the maximum value.

The arsenic and iron concentrations in samples from well 20P2 were highest in the deepest sample and decreased slightly with decreasing depth; whereas, the chromium concentrations were highest in the sample taken near the pump intake and decreased slightly with increasing depth (fig. 13*A*). Almost all arsenic was in the form of As V (shown as the difference between total dissolved As and As III) and almost all chromium was present as Cr VI (Ball and Izbicki, 2004).

Well 1N/7E-21H1 is perforated from 360 to 410, 540 to 640, and 680 to 850 ft bls in the upper and middle aquifers (fig. 13*B*). During sample collection, the pump intake was located in the middle of the well screen about 610 ft bls; therefore, water within the well was flowing downward from shallower depths and upward from deeper depths toward the pump intake. In the same manner as well 20P2, the deepest sample represents water in the aquifer at that depth, and the next deepest sample is a mixture of water that entered the well between the two sample depths. Unlike well 20P2, the shallowest sample also represents water in the aquifer at that depth, and progressively deeper samples represent mixtures of water until the depth of the pump intake. It was not possible to measure flow in the well above the pump intake using a vertical-axis flowmeter, and the percent of total flow from below the pump intake was estimated on the basis of flowmeter-calibration data.

Water sampled from well 21H1 was more alkaline than was water from well 20P2, with pH values ranging from 8.5 to 9.2, and did not contain dissolved oxygen at concentrations greater than the detection limit of 0.2 mg/L directly above the pump intake (about 590 ft bls), although dissolved oxygen is present at deeper depths.Water sampled from this well had relatively uniform dissolved-solids concentrations, ranging from 129 (at 750 ft bls) to 148 mg/L (at 360 ft bls). In addition, all the samples had similar major-ion compositions.

Arsenic and chromium concentrations were highest in samples collected below the pump intake and decreased immediately above the pump intake corresponding to the decrease in dissolved-oxygen concentrations in samples collected above the pump intake (reducing conditions); however, the iron concentrations were lowest below the pump intake and increased immediately above the pump intake (fig. 13*B*). A possible reason for the reducing conditions in the upper part of well 21H1 is that this part of the well was not properly developed, leaving drilling fluids in the gravel pack and formation. Small amounts of arsenic and most of the chromium were present in reduced forms as As III and Cr III rather than in the oxidized forms present in well 20P2 and at deeper depths within well 21H1.

Comparison of depth-dependent water-quality data from wells 20P2 and 21H1 shows that trace-element concentrations in the aquifers underlying the Copper Mountain ground-water subbasin vary spatially and with depth. Arsenic and chromium concentrations and speciation are controlled by reduction-oxidation conditions within the aquifer.

Isotopic Composition of Water from Wells

Samples collected from 14 of the wells in the study area between December 1992 and February 2002 were analyzed for the stable isotopes of oxygen (oxygen-18) and hydrogen (hydrogen-2, also called deuterium) to determine the source of water to wells and to evaluate the movement of water through the study area. Selected samples were analyzed for the radioactive isotopes of hydrogen (hydrogen-3, also called tritium) and carbon (carbon-14) to determine the age, or time since recharge, of the ground water.

Oxygen-18 and Deuterium

Oxygen-18 and deuterium are naturally occurring isotopes of oxygen and hydrogen. Oxygen-18 and deuterium abundances are expressed as ratios in delta (δ) notation as a per mil (parts per thousand) difference relative to the standard Vienna Standard Mean Ocean Water (VSMOW) (Gonfiantini, 1978). By convention, the ratio of VSMOW is 0 per mil.

Most of the world's precipitation originates from the evaporation of seawater, and the delta oxygen-18 ($\delta^{18}O$) and delta deuterium (δD) of precipitation throughout the world is linearly correlated and distributed along a line known as the global meteoric water line (fig. 14) (Craig, 1961). The $\delta^{18}O$ and δD of ground water, relative to the global meteoric water line, provides evidence of the source of the water and fractionation processes that have affected the water's stable-isotope values. For example, water from a given air mass that condensed at higher altitudes and cooler temperatures contains a greater amount of the lighter isotopes of oxygen and hydrogen and, therefore, has lighter $\delta^{18}O$ and δD values than water that condensed from the same air mass at lower altitudes and warmer temperatures. In some areas, fractionation during atmospheric condensation and precipitation, or during evaporation prior to ground-water recharge, may result in recharge waters with different $\delta^{18}O$ and δD values. Information about the source and evaporative history of water can be used to evaluate the movement of water between aquifers. Because ground water moves slowly, isotopic data typically preserve a record of ground-water recharge and movement under predevelopment conditions. This is especially useful in areas where traditional hydrologic data (such as water levels) have been altered by pumping, by changes in recharge and discharge, or as a result of human activities.

Water sampled from 14 wells in the study area had $\delta^{18}O$ values that ranged from −11 to −12.3 per mil (fig. 14), with a median value of −11.2 per mil. The δD values ranged from −76.2 to −90.1 per mil with median value of −78.8 per mil. The data plot in two distinct groups on a plot of δD as a function of $\delta^{18}O$ (fig. 14).

With the exception of wells 1N/6E-34D3–5, 1N/7E-3D1, and 22P2, ground-water samples from wells have similar $\delta^{18}O$ and δD values and plot slightly above the global meteoric water line (fig. 14). These δD values are compared with volume-weighted winter and summer precipitation δD values reported by Friedman and others (1992) for a precipitation-collection station at Joshua Tree. The δD values of the ground-water samples are similar to the δD of volume-weighted winter precipitation, but are significantly lighter (more negative) than the δD value of volume-weighted summer precipitation (fig. 14). These data are consistent with ground-water recharge from infiltration of winter precipitation and (or) subsequent streamflow rather than from infiltration of summer precipitation and (or) streamflow. In addition, the data plot near the global meteoric water line (fig. 14), indicates that little evaporation occurred prior to ground-water recharge and confirms that winter precipitation was the predominant source of ground-water recharge.

Water sampled from observation wells 1N/6E-34D3–5 completed in the lower aquifer (Tertiary sedimentary deposits) has $\delta^{18}O$ and δD values near −12.3 and −89 per mil, respectively, and plot slightly below the global meteoric water line (fig. 14). These values are lighter than the isotopic composition of present-day winter precipitation in the Joshua Tree area and reflect a different recharge history than do water from most other wells sampled. It is possible that water from these wells was recharged from a different source, where the temperature of condensation of precipitation was cooler, or that the water was recharged at a different time, when the climate was cooler than present-day conditions. For example, precipitation having a similar isotopic composition can be found in the higher altitudes of the San Bernardino Mountains (Friedman and others, 1992) outside the drainage basin, and precipitation from individual storms or precipitation during cooler and wetter winters may also be similar in composition (Izbicki and others, 2002). The age of ground water (time since ground-water recharge) and the timing of ground-water recharge are discussed in the section of this report entitled "Tritium and Carbon-14".

Water sampled from wells 1N/7E-3D1 (perforated in the upper aquifer) and 20P2 (perforated in the upper aquifer, middle aquifer, and pre-Tertiary basement complex) plots below the meteoric water line (fig. 14) and may have undergone evaporation prior to ground-water recharge. The evaporative signature of these waters may indicate that the source of the ground-water recharge was summer precipitation under a climatic regime (cooler temperature) different from present-day conditions. If evaporative effects are accounted for, the initial composition of water from well 3D1 probably was lighter than water from wells 34D3–5, and water from well 20P2 probably was similar to the composition of water from observation wells 34D3–5. The isotopically lighter data from wells 3D1 and 20P2 indicate that the source of ground-water recharge for these wells is different from that of the other wells sampled in the Joshua Tree and Copper Mountain ground-water subbasins.

Tritium and Carbon-14

Tritium is a naturally occurring radioactive isotope of hydrogen that has a half-life of 12.4 years. The concentration of tritium is measured in tritium units (TU); each TU equals 1 atom of tritium in 10^{18} atoms of hydrogen. Approximately 800 kilograms of tritium was released into the atmosphere as a result of the atmospheric testing of nuclear weapons between 1952 and 1962 (Michel, 1976). As a result, tritium concentrations in precipitation and ground-water recharge increased during that time. Tritium concentrations are not affected significantly by chemical reactions other than radioactive decay because tritium is part of the water molecule. Therefore, tritium is an excellent tracer of the movement and relative age of water on time scales ranging from recent to about 50 years before present (post 1952). In this report, ground water that has detectable tritium (greater than 0.2 TU) is interpreted as water recharged after 1952. Tritium concentrations in water from three wells (1N/6E-25M3, 1N/7E-23P1, and 1N/7E-34B1) was 0.3 TU, slightly above the detection limit, indicating little to no recharge has reached the water table since 1952.

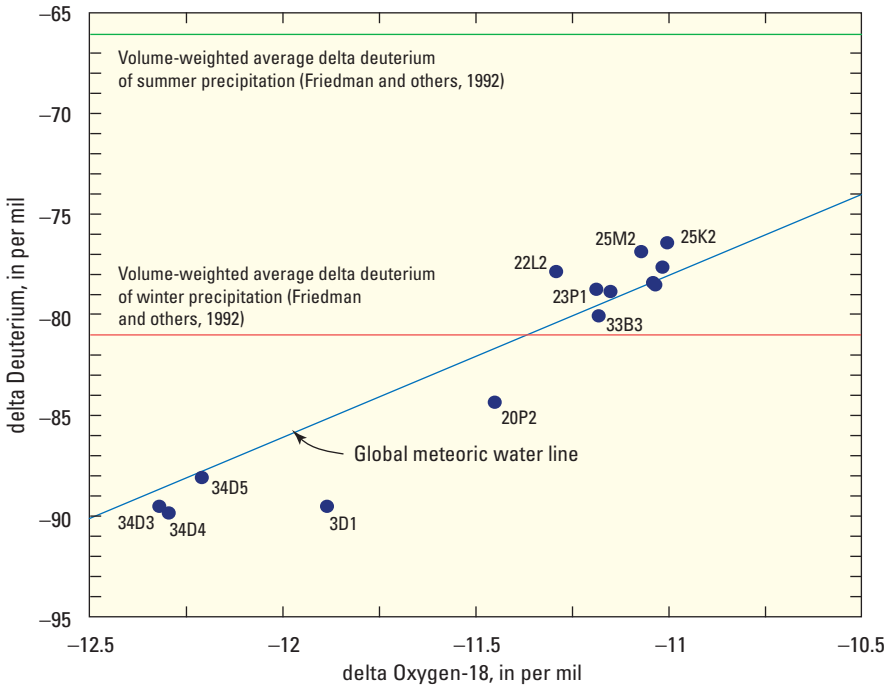

Figure 14. Relation between delta-deuterium and delta oxygen-18 from ground water sampled between August 1999 and February 2002, Joshua Tree and Copper Mountain ground-water subbasins, San Bernardino County, California.

Carbon-14 (^{14}C) is a naturally occurring radioactive isotope of carbon that has a half-life of about 5,730 years (Mook, 1980). Carbon-14 data are expressed as percent modern carbon (pmc) by comparing ^{14}C activities to the specific activity of National Bureau of Standards oxalic acid: 13.56 disintegrations per minute per gram of carbon in the year 1950 equals 100 pmc (Kalin, 2000). Carbon-14 was produced, as was tritium, by the atmospheric testing of nuclear weapons (Mook, 1980). As a result, ^{14}C activities may exceed 100 pmc in areas where ground water contains tritium. Carbon-14 activities are used to determine the age of a ground-water sample on time scales ranging from recent to more than 20,000 years before present. Carbon-14 is not part of the water molecule and, therefore, ^{14}C activities may be affected by chemical reactions that remove or add carbon to solution. In addition, ^{14}C activities are affected by the mixing of younger water that has high ^{14}C activity with older water that has low ^{14}C activity. Carbon-14 ages presented in this report do not account for changes in ^{14}C activity resulting from chemical reactions or mixing and, therefore, are considered uncorrected ages. In general, uncorrected ^{14}C ages are older than the actual age of the associated water. Izbicki and others (1995) estimated that uncorrected ^{14}C ages were as much as 30 percent older than actual ages for ground water in the regional aquifer in the Mojave River ground-water basin (not shown), about 50 mi northwest of the study area.

Carbon-14 activities in ground water sampled from wells in the Joshua Tree ground-water subbasin ranged from 2 to 72 pmc (fig. 15). These ^{14}C activities correspond to uncorrected ground-water ages ranging from about 32,300 to 2,700 years before present. The lowest ^{14}C activities, ranging from 2 to 5 pmc, were in water from the observation wells 1N/6E-34D3–5 completed in the lower aquifer. The uncorrected ^{14}C ages for water sampled from these wells are between 32,300 and 24,700 years before present. Water from these wells has the lightest $\delta^{18}O$ and δD values of wells sampled in the basin, and its isotopic composition is lighter than that of present-day precipitation measured by Friedman and others (1992), indicating that the water was recharged at a time when the climate was greatly different from present-day climatic conditions.

The highest ^{14}C activities, ranging from 71 to 72 pmc, were measured in water sampled from wells 1N/6E-25K2, 25M2, and 25M3 (perforated in the middle, upper and middle, and middle aquifers, respectively) in the Joshua Tree ground-water subbasin (fig. 15). The uncorrected ^{14}C ages for water sampled from these wells is about 2,700 years before present. As previously discussed, the $\delta^{18}O$ and δD composition of water from these wells is similar to the composition of present-day precipitation measured by Friedman and others (1992), indicating that the water was recharged under present-day climatic conditions. The proximity of these wells to Quail Wash suggests that water from the wash may have recharged the ground-water system, although measurements along the wash suggest that little recharge occurred as infiltration of streamflow during this study (2001–03) as discussed in the "Estimating Recharge Using Borehole Instrumentation" section of this report that follows.

The lowest ^{14}C activity measured in water sampled from the upper and middle aquifers in the Joshua Tree ground-water subbasin, 43 pmc, was from well 1N/7E-34B1. The uncorrected age for water sampled from this well is about 7,000 years before present. Well 34B1 is located in the eastern part of the Joshua Tree ground-water subbasin. There are no major washes located near well 34B1; therefore, the low ^{14}C activity in water sampled from this well probably resulted from small amounts of ground-water recharge along the front of the Little San Bernardino Mountains.

Carbon-14 activities in ground-water sampled from wells 1N/7E-20P2, 21H1, and 23P1 in the Copper Mountain ground-water subbasin were 32, 39, and 12 pmc, respectively. Low ^{14}C activities in water sampled from these wells indicates that the amount of recharge in the Copper Mountain ground-water subbasin was small. The low ^{14}C activity (32 pmc) measured in water from well 20P2 and the relatively light $\delta^{18}O$ and δD values of water from this well indicate that water sampled from this well has an uncorrected age of more than 10,000 years and was recharged at a time when the climate was greatly different from present-day conditions. A depth-dependent sample collected from well 20P2 at 710 ft bls (in the lower aquifer) had a ^{14}C activity of 19 pmc indicating that the water in the lower aquifer is older than the water in the upper and middle aquifers. The $\delta^{18}O$ and δD values of water from wells 21H1 and 23P1 suggests that ground-water recharge occurred under conditions similar to those of the present-day climate—despite the low ^{14}C activity (12 pmc for 23P1). A depth-dependent sample collected from well 21H1 at 820 ft bls (in the lower part of the middle aquifer) had a ^{14}C activity of 37 pmc, indicating that there is little vertical variation in ground-water age at this well. The low ^{14}C activity in water sampled from well 23P1 is probably the result of the addition of dead carbon (devoid of ^{14}C) from dissolution of carbonate aquifer materials.

Estimation of Recharge

To effectively manage the water resources within the Joshua Tree and Copper Mountain ground-water subbasins, it is important to know the quantity and distribution of recharge. Previous investigators used a percentage of precipitation falling on the watershed (Whitt and Jonker, 1998). In this study, natural recharge was estimated using direct field measurements (borehole instrumentation of temperature, matric potential, and water chemistry) and using a distributed-parameter watershed model.

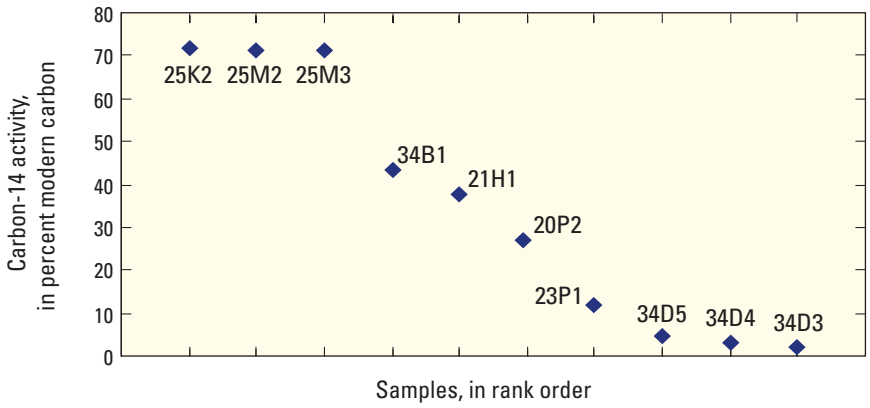

Figure 15. Uncorrected carbon-14 data from ground-water samples, Joshua Tree and Copper Mountain ground-water subbasins, San Bernardino County, California.

Estimating Recharge Using Borehole Instrumentation

Natural recharge was estimated using field measurements of temperature, matric potential, and water chemistry. The data were collected from soil cores, instruments installed in boreholes, temperature-access tubes, and infiltration tests.

Installation of Unsaturated-Zone Monitoring Sites

Four instrumented boreholes and seven temperature-access tubes were installed in or near Quail Wash and Yucca Wash (fig. 16) to collect data used to estimate the natural recharge along these washes.

Instrumented Boreholes

Instrumented boreholes were installed in the streambed of Quail Wash, near the mountain front and downstream from State Highway 62 (sites UQSW and MQSW, respectively), and at a site along Yucca Wash, downstream from the confluence with Quail Wash (site LQSW) (fig. 16). A control site, QSWC, was installed to the east of UQSW outside the active streambed. The boreholes were drilled to a depth of about 50 ft using a 10-in. hollow-stem auger. Two-foot-long split-spoon cores were collected at 5-ft intervals during drilling for later laboratory analysis. Sample collection, handling, and preservation techniques described by Izbicki and others (2000a) were used to store the samples and to minimize water loss.

A 2-in.-diameter polyvinyl chloride (PVC) access tube was installed at each site to measure temperature. Heat-dissipation sensors, packed in diatomaceous earth and fine sand were installed between the borehole annulus and the PVC access tube at 5-, 10-, 15-, 25-, and 50-ft depths. Between the sensors, the borehole annulus was backfilled with low-permeability bentonite grout to minimize movement of water through the borehole annulus. The heat-dissipation probes report temperatures to the thousandth of a degree; however, most manufacturers claim accuracies between 0.05 and 0.1^{o}C.

Heat-dissipation sensors measure temperature and provide an indirect method of measuring soil-water matric potential. In general, a heat-dissipation sensor consists of a heating element and thermocouple embedded within a porous ceramic matrix. The rate of heat dissipation in the sensor is a function of water content. Prior to installation, the heat-dissipation sensors were calibrated to relate the rate of heat dissipation to matric potential following techniques described by Flint and others (2002). The heat-dissipation sensors were activated and data were collected at 4-hour intervals by a data logger in a vault installed at land surface. Several months were required for the probes and backfill to equilibrate with the surrounding material before representative data could be collected.

The core material collected from the boreholes was analyzed for water content, matric potential, chloride, and particle size and color. Water content was measured gravimetrically and matric potential was measured using the filter-paper technique (Campbell and Gee, 1986). Chloride was leached from the core material using techniques described by Izbicki and others (2000a) and was analyzed in the laboratory using an ion-chromatograph (American Public Health Association, 1992). Particle size and color were described in the field and the laboratory using standard techniques.

Temperature Access Tubes

One-in.-diameter PVC access tubes were installed using a cone penetrometer at two sites in Yucca Wash (Bartlett and Center) and six sites in Quail Wash (MQSWC, Junction, LQSWC-north, LQSWC-south, Sunfair, and Cascade) (fig. 16). One of the access tubes was installed as a control site for MQSW (MQSWC) and two of the access tubes were installed as control sites for LQSW (LQSWC-north and -south). The depths of the access tubes ranged from 5 to 33 ft depending on the depth of penetration of the penetrometer and the stability of the resulting hole.

Analysis of Physical-Property Data

Test-drilling data show that the unsaturated zone beneath the streambed and control sites was primarily composed of sand with smaller amounts of gravel and silt. No clay layers were identified in any of the boreholes drilled for this study. The saturated hydraulic conductivity of most core material collected from the unsaturated zone ranged from about 2×10^{-3} to 9×10^{-5} centimeters per second (cm/s) (fig. 17). However, the hydraulic-conductivity value measured for the deepest sample collected at the downstream site (LQSW) was about 4×10^{-6}cm/s, a value similar to that for the buried soil layers encountered beneath other streambeds in the Mojave Desert as reported by Izbicki and others (2000b, 2002) (fig. 17). The small range in hydraulic conductivity values reflects the homogeneous nature of the deposits and the lack of alteration by soil development during deposition. Physical and thermal properties of water and soil are reported in metric units for consistency with data from previously reported studies.

The volumetric water content ranged from 0.02 to 0.19 (fig. 18). The lowest water contents were from the control site, QSWC, away from Quail Wash. The highest water contents were from the downstream site LQSW. Water-content data at site MQSW showed slightly drier conditions than data measured at site LQSW. Water-content data at site UQSW were similar to data measured at the control site. Water-content data at sites beneath streambeds were similar to water-content data collected beneath streambeds and control sites elsewhere in the Mojave Desert, as reported by Izbicki and others (2000b and 2002).

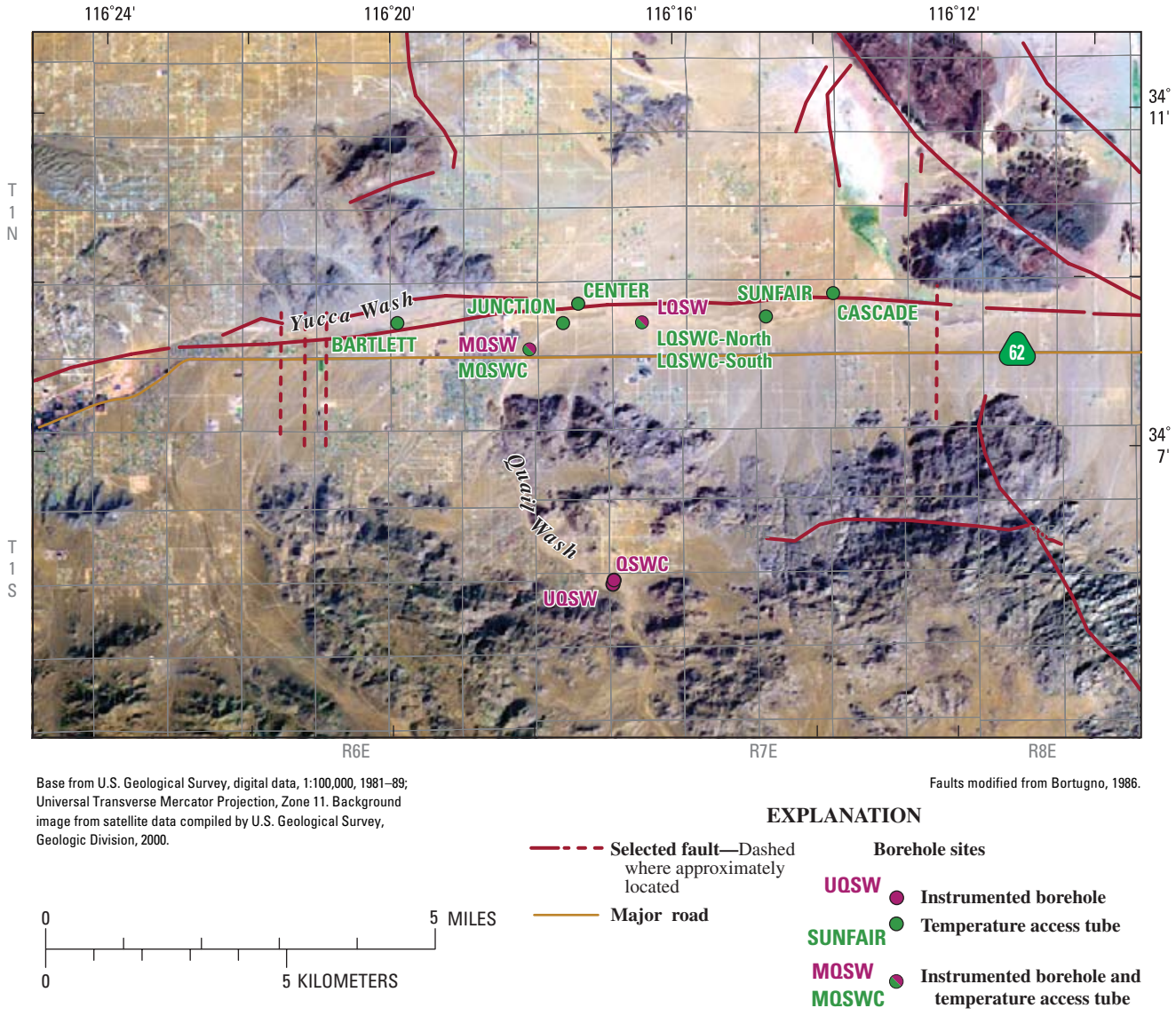

Figure 16. Locations of instrumented borehole sites, temperature-access tubes, and infiltration tests near Joshua Tree, San Bernardino County, California.

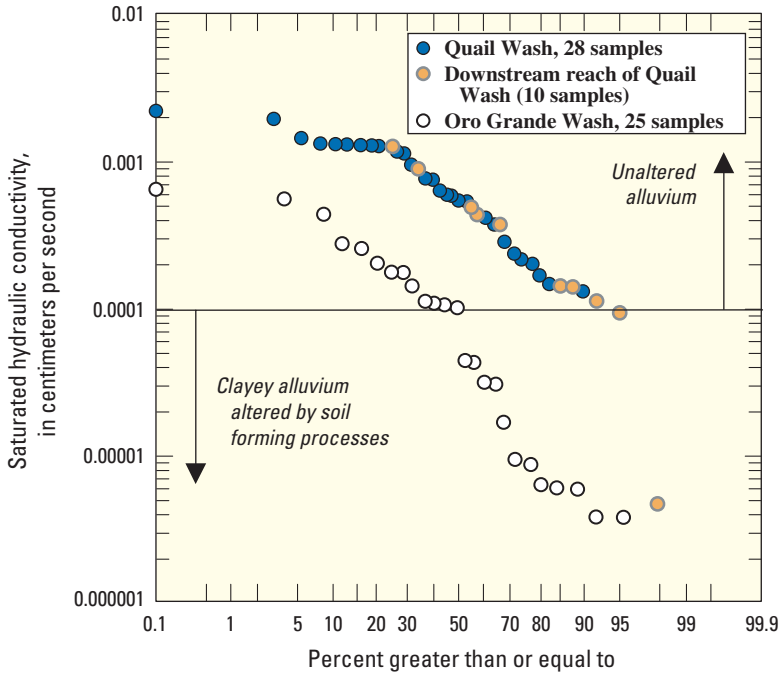

Figure 17. Saturated hydraulic conductivity for unsaturated material beneath Quail Wash near Joshua Tree, San Bernardino County, California.

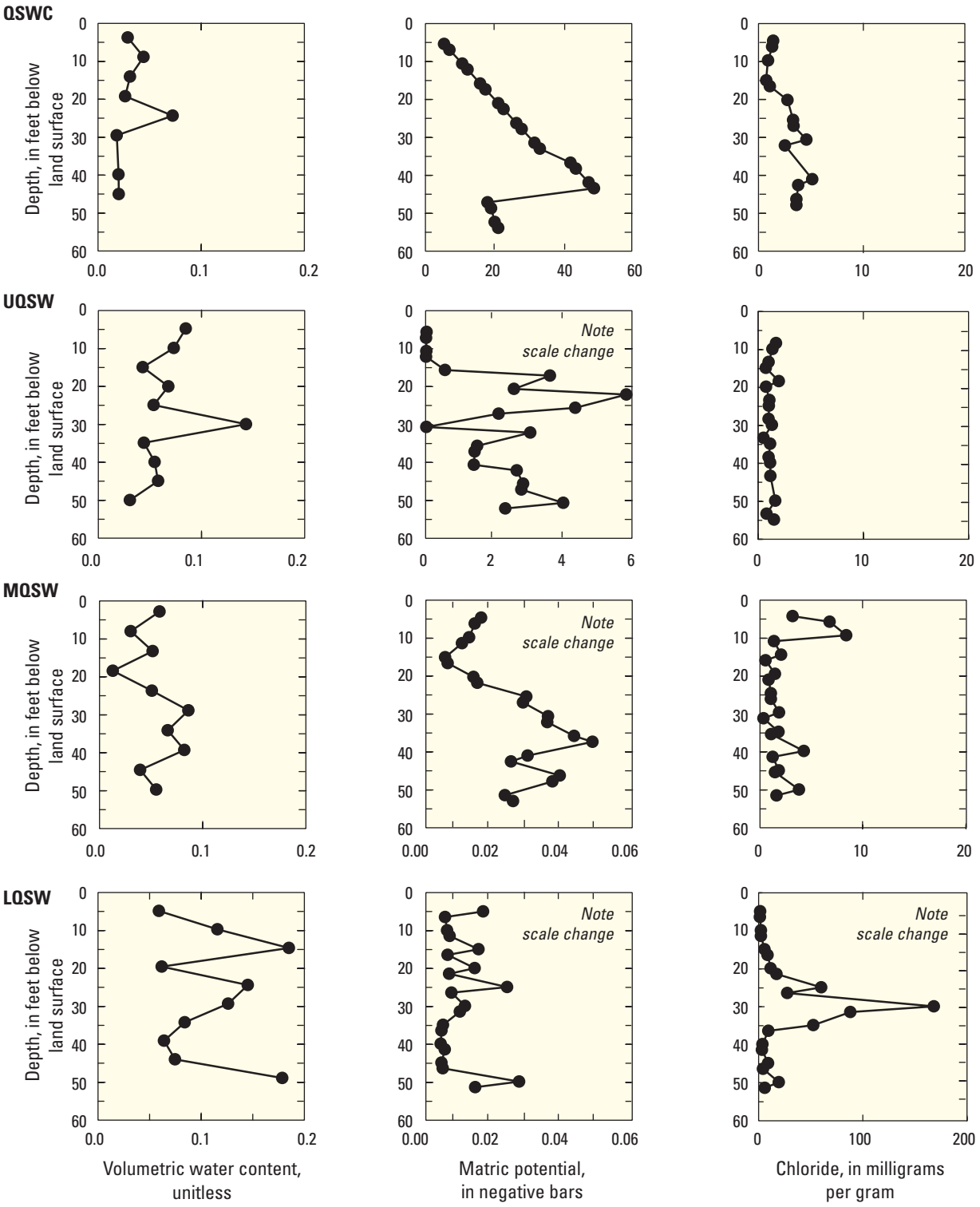

Figure 18. Water content, matric potential, and chloride data for unsaturated material at instrumented borehole sites QSWC, UQSW, MQSW, and LQSW, near Joshua Tree, San Bernardino County, California.

Matric potential, a measure of how tightly the water is held within the alluvium, ranged from −46 to greater than −0.01 bars (fig. 18). The more negative values were obtained from samples from the very dry alluvium at the control site, site QSWC, and the less negative values were obtained from samples from the downstream site, site LQSW. Matric-potential data collected from site MQSW are similar to those from site LQSW, although the matric potentials measured below a depth of about 20 ft are more negative. Matric-potential data collected from UQSW are similar to those obtained at sites LQSW and MQSW to a depth of about 15 ft. Below that depth, matric-potential values are more similar to those obtained at the nearby control site, with the exception of less negative values from about 30 ft bls (fig. 18).

Matric-potential values for samples collected beneath Quail Wash were similar to data collected by Izbicki and others (2000b, 2002) beneath streambeds elsewhere in the Mojave Desert where small amounts of natural recharge have been shown to occur under present-day climatic conditions. Matric-potential data at the control site indicated wetter conditions and were more than an order of magnitude less negative than matric-potential data collected by Izbicki and others (2000b, 2002) at sites away from streambeds elsewhere in the Mojave Desert and at similar sites in alluvial valleys throughout the desert areas of the southwestern United States as reported by Prudic (1994) and Phillips (1994). This difference may result from the location of the control site at a higher altitude near the mountain front.

The movement of liquid water in unsaturated porous material is governed by total potential gradient. Total potential is calculated as the sum of matric potential, expressed as head in units of length, and the height above an arbitrary datum, such as the water table (Jury and others, 1991). Matric-potential data measured using the filter-paper method do not incorporate solute (osmotic) effects. Solute effects are important in arid areas where soluble salts have accumulated in very dry unsaturated material, but usually are not important in wetter material common beneath streambeds (Izbicki and others, 2000b; 2002); therefore, these effects were neglected in this study. Assuming an arbitrary datum near the water table, about 400 ft bls (the depth to water at site UQSW and the control site, QSWC, is not precisely known), total-potential data are positive and consistent with gravity drainage of water through the unsaturated zone. Total-potential data from sites LQSW, MQSW, and the upper 15 ft of site UQSW approach a unit gradient with depth and appear to be draining readily under the influence of gravity.

Analysis of Chloride Data

Chloride is readily dissolved and moves with infiltrating water because it is conservative, nonvolatile, and nonreactive with aquifer materials. Consequently, chloride concentrations in the unsaturated zone are used to provide estimates of the long-term downward water flux in arid areas (Phillips, 1994). Assuming that atmospheric deposition (precipitation plus dry fallout) is the only source of chloride, low chloride concentrations in the unsaturated zone are consistent with rapid movement of water through the unsaturated zone. High concentrations are consistent with little or no movement of water through the unsaturated zone and the accumulation of chloride and other soluble salts over long periods of time.

Chloride concentrations in the unsaturated zone beneath Quail Wash ranged from less than 1 to about 170 milligrams per gram (mg/g) of alluvium. The highest concentrations were in site LQSW about 30 ft bls (fig. 18). Chloride concentrations at all sites, with the exception of site LQSW, did not exceed 10 mg/g.

The chloride concentrations in the unsaturated zone underlying the control site, QSWC, are much lower than concentrations reported at similar sites elsewhere in the Mojave Desert (Izbicki and others, 2000b) and in the arid southwestern United States (Phillips, 1994; Prudic, 1994). The low concentrations suggest that water has infiltrated through the unsaturated zone at the site in the recent geologic past and flushed the chlorides. Assuming an atmospheric deposition rate of 10 milligrams per square centimeter per year ($mg/cm^2/yr$) (Phillips, 1994), chloride may have been accumulating in the upper 50 ft of the unsaturated material underlying site QSWC for fewer than 800 years. This is much less than the 10,000 to 12,000 years of chloride accumulation estimated for similar sites in the Mojave Desert (Izbicki and others, 2000b, 2002) and the arid southwestern United States (Prudic, 1994; Phillips, 1994). It is possible that the infiltration of direct precipitation during wetter climatic periods may have resulted in the lower chloride concentrations measured below the root zone at this location. Another possible explanation is that Quail Wash may have followed a different course in the past, wetting the unsaturated zone beneath the QSWC site.

The chloride concentrations and the shape and depth of the chloride profile at site LQSW are consistent with data reported from other sites in the Mojave Desert (Izbicki and others, 2000b) and arid southwestern United States where infiltration to depths below the root zone does not occur under present-day climatic conditions (Phillips, 1994; Prudic, 1994). Assuming an atmospheric deposition rate of 10 mg/cm^2/yr (Phillips, 1994), chloride may have been accumulating in the upper 50 ft of the unsaturated material underlying site LQSW for almost 7,000 years. However, water-content and matric-potential data suggest that the unsaturated zone at this site is wet and water should move downward transporting soluble salts, such as chloride. This discrepancy can be possible only if the unsaturated zone at site LQSW was recently wetted by infiltration of streamflow from the wash. This site is the farthest from the mountain front, and the channel in this reach, which has a slope of only about 0.3 percent, meanders across the valley floor. It is possible that the stream channel may change course as streamflow erodes the channel banks. This was demonstrated in summer 2003 when a large flow eroded the bank and destroyed instrument shelters located about 20 ft from the channel. The potential for ground-water recharge from intermittent streams is enhanced in areas where the stream channel wets the same area repeatedly year after year and replenishes water in the unsaturated zone. Geomorphic processes that lead to channel migration and abandonment may not allow infrequent streamflows to wet the unsaturated zone for a long enough period of time to permit water movement to a water table several hundred feet bls (Izbicki and others, 2002).

Analysis of Temperature and Matric-Potential Data

Continuous temperature and matric-potential data were collected from the instrumented boreholes to determine annual variations in temperature at measurement depths and changes in matric potential as a result of infiltration of streamflow (fig. 19). Large changes in temperature and matric potential were measured as a result of infiltrometer tests completed as part of this study; results of those tests are discussed in the "Analysis of Infiltrometer Tests" section of this report. Temperature profiles were collected on a periodic basis from the temperature-access tubes within the instrumented boreholes (fig. 20).

Continuous Data from Instrumented Sites

Continuous temperature and matric-potential data collected from the instrumented boreholes beneath Quail Wash (UQSW, MQSW, and LQSW, and the control site, QSWC) are shown in figure 19 for the data-collection period of January 2001 to July 2003. In addition, precipitation data for one site in the town of Yucca Valley (fig. 2) is also shown in figure 19 to illustrate periods of possible infiltration.

Precipitation data show that is was drier than average during the data-collection period—especially during 2002. However, winter storms occurred on January 10, 2001; between February 25 and March 9, 2001; March 15, 2002; January 10, 2003; February 11–12, 2003; February 25, 2003; and March 15–18, 2003. Large summer storms did not occur during the data-collection period; however, a series of large summer storms in August 2000 and August 2003 just before and after the period of record resulted in destructive flows along Quail Wash. The August 2003 streamflows destroyed instrumentation in vaults at sites LQSW and MQSW.

At sites UQSW, MQSW, and LQSW, matric potential measured between January 2001 and July 2003 ranged from less negative than the entry pressure for the ceramic material of the heat-dissipation sensor, about −0.07 bars, to more negative than −150 bars (fig. 19). Matric-potential data changed annually near the surface, as a result of evaporative or transpirative water losses during the summer months, and infiltration of water after precipitation or streamflow during the winter months (fig. 19). The wetting and drying of near-surface streambed material produced wide variation in matric-potential data, which ranged over several orders of magnitude at some sites. Annual variations in matric potential dampened to more constant values with increasing depth. The most negative matric potentials at all sites beneath Quail Wash were measured at instruments 5 ft below the streambed during the summer months (fig. 19*B–D*).

Matric potentials were less negative at the downstream site, LQSW, and more negative at the upstream site, UQSW. These data suggest that larger quantities of water have infiltrated along the downstream reach of Quail Wash than along the upstream reach. One would expect that there would be greater infiltration in the upstream reach than in the downstream reach under natural predevelopment conditions. The larger quantities of infiltration along the downstream reach of Quail Wash may be the result of increased runoff from urban areas in the town of Yucca Valley and the community of Joshua Tree.

The relation between water content and matric potential is highly nonlinear. Small changes in water content at very dry sites may result in large changes in matric potential, whereas similar changes in water content at wetter sites may result in a small or negligible change in matric potential. Therefore, dry sites may have larger changes in matric potential as a result of infiltration than do wetter sites that may actually receive greater amounts of water.

Changes in matric potential with depth resulting from infiltration of streamflow are delayed in time and attenuated with depth (fig. 19*B–D*) as water moves downward through the unsaturated zone. As a result, at some sites it was possible to measure the cumulative effect of seasonal infiltration beneath the streambed in terms of matric potential but more difficult to identify the stormflow that produced the infiltrated water.

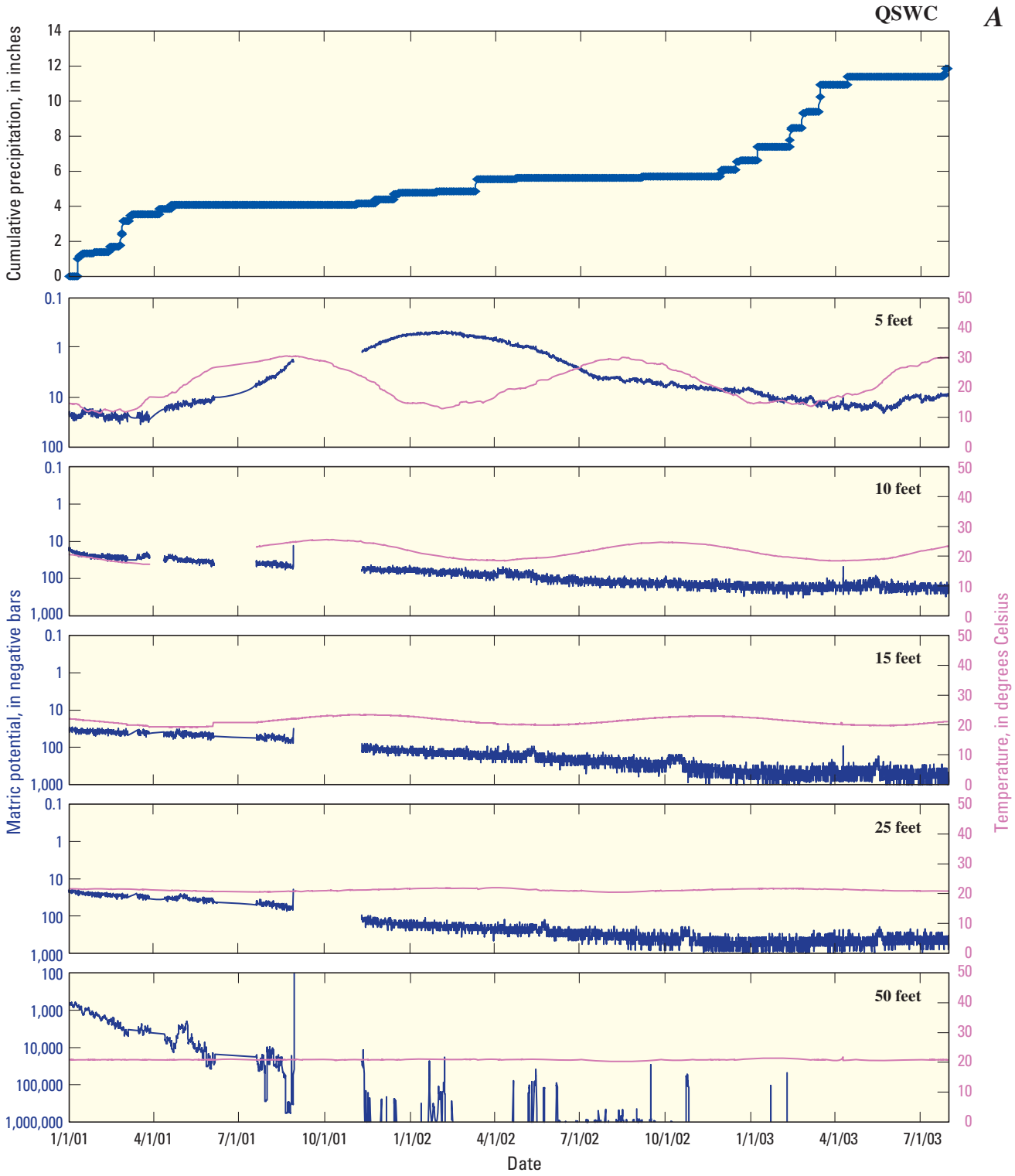

Figure 19. Cumulative precipitation measured at Yucca Valley, matric potential, and temperature at instrumented borehole sites (*A*) QSWC, (*B*) UQSW, (*C*) MQSW, and (*D*) LQSW, near Joshua Tree, San Bernardino County, California.

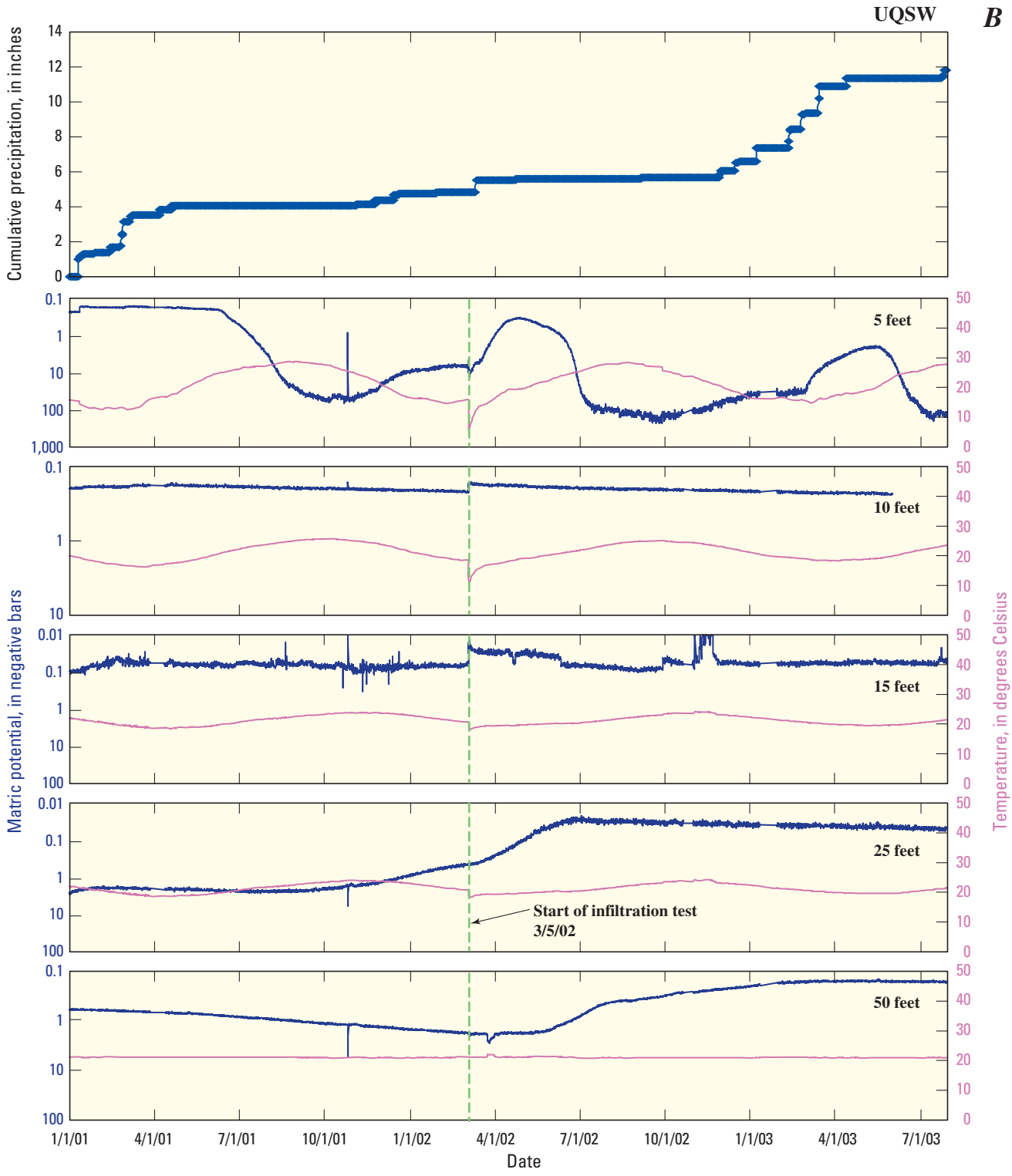

Figure 19.—Continued.

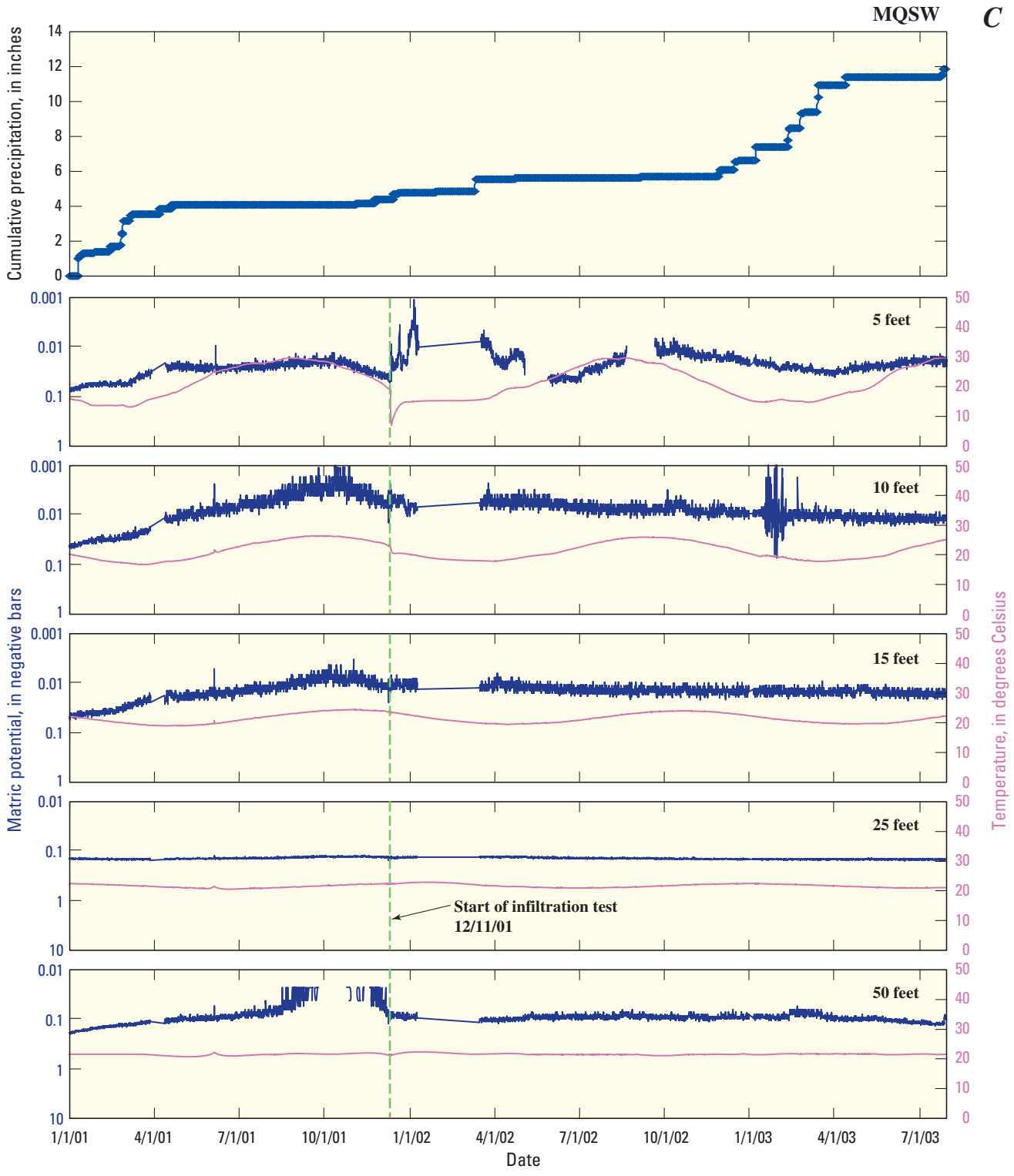

Figure 19.—Continued.

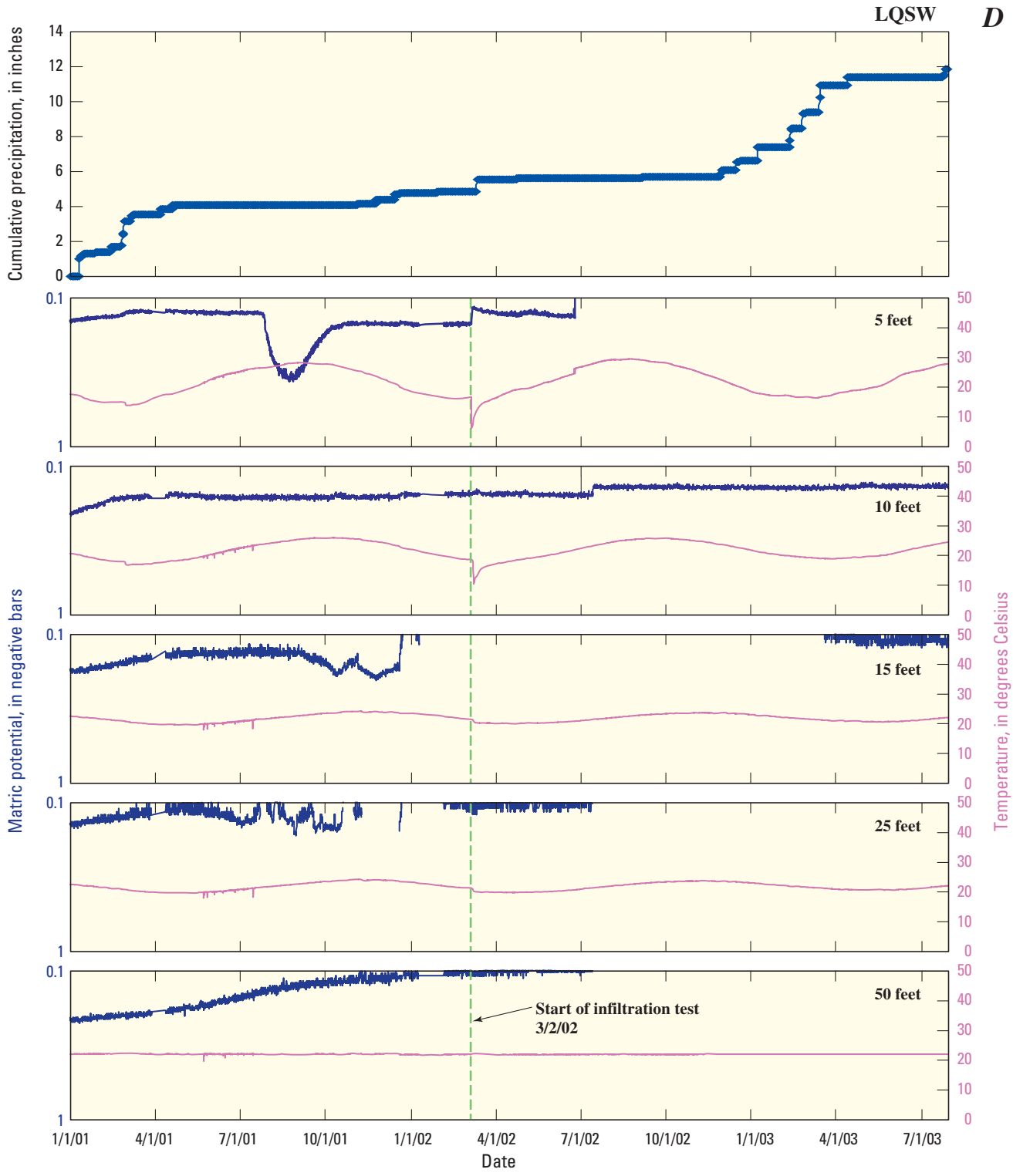

Figure 19.—Continued.

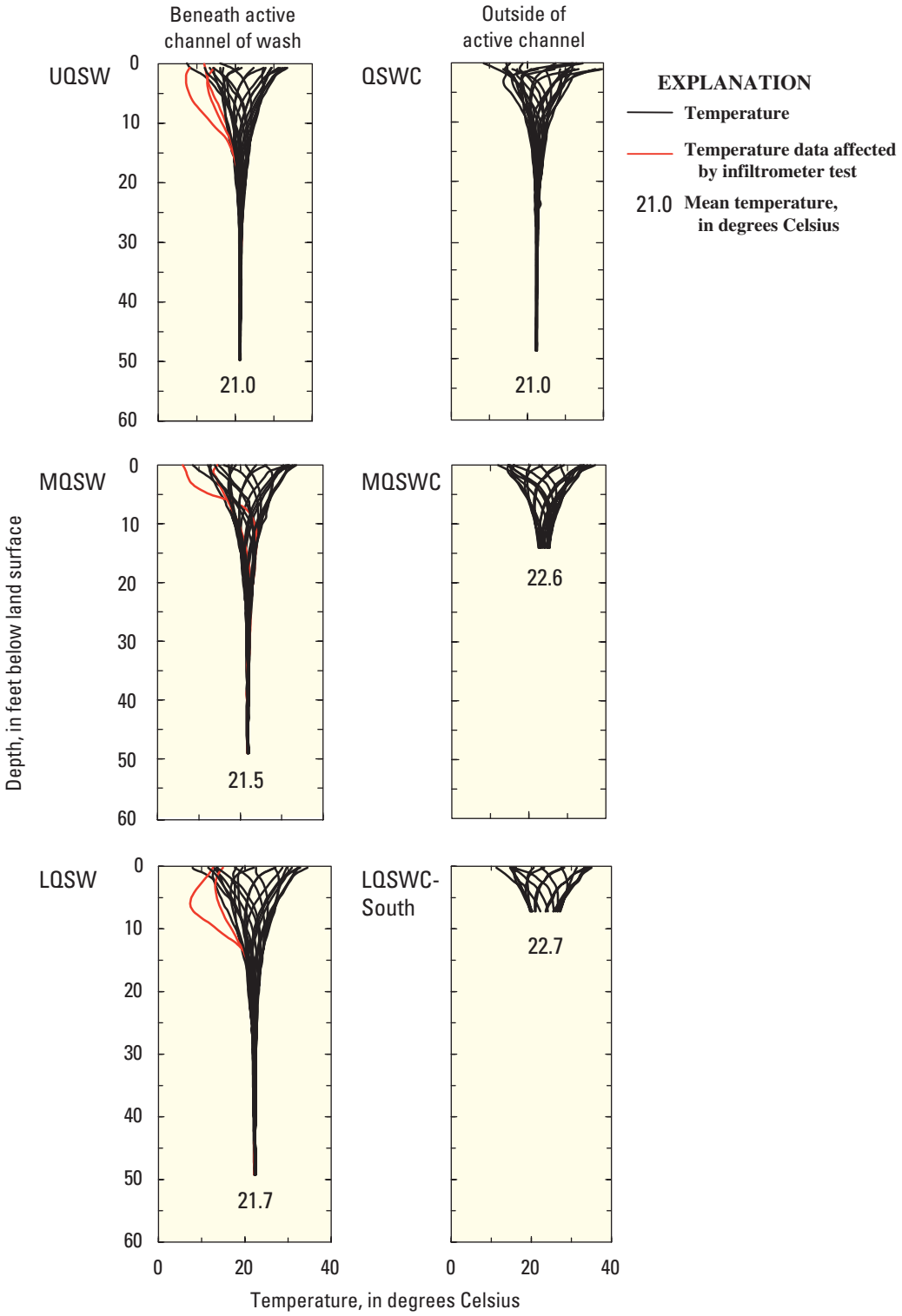

Figure 20. Temperature with depth and average temperature at instrumented borehole sites QSWC, UQSW, MQSW, and LQSW and temperature-access tube sites MQWSC and LSWC-south, near Joshua Tree, San Bernardino County, California, January 2001–July 2003.

Small changes in matric potential at 5 ft occurred at the control site, QSWC, as a result of the larger storms (fig. 19*A*). In general, water did not penetrate to depths below 5 ft and the alluvium below these depths became progressively drier during this study, eventually exceeding –10,000 bars. Decreases in matric potential (increasingly larger negative values) occurring at site QSWC suggest that a small amount of water was draining from the subsurface during this study. This could only occur if at some time in the recent past water infiltrated to depths below the root zone as a result of an infrequent large storm. The amount of water that actually drains to depths below the root zone at this site is too small to be significant for water supply. Decreases in matric potential also may be related to a gradual equilibration of the instruments to the very dry unsaturated material at this site. However, most of the equilibration occurred within the first three months of instrument installation (not shown in fig. 19*A*) and this type of delayed equilibration has not been observed at similarly dry sites elsewhere in the Mojave Desert.

Temperature data collected at the control site QSWC and sites UQSW, MQSW, and LQSW show broad annual cycles that decrease in amplitude with increasing depth (fig. 19). The occurrence and magnitude of the annual maximum and minimum temperature are progressively lagged and attenuated with increasing depth. This phenomenon is well documented in unsaturated porous material (Jury and others, 1991) and is used later in this paper to estimate thermal properties of alluvium.

Constantz and Thomas (1996, 1997) used temperature changes in streambeds to determine the onset, duration, and cessation of streamflow in arid areas. In general, changes in temperature after precipitation measured by instruments in the streambed at sites LQSW, MQSW, and UQSW were small and similar in magnitude to temperature changes measured at the control site. However, temperature changes as large as 1°C were measured by heat-dissipation sensors 5 ft below the surface of the streambed at site LQSW after the January 10 and February 25, 2001, and February 11–12, 2003, storms (fig. 19*D*). At site LQSW, temperature changes after the February 25, 2001, storm were recorded on instruments as deep as 15 ft below the streambed. Observations of the stream channel and anecdotal data provided by local residents confirm streamflow along this reach after these storms.

Temperature Data from Access Tubes

Temperature data collected at 6-week intervals from access tubes at instrumented boreholes in Quail Wash at sites UQSW, MQSW, and LQSW and at the control site, QSWC, are shown in figure 20. Temperature data also were collected at the same 6-week interval from temperature access tubes installed at the control sites MQSWC and LQSWC-south (fig. 20). Note that the mean temperatures for all the sites also are presented in figure 20.

Temperature was measured at 1-ft intervals within the access tubes at the instrumented boreholes and the temperature-access tubes using a thermistor having a precision of ± 0.1°C. The same thermistor was used throughout the study to minimize instrument variability. Temperature was measured from the bottom of the access tube toward the surface, and air flow was minimized through the access tube during measurements by covering the top of the access tube with a cloth. The temperature near the bottom of the access tube is less variable throughout the year than temperatures near the top of the access tube, and the temperature from access tubes at depths greater than about 30 ft is constant. Thus, measurements from each access tube had about the same initial temperature, minimizing the effect of changing surface temperatures on the measurements. After lowering the thermistor to the bottom of the access tube, the thermistor was allowed to equilibrate for 1 hour prior to collecting data. At deeper depths, 1 minute was required for the thermistor to equilibrate between measurement intervals. At shallower depths near land surface, as much as 15 minutes were required for the thermistor to equilibrate between measurement intervals. Temperature data collected from access tubes at the instrumented boreholes agreed with temperature data collected from heat-dissipation sensors; the mean-square error (MSE) was ± 0.025°C (Izbicki and Michel, 2002).

Near-surface temperatures measured in access tubes within 1 ft of land surface ranged from about 5 to 36°C (fig. 20) and were warmer during the summer and cooler during the winter. Temperatures converged to an average value with increasing depth and showed little seasonal variation below depths of about 30 ft (fig. 20). The control sites LQSWC-south and MQSWC are not as deep as the other sites; however, the average temperature at control site QSWC differed by only 0.1°C for the intervals 0 to 9 ft (the measurement interval at site LQSWC-south), 0 to 15 ft (the measurement interval at site MQSWC), and 0 to 30 ft (the measurement interval at site QSWC)—suggesting that average temperatures from different intervals are comparable. At the control sites, average temperatures from different intervals are comparable. The average temperature is inversely related to altitude of the site, increasing from 21.0°C at site UQSW (highest altitude) to 21.7°C at site LQSW (lowest altitude). Average annual temperatures at the sites beneath the active channel of the wash are inversely related to altitude in a manner similar to the control site, but also are related to the infiltration of streamflow during winter months.

Izbicki and Michel (2002) showed that in areas having winter-dominated precipitation regimes, winter streamflows result in a measurable difference between temperature measured in the unsaturated zone beneath intermittent stream channels and temperature measured at unsaturated-zone sites away from the channel. During this study, an average temperature difference of about 1°C was measured at sites MQSW and LQSW, and their respective control sites (fig. 20). The average temperature difference was within the measurement error of ± 0.1°C at site UQSW and its control site, QSWC (fig. 20). These data indicate that streamflow and subsequent infiltration were greater along the downstream reaches represented by sites MQSW and LQSW and less along the upstream reach near the mountain front represented by site UQSW. Increased streamflow at sites MQSW and LQSW may result from winter runoff from urbanized areas in Joshua Tree and Yucca Valley. The difference in temperature at sites beneath and away from the wash was used to estimate infiltration from streamflow in the "Estimation of Infiltration and Ground-Water Recharge" section of this report.

Analysis of Infiltrometer Tests

A 4-ft-diameter double-ring infiltrometer, having a 2-ft-diameter inner ring, was used to measure the maximum rate that water, if available, could infiltrate into the streambed. The average annual infiltration rate is less than the maximum infiltration rate because water is only infrequently available and the physical properties of the streambed, with respect to infiltration, may change between flowing and standing conditions. Data from the infiltrometer tests were also used to determine the response of instruments within boreholes to infiltration. Infiltration tests were performed along Quail and Yucca Washes at sites UQSW, MQSW, and LQSW on March 2002, December 2001, and March 2002, respectively. Tests in the washes were about 3 hours in duration. A constant head of about 1 ft was maintained in the infiltrometer during each test and the volume of water applied to both the inner and outer ring was monitored; about 1,000 gallons (gal) of water was infiltrated in the streambed during each test (fig 21*A*). To provide a strong temperature signal similar in magnitude to winter stormflows (Izbicki and Michel, 2002), the infiltrating water was chilled during the tests using a combination of water ice and dry ice (fig. 21*B*). The mass of water ice was included when calculating the total amount of water infiltrated. Dry ice was not introduced directly to the water; instead, heat exchangers were used to chill the water prior to infiltration. At the end of each test, changes in head in the infiltrometer were measured as water drained into the streambed (fig. 21*C*).

Infiltration tests also were done at selected sites on the alluvial fan away from the active channel of the wash near sites UQSW (but not at the control site QSWC), MQSW, and LQSW (note, the exact locations of the infiltration-test sites are not shown in figure 16). These tests were about 1–3 hours in duration. The water was not chilled during the tests because the tests were not done over instrumented boreholes; however, the temperature of the infiltrating water was monitored.

The results from the infiltration tests and the best-fit linear relation where the slope reflects the maximum infiltration rate are shown in figure 22. Estimated maximum infiltration rates of water beneath the active channel sites ranged from 2.0 to 3.4 feet per hour (ft/hr) (fig. 22). Infiltration data collected at most sites were slightly nonlinear—estimated rates were lower at the beginning of the test and increased as the water content of the unsaturated material beneath the infiltrometer increased. However, the effect was small and a linear approximation was used to estimate the overall infiltration rate during the test. Estimated infiltration rates were higher at site UQSW near the mountain front, and lower at sites MQSW and LQSW. The decrease in estimated infiltration rate at site MQSW may be explained by a change in the active channel at that site. The active channel of Quail Wash at site MQSW is controlled by a levee for flood control and is not located where the natural channel flowed under predevelopment conditions. Estimated maximum infiltration rates at sites away from the active channel of the wash ranged from 1.5 to 2.8 ft/hr and were generally lower than rates measured at the same location in the active channel. It is likely that infiltration rates through the alluvial deposits decrease to lower values away from the wash toward Coyote Lake.

Temperature profiles collected at 1-week intervals for 3 weeks from the temperature-access tubes within the instrumented borehole sites after the infiltrometer tests at the instrumented sites (UQSW, MQSW, and LQSW) in the active-channel are shown in red on figure 20.

Data collected from the instrumented boreholes during the infiltrometer tests indicated that temperature decreased and matric potential became less negative beneath the streambed as water infiltrated into the subsurface during the tests (figs. 19*B–D*). At site MQSW, temperature changes were as large as 10°C, 5 ft below the streambed surface, and changes were measurable to depths of about 15 ft within 10 days of the test (fig. 23). Matric-potential changes were measurable immediately at the 5-ft depth (fig. 23). Changes in matric potential resulting from infiltration of water applied during the infiltrometer tests were large in magnitude in comparison with changes resulting from infiltration of natural streamflow and were easily identified as the water moved downward through the unsaturated zone underlying the streambed (fig. 19*A*). The data show that the instruments are capable of measuring changes associated with infiltration of winter streamflows similar in duration to the infiltration tests. Because the temperature and volume of water infiltrated during the tests are known, the data provide a benchmark from which to evaluate measured changes in temperature and matric potential at the instrumented boreholes along Quail Wash.

Figure 21. Double-ring infiltrometer test on Quail Wash (*A*) water tanks maintaining constant head, (*B*) chilled infiltrating water, and (*C*) measuring falling head at the end of the test, near Joshua Tree, San Bernardino County, California, December 2001.

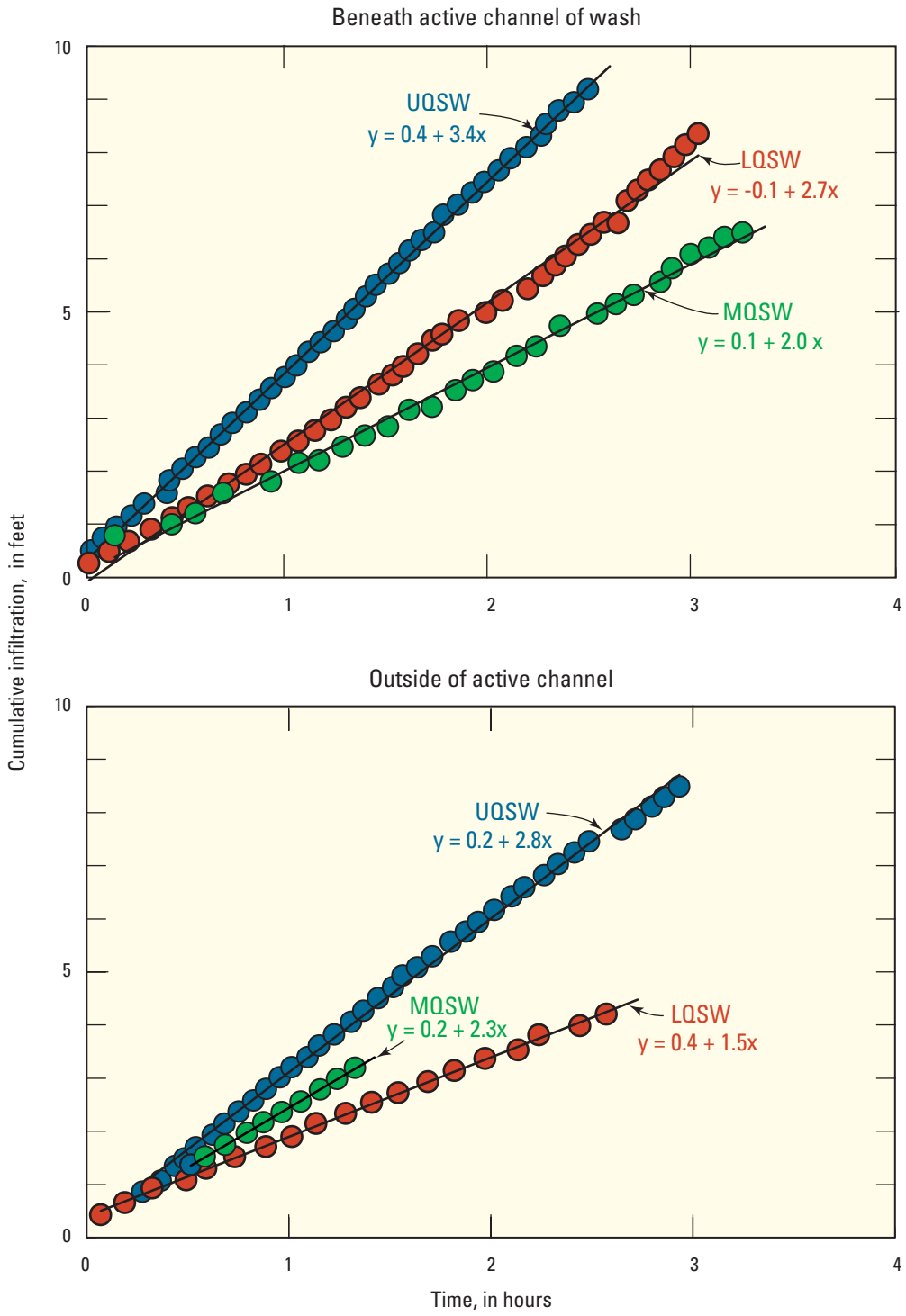

Figure 22. Infiltration at selected sites along Quail Wash with best-fit linear relation, near Joshua Tree, San Bernardino County, California.

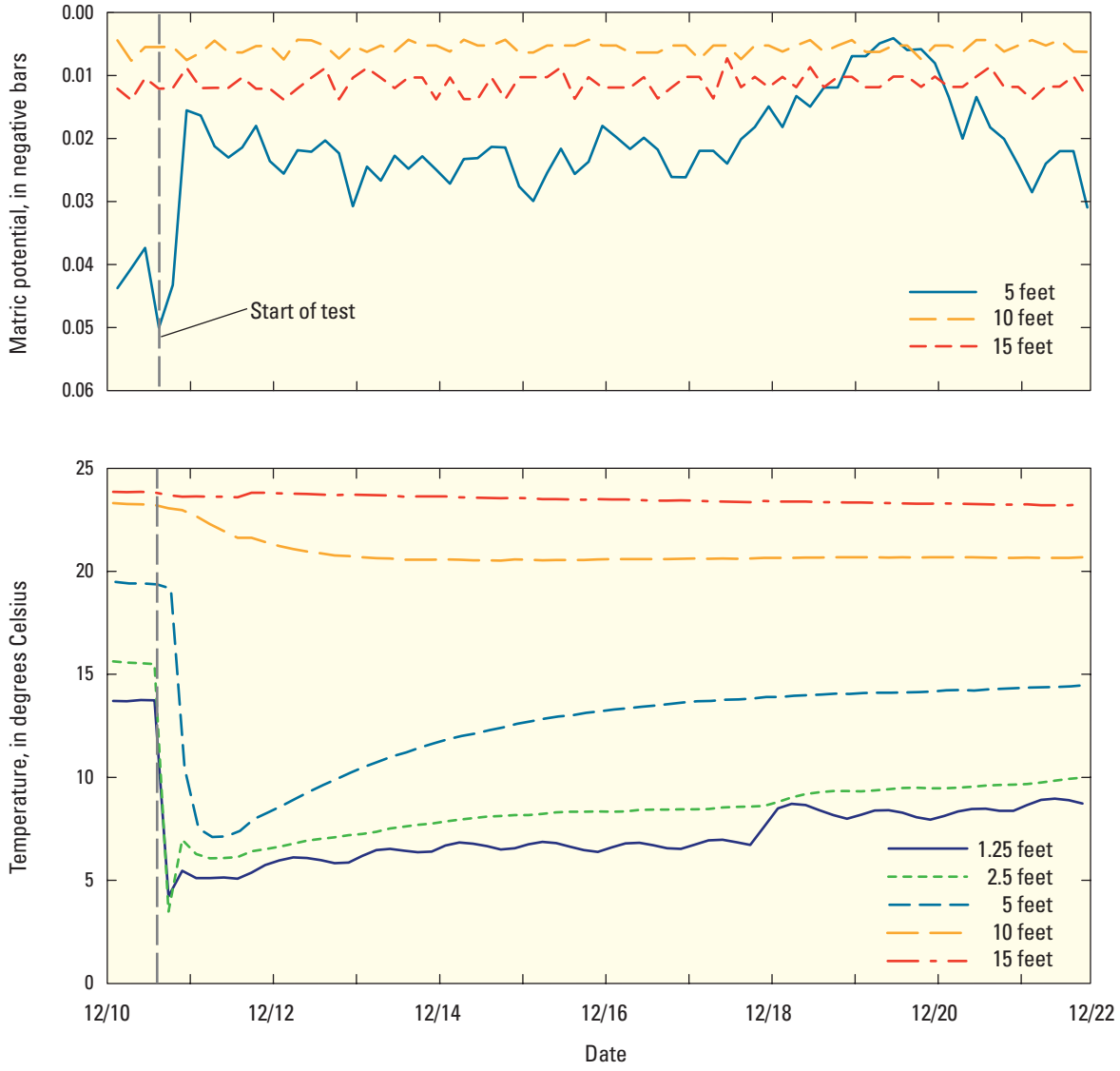

Figure 23. Temperature and matric-potential data at site MQSW after infiltration of water using a double-ring infiltrometer, Quail Wash, near Joshua Tree, San Bernardino County, California, December 6–16, 2001.

The measured changes in matric potential and temperature after the infiltration tests approximate the expected changes in these properties resulting from a single winter stormflow of duration 2.5 to 3.5 hours. The infiltration at each site was about 10 ft during the infiltration test. The measured signals are what one would expect if 60 acre-ft infiltrated along 12 miles of Quail and Yucca Washes in 3 hours (assuming a 4-ft wetted channel, which was the diameter of the double-ring infiltrometer). Examination of the data collected at sites UQSW, MQSW, and LQSW between January 2001 and July 2004 do not show changes in matric potential or temperature consistent with the infiltration test results (fig. 19*B–D*) suggesting that infiltration of this magnitude did not occur during this study.

Estimation of Infiltration and Ground-Water Recharge

The difference in temperature between the unsaturated zone beneath Quail Wash and the unsaturated zone away from the active channel of the wash was used to estimate average annual infiltration along stream reaches in the study area. The approach works well in areas where precipitation and subsequent runoff occurs primarily during the winter. The approach may underestimate infiltration in areas where large amounts of precipitation and subsequent runoff occur during the summer (Izbicki and Michel, 2002).

The computer program VS2DH (Healy and Ronan, 1996) was used to estimate temperature in unsaturated material beneath a wash and unsaturated material away from a wash given different amounts of streamflow infiltrated from the wash. The program uses a finite-difference approximation to solve equations that describe the coupled advective transport of water and heat, and the conductive transport of heat in variably saturated porous media. The simulated results were compared to measured data at sites LQSW and MQSW, and their respective controls to estimate infiltration from streamflow at those sites.

A two-dimensional, axially symmetric finite-difference grid was used for the simulations. The grid represents one-half of a perpendicular cross section through the stream channel and contains 23 active cells in the X-direction (length), 55 active cells in the Z-direction (depth), and 1 active cell in the Y-direction (width) (table 5). The horizontal cell dimension is 1.2 m. The vertical cell dimensions vary with depth; from top to bottom cells 1–20 are 1.0 m, cells 21–40 vary uniformly from 1.0–4.0 m, and cells 41–55 are 4.0 m. The horizontal dimension in the model was chosen such that the vertical boundary conditions did not affect the simulation in the area of interest near the stream channel. The distance between the instrumented boreholes within the stream channel and the temperature access tubes away from the stream channel is within the model grid. The stream was simulated as a specified flux through two nodes in the upper left of the model grid (table 5). The temperature of the infiltrating water was estimated from winter streambed-temperature data measured about 0.3 ft bls and was specified at 10°C. The volume of infiltrating water was adjusted over a range of specified fluxes. The temperature at the upper boundary was specified at 22°C on the basis of the water temperature from shallow wells sampled in the study area. The water table was used as the bottom boundary condition. No-flow and no-energy transport boundaries were specified as the vertical boundary conditions.

The hydraulic properties of the unsaturated material, including saturated hydraulic conductivity and porosity were measured. Residual moisture content was estimated from laboratory physical-property data as the moisture content of the drier core material. The thermal properties of the unsaturated material, including thermal conductivity and thermal diffusivity, were estimated from the damping of the amplitude of annual temperature data measured in the access tubes with depth using methods described by Jury and others (1991). The heat capacity of dry alluvium was calculated from measured bulk-density data using literature-derived values for water and mineral constituents (Jury and others, 1991). The contribution of organic material to the heat capacity was assumed to be small and the heat capacity of air was neglected. Vertical to horizontal anisotropy, specific storage, longitudinal and transverse dispersivity, the van Genuchten parameters (alpha and beta) were assigned from literature values (Freeze and Cherry, 1979; Hillel, 1982; Carsel and Parrish, 1988; Jury and others, 1991). The estimates of physical and thermal-property data used to estimate infiltration are given in table 5.

Initial conditions were intended to duplicate temperature and moisture conditions that approximate natural conditions in the unsaturated zone beneath and adjacent to the stream channel. To establish average moisture and temperature conditions for each recharge rate, 10 years were simulated with an average annual recharge rate and average annual temperature specified in the stream channel and along the upper boundary, respectively. To establish monthly variations in moisture and temperature conditions for each recharge rate, the model was run for an additional 5 years with the recharge applied during the 15th day of the wettest month (February). No recharge was applied during the remaining 11 months. For the purposes of the model simulations, a year began with the establishment of near isothermal conditions in the unsaturated zone during spring (April) to the next spring (March). This approximates the climatalogical year rather than the calendar or water year. Temperature along the upper boundary was set equal to the temperature measured in the unsaturated zone 1 ft bls at the control site. The average of all the monthly temperatures equaled the average annual temperature used to establish average temperature conditions within the model. It is unlikely that this procedure resulted in moisture and temperature conditions that approximated the natural system throughout the model domain, but it was believed that this procedure established conditions that closely approximated natural conditions at the depths where data were collected.

Table 5. Physical and thermal properties used to estimate infiltration at selected sites along Quail Wash, near Joshua Tree, California

[m, meter; °C, degrees Celsius; m^3, cubic meter; sec, second; J, Joules]

Parameter	Parameter value	Units
Physical and hydraulic properties		
Saturated hydraulic conductivity	3.91×10^{-6}	m/s
van Genuchten parameters		
Alpha	4.31	1/m
Beta	3.1	Unitless
Residual moisture content	.008	Unitless
Anisotropy	1	Unitless
Porosity	.33	Unitless
Longitudinal and transverse dispersivity	.5	m
Thermal properties		
Heat capacity of dry alluvium	1.033×10^6	$J/m^3/°C$
Heat capacity of water	4.187×10^6	$J/m^3/°C$
Thermal conductivity of dry alluvium	2.52×10^{-1}	J/m/sec/°C
Thermal conductivity of saturated alluvium	8.41×10^{-1}	J/m/sec/°C
Space discretization		
Number of rows	55	
Length of rows	1.0 (cells 1–20), 1.0–4.0 (cells 21–40), 4.0 (cells 41–55)	m
Number of columns	23	
Length of columns	1.2	m
Model dimensions (length × width × depth)	$113 \times 27.6 \times 1$	m
Initial conditions and boundary conditions		
Initial pressure	Equilibrium profile	
Initial temperature	22	°C
Upper boundary condition	Land surface	
Lower boundary condition	Water table	m
Side boundary conditions	No flow and no energy transport	
Time discretization and recharge periods		
Temporal discretization	1×10^{-3} (initial), 1×10^{-10} (minimum), 1×10^6 (maximum)	sec
Temporal discretization during recharge	1×10^{-4} (initial), 1×10^{-10} (minimum), 1×10^6 (maximum)	sec
Time step multiplier/reduction factor	1.2/0.8	
Maximum time step	1×10^6	sec
Number of recharge periods	99	
Length of recharge periods	1 (30)	month (days)
Recharge	Applied to 2 cells in upper left of model	
Recharge temperature	10	°C
Model solution parameters		
Convergence criterion for flow	1×10^{-3}	m
Convergence criterion for transport	1×10^{-3}	Unitless
Damping factor	.7	Unitless
Minimum/maximum iterations per time step	2/5,000	

The measured and simulated differences between the temperature in the unsaturated zone beneath the Quail Wash at site LQSW and its control is shown for October 2001 to September 2002 in figure 24. The measured temperature difference converges to about 0.5°C with depth, which corresponds to the temperature difference expected given an average infiltration rate of about 1.3 ft/yr. The measured temperature differences at site LQSW are smaller than those shown in figure 20 because the period of record only includes data for 1 year.

Streambed infiltration along Quail Wash and Yucca Wash was calculated by multiplying the average infiltration rate of 1.3 ft/yr by the bankfull width (60 ft) and length of the washes (7,800 ft along Quail Wash downstream from Route 62 to its confluence with Yucca Wash and 36,200 ft along Yucca Wash and Quail Wash from the western boundary of the study area to Sunfair temperature access tube [fig. 16]) for a total of 71 acre-ft/yr. Infiltration along the upstream reach of Quail Wash upstream from Route 62 toward the mountain front and downstream from Sunfair toward Coyote Lake was presumed to be negligible on the basis of temperature data collected at sites UQSW and QSWC, and the presence of fine-grained deposits near the lake. Infiltration and subsequent ground-water recharge may be greater than estimated because this approach is insensitive to infiltration from summer stormflows.

Data collected as part of this study show that the amount of infiltration along Quail Wash is small—especially along upstream reaches of the wash near the mountain front. What infiltration occurs along Quail Wash occurs as a result of increased runoff downstream from urbanized areas. Not all the water that infiltrates into the streambed infiltrates to depths below the root zone and becomes ground-water recharge. Some water may be transpired by vegetation along the stream banks. In addition, along the downstream reaches of Quail Wash near site LQSW the active channel may change course across the relatively flat alluvial valley floor and may not necessarily wet the same area repeatedly year after year. Geomorphic processes that lead to channel migration and abandonment may effectively strand infiltrated water in the thick, dry, unsaturated zone underlying much of the basin. Modifications to stream channels that occur as a result of development, such as levees and other flood-control structures, act to restrict the movement of the stream channel and may, over time, enhance infiltration to depths below the root zone and ultimately increase ground-water recharge. However, previous studies of water movement through thick, unsaturated zones underlying streams in the western Mojave Desert suggest that several hundred years may be required for water to infiltrate 300 ft to the underlying water table (Izbicki and others, 2000b; 2002).

Summary of Recharge Estimates Based on Borehole Instrumentation

Stream channels in the Joshua Tree area are highly permeable, with maximum infiltration rates between 2.0 and 3.4 ft/hr. Water-content and matric-potential data collected from instrumented boreholes beneath stream channels show that the unsaturated zone beneath the stream channels is wetter than the adjacent unsaturated zone. Physical and geochemical data collected at these sites show that a small amount of infiltration occurs after streamflow within the stream channel. Some of the infiltrated water moves downward to depths below the root zone and ultimately becomes ground-water recharge. Infiltrated water is more likely to reach the water table in areas where the stream channel wets the same reach year after year. If the location of the stream channel changes, infiltrated water may not reach the aquifer several hundred feet below land surface. Chloride concentrations beneath the stream channel at site LQSW are consistent with channel abandonment and changing location of the stream channel; as a result, some water infiltrated along this reach of Quail Wash may not reach the water table. Physical and geochemical data collected away from the stream channels show that direct infiltration of precipitation to depths below the root zone and subsequent ground-water recharge likely does not occur in the Joshua Tree area.

Infiltration through stream channels in the Joshua Tree area is limited by the availability of streamflow. Precipitation was less than average during the study period and there was little runoff; however, matric-potential and temperature data collected in stream channels show that the streamflow that did occur was brief in duration and subsequent infiltration was small. Changes in matric potential and temperature resulting from streamflow were less than changes after infiltration experiments. Streamflow and subsequent infiltration were greater along reaches downstream from urbanized areas where impervious surfaces increased runoff. Differences in temperature data collected beneath the stream channel and a nearby control site suggest that average infiltration rate along a reach of Quail Wash downstream from urbanized areas in Joshua Tree and Yucca Valley was as much as 1.3 ft/yr. If one assumes that this average annual infiltration rate is representative of Yucca Wash and Quail Wash downstream of its confluence with Yucca Wash, this would amount to about 71 acre-ft/yr of streamflow infiltration. Little infiltration was recorded along upstream reaches of Quail Wash closer to the mountain front.

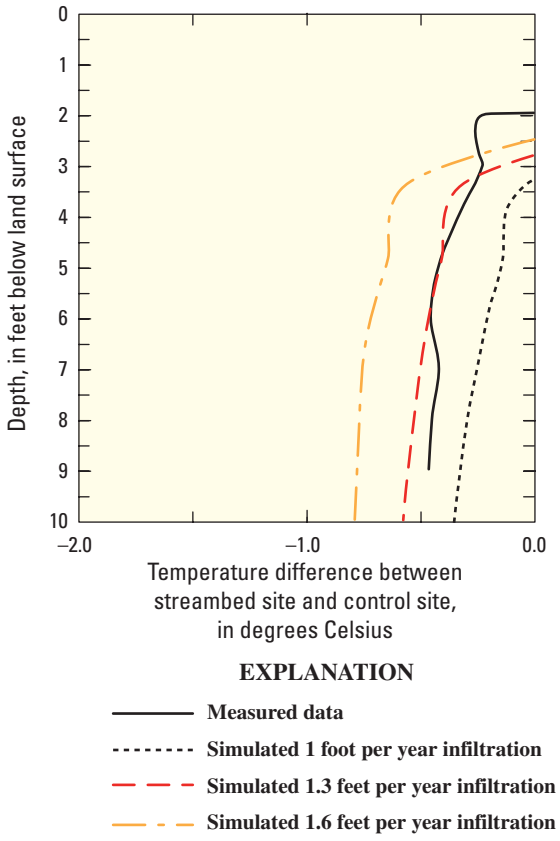

Figure 24. Measured and simulated temperature differences between site LQSW and a nearby (about 40 feet) control site LQSWC along Quail Wash, near Joshua Tree, San Bernardino County, California.

Simulated Recharge Using a Watershed Model

A deterministic, distributed-parameter, watershed-modeling approach was used to estimate the spatial and temporal distribution of naturally occurring recharge in the Joshua Tree surface-water drainage basin, which includes the Warren, Joshua Tree, and Copper Mountain ground-water subbasins. The watershed model, INFILv3, was originally developed to estimate net infiltration for the model of the Death Valley Regional Flow System (DVRFS). Net infiltration is defined as the downward drainage of water across the lower boundary of the root zone and is used to indicate potential recharge under variable climate conditions and drainage basin characteristics (Hevesi and others, 2003). Net infiltration is not necessarily equivalent to recharge because of interbasin transfer, the possible existence of transient perched zones, and processes affecting deep percolation through thick unsaturated zones. The potential for differences between net infiltration and recharge tends to increase with increased unsaturated-zone thickness, increased ground-water travel time through the unsaturated zone, increased climate variability, and increased geologic heterogeneity in the unsaturated zone. For this study, simulated net infiltration was assumed to be equivalent to the quantity of recharge in the basin.

Although uncertainty in INFILv3 model results can be high, owing to simplifying assumptions and uncertainty in model inputs, an advantage of the model (in comparison with other methods of estimating recharge, such as empirical methods or geochemistry) is that it provides a deterministic representation of the effects of climate, surface-water flow, and hydrologic processes in the upper unsaturated zone (the root zone) on the recharge estimates. In addition, the physical characteristics of the drainage basin being modeled, as defined by the topography, surficial geology, soils, and vegetation, are represented in the model. Thus, differences in the physical characteristics of the drainage basin are addressed when estimating the spatial and temporal distribution of recharge. The spatial and temporal distribution of estimated recharge can be applied to the development of transient ground-water flow models, and the effects of climate variability and changes in drainage-basin characteristics on the hydrologic system can be evaluated.

Watershed Model Description

To estimate the magnitude and distribution of recharge and surface-water runoff, in response to variable climate and drainage-basin characteristics, the INFILv3 model uses a daily water-balance model of the root zone (modeled as a variable two- to six-layered system) with a primarily deterministic representation of the processes controlling recharge. The daily water balance includes precipitation (as either rain or snow), snow accumulation, sublimation, snowmelt, infiltration into the root zone, evapotranspiration, drainage, water-content change throughout the root-zone profile, runoff (defined as excess rainfall and snowmelt) and surface water run-on (defined as runoff that is routed downstream), and recharge (simulated as drainage from the bottom root-zone layer). Potential evapotranspiration is simulated using an hourly solar radiation model to simulate daily net radiation, and daily evapotranspiration is simulated as an empirical function of root-zone water content and potential evapotranspiration. The model uses daily climate records of precipitation and air temperature from a regionally distributed network of 132 climate stations. The model also uses a spatially distributed representation of drainage-basin characteristics defined by topography, geology, soils, and vegetation to simulate daily recharge at all locations, including stream channels with intermittent streamflow in response to runoff from rain and snowmelt. The temporal distribution of daily, monthly, and annual recharge can be used to evaluate the potential effect of future climatic conditions on potential recharge. Examples of previous applications of distributed-parameter water-balance models are documented by Hatton (1998).

Calculations in the INFILv3 model are done using a grid-based representation of the drainage basin being simulated, wherein all grid cells have equal areas (here, about 885 ft by 885 ft). In areas mapped as Tertiary sedimentary and volcanic deposits and pre-Tertiary basement complex (fig. 4*A*), the root zone is represented by one to five soil layers and one underlying bedrock layer, where the number and thickness of soil layers and the thickness of the bedrock layer is dependent on the estimated total soil thickness overlying bedrock at each grid cell location. In areas mapped as Quaternary alluvial deposits (fig. 4*A*), the root zone is represented by five soil layers with no underlying bedrock layer (the root zone is underlaid by a deep-soil layer with properties defined based on the mapped unconsolidated deposit). The root zone is discretized into multiple layers to account for differences in root density and root-zone water content as a function of depth. Although the mass-balance calculations are based on water volumes (temperature effects on water density are assumed to be negligible in the volume-balance form of the continuity equation, which is based on the conservation of mass), the actual calculations are performed using water-equivalent depths. To perform simulations, the INFILv3 model requires an estimate of initial root-zone water content. For a multiyear simulation period, the simulated components of the daily water balance are summed through time to calculate total annual amounts and average annual rates. For additional information regarding the specifics of INFILv3, the reader is referred to Hevesi and others (2003).

Model Inputs

Inputs to the INFILv3 model consist of three main input groups: (1) climate and meteorological data, (2) digital-map files and associated attribute tables, and (3) model coefficients. Climate and meteorological data consist of daily climate data (temperature and precipitation), climate-station locations and altitudes, and monthly atmospheric properties. Monthly atmospheric properties consist of a set of parameters defining average monthly atmospheric conditions and were obtained from the National Climatic Data Center (Hevesi and others, 2003). Digital map files include a digital elevation model (DEM) and digitized maps of the spatial distribution of bedrock geology, soil types, and vegetation types. The attribute tables define bedrock and deep alluvium properties, soil properties, and vegetation properties representing the hydrologic characteristics of the root zone. Model coefficients include parameters for monthly climate models, parameters used to model sublimation and snowmelt, and parameters defining stream-channel characteristics.

For this study, recharge was simulated for the period of water years 1947–2003 using the INFILv3 model. The simulation required two sets of daily-climate data. The first set was the daily-climate data used by Hevesi and others (2003) to simulate net infiltration for the DVRFS model for water years 1947–99 (table 6). The second set consisted of daily-climate data for water years 2000–03 from a subset of the stations used by Hevesi and others (2003) (table 6) and from five Remote Automated Weather Stations (RAWS) located in the vicinity of the study area. Input parameters defining monthly atmospheric properties were the same for both sets of daily-climate data and climate stations.

Daily-Climate Data

The daily-climate data for water years 1947–99 were developed using daily precipitation (total accumulation) and air-temperature records (maximum and minimum daily air temperature) from 117 NCDC and 15 Nevada Test Site (NTS) climate stations in southern Nevada, southeastern California, western Arizona, and southwestern Utah that had 9 or more years of record between 1900 and 1999 (table 6). Measured snowfall depths also were included in the daily-climate data for most of the 117 NCDC stations; however, the data were not used to develop the daily-climate data for the INFILv3 model. The snowfall record was used to compare simulated daily snowfall amounts. The NCDC and NTS data can be retrieved from the following web pages located at http://www.earthinfo.com/databases/sd.htm and http://www.sord.nv.doe.gov/SORD_Rain_dailyXL.html, respectively.

The six NCDC stations located closest to the Joshua Tree surface-water drainage basin are Twentynine Palms (NCDC station code 49099), Joshua Tree (NCDC station code 44405), Joshua Tree 3 S (NCDC station code 44407), Kee Ranch (NCDC station code 44467), Morongo Valley (NCDC station code 45863), and Palm Springs (not shown) (NCDC station code 46635) (table 1 and fig. 2). The Palm Springs station is located outside the study area shown in figure 2 in the northwestern part of the Coachella Valley, southwest of the Joshua Tree surface-water drainage basin.

The daily-climate data for water years 2000–03 were developed from data collected from October 1, 1999, through December 31, 2002, at 83 NCDC stations in southern Nevada, southeastern California, western Arizona, and southwestern Utah, and from data collected for water years 1999–2003 at five RAWS stations located in the vicinity of the Joshua Tree study area (table 6). The 83 NCDC stations form a subset of the 132 stations used for the 1947–99 simulation; the subset includes those stations having precipitation and air-temperature records for water years 2000–03 and does not include the NTS stations that were included for the climate data used for the 1947–99 simulation. The five RAWS stations are Yucca Valley, Lost Horse, Covington, Burns Canyon, and Means Lake (not shown) (fig. 2, table 6). The Burns Canyon station is located to the northwest of the Joshua Tree study area and the Means Lake station is located to the north of the Joshua Tree study area (the Means Lake station is not shown in figure 2 because it is outside the area included in the figure). Data for the five RAWS stations include all daily records of precipitation and air temperature for water years 2000–03. Snowfall depth is not measured at the RAWS stations. The RAWS data can be retrieved from the following web page located at http://www.wrcc.dri.edu/wraws/scaF.html using the station names given above.

Digital Map Files and Attribute Tables

The INFILv3 model grid used for this study consists of 885-ft grid cells. Digital map data, including surface topography, surface geology, soils, and vegetation, were assigned to each cell in the INFILv3 model grid following the methods described by Hevesi and others (2003). These data were combined into the watershed input file.

The watershed input file includes (1) topographic parameters, (2) spatially distributed soil parameters, (3) spatially distributed bedrock and deep-soil parameters, and (4) spatially distributed vegetation and root-zone parameters. Root-zone properties, soil properties, and bedrock (including deep soil) properties are linked to the vegetation type, soil type, and bedrock (or deep soil) identifier in the watershed input file.

Table 6. Climate stations that provided daily-climate data used as input to the INFILv3 model of the Joshua Tree surface-water drainage basin, San Bernardino County, California

[The start and end dates indicate the period of record for the acquired data at the time of the study—these are different from the start and end dates for the simulation periods (1947–99 and 1947–2003; station name abbrevations taken from data source; NCDC, National Climatic Data Center; RAWS, Remote Automated Weather Station; NTS, Nevada Test Site; ft, feet; na, not available; *, station used during the 2000–2003 simulation; AZ, Arizona; CA, California; NV, Nevada; UT, Utah]

Station name	Station identification	State	NCDC code	Station code	Data source	Start of record	End of record	Latitude deg:min:sec	Longitude deg:min:sec	Station altitude[1] (ft)
Beaver Dam*	672	AZ	2	20672	NCDC	08/01/1956	12/31/2002	N36:53:49	W113:56:33	1,875
Bouse*	949	AZ	2	20949	NCDC	01/13/1952	12/31/2002	N33:56:35	W114:01:27	925
Bullhead City*	1050	AZ	2	21050	NCDC	11/10/1977	12/31/2002	N35:08:28	W114:34:04	540
Davis Dam # 2	2439	AZ	2	22439	NCDC	01/01/1958	07/07/1977	N35:12:00	W114:34:00	659
Ehrenberg	2787	AZ	2	22787	NCDC	07/01/1948	01/31/1977	N33:36:00	W114:32:00	322
Ehrenberg 2 E*	2790	AZ	2	22790	NCDC	02/01/1977	12/31/2002	N33:36:48	W114:28:14	465
Kingman*	4639	AZ	2	24639	NCDC	05/12/1901	12/31/2002	N35:11:00	W114:03:00	3,363
Kingman No 2	4645	AZ	2	24645	NCDC	09/01/1967	09/30/1993	N35:12:00	W114:01:00	3,539
Lake Havasu	4759	AZ	2	24759	NCDC	09/01/1967	02/28/1991	N34:27:00	W114:22:00	482
Parker*	6250	AZ	2	26250	NCDC	10/01/1893	12/31/2002	N34:09:17	W114:17:23	420
Pierce Ferry 17 SSW	6538	AZ	2	26538	NCDC	06/01/1963	07/31/1984	N35:53:00	W114:05:00	3,858
Quartzsite*	6865	AZ	2	26865	NCDC	01/17/1959	12/31/2002	N33:39:54	W114:13:38	875
Willow Beach*	9376	AZ	2	29376	NCDC	10/01/1967	12/31/2002	N35:52:07	W114:39:40	740
Yucca 1 NNE*	9645	AZ	2	29645	NCDC	01/31/1950	12/31/2002	N34:52:39	W114:08:04	1,950
Adelanto	24	CA	4	40024	NCDC	06/01/1959	06/30/1977	N34:35:00	W117:25:00	2,851
Apple Valley	244	CA	4	40244	NCDC	06/01/1959	03/31/1987	N34:31:00	W117:13:00	2,935
Backus Ranch	418	CA	4	40418	NCDC	07/01/1948	02/28/1963	N34:57:00	W118:11:00	2,651
Baker*	436	CA	4	40436	NCDC	12/01/1971	12/31/2002	N35:15:57	W116:04:25	940
Baker 9 NNW	437	CA	4	40437	NCDC	11/01/1953	03/31/1971	N35:23:00	W116:07:00	1,050
Barstow	519	CA	4	40519	NCDC	01/06/1913	03/31/1980	N34:54:00	W117:02:00	2,162
Barstow Fire Station*	521	CA	4	40521	NCDC	05/01/1980	12/31/2002	N34:53:34	W117:01:19	2,220
Benton Inspection Stn*	684	CA	4	40684	NCDC	10/01/1964	12/31/2002	N37:50:34	W118:28:42	5,460
Big Pines Park FC83B	779	CA	4	40779	NCDC	07/08/1948	09/30/1996	N34:23:00	W117:41:00	6,845
Bishop Creek Intake 2*	819	CA	4	40819	NCDC	10/01/1959	12/31/2002	N37:14:53	W118:34:53	8,154
Bishop AP*	822	CA	4	40822	NCDC	07/01/1948	12/31/2002	N37:22:16	W118:21:29	4,102
Blythe*	924	CA	4	40924	NCDC	01/01/1931	12/31/2002	N33:36:47	W114:35:50	268
Blythe FCWOS*	927	CA	4	40927	NCDC	07/01/1948	12/31/2002	N33:37:07	W114:42:51	395
Bodie*	943	CA	4	40943	NCDC	09/01/1964	12/31/2002	N38:12:43	W119:00:51	8,370
Cantil	1488	CA	4	41488	NCDC	03/01/1955	07/31/1974	N35:18:00	W117:58:00	2,011
China Lake Armitage*	1733	CA	4	41733	NCDC	07/01/1978	12/31/2002	N35:41:15	W117:41:35	2,230
Cow Creek	2092	CA	4	42092	NCDC	07/01/1948	04/22/1961	N36:32:00	W116:53:00	−151
Daggett FCWOS*	2257	CA	4	42257	NCDC	07/01/1948	12/31/2002	N34:51:13	W116:47:09	1,917
Death Valley*	2319	CA	4	42319	NCDC	04/01/1961	12/31/2002	N36:27:44	W116:52:01	−194
Deep Canyon Laboratory*	2327	CA	4	42327	NCDC	01/17/1963	12/31/2002	N33:39:05	W116:22:35	1,200
Deep Springs College*	2331	CA	4	42331	NCDC	07/01/1948	12/31/2002	N37:22:26	W117:58:49	5,225
Dunn Siding	2570	CA	4	42570	NCDC	07/08/1959	08/31/1971	N35:03:00	W116:26:00	1,611
Eagle Mountain*	2598	CA	4	42598	NCDC	07/01/1948	12/31/2002	N33:48:32	W115:27:03	973
El Mirage*	2771	CA	4	42771	NCDC	05/01/1971	12/31/2002	N34:35:21	W117:37:49	2,950
Goldstone Echo No 2*	3498	CA	4	43498	NCDC	12/01/1973	12/31/2002	N35:16:53	W116:47:04	2,950
Greenland Ranch	3603	CA	4	43603	NCDC	07/01/1948	03/31/1961	N36:27:00	W116:52:00	−168
Haiwee*	3710	CA	4	43710	NCDC	07/01/1948	12/31/2002	N36:08:20	W117:57:10	3,825
Hayfield Pumping Pla*	3855	CA	4	43855	NCDC	07/01/1948	12/31/2002	N33:42:16	W115:37:44	1,370
Hesperia	3935	CA	4	43935	NCDC	06/01/1959	06/30/1977	N34:25:00	W117:18:00	3,202

See footnote at end of table.

Table 6. Climate stations that provided daily-climate data used as input to the INFILv3 model of the Joshua Tree surface-water drainage basin, San Bernardino County, California—Continued

Station name	Station identification	State	NCDC code	Station code	Data source	Start of record	End of record	Latitude deg:min:sec	Longitude deg:min:sec	Station altitude[1] (ft)
Independence*	4232	CA	4	44232	NCDC	01/11/1927	12/31/2002	N36:47:53	W118:12:13	3,950
Indio Fire Station*	4259	CA	4	44259	NCDC	12/01/1927	12/31/2002	N33:42:31	W116:12:55	–21
Inyokern*	4278	CA	4	44278	NCDC	07/01/1948	12/31/2002	N35:39:08	W117:49:28	2,440
Inyokern Armitage	4280	CA	4	44280	NCDC	07/01/1948	06/30/1978	N35:41:00	W117:41:00	2,238
Iron Mountain*	4297	CA	4	44297	NCDC	07/01/1948	12/31/2002	N34:08:50	W115:07:19	922
Joshua Tree	4405	CA	4	44405	NCDC	06/01/1959	03/31/1974	N34:08:00	W116:19:00	2,723
Kee Ranch	4467	CA	4	44467	NCDC	07/01/1948	01/31/1979	N34:10:00	W116:32:00	4,334
Lake Sabrina*	4705	CA	4	44705	NCDC	01/01/1975	12/31/2002	N37:12:47	W118:36:49	9,065
Lancaster	4747	CA	4	44747	NCDC	07/01/1948	10/06/1972	N34:41:00	W118:07:00	2,402
Lancaster FSS*	4749	CA	4	44749	NCDC	05/01/1974	12/31/2002	N34:44:28	W118:12:42	2,338
Llano Eberle Ranch	5002	CA	4	45002	NCDC	07/01/1948	10/31/1965	N34:28:00	W117:45:00	3,822
Lucerne Valley 1 WSW	5182	CA	4	45182	NCDC	03/12/1949	09/30/1973	N34:27:00	W116:57:00	2,963
Mecca Fire Station*	5502	CA	4	45502	NCDC	07/01/1948	12/31/2002	N33:34:17	W116:04:36	–180
Mitchell Caverns*	5721	CA	4	45721	NCDC	03/11/1958	12/31/2002	N34:56:37	W115:32:49	4,350
Mojave*	5756	CA	4	45756	NCDC	07/01/1948	12/31/2002	N35:02:57	W118:09:43	2,735
Morongo Valley	5863	CA	4	45863	NCDC	10/01/1948	02/29/1972	N34:02:00	W116:35:00	2,562
Mountain Pass*	5890	CA	4	45890	NCDC	02/19/1955	12/31/2002	N35:28:14	W115:32:38	4,730
Mount San Jacinto WSP	5978	CA	4	45978	NCDC	01/01/1969	12/31/1978	N33:48:00	W116:38:00	8,425
Needles FCWOS*	6118	CA	4	46118	NCDC	07/01/1948	12/31/2002	N34:46:03	W114:37:08	890
Palmdale*	6624	CA	4	46624	NCDC	04/01/1931	12/31/2002	N34:35:16	W118:05:39	2,596
Palmdale CAA Airport	6627	CA	4	46627	NCDC	07/01/1948	03/31/1974	N34:38:00	W118:05:00	2,517
Palm Springs*	6635	CA	4	46635	NCDC	01/01/1927	12/31/2002	N33:49:39	W116:30:35	425
Parker Reservoir*	6699	CA	4	46699	NCDC	01/30/1943	12/31/2002	N34:17:25	W114:10:15	738
Randsburg*	7253	CA	4	47253	NCDC	07/01/1948	12/31/2002	N35:22:09	W117:39:09	3,570
Shoshone*	8200	CA	4	48200	NCDC	12/01/1972	12/31/2002	N35:58:19	W116:16:12	1,570
South Lake*	8406	CA	4	48406	NCDC	01/01/1975	12/31/2002	N37:10:06	W118:34:14	9,580
Thermal FAA Airport*	8892	CA	4	48892	NCDC	06/01/1950	12/31/2002	N33:37:40	W116:09:36	-112
Trona*	9035	CA	4	49035	NCDC	07/01/1948	12/31/2002	N35:45:49	W117:23:27	1,695
Twentynine Palms*	9099	CA	4	49099	NCDC	07/01/1948	12/31/2002	N34:07:41	W116:02:13	1,975
Valyermo Fire Stn 79	9250	CA	4	49250	NCDC	11/01/1972	04/30/1985	N34:27:00	W117:52:00	3,602
Valyermo Ranger Stn	9251	CA	4	49251	NCDC	07/01/1948	12/31/1971	N34:27:00	W117:51:00	3,704
Victorville Pump Pla*	9325	CA	4	49325	NCDC	07/01/1948	12/31/2002	N34:32:06	W117:18:21	2,858
Wildrose R S*	9671	CA	4	49671	NCDC	01/01/1969	01/31/2000	N36:15:56	W117:11:07	4,100
Adaven	46	NV	26	260046	NCDC	01/03/1928	02/28/1982	N38:07:00	W115:35:00	6,250
Amargosa Farms Garey*	150	NV	26	260150	NCDC	12/01/1965	12/31/2002	N36:34:18	W116:27:43	2,450
Beatty	714	NV	26	260714	NCDC	07/01/1948	11/30/1972	N36:55:00	W116:45:00	3,304
Beatty 8 N*	718	NV	26	260718	NCDC	12/01/1972	12/31/2002	N36:59:42	W116:43:08	3,550
Boulder City*	1071	NV	26	261071	NCDC	09/03/1931	12/31/2002	N35:58:48	W114:50:47	2,500
Caliente*	1358	NV	26	261358	NCDC	08/01/1928	12/31/2002	N37:37:01	W114:30:57	4,400
Desert Natl WL Range*	2243	NV	26	262243	NCDC	07/01/1948	12/31/2002	N36:26:16	W115:21:35	2,920
Desert Rock AP*	2251	NV	26	262251	NCDC	04/01/1984	12/31/2002	N36:37:14	W116:01:40	3,301
Duckwater*	2390	NV	26	262390	NCDC	09/01/1966	12/31/2002	N38:51:08	W115:38:10	5,550
Dyer*	2431	NV	26	262431	NCDC	07/01/1948	12/31/2002	N37:36:54	W118:00:38	4,900
Elgin*	2557	NV	26	262557	NCDC	03/01/1951	12/31/2002	N37:20:52	W114:32:35	3,420
Elgin 3 SE	2562	NV	26	262562	NCDC	05/01/1965	06/23/1985	N37:19:00	W114:30:00	3,301
Goldfield*	3285	NV	26	263285	NCDC	07/01/1948	12/31/2002	N37:42:29	W117:13:59	5,690
Indian Springs	3980	NV	26	263980	NCDC	07/01/1948	06/30/1964	N36:35:00	W115:41:00	3,123

See footnote at end of table.

Table 6. Climate stations that provided daily-climate data used as input to the INFILv3 model of the Joshua Tree surface-water drainage basin, San Bernardino County, California—Continued

Station name	Station identification	State	NCDC code	Station code	Data source	Start of record	End of record	Latitude deg:min:sec	Longitude deg:min:sec	Station altitude[1] (ft)
Lake Valley Steward	4384	NV	26	264384	NCDC	01/01/1971	11/30/1998	N38:19:00	W114:39:00	6,350
Las Vegas	4429	NV	26	264429	NCDC	01/01/1928	08/31/1956	N36:10:00	W115:08:00	2,011
Las Vegas AP*	4436	NV	26	264436	NCDC	01/01/1949	12/31/2002	N36:04:44	W115:09:19	2,127
Logandale	4651	NV	26	264651	NCDC	02/01/1968	01/31/1992	N36:37:00	W114:29:00	1,410
Mina*	5168	NV	26	265168	NCDC	01/01/1928	12/31/2002	N38:23:12	W118:06:21	4,550
North Las Vegas*	5705	NV	26	265705	NCDC	02/01/1951	12/31/2002	N36:14:05	W115:06:59	1,898
Overton*	5846	NV	26	265846	NCDC	07/01/1948	12/31/2002	N36:33:03	W114:27:29	1,250
Pahranagat W L Refuge*	5880	NV	26	265880	NCDC	03/01/1964	12/31/2002	N37:16:09	W115:07:11	3,400
Pahrump*	5890	NV	26	265890	NCDC	11/01/1948	12/31/2002	N36:16:43	W116:00:12	2,674
Pioche*	6252	NV	26	266252	NCDC	07/01/1948	12/31/2002	N37:56:40	W114:27:58	6,180
Rattlesnake	6630	NV	26	266630	NCDC	07/01/1948	09/18/1966	N38:27:00	W116:10:00	5,915
Red Rock Canyon St P*	6691	NV	26	266691	NCDC	05/01/1977	12/31/2002	N36:04:07	W115:27:37	3,780
Reese River O'Toole*	6746	NV	26	266746	NCDC	04/01/1972	12/31/2002	N39:03:45	W117:24:46	6,550
Sarcobatus	7319	NV	26	267319	NCDC	07/01/1948	06/30/1961	N37:16:00	W117:01:00	4,022
Searchlight*	7369	NV	26	267369	NCDC	07/01/1948	12/31/2002	N35:27:58	W114:55:18	3,540
Silverpeak*	7463	NV	26	267463	NCDC	10/16/1967	12/31/2002	N37:45:43	W117:33:55	4,260
Snowball Ranch*	7640	NV	26	267640	NCDC	09/03/1966	06/30/2002	N39:02:25	W116:11:56	7,160
Sunrise Manor Las Ve	7925	NV	26	267925	NCDC	07/01/1961	10/31/1989	N36:12:00	W115:05:00	1,821
Tempiute 4 Nw	7983	NV	26	267983	NCDC	04/29/1972	12/31/1985	N37:41:00	W115:43:00	4,892
Tonopah	8160	NV	26	268160	NCDC	01/01/1928	06/10/1954	N38:04:00	W117:14:00	6,024
Tonopah FCWOS*	8170	NV	26	268170	NCDC	06/11/1954	12/31/2002	N38:03:04	W117:05:25	5,395
Twin Springs Fallini*	8443	NV	26	268443	NCDC	10/01/1985	12/31/2002	N38:12:12	W116:10:33	5,300
Valley of Fire St Pk*	8588	NV	26	268588	NCDC	12/01/1972	12/31/2002	N36:25:47	W114:30:47	2,000
Enterprise*	2558	UT	42	422558	NCDC	08/01/1954	12/31/2002	N37:34:22	W113:42:32	5,320
Gunlock Powerhouse*	3506	UT	42	423506	NCDC	07/01/1948	12/31/2002	N37:16:50	W113:43:42	4,110
St. George*	7516	UT	42	427516	NCDC	01/01/1928	12/31/2002	N37:06:25	W113:33:40	2,770
Veyo Powerhouse*	9136	UT	42	429136	NCDC	08/27/1957	12/31/2002	N37:21:08	W113:40:00	4,600
Rainier Mesa	na	CA	na	na	NTS	03/01/1959	01/31/2000	N37:11:28	W116:12:52	7,491
Buster Jangle Y	na	CA	na	na	NTS	02/01/1960	01/31/2000	N37:03:46	W116:03:06	4,068
Cane Springs	na	CA	na	na	NTS	09/01/1964	01/31/2000	N36:48:44	W116:05:26	4,000
Desert Rock	na	CA	na	na	NTS	10/01/1963	01/31/2000	N36:37:16	W116:01:30	3,251
Jackass Flats	na	CA	na	na	NTS	01/01/1959	01/31/2000	N36:47:05	W116:17:17	3,422
40 Mile Canyon	na	CA	na	na	NTS	02/01/1960	01/31/2000	N37:02:57	W116:17:12	4,820
Little Feller 2	na	CA	na	na	NTS	08/01/1976	01/31/2000	N37:07:05	W116:18:11	5,118
Mercury	na	CA	na	na	NTS	03/01/1971	01/31/2000	N36:39:39	W116:00:33	3,770
Mid Valley	na	CA	na	na	NTS	09/01/1964	01/31/2000	N36:58:21	W116:10:16	4,659
Pahute Mesa 1	na	CA	na	na	NTS	01/01/1964	01/31/2000	N37:14:56	W116:26:12	6,549
Phs Farm	na	CA	na	na	NTS	10/01/1964	01/31/2000	N37:12:32	W116:02:16	4,564
Rock Valley	na	CA	na	na	NTS	03/01/1963	01/31/2000	N36:41:07	W116:11:29	3,399
Tippipah Springs 2	na	CA	na	na	NTS	05/01/1960	01/31/2000	N37:03:11	W116:11:26	4,981
Well 5B	na	CA	na	na	NTS	09/01/1963	01/31/2000	N36:48:07	W115:57:52	3,081
Yucca Dry Lake	na	CA	na	na	NTS	01/01/1959	01/31/2000	N36:57:23	W116:02:48	3,924
Burns Canyon*	na	CA	na	na	RAWS	08/01/1991	09/30/2003	N34:12:37	W116:38:02	6,000
Covington*	na	CA	na	na	RAWS	07/01/2001	09/30/2003	N34:03:12	W116:20:03	4,646
Lost Horse*	na	CA	na	na	RAWS	09/01/1991	09/30/2003	N34:01:04	W116:11:16	4,200
Means Lake*	na	CA	na	na	RAWS	11/01/1997	09/30/2003	N34:23:26	W116:31:01	2,900
Yucca Valley*	na	CA	na	na	RAWS	05/01/1990	09/30/2003	N34:07:24	W116:24:28	3,260

[1]Datum unknown.

Topographic Parameters

The surface-altitude value for each grid cell was determined by resampling the 30-m DEM developed for the Mojave Desert region (Utah State University, 1998) resulting in a 270-m DEM. The surface-altitude values were required to model potential evapotranspiration and to model spatially distributed daily-climate data. In addition, the 270-m DEM was used to develop topographic parameters that are used to simulate potential evapotranspiration and the routing of surface-water flow (Hevesi and others, 2003). Topographic parameters include slope, aspect, streamflow-routing parameters, the skyview parameter, and 36 blocking-ridge angles. The skyview parameter defines the percentage of open sky used to simulate incoming solar radiation (Flint and Childs, 1987) and is calculated using 36 blocking-ridge angles. The 36 blocking-ridge angles were defined for each 10-degree arc along the horizon using the 270-m DEM to address the effects of shading by surrounding terrain on simulated net radiation (Flint and Childs, 1987).

The surface-water flow-routing parameters for each grid cell were defined using the 270-m DEM data following the approach described by Hevesi and others (2003). The surface-water flow-routing parameters were used to determine the watershed (drainage basin) modeling domains covering the Joshua Tree surface-water drainage basin. The total surface-water model area and the mapped surface-water drainage basins (California Department of Forestry and Fire Protection, 1999) are shown in figure 2. Note that the model area and mapped basins do not match exactly because the resolution of the DEM is too coarse to capture the more subtle drainage boundaries that typically occur on alluvial fans and across the relatively flat-lying areas of desert basins.

The Joshua Tree surface-water drainage basin was modeled as a single watershed-modeling domain (JOSH1 in figure 2). The JOSH1 model domain consists of 8,871 model grid cells and covers 250 mi^2. The 19 largest surface-water subbasins with distinct channels upstream from the Joshua Tree and Copper Mountain ground-water model area in the JOSH1 model domain are shown in figure 2 and include a total of 7,588 cells covering 214 mi^2. The largest of these subbasins are CM18 (Quail Wash), consisting of 3,608 cells and covering 102 mi^2, and WV01 (Yucca Wash), consisting of 1,934 cells and covering 54 mi^2. Also shown in figure 2 are small, unnamed, surface-water subbasins that did not have distinct channels. The subbasins covered about 10 mi^2 and the ground-water model area covered about 26 mi^2. For the surface-water subbasins within JOSH1, the number of model cells, areas, and average altitude are given in table 7.

Spatially Distributed Soil Parameters

Spatially distributed soil parameters include soil thickness, porosity, the wilting-point water content, a drainage-function coefficient, and saturated hydraulic conductivity. These parameters were estimated using the State Soil Geographic Database (STATSGO) digital map and associated attribute tables compiled by the U.S. Department of Agriculture (1994). The Joshua Tree surface-water drainage basin includes 12 different STATSGO map unit identifiers (MUIDs) (fig. 25). The STATSGO data were applied using methods described by Hevesi and others (2003) to develop the INFILv3 input soil parameters presented in table 8.

For this study, a maximum root-zone depth of about 20 ft was assumed for all areas mapped as Quaternary alluvial deposits and a maximum root-zone depth of about 6.5 ft was assumed for all other geologic units (fig. 4*A*). The soil depth of each of the five modelled root-zone layers for all STATSGO MUIDs in the Joshua Tree study area is presented in table 8.

Spatially Distributed Bedrock and Deep-Soil Parameters

Spatially distributed bedrock and deep-soil parameters were developed using the digital geologic map and associated attribute tables for the Mojave Desert region compiled by Bedford and Miller (1997). The digital geologic map for the Mojave Desert region defines 10 different geologic units in the Joshua Tree study area (fig. 4*A*). Of the 10 geologic units, 2 are unconsolidated (deep soils underlying the root zone) and 8 are considered to be bedrock units. Each geologic unit is assigned an effective root-zone porosity and a maximum and minimum hydraulic conductivity (table 9). The assigned values of effective root-zone porosity and hydraulic conductivity are generally consistent with the values assigned to equivalent geologic units that were used in the calibrated DVRFS model (Hevesi and others, 2003).

Spatially Distributed Vegetation and Root-Zone Parameters

Spatially distributed vegetation parameters (vegetation type and cover) and root-zone parameters (maximum root-zone depth and root density as a function of depth) were developed using the California Gap Analysis Program (GAP) digital map and associated attribute table compiled by the U.S. Geological Survey (2000). For the Joshua Tree study area, 13 different vegetation types are defined using the GAP data; the dominant vegetation types include creosote scrub for the lower altitudes in the northern part of the study area, desert mixed scrub and blackbrush for intermediate altitudes, and pinyon-juniper woodland for the higher altitudes in the Little San Bernardino Mountains (fig. 26). The vegetation and root-zone parameters are presented in table 10. Note that the resolution of the GAP data in the study area is too coarse to discern changes in type or density of vegetation along intermittent stream channels (fig. 26); therefore, this vegetation was not addressed explicitly in the INFILv3 model.

Table 7. Modeled surface-water drainage basins, Joshua Tree surface-water drainage basin, San Bernardino County, California

[ft, feet; in./yr, inches per year; acre-ft/yr, acre feet per year; mi^2, square mile; —, not available; na, not applicable; asl, above sea level]

Surface-water drainage basin					
Subbasin No.	INFILv3 identifier	Number of cells	Area (mi^2)	Area (acres)	Average altitude (ft asl)
Warren Valley surface-water drainage basin					
WV01	YUCC1	1,934	54.44	34,839	3,974
Copper Mountain surface-water drainage basin					
CM01	JTN00	174	4.90	3,134	3,491
CM02	JTN01	31	.87	558	3,242
CM03	JTN02	28	.79	504	2,602
CM04	JTN03	994	27.98	17,906	3,158
CM05	JTN04	139	3.91	2,504	2,725
CM06	JTN05	262	7.37	4,720	2,749
CM07	JTN06	25	.70	450	3,120
CM08	JTN07	19	.53	342	2,892
CM09	JTN08	15	.42	270	2,602
CM10	JTS00	188	5.29	3,387	3,784
CM11	JTS01	44	1.24	793	3,336
CM12	JTS02	28	.79	504	3,287
CM13	JTS03	26	.73	468	3,847
CM14	JTS04	19	.53	342	3,785
CM15	JTS05	26	.73	468	3,290
CM16	JTS06	14	.39	252	3,162
CM17	JTS07	14	.39	252	3,156
CM18	QWSH2	3,608	101.55	64,994	4,359
Total		7,588	213.55	136,687	na
Modeled Joshua Tree surface-water drainage basin (JOSH1)		8,871	249.69	159,801	3,761
Area of ground-water model within the Joshua Tree surface-water drainage basin		914	25.73	16,465	2,571

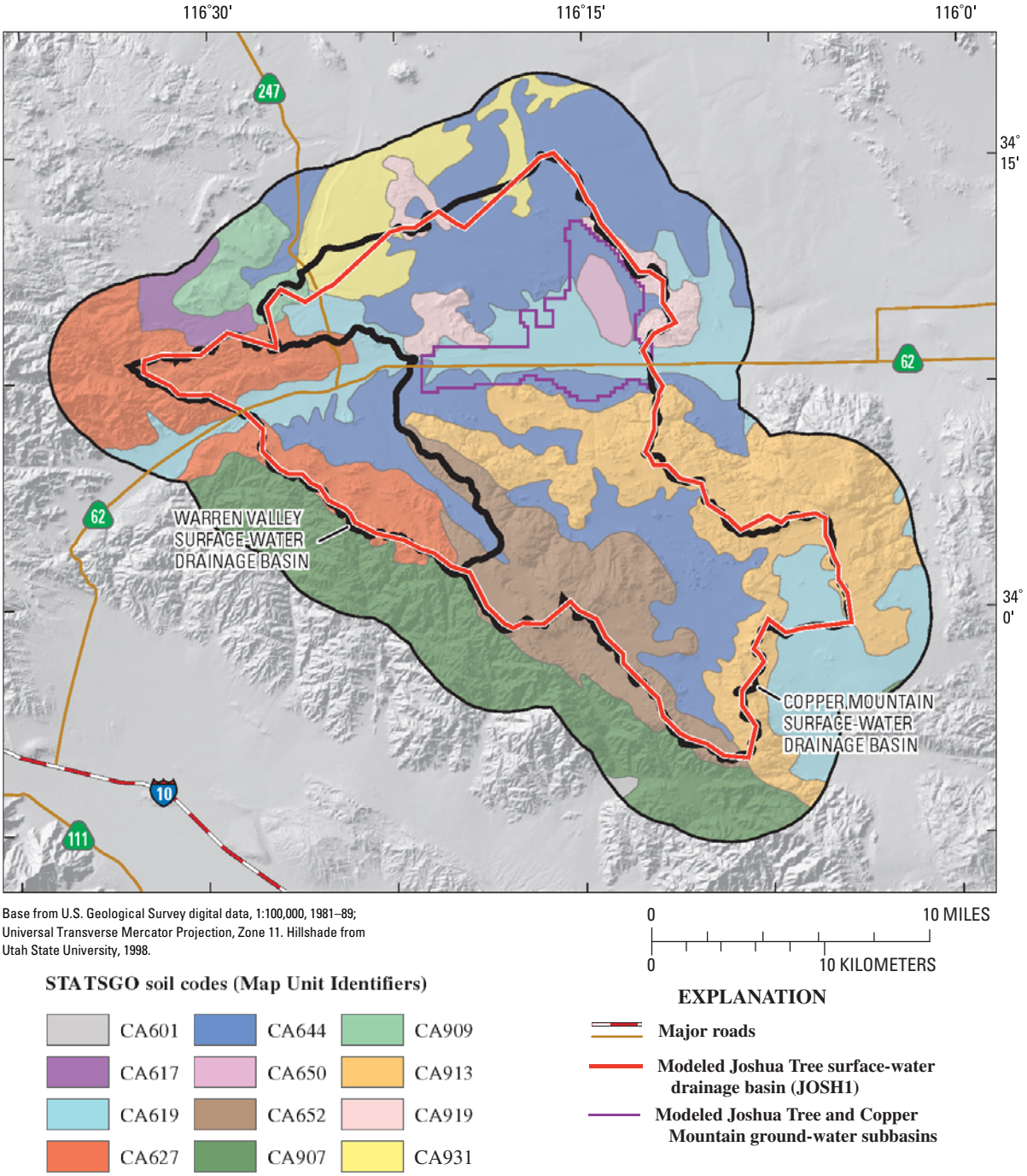

Figure 25. State Soil Geographic Database (STATSGO) soil types, Warren Valley and Copper Mountain surface-water drainage basins, San Bernardino County, California.

Table 8. Estimated soil parameters used in the INFILv3 watershed model, Joshua Tree surface-water drainage basin, San Bernardino County, California

[ft, feet; STATSGO, state soil geographic database; MUID, map unit identifier; ft/sec, feet per second]

STATSGO			Estimated soil properties				
Map code (MUID)	Number of soil components	Average number of soil layers	Soil depth (ft)	Porosity	Wilting point	Drainage parameter	Saturated hydraulic conductivity (ft/sec)
CA601	9	2	5.00	0.346	0.004	2.219	7.3×10^{-5}
CA617	11	4	5.10	.359	.032	4.261	2.8×10^{-5}
CA619	21	3	5.35	.354	.052	5.043	1.9×10^{-5}
CA627	8	2	.87	.405	.066	5.721	1.6×10^{-5}
CA644	17	5	7.25	.374	.044	4.249	2.9×10^{-5}
CA650	7	2	5.00	.358	.197	12.267	1.3×10^{-6}
CA652	13	3	2.82	.375	.041	4.318	2.7×10^{-5}
CA907	18	1	.47	.369	.026	4.313	2.5×10^{-5}
CA909	17	1	1.09	.387	.030	4.378	2.7×10^{-5}
CA913	15	1	.55	.378	.034	4.338	2.7×10^{-5}
CA919	14	3	1.35	.373	.048	4.808	2.2×10^{-5}
CA931	19	4	5.01	.352	.013	3.004	4.9×10^{-5}

Table 9. Estimated bedrock and deep-soil parameters used in the INFILv3 watershed model, Joshua Tree surface-water drainage basin, San Bernardino County, California

[ft/sec, feet per second]

Map unit	Geologic unit	Geologic unit age	Estimated root-zone porosity	Estimated hydraulic conductivity (ft/sec)	
				Minimum	Maximum
Qsu	Undifferentiated surficial deposits	Quaternary-Pliocene	0.35	7.6×10^{-5}	7.6×10^{-5}
Qp	Dry-lakebed deposits	Quaternary-Pliocene	.15	3.8×10^{-8}	3.8×10^{-8}
Tsy	Young sedimentary rocks	Tertiary	.35	3.8×10^{-9}	3.8×10^{-6}
Tvy	Young volcanic rocks	Tertiary	.02	3.8×10^{-13}	3.8×10^{-10}
Kg	Granitoid rocks	Cretaceous	.01	7.6×10^{-13}	7.6×10^{-10}
Jg	Granitoid rocks	Jurassic	.005	7.6×10^{-15}	7.6×10^{-12}
TRg	Granitoid rocks	Triassic	.01	7.6×10^{-13}	7.6×10^{-10}
ZXsg	Sedimentary rocks and gneiss	PreCambrian	.01	7.6×10^{-14}	7.6×10^{-11}
Xg	Granitoid rocks	PreCambrian	.005	7.6×10^{-15}	7.6×10^{-12}
Xm	Metamorphic rocks	PreCambrian	.01	7.6×10^{-14}	7.6×10^{-11}

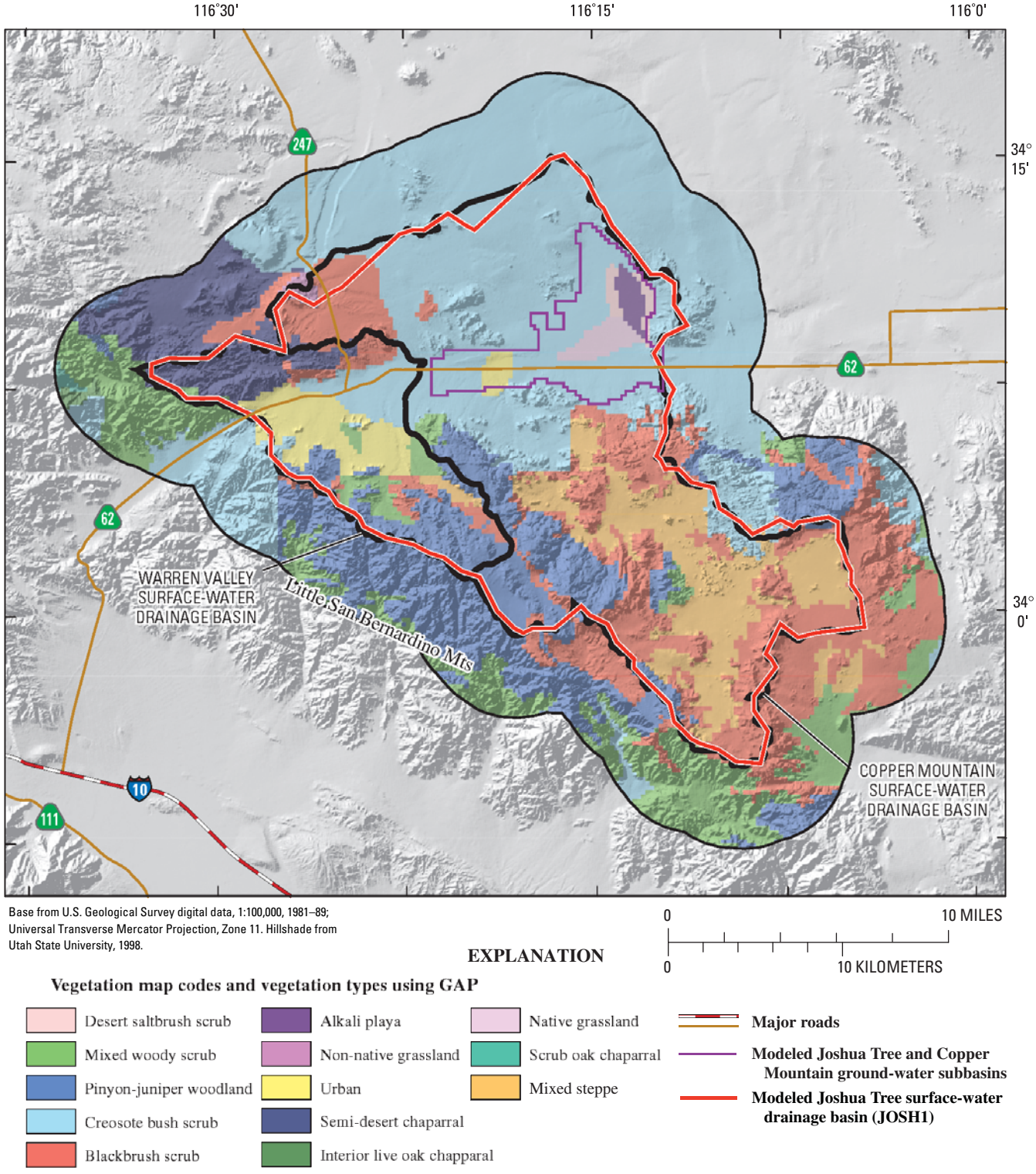

Figure 26. Vegetation types, defined using California Gap Analysis Program data, Warren Valley and Copper Mountain surface-water drainage basins, San Bernardino County, California.

Table 10. Estimated vegetation and root-zone parameters used in the INFILv3 watershed model, Joahua Tree surface-water drainage basin, San Bernardino County, California

[Numbers presented are simulated results and do not imply any level of accuracy]

Gap Analysis Program (GAP)		Estimated vegetation cover (percent)	Modeled root-zone layers					
			Soil layers					Bedrock layer
Map code	Vegetation type		Layer 1	Layer 2	Layer 3	Layer 4	Layer 5	Layer 6
			Maximum layer thickness (meters)					
			0.1	0.2	0.7	2.0	3.0	2.0
			Estimated root density (percent)					
3	Desert Saltbrush Scrub	25	25	25	12.5	6.25	2.5	1.25
10	Mojave Mixed Woody Scrub	30	30	30	15	7.5	3	1.5
16	Mojavean Pinyon and Juniper Woodland	50	50	50	25	12.5	5	2.5
18	Mojave Creosote Bush Scrub	30	30	30	15	7.5	3	1.5
22	Blackbrush Scrub	35	35	35	17.5	8.75	3.5	1.75
32	Alkali Playa	0	0	0	0	0	0	0
43	Non-Native Grassland	35	35	35	17.5	8.75	3.5	1.75
44	Urban	25	25	25	12.5	6.25	2.5	1.25
59	Semi-Desert Chaparral	50	50	50	25	12.5	5	2.5
61	Interior Live Oak Chaparral	60	60	60	30	15	6	3
64	Desert Native Grassland	30	30	30	15	7.5	3	1.5
67	Scrub Oak Chaparral	70	70	70	35	17.5	7	3.5
68	Mojave Mixed Steppe	40	40	40	20	10	4	2

Model Coefficients

Monthly climate-regression models were used to spatially distribute the daily climate data using a modified inverse-distance-squared interpolation (Hevesi and others, 2003). The regression models were developed for the Death Valley and Mojave Desert regions using climate-station altitudes, the average monthly precipitation values, and maximum and minimum daily air temperatures for the 132 NCDC and NTS stations used for the 1947–2003 simulation. Coefficients for modeling snowmelt, sublimation, and stream-channel characteristics were identical to those used by Hevesi and others (2003) for simulating net infiltration in the DVRFS model.

Model Outputs

Model outputs include (1) annual, monthly, and daily time series results for simulated components of the water balance, expressed as the mean simulation result for all grid cells and also as the simulation result for specified grid locations; (2) spatially distributed simulation results for all components of the water balance, including the daily, annual, and average annual results at all grid cells; and (3) summary statistics for model inputs and outputs, including the mean, maximum, and minimum values for all grid cells in the model domain. The time-series results were used to compare simulated streamflow with measured streamflow records, to compare simulated precipitation and snowfall with measured precipitation and snowfall, and to analyze the temporal distribution of the simulated water-balance components. The spatially distributed simulation results were used to analyze the spatial distribution of the simulated water-balance components and to develop the potential recharge estimates for the ground-water flow model.

Evaluation of Model Calibration (1950–2003)

The INFILv3 model used to develop recharge estimates for the Joshua Tree study area was based on the calibrated DVRFS model. The INFILv3 model used to estimate recharge for the DVRFS model was calibrated using streamflow records from 31 gaging sites and basinwide estimates of recharge for 42 hydrographic areas in the Death Valley region (Hevesi and others, 2003). Note that none of the 31 gaging sites were located within the Joshua Tree study area. The model data defining drainage basin characteristics for the Joshua Tree study area (such as soil, bedrock, and vegetation parameters) are somewhat different from those used to calibrate the DVRFS model; however, the same data sources (STATSGO and GAP) were used to develop soil and vegetation input parameters for both study areas, and the geology in the southwestern part of the Death Valley region includes granitic and metamorphic rock types representative of the geology for the Joshua Tree study area.

Although the INFILv3 model used in this study was not calibrated to the specific area of the Joshua Tree study area, model performance was evaluated using a comparison of simulated and measured precipitation, snowfall, and streamflow. For evaluating simulated precipitation, the spatial distribution of simulated average annual precipitation was compared with average annual precipitation estimated using a regression-based precipitation model [Parameter Regression on Independent Slope Model (PRISM) (Daly and others, 1994)]. The simulated daily, monthly, and annual time-series of precipitation and snowfall depth at the Joshua Tree 3 S climate station was compared with the measured record. Simulated daily, monthly, and annual streamflow was compared with measured streamflow at the four gaging sites in the vicinity of the Joshua Tree surface-water drainage basin: Quail Wash (USGS station number 10253320, QUAIL WASH NR JOSHUA TREE CA), Fortynine Palms Creek (USGS station number 10253350, FORTYNINE PALMS C NR TWENTYNINE PALMS CA), Long Creek (USGS station number 10257800, LONG C NR DESERT HOT SPRINGS CA), and Pipes Creek (USGS station number 10260200, PIPES C NR YUCCA VALLEY CA). The PRISM-estimated average annual precipitation data for 1961–90 can be retrieved from the following web site located at http://www.ocs.orst.edu/prism/state_products/maps.phtml?id=CA.

To develop estimates of natural recharge for the Joshua Tree study area, the INFILv3 model was applied to simulate daily recharge for water years 1947–2003. The initial conditions for the 1947–2003 simulation were defined using an assumed initial water content for soils that was 20 percent greater than the calculated wilting-point water content for each soil type and an initial water content of zero for the bedrock layer of the root zone. To reduce the dependency of the results on the assumed initial water content, the first 3 years of the simulation period (1947–49) were not included in the calculation of the average-annual water-balance terms.

1950–99 Simulated Results

The simulated 50-year average daily recharge rate for 1950–99 was used to develop boundary conditions for the ground-water flow model of the Joshua Tree and Copper Mountain ground-water subbasins. The 1950–99 watershed simulation results for all components of the water balance were evaluated for JOSH1 (tables 11 and 12). In table 11, the results are given in terms of the basin-wide, average rates, and in table 12, the results are given in terms of the basin-wide, volumetric flowrates.

Table 11. Summary of water-balance results: basinwide average rates for the water year 1950–99 simulation, Joshua Tree surface-water drainage basins, San Bernardino County, California

[Numbers presented are simulated results and do not imply any level of accuracy; IN, mass balance inflow; OUT, mass balance outflow; NI, not included in mass balance calculation; —, not available]

Subbasin No.	INFILv3 identifier	(IN) Precip-itation	(NI) Snowfall	(OUT) Sublimation	(OUT) Evapotrans-piration	(OUT) Change in storage	(NI) Runoff	(OUT) Total recharge	(IN) Surface water inflow	(OUT) Surface water outflow
Warren Valley surface-water drainage basin										
WV01	YUCC1	7.58453	.23052	.01349	7.31649	–.02633	.46236	.21447	.00000	.06641
Copper Mountain surface-water drainage basin										
CM01	JTN00	6.78328	0.08775	0.00515	6.79369	–0.02318	0.11467	0.00004	0.00000	0.00758
CM02	JTN01	6.41146	.05088	.00298	6.41903	–.01694	.04043	.00004	.00000	.00635
CM03	JTN02	5.13772	.01271	.00108	5.14242	–.00578	.01109	.00000	.00000	.00000
CM04	JTN03	6.27065	.05953	.00367	6.26759	–.02074	.04914	.01946	.00000	.00068
CM05	JTN04	5.58693	.01904	.00149	5.60222	–.01678	.00066	.00000	.00000	.00000
CM06	JTN05	5.57405	.01757	.00139	5.58864	–.01598	.00021	.00000	.00000	.00000
CM07	JTN06	6.21342	.04268	.00288	6.19540	.00017	.06945	.00003	.00000	.01493
CM08	JTN07	5.94626	.03272	.00233	5.94383	–.01183	.03607	.00000	.00000	.01193
CM09	JTN08	5.13640	.01221	.00094	5.13394	–.00039	.01243	.00000	.00000	.00191
CM10	JTS00	6.52608	.09693	.00552	6.11098	–.00011	.53226	.03226	.00000	.37743
CM11	JTS01	6.17292	.04742	.00253	5.88479	.00598	.39492	.13837	.00000	.14125
CM12	JTS02	5.85642	.03887	.00188	5.66311	.01330	.33959	.11412	.00000	.06402
CM13	JTS03	7.08100	.11996	.00623	6.83423	–.00230	.75971	.21387	.00000	.02897
CM14	JTS04	6.97383	.12794	.00562	6.83119	.02299	.73673	.08456	.00000	.02947
CM15	JTS05	6.19580	.04449	.00259	5.86784	.00057	.41894	.00713	.00000	.31767
CM16	JTS06	5.62345	.02774	.00131	5.53383	.01750	.27515	.00806	.00000	.06274
CM17	JTS07	5.74782	.03061	.00164	5.70928	.00229	.23946	.01017	.00000	.02444
CM18	QWSH2	7.36932	.30014	.01821	7.28527	–.01160	.24441	.04497	.00000	.03247
Joshua Tree and Copper Mountain ground-water subbasins		5.37523	.01645	.00118	5.50225	–.04939	.16791	.11497	—	—
Joshua Tree surface-water drainage basin [JOSH1]		6.87483	.18842	.01134	6.78305	–.01970	.24933	.08179	.00000	.01835

Table 12. Summary of water-balance results: basinwide volumes for the water year 1950–99 simulation, Joahua Tree surface-water drainage basins, San Bernardino County, California

[Numbers presented are simulated results and do not imply any level of accuracy; IN, mass balance inflow; OUT, mass balance outflow; NI, not included in mass balance calculation]

Subbasin No.	INFILv3 identifier	(IN) Precip-itation	(NI) Snowfall	(OUT) Subli-mation	(OUT) Evapo-trans-piration	(OUT) Change in storage	(NI) Runoff	(OUT) Total recharge	(IN) Surface water inflow	(OUT) Surface water outflow
Warren Valley surface-water drainage basin										
WV01	YUCC1	22,019.685	669.257	39.154	21,241.51	–76.446	1,342.343	622.652	.00	192.813
Copper Mountain surface-water drainage basin										
CM01	JTN00	1,771.802	22.920	1.345	1,774.52	–6.054	29.951	0.011	0.00	1.979
CM02	JTN01	298.363	2.368	.139	298.72	–.788	1.881	.002	.00	.296
CM03	JTN02	215.951	.534	.045	216.15	–.243	.466	.000	.00	.000
CM04	JTN03	9,356.755	88.823	5.478	9,352.18	–30.947	73.325	29.039	.00	1.010
CM05	JTN04	1,165.772	3.972	.311	1,168.96	–3.502	.137	.000	.00	.000
CM06	JTN05	2,192.291	6.911	.548	2,198.03	–6.287	.084	.000	.00	.000
CM07	JTN06	233.183	1.602	.108	232.51	.006	2.606	.001	.00	.560
CM08	JTN07	169.599	.933	.066	169.53	–.337	1.029	.000	.00	.340
CM09	JTN08	115.658	.275	.021	115.60	–.009	.280	.000	.00	.043
CM10	JTS00	1,841.774	27.355	1.558	1,724.62	–.030	150.213	9.104	.00	106.518
CM11	JTS01	407.727	3.132	.167	388.70	.395	26.085	9.139	.00	9.330
CM12	JTS02	246.159	1.634	.079	238.03	.559	14.274	4.797	.00	2.691
CM13	JTS03	276.372	4.682	.243	266.74	–.090	29.652	8.347	.00	1.131
CM14	JTS04	198.907	3.649	.160	194.84	.656	21.013	2.412	.00	.841
CM15	JTS05	241.823	1.736	.101	229.02	.022	16.351	.278	.00	12.399
CM16	JTS06	118.184	.583	.028	116.30	.368	5.783	.169	.00	1.319
CM17	JTS07	120.797	.643	.035	119.99	.048	5.033	.214	.00	.514
CM18	QWSH2	39,913.543	1,625.603	98.608	39,458.31	–62.801	1,323.772	243.549	.00	175.877
Joshua Tree and Copper Mountain ground-water subbasins		7,375.122	22.575	1.613	7,549.41	–67.760	230.386	157.746	510.237	244.351
Joshua Tree surface-water drainage basin [JOSH1]		91,550.427	2,509.088	150.967	90,328.29	–262.371	3,320.282	1,089.187	.00	244.351

Simulated 1950–99 Precipitation, Evapotranspiration, Snowfall, and Sublimation

The average annual precipitation rates simulated by INFILv3 and estimated by PRISM are similar, but not identical (figs. 27 and 28). For the general area of the Joshua Tree and Copper Mountain ground-water model, spatially distributed precipitation rates simulated by INFILv3 and estimated by PRISM are in good agreement (–2 to 1.4 in.). For the higher altitudes in the Little San Bernardino Mountains, simulated precipitation rates using INFILv3 tend to be lower than the PRISM estimates. The difference between basinwide simulated precipitation and estimated precipitation using PRISM is greatest for the modeled Warren Valley surface-water drainage basin (WV01) (fig. 28; fig. 2).

The differences between the INFILv3 and PRISM results may be the result of using different simulation horizons, DEMs, climate data, and approaches to addressing orographic influences on precipitation. The INFILv3 average is based on 1950–99 simulated results and the PRISM average is based on 1961–90 estimated results. INFILv3 uses a 270-m DEM and PRISM uses a 4,000-m DEM (Spatial Climate Analysis Service, 2004). The climate data used in INFILv3 may be of shorter duration but more site-specific than those used in PRISM. A discussion describing the differences in which orographic influences are addressed is beyond the scope of this report; however, INFILv3 uses a much simpler approach than does PRISM [see Hevesi and others (2003) for INFILv3 and Daly and others (1994) for PRISM].

Precipitation and evapotranspiration are the primary components of the water balance for JOSH1; most, if not all, of the precipitation is lost to evapotranspiration (tables 11 and 12). The simulated 1950–99 average annual evapotranspiration is similar to the simulated precipitation in magnitude and distribution (evapotranspiration is higher for basins with higher precipitation), indicating that evapotranspiration is more dependent on the availability of water than on the potential evapotranspiration rate. For the Joshua Tree and Copper Mountain ground-water model area, the simulated evapotranspiration volume (7,549 acre-ft/yr) is greater than the precipitation volume (7,375 acre-ft/yr) because the contribution of surface-water inflow to the area increases the availability of water for evapotranspiration (table 12).

For most areas in JOSH1, the average annual snowfall and sublimation are very small (less than 0.1 in./yr) (table 11). The total average annual snowfall volume in JOSH1 is 2,509 acre-ft/yr (table 12), or 2.7 percent of the average annual precipitation volume. The annual snowmelt volume is equal to annual snowfall minus annual sublimation, and equaled 2,358 acre-ft/yr (table 12). The highest basinwide average annual snowfall was simulated for CM18 (0.3 in./yr) and WV01 (0.23 in./yr) (table 11). In terms of the simulated volumes, the average annual snowfall volume is 1,626 acre-ft/yr for CM18 and 669 acre-ft/yr for WV01 (table 12). For the ground-water model area, the 50-year average annual snowfall is only 0.02 in./yr, which is an order of magnitude less than the recorded average annual snowfall depth (assumed water equivalent) of 0.21 in./yr measured at the Joshua Tree climate station (table 13).

Comparison of Simulated and Measured 1974–77 Precipitation at Joshua Tree 3 S

A comparison of simulated daily and monthly precipitation with measured precipitation for the Joshua Tree 3 S climate station is shown in figure 29. The daily results indicated satisfactory model performance in simulating the timing and frequency of storms; however, there are some significant differences between the simulated and measured amounts of precipitation, mainly in May and September 1976 (fig. 29*A*). The differences in the daily results are probably caused by the inherent stochastic nature of measured precipitation data. In order to address the stochasticity of precipitation data, an increased spatial density of measuring stations would be required. The monthly results indicated a good match between the simulated and measured amounts of precipitation (fig. 29*B*). The total simulated precipitation amount for the period of record at Joshua Tree 3 S was 19.39 in., which was slightly greater than the measured precipitation amount of 17.08 in.

Simulated 1950–99 Surface-Water Runoff and Outflow

The simulated 1950–99 average annual surface-water runoff is shown in figure 30. High runoff rates (1.5–2.0 in./yr) were simulated for the San Bernardino and Little San Bernardino Mountains, along the western boundary of the surface-water drainage basin because of the combined effects of higher precipitation, thinner soils overlying impermeable bedrock, and steeper terrain. Runoff for most lower altitudes locations in the northern and northeastern part of the surface-water drainage basin, including the Joshua Tree and Copper Mountain ground-water model area, was low (0–0.1 in./yr). Runoff for the dry lakebed of Coyote Lake was slightly higher (0.75–1 in./yr) than runoff for the surrounding alluvial fans because of the lower permeability soils for the dry lakebed.

Simulated surface-water outflow to Coyote Lake is 244 acre-ft/yr, about 7 percent of the average annual runoff of 3,320 acre-ft/yr. In addition, the simulated surface-water outflow from the subbasins is less than 50 percent of the runoff generated as excess rainfall and snowmelt within the subbasin, with the exception of CM10 and CM15 (table 12). These results indicate that most of the generated runoff volume infiltrates into the root zone as channel losses during the downstream routing of run-on.

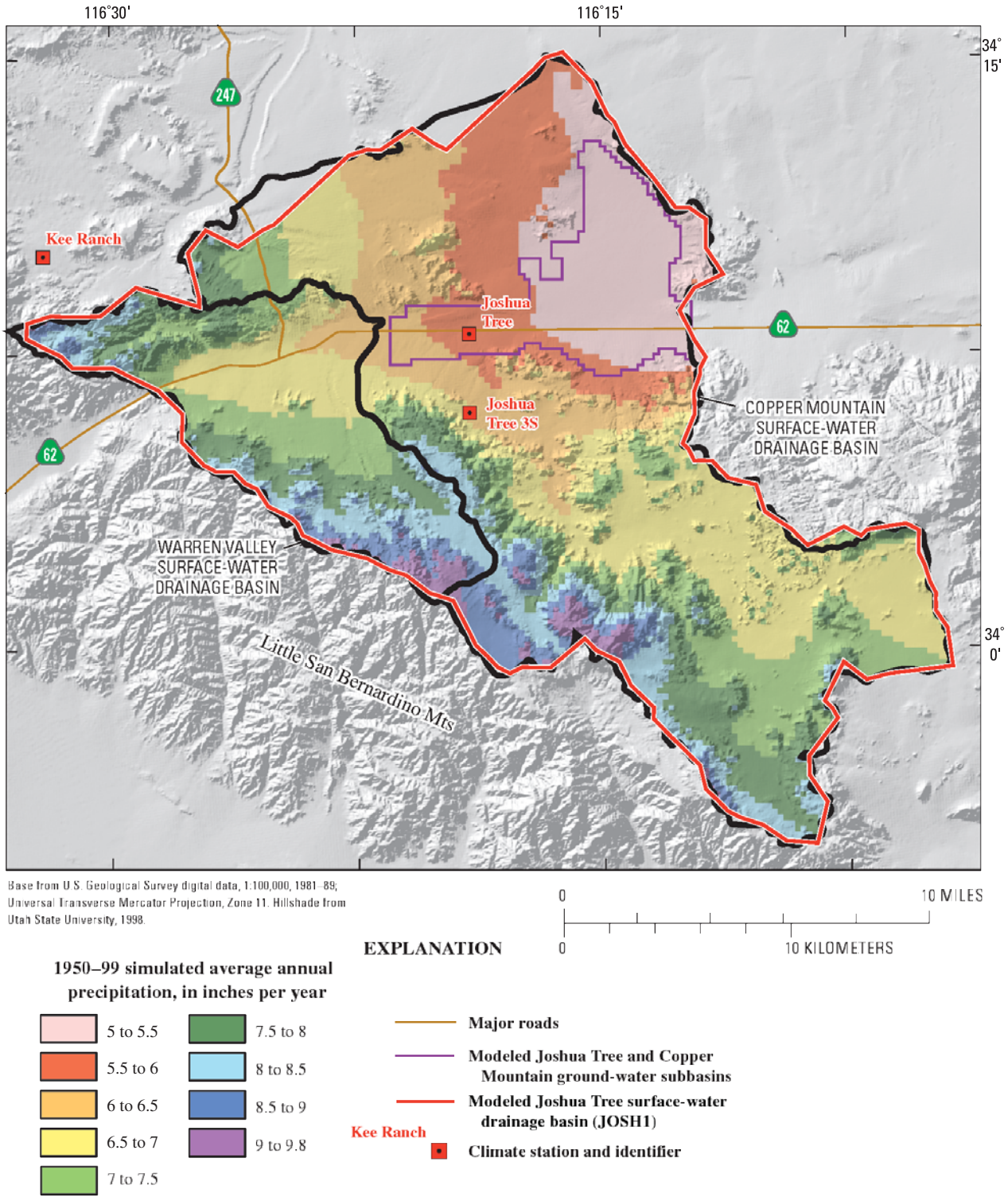

Figure 27. 1950–99 average annual precipitation simulated using the INFILv3 model, Joshua Tree surface-water drainage basin, San Bernardino County, California.

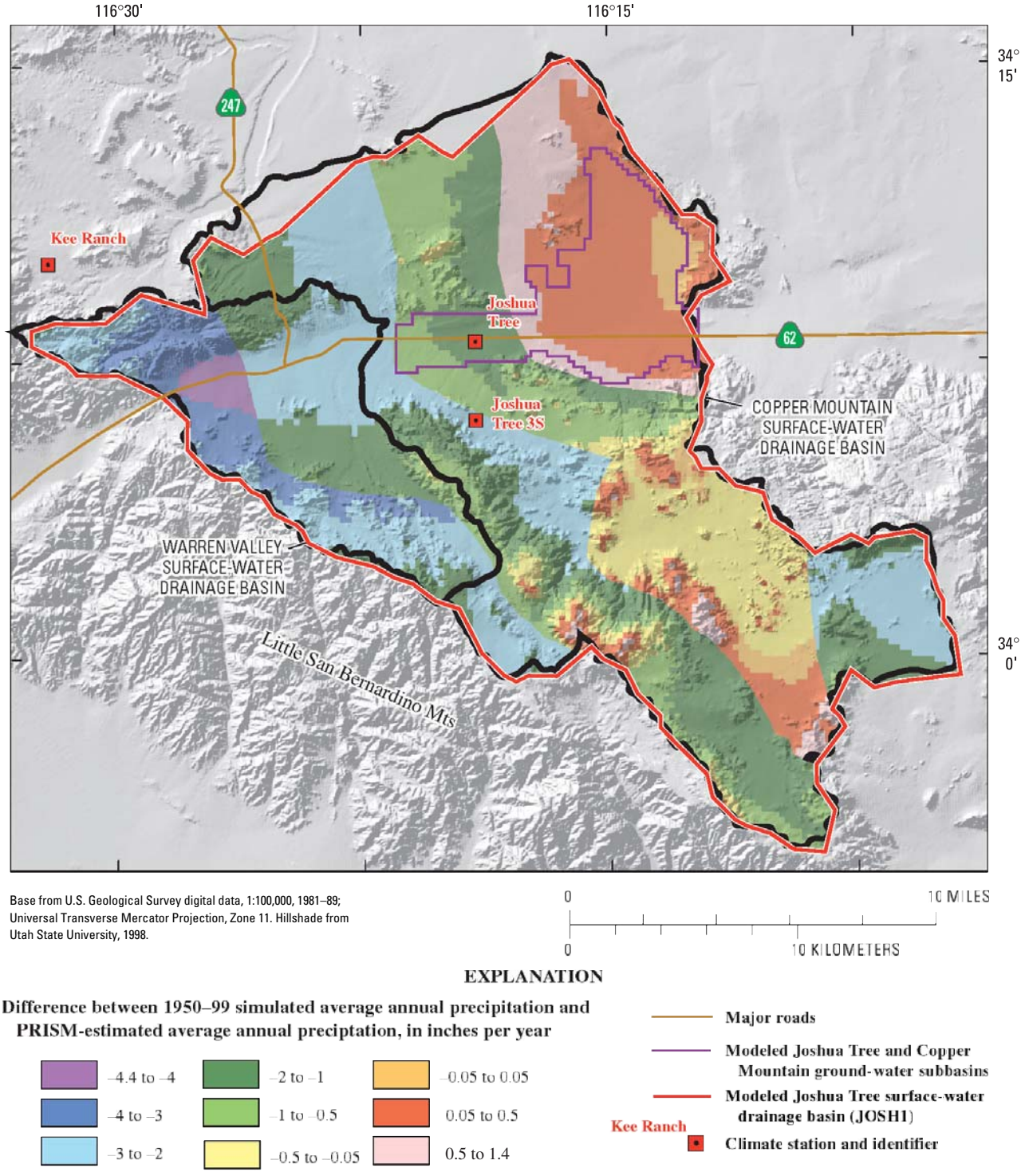

Figure 28. Difference between 1950–99 simulated average annual precipitation using the INFILv3 model and estimated average annual precipitation using PRISM, Joshua Tree surface-water drainage basin, San Bernardino County, California. Positive values indicate that the INFILv3 values are greater than the PRISM values.

Table 13. Summary of daily climate records for four National Weather Service stations within and adjacent to the Joshua Tree surface-water drainage basin, San Bernardino County, California

[in./yr, inches per year; °F, degrees Farenheit; ft, feet; —, not available; m, meters; asl, above sea level; NCDC, National Climatic Data Center]

						Daily precipitation						
Daily climate recording station			Station location coordinates (UTM, zone 11)				Total precipitation	Snow-fall	Daily maximum air temperature		Daily minimum air temperature	
Se-quence number	Station name	NCDC code	Easting (m)	Northing (m)	Station elevation (ft asl)	Number of years in record	Annual average (in./yr)	Annual average (in./yr)	Number of years in record	Daily average (°F)	Number of years in record	Daily average (°F)
1	Twenty-nine Palms	49099	588807	3776455	1,975.162	50	4.13	0.09	50	84.2	50	51.8
59	Joshua Tree	44405	563008	3776956	2,723.23	14	4.84	.21	0	—	0	—
60	Kee Ranch	44467	543013	3780539	4,334.201	27	8.31	.055	0	—	0	—
77	Morongo Valley	45863	538464	3765736	2,562.461	18	7.83	.34	0	—	0	—

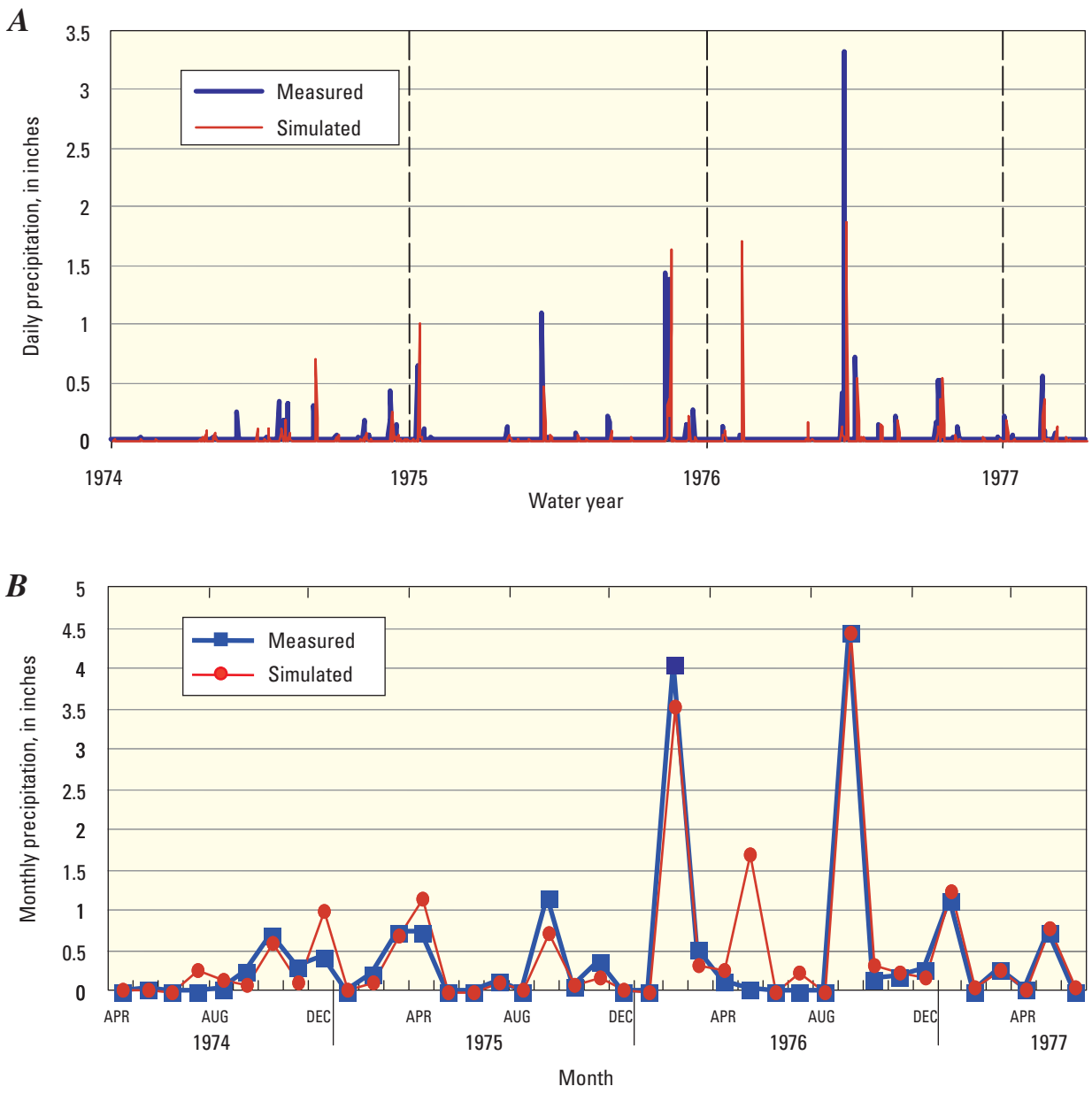

Figure 29. Measured and simulated precipitation at Joshua Tree 3 S climate station: (*A*) daily precipitation and (*B*) monthly precipitation from April 1, 1974, through June 30, 1977, San Bernardino County, California.

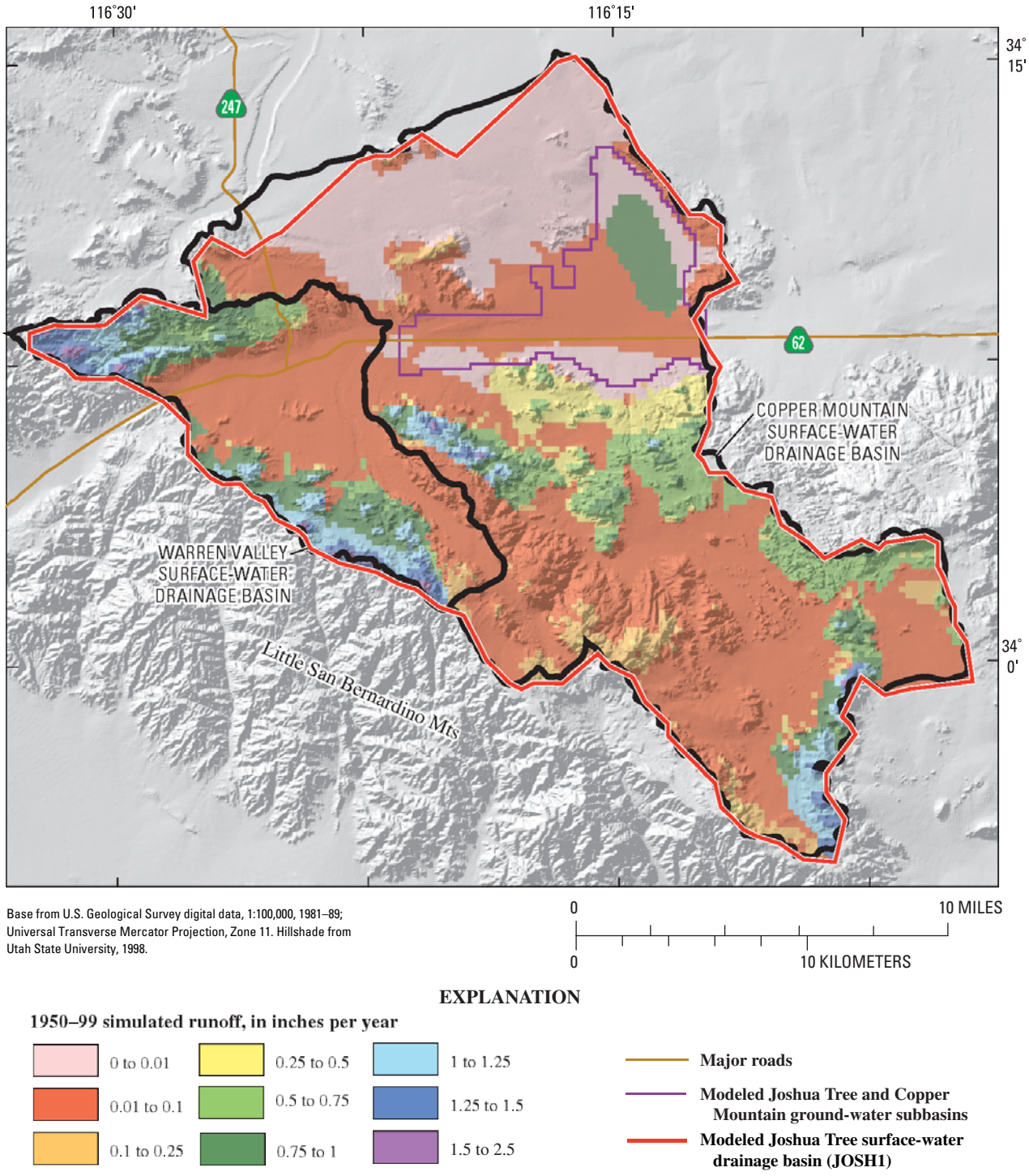

Figure 30. 1950–99 simulated average annual runoff using the INFILv3 model, Joshua Tree surface-water drainage basin, San Bernardino County, California.

Comparison of Simulated and Measured Streamflow

A comparison of simulated daily streamflow with measured streamflow at two gaging sites in the Joshua Tree study area on the south flank of the Little San Bernardino Mountains [Quail Wash (USGS station number 10253320) and Fortynine Palms Creek (USGS station number 10253350)] is presented in table 14. Of these sites, Quail Wash is the only stream that contributes water to the Joshua Tree surface-water drainage basin. The simulated total annual streamflow for the Quail Wash site is 10 times greater than measured; however, both the measured and simulated values are small. Fortynine Palms Creek is east of the study area and the simulated total annual streamflow is nearly two times greater than measured. For the summer months (July through September), simulated streamflow is zero at Quail Wash and Fortynine Palms Creek while measured streamflow at each gage was small (table 15). For the fall, winter, and spring months (October through June), simulated total streamflow is greater than measured streamflow at both gaging stations (table 16). These results indicate that the INFILv3 model reasonably estimates total streamflow from the south flank of the Little San Bernardino Mountains, although the model underestimates the contribution of summer streamflow and overestimates the contribution of winter storms.

Simulated 1950–99 Average Annual Recharge

The simulated 1950–99 average annual recharge results are shown in figure 31. In general, results from the INFILv3 watershed model indicate that recharge throughout JOSH1 is dependent on runoff generation and the subsequent infiltration of surface water run-on routed to downstream locations. These locations include major stream channels as well as the upper parts of alluvial fans downslope from more rugged terrain characterized by outcropping bedrock and thin soils. The high recharge occurs in response to the large volume of run-on that infiltrates the root zone at locations underlain by thick alluvium, and then continues to drain down through the root zone over many days and months following the occurrence of streamflow. Most of the infiltrated run-on in JOSH1 eventually is lost to evapotranspiration; only a small percentage contributes to recharge (table 12).

The average annual simulated recharge in JOSH1 is about 1,090 acre-ft/yr (table 12), with 195 acre-ft/yr infiltrating in the Warren subbasin ground-water model area (not shown in table 12), 158 acre-ft/yr infiltrating in the Joshua Tree and Copper Mountain subbasins ground-water model area, and the balance infiltrating in the area outside of the ground-water subbasins. Recall, INFILv3 simulated 244 acre-ft/yr as surface-water outflow to Coyote Lake; it was assumed that this water is evaporated because of the impermeable dry-lakebed deposits (Qp) at Coyote Lake. The areal distribution of recharge within the ground-water model areas is shown in figure 32. Most of the simulated recharge occurs along Water Canyon and Yucca Wash in the Warren subbasin and along Yucca Wash and Quail Wash in the Joshua Tree and Copper Mountain ground-water subbasins (fig. 32). In addition, simulated recharge rates between 0.1 and 0.5 in./yr occurs along the flanks of the Little San Bernardino Mountains. The recharge value estimated using INFILv3 for the Warren subbasin ground-water model area is about twice that estimated by Nishikawa and others (2003). The area outside of the ground-water subbasins is underlain by the pre-Tertiary basement complex (fig. 4*A*); most of the infiltration that occurs in this area probably does not reach the ground-water subbasins. INFILv3 simulates infiltration in the thin veneer of alluvium that overlies the pre-Tertiary basement complex; however, most of this infiltrated water probably follows the surface of the basement complex and eventually discharges at seeps and springs where the water is lost to evapotranspiration.

2000–03 Simulated Infiltration/Recharge

The INFILv3 model was applied to simulate recharge and streamflow for water years 2000–03 to compare with the field observations collected for this study and to evaluate the temporal variability of potential recharge. The reader is referred to the "Estimating Recharge Using Borehole Instrumentation" section of this report for field-measurement results.

The 2000–03 simulation period is the driest 4-year period from 1950–2003 in terms of precipitation and runoff (table 17). All simulated 2000–03 runoff occurred in response to summer precipitation. During this period, a series of large storms in August 2000 and August 2003 resulted in observed outflow to Coyote Lake; there were no other events that resulted in outflow. The watershed model successfully simulated the outflow time series (fig. 33).

The monthly time-series of simulated recharge for water years 2000–03 shows a well-defined trend of decreasing recharge rates, with no apparent correlation to the simulated precipitation (fig. 33). These results indicate that recharge for 2000–03 occurred as long-term gravity drainage from residual moisture in the lower part of the root zone in response to wetter-than-average conditions and episodes of significant recharge during the 1992–95 period. The simulated results also indicate that most of the residual moisture and, thus, long-term recharge, occurs in the deeper root zones assumed to be present in the alluvial channel locations that are subject to surface-water run-on. Precipitation during the 2000–03 simulation period did not result in significant contributions to recharge. Continuous temperature and matric-potential data collected between January 2001 and July 2003 from the instrumented boreholes beneath Quail Wash indicated that small amounts of infiltration occurred during this period, supporting the modeled results.

Table 14. Comparison of simulated and measured streamflow for all months, Joshua Tree surface-water drainage basin, San Bernardino County, California

[USGS, U.S. Geological Survery; na, not available; acre-ft, acre feet]

Water year	Number of days in record	Measured streamflow for water year		Simulated streamflow for water year	
		Number of days with flow	Total flow (acre-ft)	Number of days with flow	Total flow (acre-ft)
Quail Wash (USGS station number 10253320)					
1964	183	0	0.0	0	0.0
1965	365	0	0.0	0	0.0
1966	365	0	0.0	4	86.0
1967	365	1	0.2	0	0.0
1968	366	1	0.4	0	0.0
1969	365	1	0.1	0	0.0
1970	365	3	7.3	0	0.0
1971	365	1	1.0	0	0.0
Total	2,739	7	9.0	4	86.0
Average	na	0.9	1.1	0.5	10.8
Fortynine Palms Creek (USGS station number 10253350)					
1963	365	6	155.1	0	0.0
1964	366	3	149.0	2	373.0
1965	365	1	99.2	0	0.0
1966	365	1	6.5	21	909.5
1967	365	1	115.1	0	0.0
1968	366	0	0.0	0	0.0
1969	365	0	0.0	0	0.0
1970	365	5	52.5	0	0.0
1971	365	5	91.1	0	0.0
Total	3,287	22	668.5	23	1,282.5
Average	na	2.4	74.3	2.6	142.5

Table 15. Comparison of simulated and measured streamflow for July–September, Joshua Tree surface-water drainage basin, San Bernardino County, California

[USGS, U.S. Geological Survey; na, not available; acre-ft, acre feet]

Water year	Number of days in record	Measured streamflow for July–September			Simulated streamflow for July–September		
		Number of days with flow	Total flow (acre-ft)	Maximum daily flow (acre-ft)	Number of days with flow	Total flow (acre-ft)	Maximum daily flow (acre-ft)
Quail Wash (USGS station number 10253320)							
1964	183	0	0.0	0.0	0	0.0	0.0
1965	365	0	0.0	0.0	0	0.0	0.0
1966	365	0	0.0	0.0	0	0.0	0.0
1967	365	1	0.2	0.2	0	0.0	0.0
1968	366	1	0.4	0.4	0	0.0	0.0
1969	365	0	0.0	0.0	0	0.0	0.0
1970	365	2	6.7	3.6	0	0.0	0.0
1971	365	1	1.0	1.0	0	0.0	0.0
Total	2,739	5	8.3	5.2	0	0.0	0.0
Average	na	0.6	1.0	0.7	0	0.0	0.0
Fortynine Palms Creek (USGS station number 10253350)							
1963	365	6	155.1	119.0	0	0.0	0.0
1964	366	1	1.4	1.4	0	0.0	0.0
1965	365	1	99.2	99.2	0	0.0	0.0
1966	365	0	0.0	0.0	0	0.0	0.0
1967	365	1	115.1	115.1	0	0.0	0.0
1968	366	0	0.0	0.0	0	0.0	0.0
1969	365	0	0.0	0.0	0	0.0	0.0
1970	365	5	52.5	39.7	0	0.0	0.0
1971	365	5	91.1	41.7	0	0.0	0.0
Total	3,287	19	514.4	416.1	0	0.0	0.0
Average	na	2.1	57.2	46.2	0	0.0	0.0

Table 16. Comparison of simulated and measured streamflow for October–June, Joshua Tree surface-water drainage basin, San Bernardino County, California

[USGS, U.S. Geological Survey; na, not available; acre-ft, acre feet]

Water year	Number of days in record	Measured streamflow for October–June			Simulated streamflow for October–June		
		Number of days with flow	Total flow (acre-ft)	Maximum daily flow (acre-ft)	Number of days with flow	Total flow (acre-ft)	Maximum daily flow (acre-ft)
Quail Wash (USGS station number 10253320)							
1964	183	0	0.0	0.0	0	0.0	0.0
1965	365	0	0.0	0.0	0	0.0	0.0
1966	365	0	0.0	0.0	4	86.0	50.0
1967	365	0	0.0	0.0	0	0.0	0.0
1968	366	0	0.0	0.0	0	0.0	0.0
1969	365	1	0.1	0.1	0	0.0	0.0
1970	365	1	0.6	0.6	0	0.0	0.0
1971	365	0	0.0	0.0	0	0.0	0.0
Total	2,739	2	0.7	0.7	4	86.0	50.0
Average	na	0.3	0.1	0.1	0.5	10.8	6.3
Fortynine Palms Creek (USGS station number 10253350)							
1963	365	0	0.0	0.0	0	0.0	0.0
1964	366	2	147.6	136.9	2	373.0	276.5
1965	365	0	0.0	0.0	0	0.0	0.0
1966	365	1	6.5	6.5	21	909.5	280.3
1967	365	0	0.0	0.0	0	0.0	0.0
1968	366	0	0.0	0.0	0	0.0	0.0
1969	365	0	0.0	0.0	0	0.0	0.0
1970	365	0	0.0	0.0	0	0.0	0.0
1971	365	0	0.0	0.0	0	0.0	0.0
Total	3,287	3	154.1	143.4	23	1,282.5	556.8
Average	na	0.3	17.1	15.9	2.6	142.5	61.9

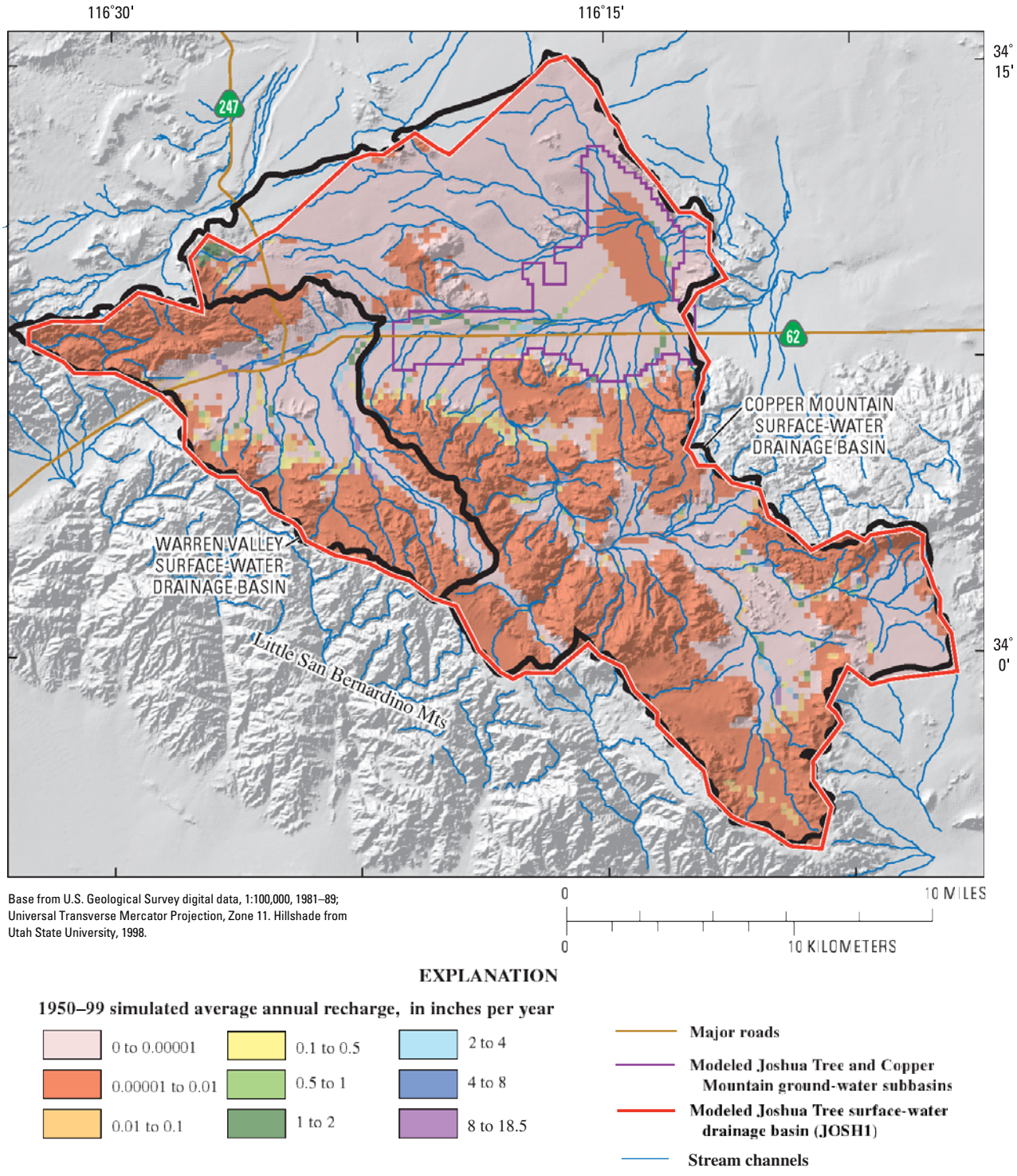

Figure 31. 1950–99 simulated average annual recharge using the INFILv3 model, Joshua Tree surface-water drainage basin, San Bernardino County, California.

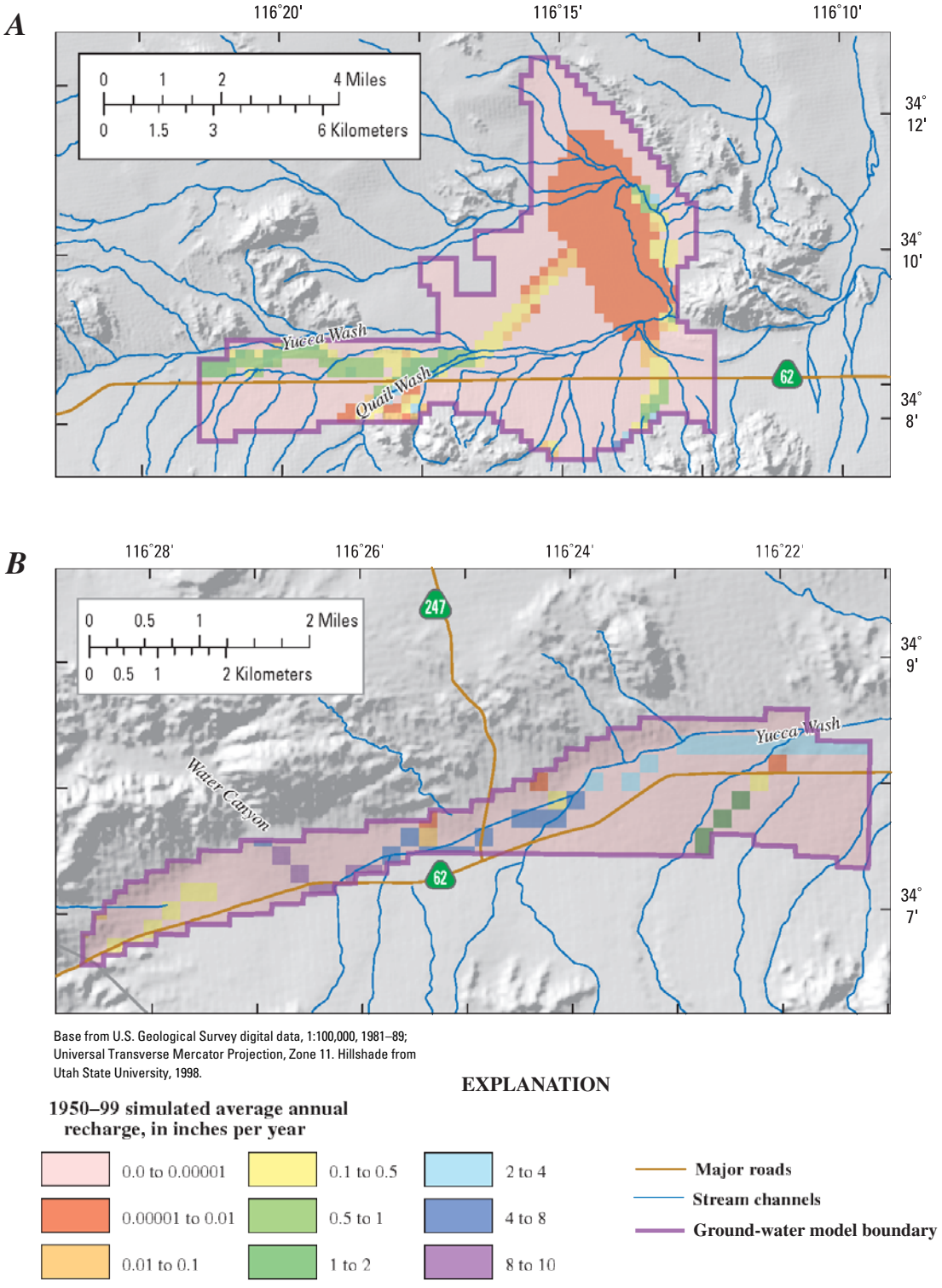

Figure 32. 1950–99 simulated average annual recharge using the INFILv3 model for the (*A*) Joshua Tree and Copper Mountain ground-water model grid only and the (*B*) Warren Valley ground-water model grid (Nishikawa and others, 2003), Joshua Tree surface-water drainage basin, San Bernardino County, California.

Table 17. Comparison of results for the 1950–99 and 2000–03 simulations, Joshua Tree surface-water drainage basin, San Bernardino County, California

[Numbers presented are simulated results and do not imply any level of accuracy; na, not available; in., inches]

	Precipitation	Snow-fall	Sub-limation	Evapo-trans-piration	Change in root-zone storage	Runoff	Outflow	Recharge	Water balance check
Results for 1950–99 simulation									
Average for water years 1950–99 (in.)	6.91	0.1921	0.01158	6.81	–0.0193	0.2600	0.01960	0.08753	0.00018
Maximum for water years 1950–99 (in.)	16.72	1.3236	.08635	14.48	2.5335	1.8651	.71659	.87784	na
Maximum water year	1983	1979	1979	1983	1976	1979	1979	1978	na
Maximum 4-year average (in.)	11.72	.4631	.03218	11.05	.6504	1.1765	.21578	.45004	na
Maximum 4-year period (water years)	1977–80	1965–68	1965–68	1977–80	1976–79	1977–80	1976–79	1978–81	na
Minimum for water years 1950–99 (in.)	1.75	.0000	.00000	1.87	–2.0716	.0000	.00000	.00088	na
Minimum water year	1956	1984	1984	1956	1998	1956	1999	1965	na
Minimum 4-year average (in.)	4.51	.0291	.00056	4.58	–0.6139	.0177	.00000	.00130	na
Minimum 4-year period (water years)	1959–62	1989–92	1989–92	1959–62	1984–87	1959–62	1986–89	1962–65	na
Results for 2000–03 simulation									
Water year 2000 (in.)	3.45	.0098	.00114	3.54	–.0986	.0132	.00066	.00515	.00000
Water year 2001 (in.)	4.59	.0241	.00086	4.66	–.0756	.0028	.00000	.00386	.00000
Water year 2002 (in.)	.96	.0013	.00001	1.02	–.0604	.0000	.00000	.00241	.00000
Water year 2003 (in.)	7.36	.0001	.00000	7.35	.0011	.0516	.00870	.00178	.00000
Average for water years 2000–03 (in.)	4.09	.0088	.00050	4.14	–.0584	.0169	.00234	.00330	.00000

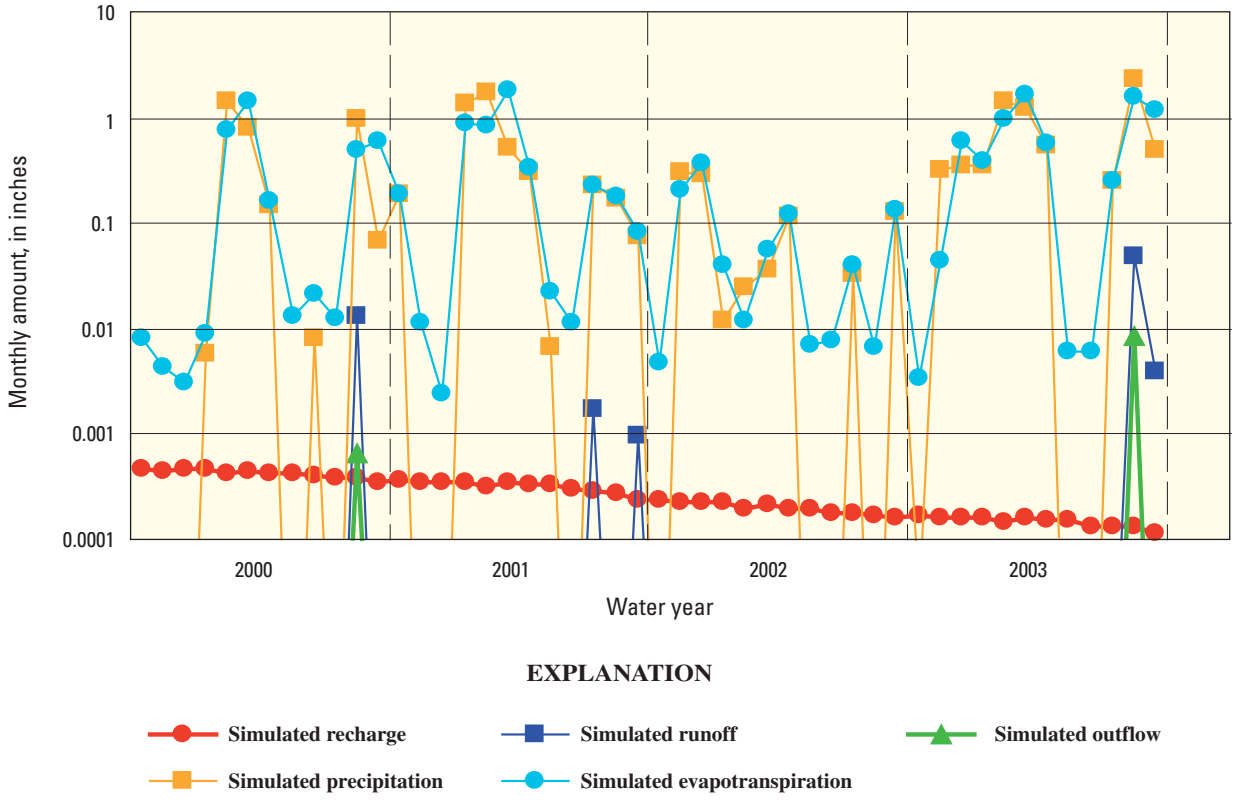

Figure 33. Simulated monthly recharge precipitation, runoff, evapotranspiration, and outflow for water years 2000–03, Joshua Tree surface-water drainage basin, San Bernardino County, California.

Time-Series Results and Temporal Variability in Simulated Recharge

Annual Results for Water Years 1950–2003

Annual (water year) basinwide average results for the simulated 1950–2003 water-balance terms for the modeled Joshua Tree surface-water drainage basin indicate significant year-to-year variability for all components of the water balance (fig. 34). There were a significant recharge event in water years 1978 and 1993 (both at least 11,000 acre-ft/yr) (fig. 34*A*). Simulated outflow shows the highest year-to-year variability with the maximum outflow of 8,800 acre-ft occurring in water year 1979 (fig. 34*B*).

The 1950–2003 annual (water year) time series of simulated recharge and the 5- and 10-year moving mean recharge rate were compared with the annual time-series of the El Nino-Southern Oscillation (ENSO) and the Pacific Decadal Oscillation (PDO) phases (fig. 35). The ENSO and PDO phases are based on monthly sea-surface temperature anomalies in the Pacific Ocean and are used as indicators of climate variability (Philander, 1990; Mantua and others, 1997). The 2 water years with the highest annual recharge (1978 and 1993) occurred during extended positive ENSO periods in conjunction with a positive PDO phase that occurred from 1977 through 1998. These infrequent occurrences of much higher-than-average annual recharge have a strong effect on the calculated time-averaged recharge rates; the 10-year mean recharge rate increases from a relatively low 400 acre-ft/yr in 1977 to a maximum of 3,100 acre-ft/yr in 1986, decreases back to 400 acre-ft in 1992, and then increases to 1,700 acre-ft/yr in 1999. In contrast, annual recharge is less than 200 acre-ft/yr from 1997 through 1999, indicating relatively dry conditions.

Average Monthly Results and Seasonal Variability

Average monthly results for all terms of the water balance were calculated using the 1950–2003 simulation results for JOSH1 (fig. 36). January is the wettest month in terms of precipitation (with an average monthly precipitation of about 1.1 in.) (fig. 36*A*), and February and March are the wettest months in terms of recharge (with an average monthly recharge of about 0.03 in.) (fig. 36*B*). June is the driest month in terms of precipitation (with average monthly precipitation of about 0.05 in.) and November is the driest month in terms of recharge (with an average monthly recharge of about 0.002 in.). The average evapotranspiration is highest for March (about 1.1 in.) and lowest for June (about 0.2 in.). March has the highest average evapotranspiration because of the high residual root-zone moisture caused by high precipitation in December–March (fig. 36*A*). June has the lowest average evapotranspiration because of the low residual root-zone moisture caused by low precipitation in April–June (fig. 36*A*). Average monthly precipitation exceeds average monthly evaporation for November, December, January, February, and September.

The monthly results indicate that recharge primarily occurs in response to December through March precipitation. Through the spring, summer, and fall months (April through November), recharge decreases (fig. 36*B*). Summer (July through September) precipitation does not provide a significant contribution to recharge. Recharge for summer months occurs primarily in response to increased moisture in the lower root-zone layers left over from infiltrated winter precipitation and surface-water run-on.

In contrast to monthly recharge, monthly runoff and surface-water outflow indicate a strong response to both winter and summer precipitation. Simulated average monthly runoff for July through September is comparable in magnitude to simulated average monthly runoff for March and December (fig. 36*B*). The ratio of runoff to outflow is the highest for the summer months (July through September) owing to the shorter assumed storm duration of 2 hours for summer precipitation (compared with a 12-hour duration assumed for winter, autumn, and spring precipitation). Streamflow simulated for the summer months is more likely to discharge into Coyote Lake dry lakebed (and subsequently evaporate), in comparison with winter through spring streamflow, which is more likely to infiltrate into the streambed before reaching the dry lakebed.

Watershed-Model Limitations

The water-balance method used in the INFILv3 model has many simplifying assumptions concerning the physics of unsaturated ground-water flow. For example, the water-balance calculations assume that the process of vapor flow and the effects of temperature on water density are negligible. Water density was assumed constant, allowing the governing equations in the water-balance model to be applied as a volume balance rather than as a mass balance. In each grid cell of the model domain, water was assumed to move vertically downward in soil and bedrock; lateral inflow or outflow in the subsurface between grid cells was assumed to be negligible. Recharge was assumed to occur as gravity drainage under a unit gradient. The effect of capillary forces on unsaturated flow in the root zone was not included in the model.

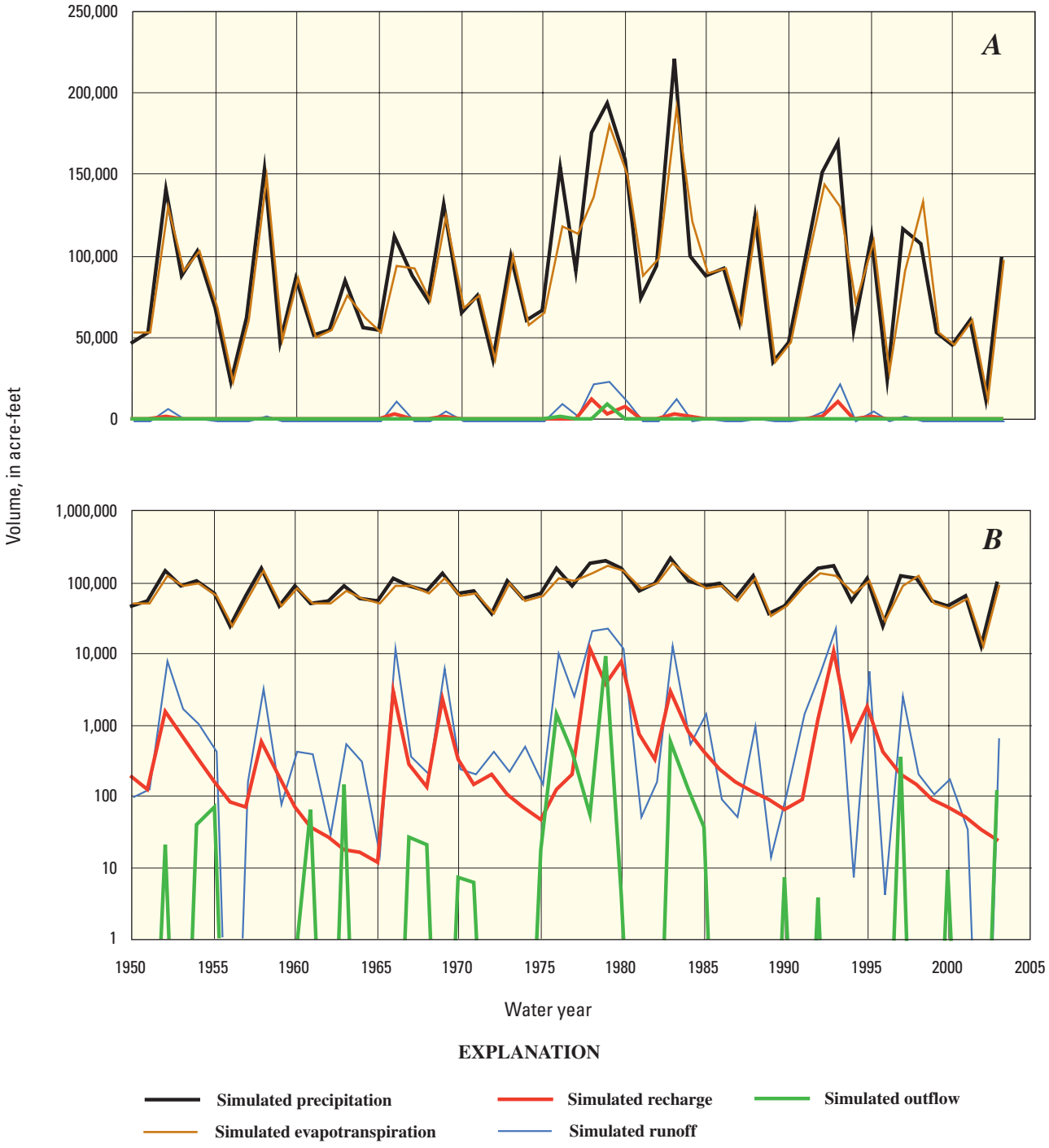

Figure 34. Simulated annual time-series of water-balance terms for water years 1950–2003 using (*A*) a linear scale and (*B*) a logarithmic scale, Joshua Tree surface-water drainage basin, San Bernardino County, California.

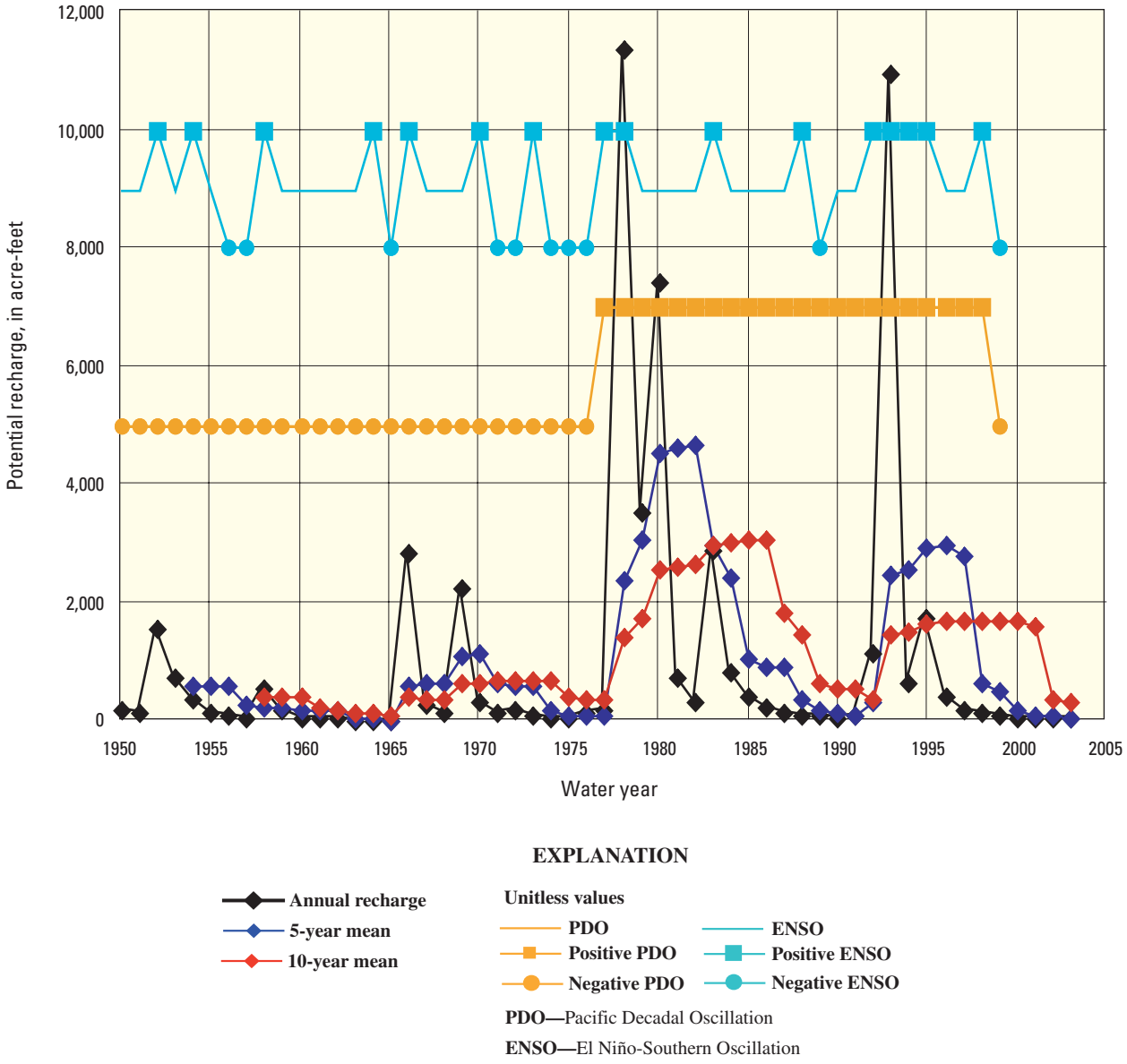

Figure 35. Pacific Decadal Oscillation (PDO) and the El Nino-Southern Oscillation (ENSO) climate cycles with temporal variability in simulated average potential recharge, Joshua Tree surface-water drainage basin, San Bernardino County, California.

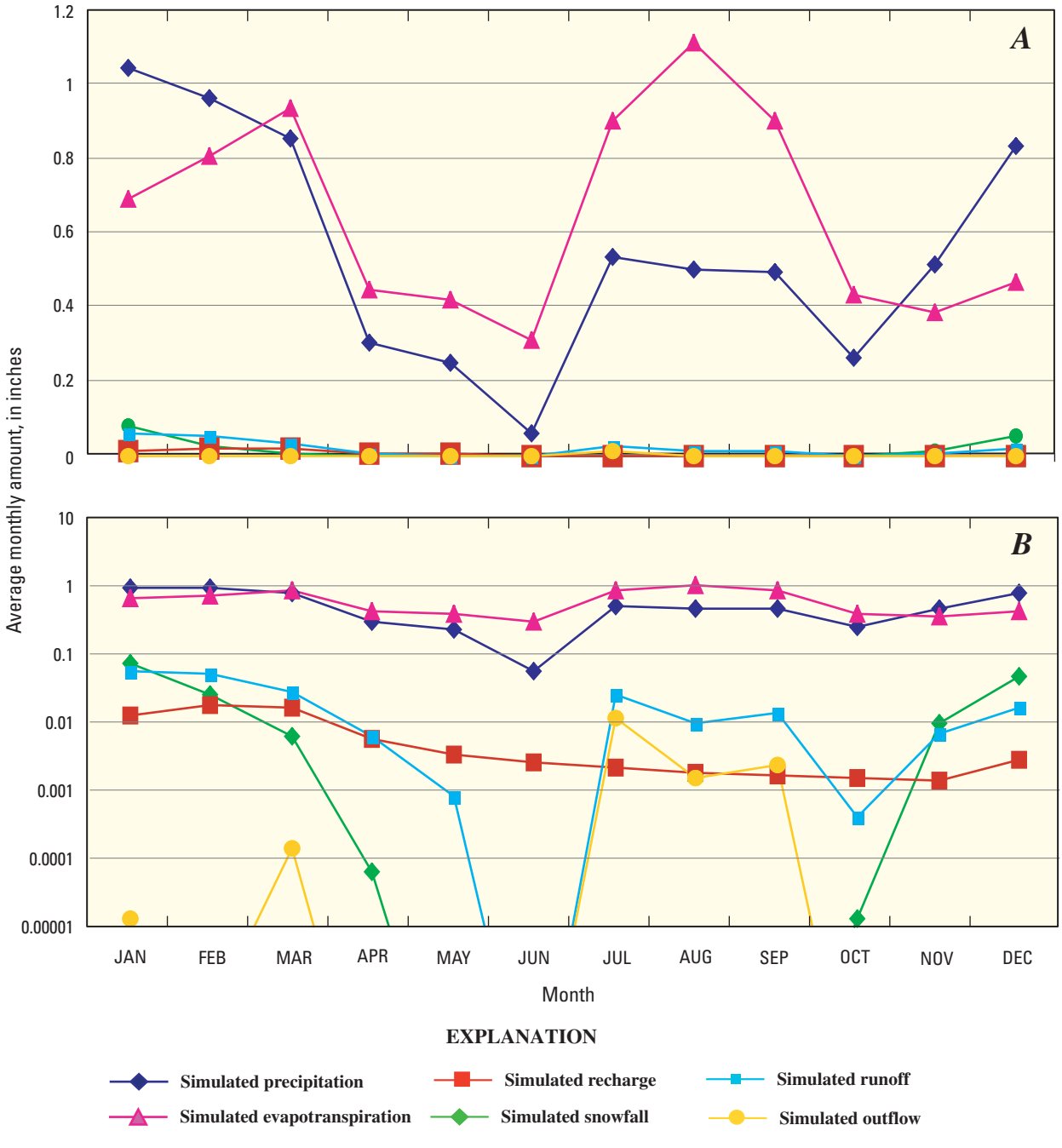

Figure 36. Simulated average monthly precipitation, evapotranspiration, snowfall, recharge, runoff, and outflow for water years 1950–2003 using (*A*) a linear scale and (*B*) a logarithmic scale, Joshua Tree surface-water drainage basin, San Bernardino County, California.

The INFILv3 model simulates streamflow originating as runoff and as subsequent overland flow, but it does not simulate streamflow originating as base flow from deep ground-water discharge or as through-flow from perched zones, such as the alluvium-bedrock contact in washes. Thus, a major assumption applied in this method of calibration is that overland flow, generated in response to rainfall or snowmelt, is the primary component of streamflow measured in the Joshua Tree study area. Simulation of daily streamflow in the INFILv3 model is based on a daily routing algorithm that assumes episodic streamflows with durations less than 24 hours. Simulated streamflow either discharges from the drainage basin or infiltrates into the root zone in the daily time step. Temporary perched ground-water systems, which may be an important component of streamflow and spring discharge for the higher altitudes, is not represented by the INFILv3 model. In addition, dispersive streamflow, which can be an important characteristic of streamflow and overland flow across alluvial fans and basins, is not directly represented in the surface-water flow-routing algorithm. All surface-water flow is simulated as convergent streamflow.

Sources of model uncertainty include input parameters such as the hydraulic conductivity of bedrock, soil thickness, soil hydrologic properties, parameters used to define stream-channel characteristics, root-zone depth, and root density as a function of depth. Additional sources of model uncertainty include the limitation of the model in representing the spatial and temporal distribution of precipitation and air temperature using available climate records and the limitation of the model in representing runoff generation and subsequent streamflow using assumed durations for precipitation, snowmelt, and streamflow. Recall, coefficients for modeling snowmelt, sublimation, and stream-channel characteristics were identical to those used by Hevesi and others (2003) for simulating net infiltration in the DVRFS model. The use of these parameters in the Joshua Tree area may result in small errors in estimating potential evapotranspiration; however, these errors are probably insignificant in comparison with other sources of uncertainty in the simulation of actual evapotranspiration (such as, root density).

Summary of Simulation Results Using the INFILv3 Watershed Model

The average annual simulated recharge in JOSH1 is about 1,090 acre-ft/yr, with 195 acre-ft/yr in the Warren subbasin ground-water model area and 158 acre-ft/yr infiltrating in the Joshua Tree and Copper Mountain subbasins ground-water model area. The simulated total annual streamflow is 2 to 10 times greater than the measured total annual streamflow, indicating that the recharge values estimated using INFILv3 may be overestimated. Recall that the INFILv3 model was calibrated for the large-scale DVRFS model; therefore, reconceptualization and recalibration of the model may be required to more accurately simulate watershed conditions in the Joshua Tree study area.

Results from the INFILv3 watershed model indicate that recharge and potential recharge throughout the Joshua Tree surface-water drainage basin is strongly dependent on winter-season runoff generation during wetter than average periods and the subsequent infiltration of surface water run-on routed to downstream locations. These locations include major stream channels as well as the upper parts of alluvial fans downslope from more rugged terrain characterized by outcropping bedrock and thin soils. The high recharge occurs in response to the large volume of run-on that infiltrates the root zone at locations underlain by thick alluvium, and then continues to drain down through the root zone over many days and months following the occurrence of streamflow. Above-normal summer precipitation, including storms characterized by high-intensity precipitation conducive to runoff generation, generally does not result in significant recharge, even when conditions are wet enough to cause surface-water discharge into the Coyote Lake dry lakebed. These simulated results are supported by the isotopic data that indicate that winter precipitation is the predominant source of ground-water recharge.

The 2000–03 simulation results indicate that recharge occurred as long-term gravity drainage from residual moisture in the lower part of the root zone in response to wetter than average conditions and episodes of significant recharge during the 1992–95 period. The simulated results also indicate that most of the residual moisture and, thus, long-term recharge, occurs in the deeper root zones estimated for the alluvial channel locations that are subject to surface-water run-on. Precipitation during the 2000–03 simulation period does not result in significant contributions to recharge because of insufficient winter precipitation.

Ground-Water Flow Model

To better understand the physics and dynamics of ground-water flow in the Joshua Tree and Copper Mountain ground-water subbasins, a numerical flow model of the subbasins was developed for the period 1958–2001. The ground-water flow model was developed using MODFLOW-2000 (MF2K) (Harbaugh and others, 2000).

MF2K is a finite-difference model that simulates ground-water flow in a three-dimensional heterogeneous and anisotropic medium provided that the fluid has constant density (Harbaugh and others, 2000). For additional information regarding MF2K, the reader is referred to Harbaugh and others (2000).

Model Discretization

Spatial Discretization

The grid spacing of the MF2K finite-difference model grid is about 820 ft by 820 ft (fig. 37). The areal model domain was based initially on geohydrologic data collected by previous investigators and collected for this study. Estimates of average aquifer properties were assigned to the representative cell volume, and average hydraulic head was calculated at the center, or node, of each cell.

The vertical layering is shown along with the relative thicknesses and the altitudes of the model layers in figure 38. The aquifer system was vertically discretized into three model layers: model layer 1 represents the upper aquifer, model layer 2 represents the middle aquifer, and model layer 3 represents the lower aquifer.

In most areas, the bottom of model layer 1 and the bottom of model layer 2 were assumed to be uniformly flat (fig. 38) and to correspond with approximated geologic contacts. The top altitude of model layer 1 represents the water table and was defined using data from a modified DEM of the subbasins (Steven Predmore, USGS, written commun., 2002); the bottom altitude corresponds to the bottom of the upper aquifer at 2,000 ft asl, except in areas where the basement-complex altitude is greater than 2,000 ft asl. Model layer 1 has a variable thickness, which ranges from 1 to 360 ft assuming that the entire thickness of the layer is available for ground-water storage. The top altitude of model layer 2 is 2,000 ft asl, except in areas where the basement-complex altitude is greater than 2,000 ft asl; the bottom altitude corresponds to the bottom of the middle aquifer at 1,550 ft asl, except in areas where the basement-complex altitude is greater than 1,550 ft. Model layer 2 has a variable thickness that ranges from 230 to 450 ft. If the basement-complex altitude is greater than the top of the model layer, then the model cell is inactive in that layer. The top altitude of model layer 3 is 1,550 ft asl and the bottom altitude is based on the depth to basement complex determined by gravity measurements (fig. 38). Model layer 3 has a variable thickness that ranges from 0 to 1,180 ft.

The geologic and geophysical logs collected from the multiple-well monitoring site 1N/6E-34D3-5 indicate that at this site the upper aquifer is unsaturated, and that Tertiary sedimentary and volcanic deposits were encountered at about 2,200 ft asl (fig. 6*B*). Therefore, the bottom altitude of model layer 1 was raised to 2,200 ft asl in the area between the Yucca Barrier and the inferred north-south trending fault (located between wells 1N/6E-34D3-5 and 34D2), to reflect the geologic properties found at site 1N/6E-34D3–5. The bottom altitude of model layer 2 was unchanged and the bottom altitude of model layer 3 was based on the depth to basement complex determined by gravity measurements. Model layer 1 represents the middle aquifer and model layers 2 and 3 represent the lower aquifer in the model domain west of the inferred fault (fig. 38).

Temporal Discretization

MF2K allows the modeler to simulate the first stress period as steady state and the following stress periods as transient state. Two different stress-period lengths were used for the transient-state simulation period of 1958–2001. The period 1958–75 was simulated using annual stress periods because only annual pumping data were available. The period 1976–2001 was simulated using monthly stress periods because monthly pumping data were available. The total number of transient-state stress periods was 330. Four time steps per stress period were used.

To determine the adequacy of the transient temporal discretization, the time-varying mass-balance errors and the final mass-balance error were considered. In general, the time-varying mass-balance errors should not fluctuate in an unstable manner and the final mass-balance errors should be relatively small. The ground-water flow error fluctuated somewhat in early time but did not fluctuate for most of the simulation and was about −0.15 percent over the last 240 stress periods (fig. 39). The time-varying and final mass-balance errors indicate that the temporal discretizations were adequate.

Model Boundaries

For the ground-water flow model, three types of boundary conditions were used: no-flow, specified-flux, and general-head. A no-flow boundary indicates that there is no exchange of water between the model cell and the domain outside the model. All lateral model boundaries, with the exception of the western, eastern, and northern boundaries, which are bounded by other subbasins, were simulated as no-flow boundaries (fig. 37). For the most part, these no-flow boundaries correspond to locations where gravity data indicate that the basement complex is at, or near, the water-table altitude. The bottom of the model corresponds with the top of the basement complex as defined by the gravity data. It was assumed that the basement complex yields little to no water to the ground-water flow system.

A specified-flux boundary indicates that water flows into or out of the model domain at a specified rate that remains constant for the entire stress period. Specified-flux boundary conditions were used to simulate inflow across the Yucca barrier from the Warren subbasin to the west and natural recharge (fig. 37).

A general-head boundary simulates a source of water outside the model area that either supplies, or receives water from, adjacent cells at a rate proportional to the hydraulic-head differences between the source and the model cells (Harbaugh and others, 2000). The constant of proportionality is the hydraulic conductance whose value is determined during the calibration process. General-head boundaries were located at the eastern and northern ends of the model corresponding to approximate locations of boundaries with other ground-water subbasins (fig. 37).

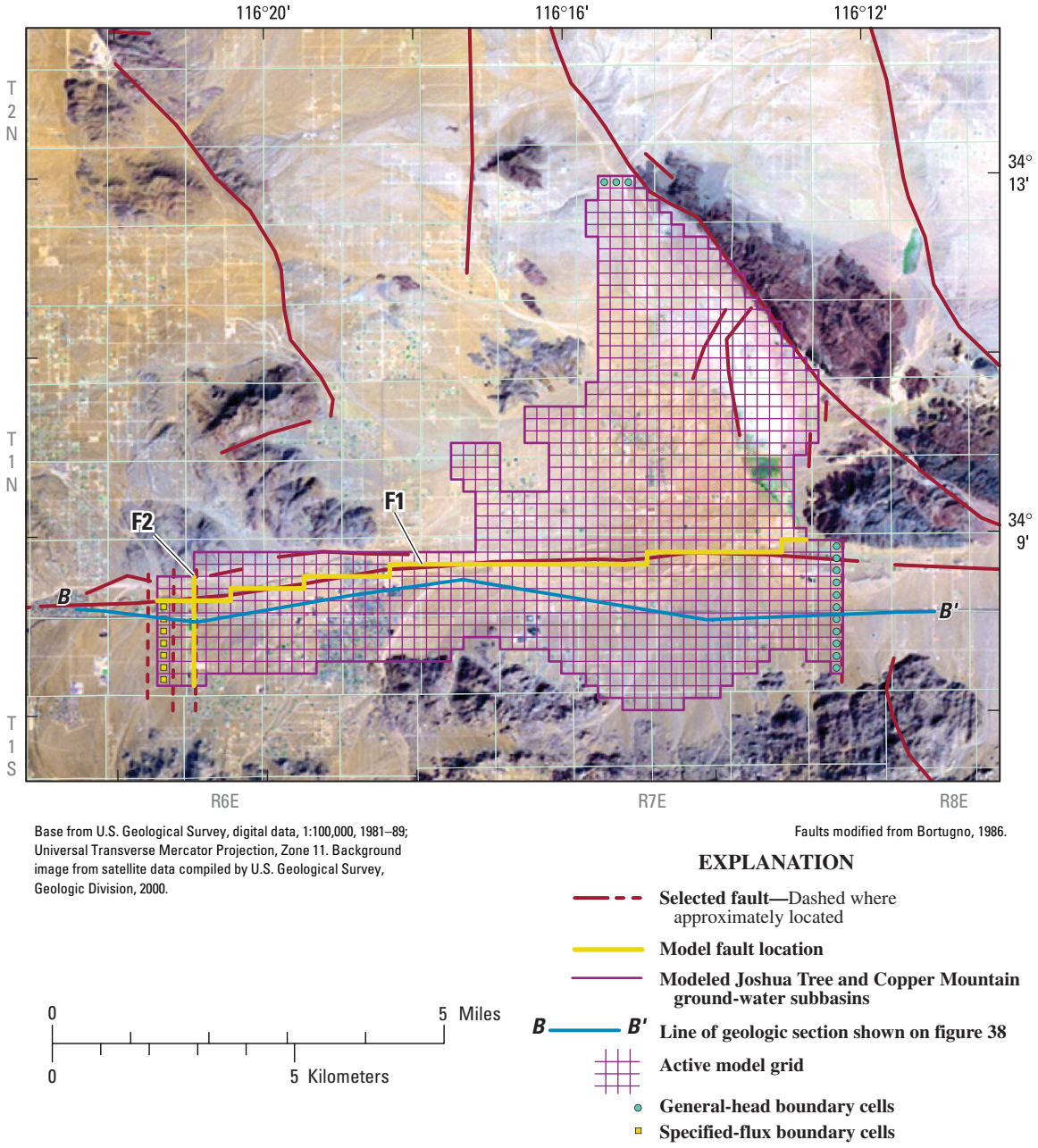

Figure 37. Model grid, active cells, modeled faults, specified-flux boundaries, and general-head boundaries for the ground-water flow model of the Joshua Tree and Copper Mountain ground-water subbasins, San Bernardino County, California.

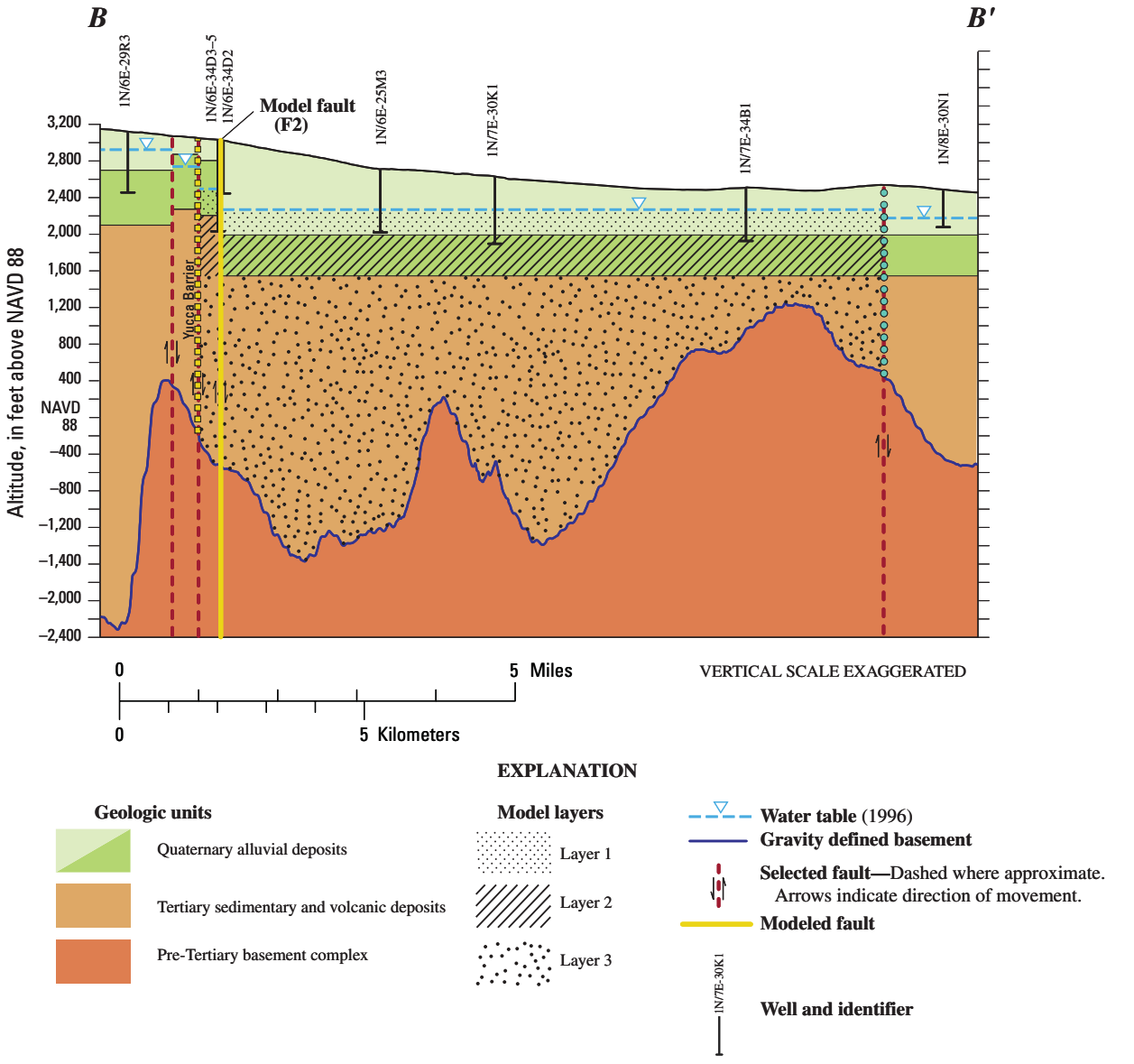

Figure 38. Vertical discretization along section line *B–B′* of the ground-water flow model of the Joshua Tree and Copper Mountain ground-water subbasins, San Bernardino County, California.

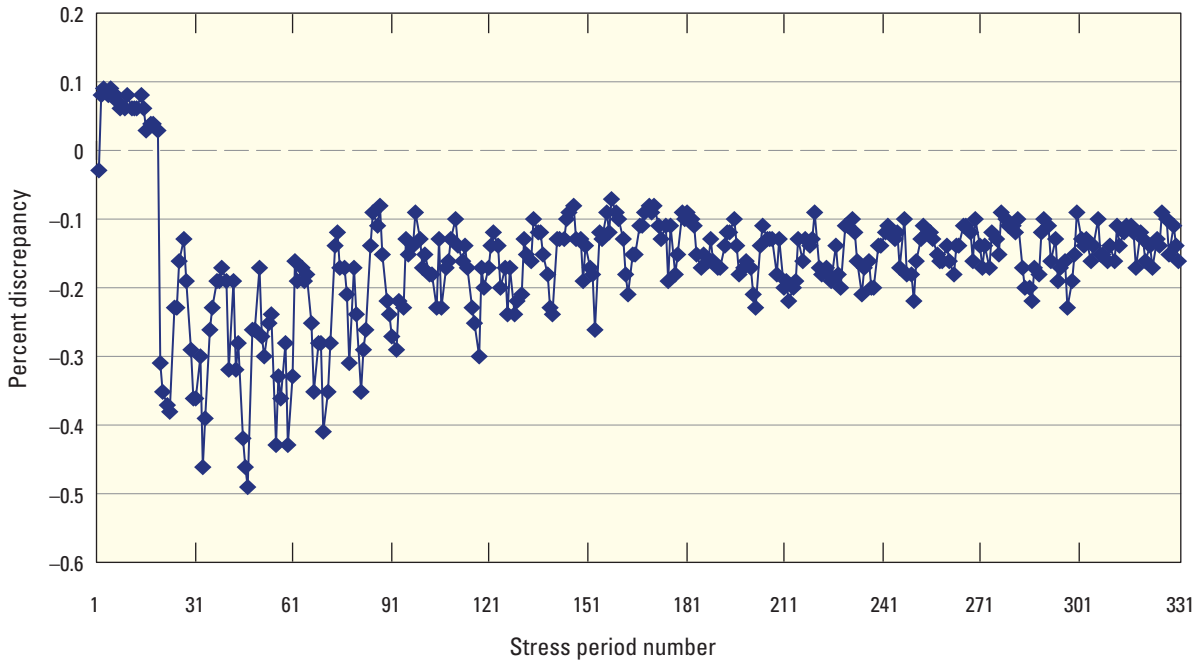

Figure 39. Time-varying mass-balance errors by stress period for the ground-water flow model of the Joshua Tree and Copper Mountain ground-water subbasins, San Bernardino County, California.

Subsurface Properties

Model-layer properties [horizontal and vertical hydraulic conductivity, specific storage, specific yield, hydraulic characteristic (used to simulate faults), and boundary conditions] affect the rate at which simulated water moves through an aquifer, the volume of water in storage, and the rate and areal extent of changes in ground-water levels caused by ground-water pumping and (or) recharge. For this study, some of the aquifer-system properties (hydraulic conductivity, specific storage, and specific yield) were estimated initially from well logs, specific-capacity tests, and published literature. Final estimates of these properties were made using a trial-and-error approach under predevelopment and transient-state conditions (table 18).

Most aquifer-system properties (such as hydraulic conductivity and specific storage) are continuous functions of the spatial variables; therefore, the number of property values could be infinite. For estimation purposes, the infinite number of property values may be reduced through parameterization (Yeh, 1986). In general for this study, the hydraulic-conductivity and storage distributions for each model layer were assumed to be homogeneous. In addition, it was assumed that the hydraulic-conductivity distribution was anisotropic.

Hydraulic Conductivity

A medium has a hydraulic conductivity (K) of unit length per unit time if it will transmit in unit time a unit volume of ground water at the prevailing viscosity through a cross section of unit area, measured at right angles to the direction of flow, under a hydraulic gradient of unit change in head through unit length of flow (Lohman, 1979). MF2K requires defined horizontal and vertical hydraulic-conductivity values for unconfined and confined aquifers. Initial estimates of K values were derived from aquifer tests, specific-capacity tests, and drillers' logs.

Storage Coefficient and Specific Yield

The storage coefficient (also known as storativity, S) of a saturated confined aquifer of thickness b is the volume of water that an aquifer releases from storage per unit of surface area of aquifer per unit decline in the component of hydraulic head normal to that surface (Freeze and Cherry, 1979). For confined aquifers, water is released from storage when pumping causes a decrease in pore-fluid pressure (hydraulic head or head is equal to the pore-fluid pressure divided by the specific weight of water) that increases the intergranular stress transmitted by the solid skeleton of the aquifer and results in a small reduction in porosity. The decrease in pore-fluid pressure produces a slight expansion of water. The combination of the small reduction in porosity and the slight expansion of the water results in a certain volume of water being released from storage (Bear, 1979). The specific yield (Sy) for an unconfined aquifer is the volume of water released from storage per unit surface area of aquifer per unit decline in the water table (Freeze and Cherry, 1979). For unconfined aquifers, water is released from storage when a decline in ground-water level results in the desaturation of the porous medium. Sy was specified for model layer 1 and S [specifically, specific storage ($Ss = S/b$)] was specified for model layers 2 and 3.

Faults

Faults may be barriers to ground-water flow. The faults in the Joshua Tree ground-water basin were modeled using the Horizontal-Flow-Barrier (HFB) Package (Hsieh and Freckleton, 1993). The HFB package simulates faults as thin, vertical, low-permeability geologic features that impede the horizontal flow of ground water. Faults are approximated as a series of horizontal-flow barriers conceptually situated between pairs of adjacent cells in the finite-difference grid (Hsieh and Freckleton, 1993). Flow across a simulated fault is proportional to the hydraulic-head difference between adjacent cells. The constant of proportionality is the hydraulic characteristic (t^{-1}) and is equal to the barrier hydraulic conductivity divided by the width of the horizontal-flow barrier. The hydraulic-characteristic value was determined during the calibration process.

Two faults were simulated as internal barriers to ground-water flow; the fault locations are shown in figure 37. Model fault F1 follows the Pinto Mountain Fault as mapped in figure 4*B*; however, its trace was changed near the eastern end of the basin because measured water levels at wells 1N/7E-25E1 and 25E2 were similar to other water levels measured south of the fault (fig. 37). Model fault F2 corresponds to a fault associated with the Yucca Barrier; it was inferred that this unnamed fault is located between monitoring wells 1N/6E-34D5 and 1N/6E-34D2 (dry) (fig. 4*B*) because the water-level altitude measured at well 34D5 is 80 ft higher than the bottom altitude of well 34D2.

Initially, the hydraulic-characteristic value for each fault was set to a large value allowing ground water to flow freely across the faults. Through the calibration process, the hydraulic-characteristic values were lowered such that the simulated hydraulic heads closely matched measured water levels.

Table 18. Initial and final ground-water flow model parameter estimates, Joshua Tree and Copper Mountain ground-water subbasins, San Bernardino County, California

[K, hydraulic conductivity in feet per day; Kz, vertical hydraulic conductivity in feet per day; Sy, specific yield in feet per feet; Ss, specific storage in per feet; F1, hydraulic characteristic of Pinto Mountain Fault, in per day; F2, hydraulic characteristic of inferred north-south trending fault, in per day; GHBN, general-head conductance northern boundary in feet squared per day; GHBS, general-head conductance southern boundary in feet squared per day; Rech, recharge in acre-feet per year; na, not applicable; ( ), initial estimates]

Parameter	Layer 1		Layer 2		Layer 3
	East of fault 2	West of fault 2	East of fault 2	West of fault 2	
K	(60.0) 60.0	(5.00) 5.00	(5.00) 5.00	(0.500) 0.500	(0.500) 0.500
Kz	(.600) .600	(.0500) .0500	(.0500) .0500	(.00500) .00500	(.00500) .00500
Sy	(.1) .2	(.1) .2	na	na	na
Ss	na	na	(1.00×10^{-3}) 1.00×10^{-6}	(1.00×10^{-3}) 1.00×10^{-6}	(1.00×10^{-6}) 1.00×10^{-6}
F1	(60.0) 3.80×10^{-7}	(60.0) 3.80×10^{-7}	(60.0) 3.80×10^{-7}	(60.0) 3.80×10^{-7}	(60.0) 3.80×10^{-7}
F2	(60.0) 6.50×10^{-7}	(60.0) 6.50×10^{-7}	(60.0) 6.50×10^{-7}	(60.0) 6.50×10^{-7}	(60.0) 6.50×10^{-7}
GHBN	(1,076) 10.76	(1,076) 10.76	(1,076) 10.76	(1,076) 10.76	(1,076) 10.76
GHBS	(1,076) 1.08×10^{-6}	(1,076) 1.08×10^{-6}	(1,076) 1.08×10^{-6}	(1,076) 1.08×10^{-6}	(1,076) 1.08×10^{-6}
Rech	(158) 123.0	(158) 123.0	na	na	na

Model Inflow

Potential sources of model inflow include natural inflow and infiltration of septic-tank effluent. Natural ground-water inflow to the Joshua Tree ground-water subbasin occurs primarily as underflow across the Yucca Barrier from the Warren subbasin and as recharge of runoff from washes along the Little San Bernardino Mountains. Nishikawa and others (2003) reported an average rate for underflow from the Warren ground-water subbasin to the Joshua Tree ground-water subbasin of 85.5 acre-ft/yr. This rate was assumed to be a long-term average and was simulated along the western boundary of the Joshua Tree ground-water subbasin as a specified flux. The final simulated underflow flux rate was about 84 acre-ft/yr.

The recharge of runoff was estimated using the INFILv3 watershed model (Hevesi and others, 2003) as described in the "Simulated Recharge Using a Watershed Model" section of this report. The average annual recharge simulated by INFILv3 in the modeled Joshua Tree surface-water drainage basin (fig. 2) is about 1,090 acre-ft/yr (623 acre-ft/yr infiltrating in the Warren Valley surface-water drainage basin and 467 acre-ft/yr infiltrating in the Copper Mountain surface-water drainage basin) with 158 acre-ft/yr infiltrating in the Joshua Tree and Copper Mountain subbasins ground-water model area (table 12). The final calibrated flux owing to recharge was reduced to 123 acre-ft/yr, and the final distribution of recharge is shown in figure 32. A specified-flux boundary condition was applied to the uppermost active model layer to simulate the recharge of runoff.

The only form of wastewater treatment in the Joshua Tree ground-water subbasin is the use of septic tanks. Assuming that pumpage in the winter months (December–March) is representative of the average pumping and assuming that 73 percent of the pumped ground water is returned by way of septage, then the average potential recharge flux from 1977 to 2001 is as much as 660 acre-ft/yr. However, during the calibration process it was found that the recharge flux from septic tanks resulted in overestimated hydraulic heads, indicating that the septage had not yet traveled through the unsaturated zone. In many areas, increased nitrate concentrations in ground water are associated with septage-recharge flux (Bouwer, 1978). The absence of increased nitrate concentrations in JBWD wells supports the modeling results that an insignificant volume of septage has reached the water table; however, this source of water may eventually reach the water table. Flint and Ellett (2004) simulated the flow of septage through a 600-ft thick unsaturated zone in a desert environment and the results indicated that after 40 years of application the septage traveled about 230 ft.

Model Outflow

Ground-water outflow from the Joshua Tree and Copper Mountain ground-water subbasins occurs primarily as pumpage and ground-water underflow along the northern and eastern boundaries of the subbasins. Evapotranspiration was not simulated explicitly because the depth to ground water was such that this ground-water discharge probably did not occur.

Pumpage

Pumpage data on a per-well basis were not available for the period 1958–64; however, Lewis (1972) reported total annual pumpage for public supply for this period. For this simulation period, public-supply pumpage was evenly divided among production wells assumed to be or known to be actively pumped in a given year.

Pumpage data from 1965–2001, with the exception of most of 1977, were supplied by Joshua Basin Water District (Mark Meeler, Joshua Basin Water District, written commun., 2002). Pumpage data were reported on an annual basis from 1965 to 1975 and on a monthly basis from 1976 to 2001. The missing monthly data from 1977 (February through December) were linearly interpolated using the reported 1976 and 1978 monthly data. The total volume of pumpage from 1958 to 2001 was about 42,200 acre-ft (fig. 8).

Pumpage data were simulated using the multi-node well (MNW) package (Halford and Hanson, 2002). In general, the MNW package distributes vertically the total pumpage on the basis of the hydraulic conductivity of the model layers penetrated by the well and the screened interval of the well. For additional information regarding the MNW package, the reader is referred to Halford and Hanson (2002).

Ground-Water Underflow

Ground-water underflow out of the model area can occur along the eastern and northern edges of the Joshua Tree and Copper Mountain ground-water subbasins. This underflow was simulated using a general-head boundary (fig. 37). A general-head boundary is used to simulate a source of water outside the model area that either supplies water to, or receives water from, the model at a rate proportional to the hydraulic-head differences between the source and the model. The constant of proportionality is termed the conductance (L^2t^{-1}).

Initially, the conductance values were set to large values allowing ground water to flow freely across the boundaries. Through the calibration process, the conductance values were lowered such that the simulated hydraulic heads closely matched measured water levels.

Model Calibration

The ground-water flow model of the Joshua Tree and Copper Mountain ground-water subbasins was calibrated using a trial-and-error process in which the initial estimates of the aquifer properties were iteratively adjusted to improve the match between simulated hydraulic heads and measured ground-water levels. Measured ground-water levels for predevelopment conditions and for the period 1958–2001 were used to calibrate the ground-water flow model. The calibration process involved iteratively adjusting the parameters to minimize hydrologic-budget error, match measured water levels, and simulate reasonable boundary fluxes.

Measured ground-water levels collected prior to 1958 were used to calibrate the ground-water flow model for predevelopment conditions because these data yielded the most complete dataset when pumpage was relatively low. Measured ground-water levels from 1958 to 2001 were used to calibrate the ground-water flow model for transient conditions caused by stresses within the basin. Changes in the hydrologic conditions from 1958 to 2001 are the result of stress on the aquifer system caused by ground-water pumping (all other stresses, that is, natural recharge and boundary fluxes, are held constant). Seasonal and long-term climatic variations also can influence hydrologic conditions, but they are not addressed in this study. The magnitude of variability in the simulated hydraulic heads is dependent on ground-water pumping, natural recharge, boundary conditions, hydraulic parameters (*K*, *Sy*, and *Ss*), and fault parameters (hydraulic characteristic).

Measured annual pumpage data from 1958 to 1975 and monthly pumpage from 1976 to 2001 were simulated using the MNW package (Halford and Hanson, 2002). Average annual recharge estimated using INFILv3 were simulated as a specified flux to model-layer 1.

The general-head boundary parameters were estimated through calibration such that the simulated hydraulic heads approximated measured predevelopment water levels (pre-1958 ground-water levels). Two general-head boundaries were located at the eastern and northern ends of the model to simulate ground-water underflow (fig. 37). Water levels on the eastern end of the Joshua Tree ground-water subbasin were about 2,255 ft asl in the late 1960s (Lewis, 1972); therefore, the head of the general-head boundaries for each model layer was set equal to 2,255 ft. Water levels on the northern end of the Copper Mountain ground-water subbasin were based on water-level measurements made at a well owned by the Surprise Springs Water Agency (2N/7E-20Q1) and were set equal to about 2,150 ft asl. The initial conductance values were 1076.0 ft^2/d, which allowed water to freely leave the basin. The final general-head-conductance values for the eastern and northern boundaries were 1.08×10^{-6} and 10.76 ft^2/d, respectively.

The initial estimates of hydraulic conductivity for model layers 1-3 east of model fault F2 were 60.0, 5.0, and 0.5 feet per day (ft/d), respectively. West of F2, the initial estimates of hydraulic conductivity for model layers 1–3 were 5.0, 0.5, and 0.5 ft/d, respectively. Recall that the upper aquifer is unsaturated west of F2; therefore, only the middle and lower aquifers are present in this part of the Joshua Tree ground-water subbasin. Through the calibration process it was found that these initial values were reasonable, and therefore, they were not changed.

The initial estimate of the anisotropy ratio was 100:1; that is, the horizontal hydraulic conductivity was 100 times greater than the vertical hydraulic conductivity. Other ratios were tested during the calibration process; however, changing this ratio did not have a significant effect. Therefore, the ratio of 100:1 was retained, and the final calibrated vertical hydraulic conductivity values for model layers 1–3 east of model fault F2 were 0.6, 0.05, and 0.005 ft/d, respectively and west of F2 were 0.05, 0.005, and 0.005 ft/d, respectively.

The initial estimates of storage properties for model layers 1-3 were 0.1 ft/ft, 1.0×10^{-3}/ft, and 1.0×10^{-6}/ft, respectively. The first value is an estimate of *Sy* for the unconfined model layer 1, and the second and third values are estimates of *Ss* for the confined model layers 2 and 3. The final calibrated values for model layers 1–3 were 0.2 ft/ft, 1.0×10^{-6}/ft, and 1.0×10^{-6}/ft, respectively.

Flow across a simulated fault is proportional to the hydraulic characteristic (Hsieh and Freckleton, 1993). The initial hydraulic-characteristic values for all the faults were set equal to the largest value of hydraulic conductivity (60.0 ft/d) divided by the assumed width of the fault (1 ft), allowing unrestricted hydraulic connection across the faults. To reproduce the measured water levels, it was necessary to simulate faults F1 and F2 (fig. 37) by decreasing the initial hydraulic-characteristic values by as much as nine orders of magnitude (table 18).

Simulated Hydraulic Heads

Areal Distribution: Predevelopment and 2001

Simulated model-layer 1 hydraulic heads with water-level measurements at selected wells for predevelopment conditions (pre-1958) and at the end of the simulation period (December 31, 2001) are shown in figure 40. Faults divide the subbasins into three subareas: west of the inferred north-south trending fault (F2), south of the Pinto Mountain Fault (F1) and east of F2, and north of the Pinto Mountain Fault. Simulated predevelopment hydraulic heads west of F2 range from about 2,650 to more than 2,700 ft asl (fig. 40*A*). Simulated predevelopment hydraulic heads east of F2 and south of the Pinto Mountain Fault range from about 2,300 to 2,350 ft asl. Simulated predevelopment hydraulic heads north of the Pinto Mountain Fault are less than 2,200 ft asl. The model results are consistent with measured water levels and indicate that ground water initially flows west to east and then flows northward exiting the Copper Mountain ground-water subbasin through the northern boundary.

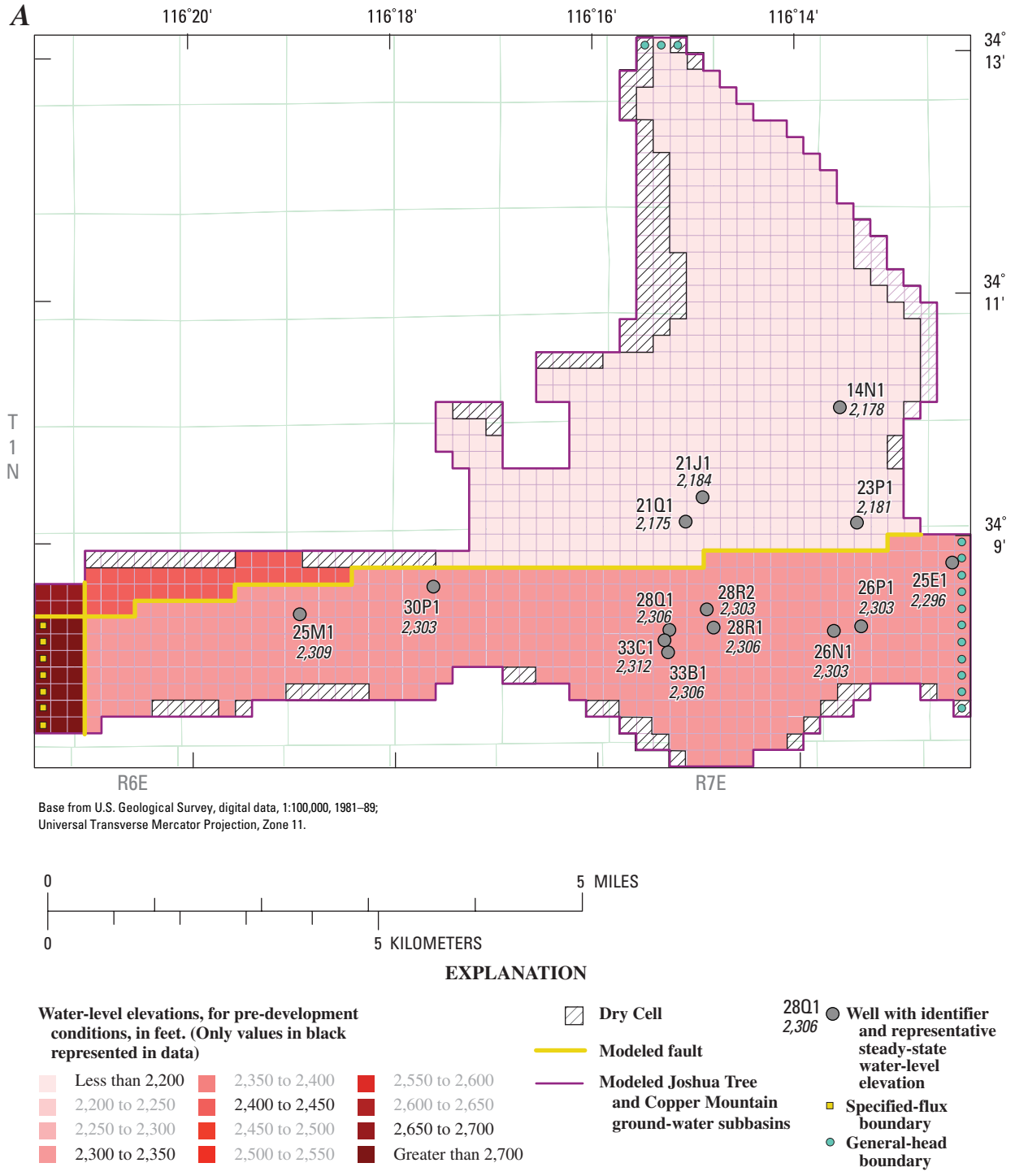

Figure 40. Areas of similar simulated model layer 1 hydraulic head and measured water levels for (*A*) steady-state and (*B*) December 2001, Joshua Tree and Copper Mountain ground-water subbasins, San Bernardino County, California.

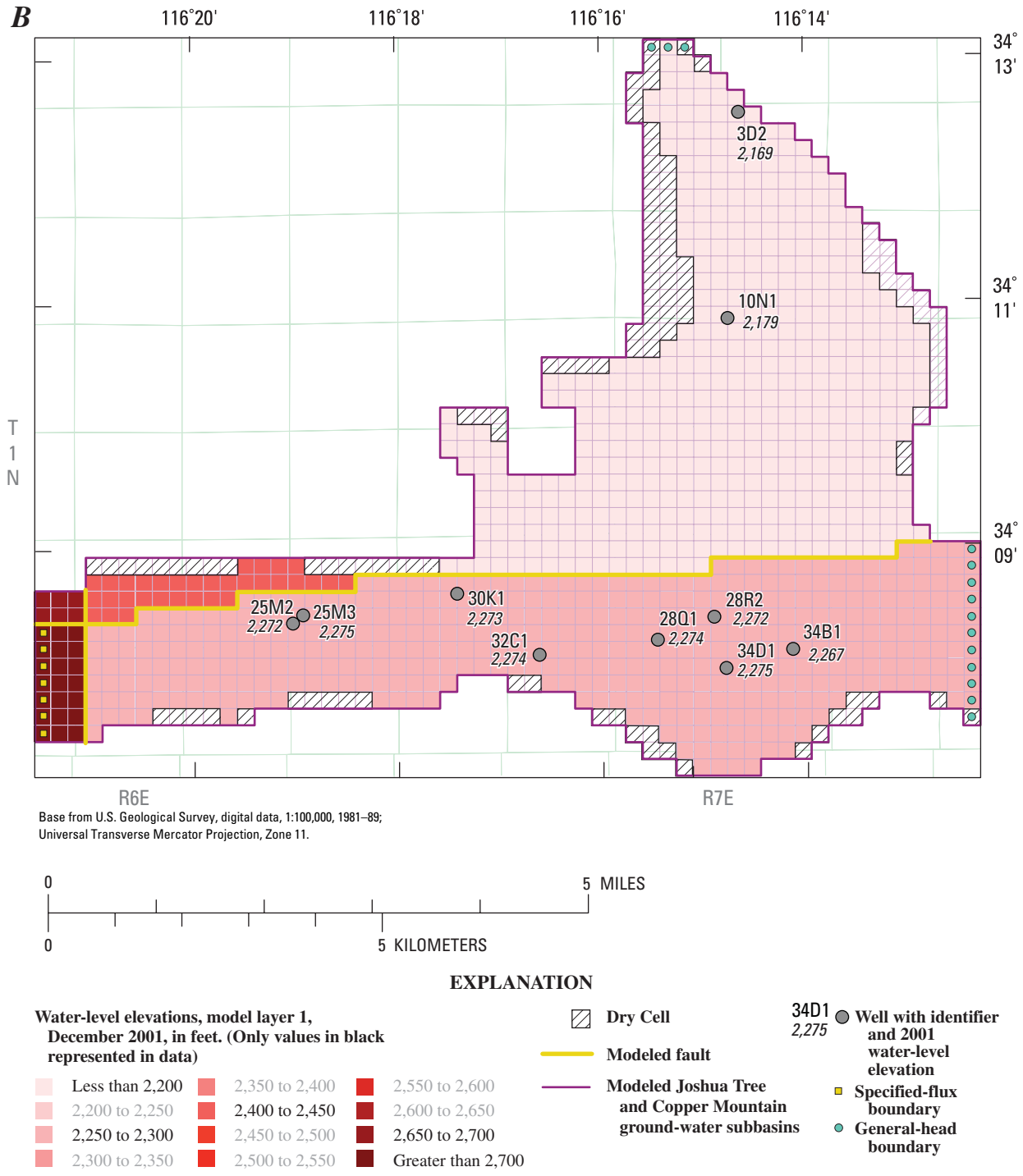

Figure 40.—Continued.

Simulated December 2001 hydraulic heads west of F2 range from about 2,650 to more than 2,700 ft asl. Simulated December 2001 hydraulic heads east of F2 and south of the Pinto Mountain Fault range from about 2,250 to 2,300 ft asl and, although not shown on figure 40*B*, there is a water-level depression near wells 1N/6E-25M2 and M3 (fig. 40*B*). Simulated December 2001 hydraulic heads north of the Pinto Mountain Fault range from about 2,165 to 2,181 ft asl. The 2001 model results are also consistent with measured water levels and indicate that, in general, the predevelopment ground-water paths are maintained through the simulation period.

Simulated Hydrographs

Simulated hydraulic heads and measured water levels for selected wells are shown in figure 41; only one of these wells, 1N/7E-32C1, has a long-term record. The simulated hydraulic heads for model layers 1–3 are shown in figure 41 for comparison with the measured water levels.

Wells 1N/6E-34D3-5, located west of model fault F2, were installed in 1999; therefore, the period of record for these wells is short. The simulated and measured hydrographs for well 1N/6E-34D4, which is perforated in Tertiary sedimentary and volcanic deposits (model layer 2), is shown in figure 41*A*. Note that in the ground-water flow model, well 34D4 is located near fault F2 where the simulated hydraulic gradient is very steep because of the low hydraulic-characteristic value. Therefore, the simulated hydraulic head shown in figure 41*A* is an average of the simulated hydraulic heads at two model cells adjacent to the well location in the east-west direction. The measured water levels are between the high simulated hydraulic heads for model layers 1 and 2 and the low values for model layer 3. The sudden decline in measured water levels (8 ft) following the Hector Mine earthquake (October 16, 1999) is not captured by the simulated data; however, the simulated results in later time follow the general trend of the measured data.

Well 1N/6E-25M2, located south of the Pinto Mountain Fault and in the community of Joshua Tree, has a short period of record (fig. 41*B*). Well 25M2 was drilled in 1961 and is perforated in model layer 1. The simulated hydraulic heads match the measured data very well.

Well 1N/7E-32C1, located south of the Pinto Mountain Fault, has a fairly long period of record; however, data were not collected between 1972 and 1993 (fig. 41*C*). Well 32C1 was drilled in 1952 and is perforated in model layer 1. The measured drawdown that occurred in the late 1960s was not reflected in the simulated hydraulic heads; however, the general trend in measured water levels are reflected in the model layer 1 simulated hydraulic heads.

Well 1N/7E-14N1 is located in the Copper Mountain ground-water subbasin, north of the Pinto Mountain Fault. Well 14N1 was drilled in 1943 and is perforated in model layer 1. The simulated hydraulic heads for all model layers followed closely the trend in measured water levels; however, the simulated values were about 5 ft lower than the measured values (fig. 41*D*).

Simulated Water Budget

The simulated water budgets for predevelopment conditions, the end of the transient simulation (December 2001), and cumulative volumes from 1958 to 2001 are shown in table 19. Recall that for all simulations, recharge is an input parameter that is held constant and that pumpage is based on historical data. The model simulates the inflows to and outflows from the general-head boundaries, as well as changes in storage.

For predevelopment conditions the mass-balance error was 0 percent; the inflow rate was about 207 acre-ft/yr (123 acre-ft/yr of recharge and 84 acre-ft/yr of ground-water inflow across the Yucca Barrier) and the outflow rate was about 207 acre-ft/yr. Ground water exited the Copper Mountain ground-water basin through the northern boundary. Note that by definition for predevelopment/steady-state conditions, there is no change in storage.

For December 2001 conditions, the inflow rate was about 207 acre-ft/yr (123 acre-ft/yr of recharge and 84 acre-ft/yr of ground-water inflow across the Yucca Barrier) and the outflow rate was about 1.53×10^3 acre-ft/yr (1.33×10^3 acre-ft/yr of pumpage and 199 acre-ft/yr of ground-water outflow through the northern boundary) (table 19). The ground-water pumpage resulted in 1.32×10^3 acre-ft/yr of water being removed from storage.

For the entire simulation period of 1958–2001, the cumulative inflow volume was about 9.10×10^3 acre-ft (5.41×10^3 acre-ft of recharge and 3.69 x 103 acre-ft of ground-water inflow across the Yucca Barrier) and the cumulative outflow volume was about 5.11×10^4 acre-ft (4.22×10^4 acre-ft of pumpage and 8.88×10^3 acre-ft of ground-water outflow through the northern boundary) (table 19). Of the total pumpage, the model simulated that 99 percent (4.19×10^4 acre-ft) was removed from ground-water storage (table 19). This decrease in storage explains the decline in measured ground-water levels.

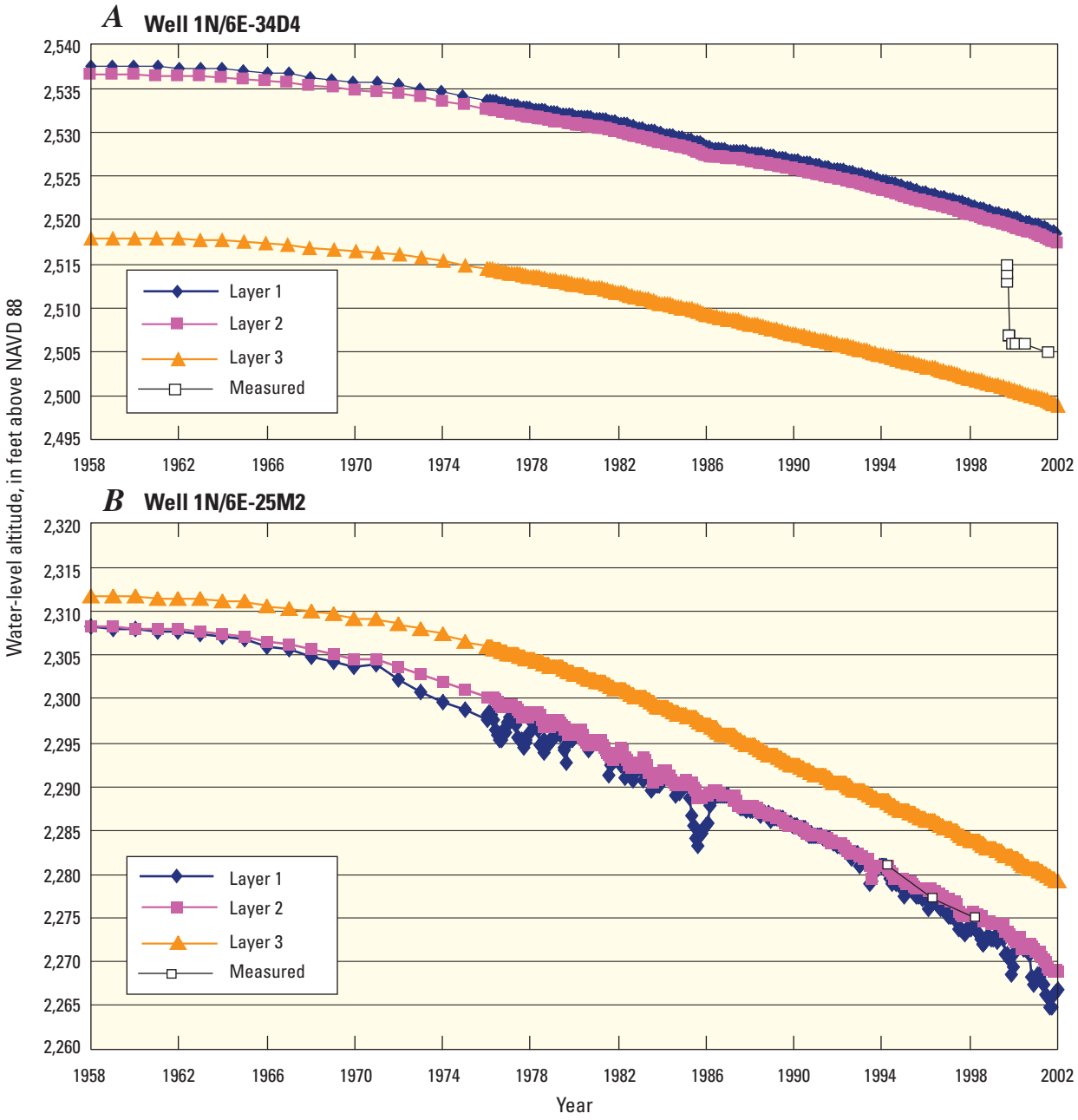

Figure 41. Mmeasured water levels and simulated hydraulic heads for perforated model layers for wells (*A*) 1N/6E-34D4, (*B*) 1N/6E-25M2 (JBWD #2), (*C*) 1N/7E-32C1, and (*D*) 1N/7E-14N1, Joshua Tree and Copper Mountain ground-water subbasins, San Bernardino County, California.

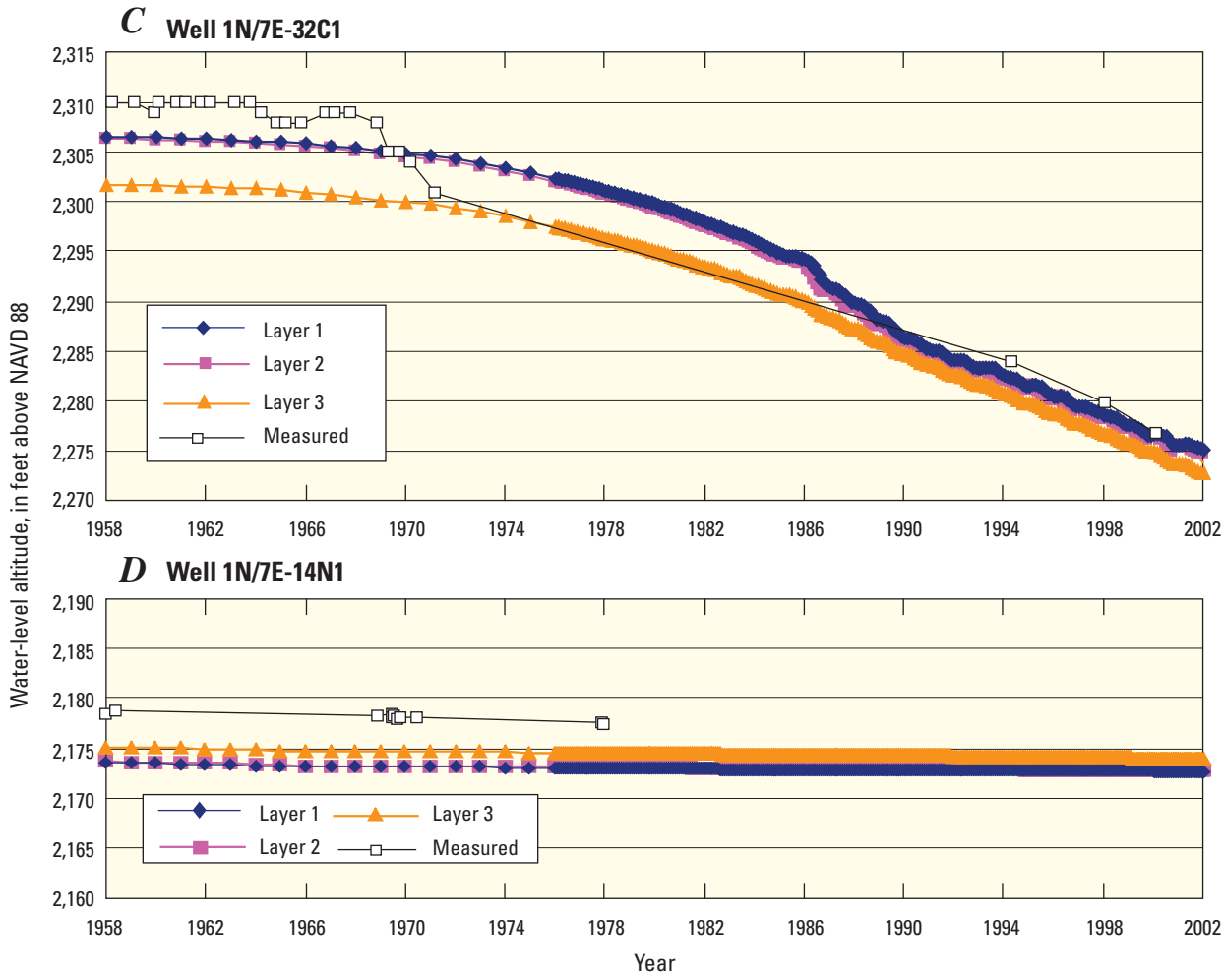

Figure 41.—Continued.

Table 19. Simulated water budgets for predevelopment and December 2001conditions, and cumulative volumes, Joshua Tree and Copper Mountain ground-water subbasins, San Bernardino County, California

[acre-ft, acre feet; acre-ft/yr, acre feet per year]

	Water budget components	Water budget values
Predevelopment		
Inflow (acre-ft/yr)		
	Recharge	123
	Specified flux	84.0
	Total	207
Outflow (acre-ft/yr)		
	Pumpage	0
	Head-Dependent Boundary	207
	Total	207
	Outflow-Inflow	0
	Storage Depletion	0
End of transient simulation (December 2001)		
Inflow (acre-ft/yr)		
	Recharge	123
	Specified flux	84.0
	Total	207
Outflow (acre-ft/yr)		
	Pumpage	1.33×10^3
	Head-Dependent Boundary	199
	Total	1.53×10^3
	Outflow-Inflow	1.32×10^3
	Storage Depletion	1.32×10^3
Cumulative (1958–2001)		
Inflow (acre-ft)		
	Recharge	5.41×10^3
	Specified flux	3.69×10^3
	Total	9.10×10^3
Outflow (acre-ft)		
	Pumpage	4.22×10^4
	Head-Dependent Boundary	8.88×10^3
	Total	5.11×10^4
	Outflow-Inflow	4.20×10^4
	Storage Depletion	4.19×10^4

Model Fit

Measured water levels and simulated transient-state hydraulic heads for selected wells from predevelopment (pre1958) to 2001 closely follow a 1:1 correlation line (fig. 42). If the model simulated measured data perfectly, then all the data would lie on the 1:1 correlation line. Most wells in the Joshua Tree and Copper Mountain ground-water subbasins are perforated in model layer 1 only and three wells (1N/6E-34D3-5) are perforated in model layer 2; the simulated hydraulic heads from model layer 1 are compared with measured data directly. However, for wells that are perforated in model layers 1 and 2, MF2K calculates a composite simulated hydraulic head that is a weighted function of the simulated heads from the respective model layers. The weights are functions of the perforated interval and the hydraulic conductivity of the model layers and sum to 1.0 (Hill and others, 2000). The composite simulated hydraulic heads are compared with measured water levels from multi-layer wells in figure 42. The sum of squared errors equaled 6.15×10^3 ft^2, and with 353 observations the root-mean-squared error equaled 4.17 ft.

Sensitivity Analysis

Sensitivity analysis is a procedure that evaluates the model sensitivity to variations in the input parameters. The procedure involves keeping all input parameters constant except for the one being analyzed. For this study, there were nine parameters; horizontal and vertical hydraulic conductivity and storage (specific storage and specific yield) varied by layer, yielding 15 parameters (table 18). MF2K was used to generate composite-scaled sensitivity values for each parameter. Composite-scaled sensitivities are calculated in MF2K for each parameter using the scaled sensitivities for all observations. Composite-scaled sensitivities are unitless and indicate the total amount of information provided by the observations for the estimation of one parameter (Hill, 1998). In general, the larger the value of the composite-scaled sensitivity for a particular parameter, the greater the model's sensitivity to changes in that parameter.

The composite-scaled sensitivity values for all the parameters are shown in figure 43. Hill (1998) stated that it is likely that a parameter-estimation routine will not be able to estimate those parameters whose composite-scaled sensitivity values are less than about 0.01 times the largest value (here, about 19). These results indicate that the simulated hydraulic heads are most sensitive (greater than 0.19) to changes in the following parameters: F2 hydraulic characteristic, F1 hydraulic characteristic, recharge, layer 1 hydraulic conductivity, layer 3 hydraulic conductivity, north general-head boundary conductance, layer 1 specific yield, and layer 3 vertical hydraulic conductivity.

Ground-Water Flow Model Limitations

When applied carefully, a numerical ground-water flow model can be useful for projecting aquifer responses to various changes in aquifer stresses; however, a model is a highly idealized approximation of the actual system and is based on average and estimated conditions. Perhaps the biggest limitation is the failure of an idealized, lumped-parameter model to capture a complex hydrogeologic setting. The capability of the model to reliably project aquifer responses is also related to the accuracy of the input data used in the model calibration and is inversely related to the magnitude of the proposed changes in the stresses being applied to the model as well as to the length of the simulation horizon.

In this study, the ground-water flow model was calibrated using manual trial-and-error techniques. Owing to the complexity and unknowns of the system being represented, it is worth noting that model construction and calibration (formal or not) result in a nonunique product and that model predictions are subject to potentially large errors (Konikow and Bredehoeft, 1992). Automated approaches could be used in subsequent studies to more formally characterize uncertainties in the parameters and perhaps improve the fit of the model to calibration data (Yeh, 1986).

In this model, septage was not simulated as a source of recharge; however, this source of recharge may reach the water table. In order to simulate future conditions, the timing and quantity of this potential source of recharge should be considered.

Summary and Conclusions

The Joshua Basin Water District (JBWD) supplies water to the community of Joshua Tree from the underlying Joshua Tree ground-water subbasin. The JBWD is concerned with the long-term sustainability of the underlying aquifer and plans to construct production wells in the adjacent Copper Mountain ground-water subbasin to help meet future demands.

The objectives of this study were to (1) improve the understanding of the geohydrologic framework of the Joshua Tree and Copper Mountain ground-water subbasins, (2) determine the distribution and quantity of recharge using field and numerical techniques, and (3) develop a ground-water flow model that can be used to help manage the water resources of the region. These objectives were accomplished by collecting ground-water-level and water-quality data for the subbasins and assessing the current state of the subbasins. In addition, field measurements and a distributed-parameter watershed model were used to estimate the amount of recharge in the subbasins. The water-level, water-quality, and recharge data were then used to constrain the ground-water flow model.

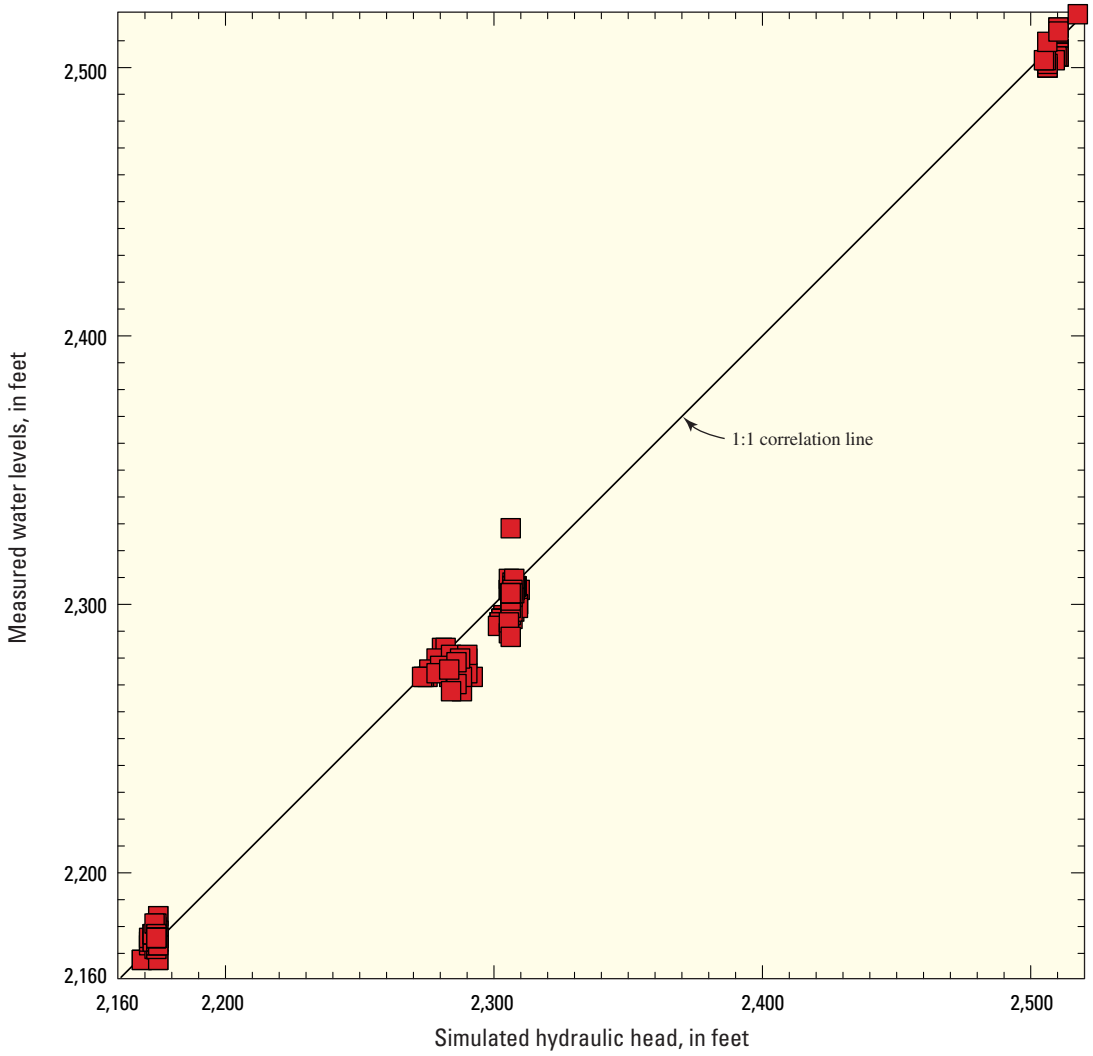

Figure 42. Relation between simulated hydraulic heads and measured water levels, with 1:1 best-fit line, Joshua Tree and Copper Mountain ground-water subbasins, San Bernardino County, California.

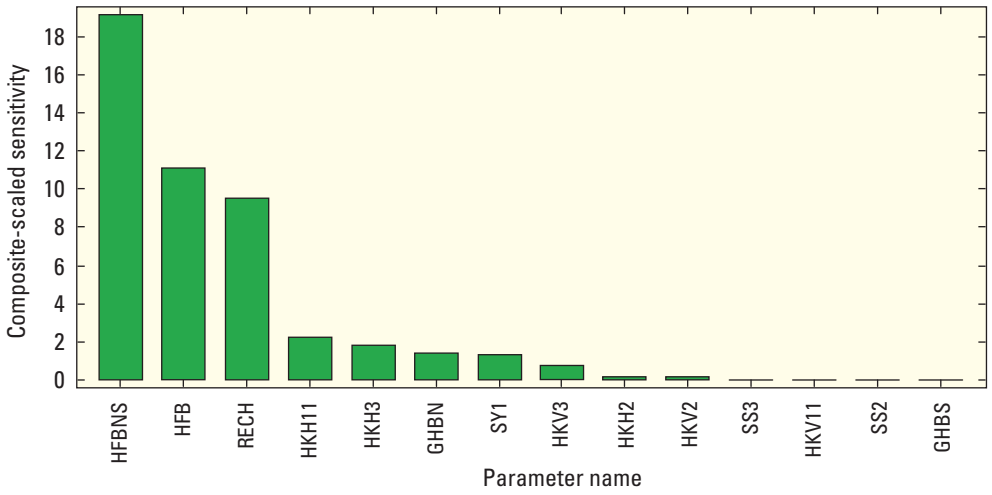

EXPLANATION

HFBNS—Fault 2 hydraulic characteristic
HFB—Fault 1 hydraulic characteristic
RECH—Recharge
HKH11—Layer 1 horizontal hydraulic conductivity
HKH3—Layer 3 horizontal hydraulic conductivity
GHBN—Northern general-head boundary conductance
SY1—Layer 1 specific yield
HKV3—Layer 3 vertical hydraulic conductivity
HKH2—Layer 2 horizontal hydraulic conductivity
HKV2—Layer 2 vertical hydraulic conductivity
SS3—Layer 3 specific storage
HKV11—Layer 1 vertical hydraulic conductivity
SS2—Layer 2 specific storage
GHBS—Eastern general-head boundary conductance

Figure 43. Composite-scaled sensitivities for the ground-water flow model, Joshua Tree and Copper Mountain ground-water subbasins, San Bernardino County, California.

The geohydrologic framework of the Joshua Tree and Copper Mountain ground-water subbasins was defined by summarizing previously published research, completing a gravity survey, and collecting geologic and hydrologic data from existing production and monitoring wells. On the basis information from of available lithologic and geophysical logs, the ground-water system was subdivided vertically into three aquifers: the upper, middle, and lower aquifers. Geologic mapping and water-level data indicated that two faults cross the subbasins and have either juxtaposed pre-Tertiary basement complex against unconsolidated alluvial deposits or displaced preferential flow paths in unconsolidated alluvial deposits. This juxtaposition and displacement, along with cementation, compaction, and extreme deformation of the water-bearing deposits adjacent to faults can create low-permeability zones that can act as partial or complete barriers to ground-water flow, thereby compartmentalizing the ground-water flow system.

The sources of ground-water inflow to the subbasins are infiltration of stormflow runoff, ground-water underflow from the neighboring Warren ground-water subbasin, and septage. Natural ground-water outflow exits through the northern boundary of the Copper Mountain ground-water subbasin; ground-water levels are too deep for significant evapotranspiration to occur. Significant ground-water development did not start until 1958.

Published ground-water data for 1996 were used to describe ground-water levels and movement in the study area. A long-term hydrograph indicates a water-level decline of about 35 ft from the late 1950s to 1998 in the south-central part of the Joshua Tree ground-water subbasin.

The water-quality data indicated that dissolved-solids and nitrate concentrations were below regulatory limits; however, fluoride concentrations in the lower aquifer exceeded regulatory limits. In general, arsenic and chromium concentrations were below regulatory limits except for samples from wells 1N/6E-34D3–5, perforated in the lower aquifer, which had arsenic concentrations of 26, 29, and 36 µg/L, respectively, exceeding the USEPA MCL of 10 µg/L. Oxygen-18 and deuterium data indicate that winter precipitation is the predominant source of ground-water recharge. The tritium concentrations in three wells were slightly above the detection limit, indicating little to no recharge has reached the water table since 1952. The carbon-14 data indicated that the uncorrected ground-water ages ranged from about 32,300 to 2,700 years before present.

Instrumented boreholes were installed in selected washes and at a nearby control site to determine the distribution and quantity of recharge. Core material and cuttings from the boreholes were analyzed for physical, chemical, and hydraulic properties. Instruments installed in the boreholes were monitored to measure changes in matric potential and temperature. Borehole data were supplemented with temperature data collected from access tubes installed at additional sites along study washes. Streambed hydraulic properties and the response of instruments to infiltration were measured using infiltrometers. Physical and geochemical data collected away from the stream channels show that direct areal infiltration of precipitation to depths below the root zone and subsequent ground-water recharge do not occur in the Joshua Tree area. Streamflow and subsequent infiltration measured during the study were greatest along reaches downstream from urbanized areas where impervious surfaces increased runoff. Differences in temperature data collected beneath the stream channel and a nearby control site suggest that average infiltration along a reach of Quail Wash downstream from urbanized areas in Joshua Tree and Yucca Valley was as much as 1.3 ft/yr. Extrapolating this value to a basin-scale yields a total of 71 acre-ft/yr of streamflow infiltration in the study area.

Results from the distributed-parameter watershed model indicate that most of the recharge likely occurs during anomalously wet periods, or even isolated occurrences of extreme storms, that are separated by relatively long (multi-year to multi-decade) periods of negligible recharge. In other words, the average climate condition for the study area likely does not generate significant recharge relative to the recharge generated during anomalously wet years or storm periods. This indicates that recharge for the study area may be very sensitive to potential changes in climate or to variations owing to normal climate cycles.

The spatially distributed estimates of recharge indicate that runoff generation and subsequent surface-water flow (including both overland flow and channelized streamflow) are the dominant hydrologic processes controlling recharge. For the Joshua Tree and Copper Mountain ground-water subbasins, recharge primarily occurs along active stream channels in response to infiltrated surface water. The average annual simulated recharge for the entire Joshua Tree surface-water drainage basin is about 1,090 acre-ft/yr, with 158 acre-ft/yr infiltrating in the Joshua Tree and Copper Mountain subbasins ground-water model area. The simulated total annual streamflow is 2 to 10 times greater than the measured total annual streamflow, indicating that the recharge values estimated using INFILv3 may be overestimated.

Results from the INFILv3 watershed model indicate that recharge throughout the modeled Joshua Tree surface-water drainage basin is strongly dependent on winter-season runoff generation during wetter than average periods and the subsequent infiltration of surface water run-on routed to downstream locations. These simulated results are supported by the isotopic data that indicate that winter precipitation is the predominant source of ground-water recharge.

Data collected during the study were used to develop and calibrate a ground-water flow model of the Joshua Tree and Copper Mountain ground-water subbasins using MODFLOW-2000. The simulation period of the ground-water flow model was 1958–2001. Recharge was simulated using the recharge estimates from the watershed model. The model was calibrated using a trial-and-error approach using water-level data collected between 1958 and 2001. The MODFLOW-2000 sensitivity process was used for the sensitivity analysis. In order to better match the measured data, low fault-hydraulic-characteristic values were required, thereby compartmentalizing the Joshua Tree and Copper Mountain ground-water subbasins. The calibrated model matched measured water-level declines in the ground-water subbasins. The simulated total natural inflow was about 207 acre-ft/yr, composed of 123 acre-ft/yr of recharge and 84 acre-ft/yr of underflow from the adjacent Warren ground-water subbasin. The simulated value of recharge is very close to those values estimated using measured temperature differences (120 acre-ft/yr) and a distributed-parameter watershed model (158 acre-ft/yr). The cumulative volume of water pumped from the ground-water subbasins between 1958–2001 was 42,210 acre-ft; of this total pumpage, the model simulated that 99 percent (41,930 acre-ft) was removed from ground-water storage. This decrease in storage explains the 35-ft decline in measured ground-water levels. Septage was not simulated as a source of recharge; however, this source of recharge may reach the water table. In order to simulate future conditions, the timing and quantity of this potential source of recharge should be considered.

References Cited

American Public Health Association, 1992, Standard methods for examination of water and wastewater (18th ed.): variously paged.

Ball, J.W., and Izbicki, J.A., 2004, Occurrence of hexavalent chromium in ground water in the western Mojave Desert, California: Applied Geochemistry, v. 19, p. 1123–1135.

Bear, Jacob, 1979, Hydraulics of groundwater: New York, McGraw-Hill, 569 p.

Bedford, D.R., and Miller, D.M., compilers, 1997, Bedrock geology database for the Mojave Desert Ecoregion, in ARC/INFO data layers CD-ROM, Mojave Desert Ecosystem Program: Logan, Utah, Utah State University Press.

Bouwer, Herman, 1978, Groundwater hydrology: New York, McGraw-Hill, 480 p.

California Department of Forestry and Fire Protection, 1999, California watersheds (CALWATER 2.2): California Department of Forestry and Fire Protection data available on the World Wide Web, accessed September 2000, at URL http://gis.ca.gov/meta.epl?oid=5298.

California Department of Health Services, 2003, MCLs, DLRs, and unregulated chemicals requiring monitoring: California Department of Health Services data available on the World Wide Web, accessed October 17, 2003, at URL http://www.dhs.ca.gov/ps/ddwem/chemicals/MCL/mclindex.htm.

California Irrigation Management Information System, 2002, California ETo zones map: California Department of Water Resources data available on the World Wide Web, accessed April 29, 2002, at URL http://www.cimis.water.ca.gov/.

Campbell, G.S., and Gee, W.G., 1986, Water potential measurement using the filter paper technique, in Klute, A.L., ed., Methods of soil analysis, Part 1, Physical and mineralogical methods (2d ed.): Madison, Wisc., American Society of Argonomy, chap. 25, p. 628–630.

Carsel, R.F., and Parrish, R.S., 1988, Developing joint probability distributions of soil water retention characteristics: Water Resources Research, v. 24, no. 5, p. 755–769.

Chow, V-T., Maidment, D.R., and Mays, L.W., 1988, Applied hydrology: New York, McGraw-Hill, 572 p.

Christensen, A.H., and Fields-Garland, L.S., 2001, Concentrations for total dissolved solids, boron, fluoride, and nitrite-nitrate for wells sampled in the Mojave Water Agency management area, California, 1991–97: U.S. Geological Survey Open-File Report 01-84, 1 CD-ROM.

Constantz, James, and Thomas, C.L., 1996, The use of streambed temperature profiles to estimate depth, duration, and rate of percolation beneath arroyos: Water Resources Research, v. 32, no. 12, p. 3597–3602.

Constantz, James, and Thomas, C.L., 1997, Streambed temperature profiles as indicators of percolation characteristic beneath arroyos in the middle Rio Grande basin, USA: Hydrologic Processes, v. 11, p. 1621–1634.

Craig, Harmon, 1961, Isotopic variations in meteoric waters: Science, v. 133, p. 1702–1703.

Daly, Christopher, Neilson, R.P., and Phillips, D.L., 1994, A statistical-topographic model for mapping climatological precipitation over mountainous terrain: Journal of Applied Meteorology, v. 33, p. 140–158.

Dibblee, T.W., Jr., 1967, Geologic map of the Joshua Tree Quadrangle, San Bernardino and Riverside Counties, California: U.S. Geological Survey Miscellaneous Geologic Investigations Map I-516.

EarthInfo Inc., 2003, NCDC summary of the day. West 2, 2002: Boulder, Colo., EarthInfo Inc., CD ROM.

Eckenfelder, W.W., Jr., 1980, Principles of water quality management: Boston, CBI Publishing Company, Inc., 717 p.

Flint, A.L., Campbell, G.S., Ellett, K.M., and Calissendorff, 2002, Calibration and temperature correction of heat dissipation matric potential sensors: Journal Soil Science Society of America, v. 66, p. 1439–1445.

Flint, A.L., and Childs, S.W., 1987, Calculation of solar radiation in mountainous terrain: Journal of Agricultural and Forest Meteorology, v. 40, p. 233–249.

Flint, A.L., and Ellett, K.M., 2004, The role of the unsaturated zone in artificial recharge at San Gorgonio Pass, California: Vadose Zone Journal, v. 3, p. 763–774.

Freeze, R.A., and Cherry, J.A., 1979, Groundwater: Englewood Cliffs, N.J., Prentice-Hall, 604 p.

Friedman, Irving, Smith, G.I., Gleason, J.D., Warden, Augusta, and Harris, J.M., 1992, Stable isotopic composition of waters in southeastern California: 1. Modern precipitation: Journal of Geophysical Research, v. 97, no. D5, p. 5795–5812.

Gonfiantini, Roberto, 1978, Standards for stable isotope measurements in natural compounds: Nature, v. 271, p. 534–536.

Halford, K.J., and Hanson, R.T., 2002, User guide for the drawdown-limited, multi-node well (MNW) package for the U.S. Geological Survey's modular ground-water flow model, versions MODFLOW-96 and MODFLOW-2000: U.S. Geological Survey Open-File Report 02-293, 33 p.

Harbaugh, A.W., Banta, E.R., Hill, M.C., and McDonald, M.G., 2000, MODFLOW-2000, the U.S. Geological Survey modular ground-water flow model—User guide to modularization concepts and the ground-water flow process: U.S. Geological Survey Open-File Report 00-92, 121 p.

Hatton, T.J., 1998, Catchment scale recharge modeling, Part 4, in The basics of recharge and discharge: Collingwood, Victoria, Australia, CSIRO Publishing, 19 p.

Healy, R.W., and Ronan, A.D., 1996, Documentation of computer program VS2DH for simulation of energy transport in variably saturated porous media -- modification of the U.S. Geological Survey's computer program VS2DT: U.S. Geological Survey Water-Resources Investigations Report 96-4230, 36 p.

Hevesi, J.A., Flint, A.L., and Flint, L.E., 2003, Simulation of net infiltration and potential recharge using the distributed-parameter watershed model, INFILv3, of the Death Valley Region, Nevada and California: U.S. Geological Survey Water-Resources Investigations Report 03-4090, 161 p.

Hill, M.C., 1998, Methods and guidelines for effective model calibration: U.S. Geological Survey Water-Resources Investigations Report 98-4005, 90 p.

Hill, M.C., Banta, E.R., Harbaugh, A.W., and Anderman, E.R., 2000, MODFLOW-2000, the U.S. Geological Survey modular ground-water flow model--User guide to the observation, sensitivity, and parameter-estimation processes and three post-processing programs: U.S. Geological Survey Open-File Report 00-184, 209 p.

Hillel, Daniel, 1982, Introduction to soil physics: New York, Academic Press, 364 p.

Hsieh, P.A., and Freckleton, J.R., 1993, Documentation of a computer program to simulate horizontal-flow barriers using the U.S. Geological Survey's modular three-dimensional finite-difference ground-water flow model: U.S. Geological Survey Open-File Report 92-477, 32 p.

Izbicki, J.A., Clark, D.A., Pimentel, M.I., Land M.T., Radyk, John, and Michel, R.L., 2000a, Data from a thick unsaturated zone underlying Oro Grande and Sheep Creek Washes in the western part of the Mojave Desert, near Victorville, San Bernardino County, California: U.S. Geological Survey Open-File Report 00-262, 133 p.

Izbicki, J.A., Christensen, A.H., and Hanson, R.T., 1999, U.S. Geological Survey combined well-bore flow and depth-dependent water sampler, U.S. Geological Survey Fact Sheet FS-196-99, http://ca.water.usgs.gov/archive/reports/fs19699.pdf

Izbicki, J.A., Danskin, W.R., and Mendez, G.O., 1997, Chemistry and isotopic composition of ground water along a section near the Newmark area, San Bernardino County, California; U.S. Geological Survey Water-Resources Investigations Report 97-4179, 27 p.

Izbicki, J.A., and Martin, Peter, 1997, Use of isotopic data to evaluate recharge and geologic controls on the movement of ground water in Las Posas Valley, Ventura County, California: U.S. Geological Survey Water-Resources Investigations Report 97-4035, 12 p.

Izbicki, J.A., and Michel, R.L., 2002, Use of temperature data to estimate infiltration from intermittent streams in the western Mojave Desert, USA, in Foo, D.Y., ed., Balancing the ground water budget: Proceedings of the International Association of Hydrogeologists, Darwin, Australia, May 12-14, 2002, 1 CD-ROM.

Izbicki, J.A., Michel, R.L., and Martin, Peter, 1995, Source, movement and age of groundwater in the upper part of the Mojave River basin, California, U.S.A., in Adar, E.M., and Leibundgut, Christian, eds., Application of tracers in arid zone hydrology: International Association of Hydrological Sciences, no. 232, p. 43–56.

Izbicki, J.A., Radyk, John, and Michel, R.L., 2000b, Water movement through a thick unsaturated zone underlying an intermittent stream in the western Mojave Desert, southern California, USA, Journal of Hydrology, v. 238, p. 194–217.

Izbicki, J.A., Radyk, John, and Michel, R.L., 2002, Movement of water through the thick unsaturated zone underlying Oro Grande and Sheep Creek Washes in the western Mojave Desert, USA: Hydrogeology Journal, v. 10, p. 409–427.

Jury, W.A., Gardner, W.R., and Gardner, W.H., 1991, Soil Physics (5th ed.): New York, John Wiley & Sons, 328 p.

Kalin, R.M., 2000, Radiocarbon dating of groundwater systems, in Cook, P.G., and Herczeg, A.L., (eds.), Chapter 4: Environmental tracers in subsurface hydrology, Boston, Kluwer Academic Publishers, p. 111–144.

Konikow, L.F., and Bredehoeft, J.D., 1992, Validation of geohydrological models: part 1: Advances in Water Resources, v. 15, no. 1, p. 75–83.

Lewis, R.E., 1972, Ground-water resources of the Yucca Valley-Joshua Tree area, San Bernardino County, California: U.S. Geological Survey Open-File Report, 51 p.

Lohman, S.W., 1979, Ground-water hydraulics: U.S. Geological Survey Professional Paper 708, 70 p.

Londquist, C.J., and Martin, Peter, 1991, Geohydrology and ground-water-flow simulation of the Surprise Spring Basin aquifer system, San Bernardino County, California: U.S. Geological Survey Water-Resources Investigations Report 89-4099, 41 p.

Mantua, N.J., Hare, S.R., Zhang, Y., Wallace, J.M., and Francis, R.C., 1997, A Pacific interdecadal climate oscillation with impacts on salmon production: Bulletin of the American Meteorological Society, v. 78, p. 1069–1079.

Mendez, G.O., and Christensen, A.H., 1997, Regional water table (1996) and water-level changes in the Mojave River, Morongo, and the Fort Irwin ground-water basins, San Bernardino County, California: U.S. Geological Survey Water-Resources Investigations Report 97-4160, 34 p., 1 pl.

Michel, R.L., 1976, Tritium inventories of the world oceans and their implications: Nature, v. 263, p. 103–106.

Mook, W.G., 1980, The dissolution-exchange model for dating of groundwater with 14C, in Fritz, P. and Fontes, J.C., eds., Handbook of Environmental Isotopes Geochemistry, v. 1, Amsterdam, Elsevier, p. 50–74.

Nishikawa, Tracy, Densmore, J.N., Martin, Peter, and Matti, Jonathan, 2003, Evaluation of the source and transport of high nitrate concentrations in ground water, Warren subbasin, California: U.S. Geological Survey Water-Resources Investigations Report 03-4009, 133 p.

Philander, S.G., 1990, El Nino, La Nina, and the Southern Oscillation: New York, Academic Press, 291 p.

Phillips, F.M., 1994, Environmental tracers for water movement in desert soils of the American Southwest: Soil Science of America Journal v. 58, p. 15–24.

Piper, A.M., 1945, A graphic procedure in the geochemical interpretation of water analysis: American Geophysical Union Transactions, 25th Annual Meeting, p. 914–928.

Prudic, D.E., 1994, Estimates of percolation rates and ages of water in unsaturated sediments at two Mojave Desert sites, California–Nevada: U.S. Geological Survey Water-Resources Investigations Report 94-4160, 19 p.

Pyke, C.W., 1972, Some meteorological aspects of the seasonal distribution of precipitation in the Western United States and Baja California: University of California, Water Resources Center Contribution 139, 205 p.

Roberts, C.W., Jachens R.C., Katzenstein, A.M., Smith, G.A., and Johnson, R.U., 2002, Gravity map and data of the eastern half of the Big Bear Lake, 100,000 scale quadrangle, California, and analysis of the depths of several basins: U.S. Geological Survey Open-file Report 02-353, accessed October 4, 2002, at URL http://geopubs.wr.usgs.gov/open-file/of02-353/.

Spatial Climate Analysis Service, 2004, PRISM products, accessed August 25, 2004, at URL http://www.ocs.orst.edu/prism/products/.

Trayler, C.R., and Koczot, K.M., 1995, Regional water table (1994) and water-level changes in the Morongo Basin, San Bernardino County, California: U.S. Geological Survey Water-Resources Investigations Report 95-4209, scale 1:125,000,
1 sheet.

Umari, A.M.J., Martin, Peter, Schroeder, R.A., Duell, Jr., L.F.W., and Fay, R.G., 1995, Potential for ground-water contamination from movement of wastewater through the unsaturated zone, Upper Mojave River Basin, California: U.S. Geological Survey Water-Resources Investigations Report 93-4137, 83 p.

U.S. Department of Agriculture, 1994, State Soil Geographic (STATSGO) Data Base—Data use information, Misc. Pub. no. 1492.

U.S. Environmental Protection Agency, 2003a, National secondary drinking water regulations: U.S. Environmental Protection Agency data available on the World Wide Web, accessed on October 16, 2003, at URL http://www.epa.gov/safewater/mcl.html#sec.

U.S. Environmental Protection Agency, 2003b, List of contaminants and their MCLs: U.S. Environmental Protection Agency data available on the World Wide Web, accessed on October 16, 2003, at URL http://www.epa.gov/safewater/mcl.html#mcls.

U.S. Geological Survey, 2000, (westveg.text) Gap Analysis Program: U.S. Geological Survey data available on the World Wide Web, accessed August 16, 2000, at http://www.gap.uidaho.edu/Regional GAP/regionalftp.htm.

Utah State University, compilers, 1998, Digital elevation data consisting of elevation in meters, slope, aspect and a shaded relief, in Elevation CD-ROM, Mojave Desert Ecosystem Program: Logan, Utah, Utah State University Press.

Whitt, Allen, and Jonker, Kevin, 1998, Groundwater survey of the Joshua Tree and Copper Mountain subbasins, Joshua Tree, California: Western Water Surveys report prepared for the Joshua Basin Water District, variously paged.

Yeh, W. W-G., 1986, Review of parameter identification procedures in groundwater hydrology: the inverse problem: Water Resources Research, v. 22, no. 1, p. 95–108.